DISSERTATION

submitted to the

Combined Faculties for the Natural Sciences and for Mathematics

of the **Ruperto-Carola University of Heidelberg, Germany**

for the degree of

Doctor of Natural Sciences

presented by

Diplom-Molekularmedizinerin **Noemi Bender,**

born in Bad Neuenahr, Germany

Oral-examination: 19.12.2016

Molecular Mechanisms of Macrophage Activation induced by the synergistic effects of Low dose irradiation and adoptive T cell therapy

Referees: Prof. Dr. Philipp Beckhove
Prof. Dr. Stefan Eichmüller

The work described in this thesis was performed from 2012 to 2016 in the Department of **Translational Immunology** at the National Center for Tumour Diseases (Nationales Centrum für Tumorerkrankungen - **NCT**) of the German Cancer Research Center (Deutsches Krebsforschungszentrum - **DKFZ**) in Heidelberg, Germany under the supervision of Prof. Dr. Philipp Beckhove.

Eidesstattliche Versicherung

Hiermit erkläre ich, dass ich die vorliegende Dissertation selbst verfasst und mich dabei keiner anderen als der von mir ausdrücklich bezeichneten Quellen und Hilfen bedient habe. Des Weiteren erkläre ich, dass ich an keiner Stelle ein Prüfungsverfahren beantragt oder die Dissertation in dieser oder einer anderen Form bereits anderweitig als Prüfungsarbeit verwendet oder einer anderen Fakultät als Dissertation vorgelegt habe.

Heidelberg, 21.10.2016

Noemi Bender

Parts of this thesis have been published:

Klug, F., Prakash, H., Huber, P. E., Seibel, T., **Bender, N.**, Halama, N., Pfirschke, C., Voss, R. H., Timke, C., Umansky, L.*, et al.* (2013). **Low-dose irradiation programs macrophage differentiation to an iNOS(+)/M1 phenotype that orchestrates effective T cell immunotherapy**. Cancer cell *24*, 589-602.

Conference and workshop presentations:

Bender N, Klug F, Prakash H, Seibel T, Umansky L, Klapproth K, Beckhove P
Poster presentation: ***"*Local low dose irradiation triggers Macrophage-dependent T cell infiltration"**, CIMT (Cancer Immunotherapy) 11th Annual Meeting, Mainz, Germany, 2013.

Bender N, Klug F, Prakash H, Seibel T, Klapproth K, Halama N, Timke C, Schäkel K, Garbi N, Weitz J, Schmitz-Winnenthal H, Huber P, Hämmerling G, Beckhove P
Oral presentation: ***"*Local low dose irradiation triggers macrophage-dependent T-cell infiltration"**, 8th ENII Summer School in Advanced Immunology, Capo Caccia, Sardinia, Italy, 2013.

Bender N, Klug F, Prakash H, Seibel T, Umansky L, Klapproth K, Halama N, Timke C, Schäkel K, Garbi N, Weitz J, Schmitz-Winnenthal H, Huber P, Hämmerling G, Beckhove P
Poster presentation: ***"*Local low dose irradiation triggers macrophage-dependent T-cell infiltration"**, DKFZ PhD Retreat, Weil der Stadt, Germany, 2013.

Bender N, Klug F, Prakash H, Seibel T, Umansky L, Klapproth K, Halama N, Timke C, Schäkel K, Garbi N, Weitz J, Schmitz-Winnenthal H, Huber P, Hämmerling G, Beckhove P
Poster presentation: ***"*Local low dose irradiation triggers macrophage-dependent T-cell infiltration"**, DKFZ Poster Presentation, Heidelberg, Germany, 2013.

Bender N, Klug F, Prakash H, Seibel T, Nögel L, Klapproth K, Halama N, Huber P, Hämmerling G, Beckhove P
Poster presentation: ***"*Macrophage-dependent tumour immune rejection induced by local low dose irradiation"**, CIMT (Cancer Immunotherapy) 12th Annual Meeting, Mainz, Germany, 2014.

ABSTRACT

The detection of cancerous cells by the immune system elicits spontaneous antitumour immune responses. Still, during their progression, tumours acquire characteristics that enable them to escape immune surveillance. Cancer immunotherapy aims to reverse tumour immune evasion by activating and directing the immune system against transformed tumour cells. However, the tumours' intrinsic resistance mechanisms limit the success of many immunotherapeutic approaches. The functionally and morphologically abnormal tumour vasculature forms a physical barrier and prevents the entry of tumour-reactive immune effector cells, while the immunosuppressive tumour microenvironment impairs their function. To block tumour immune evasion, therapeutic strategies are being developed that combine cancer immunotherapy with treatment modalities, such as radiotherapy, that reprogram the tumour microenvironment to increase treatment efficacies and improve clinical outcome. In various preclinical models radiotherapy was shown to enhance the efficacy of adoptive T cell therapy. Our group showed that in the RIP1-TAg5 mouse model of spontaneous insulinoma, the transfer of *in vitro*-activated tumour-specific T cells induces T cell infiltration and promotes long-term survival only in combination with neoadjuvant local low dose irradiation (LDI). These treatment effects were mediated by $iNOS^+$ macrophages.

In this thesis, we investigated the mechanisms underlying the improved T cell infiltration and prolonged survival upon combination therapy with adoptive T cell transfer and local LDI. We demonstrate that combination therapy leads to a normalization of the aberrant tumour vasculature and endothelial activation, an increase in intratumoural macrophages, a reduction of intratumoural myeloid derived suppressor cells and, most importantly, to tumour regression. These findings suggest that this treatment inhibits tumour immune suppression but also facilitates immune effector cell infiltration through the normalization of the tumour vasculature, finally leading to tumour immune rejection. Inhibition of the inducible nitric oxide (NO) synthase (iNOS) revealed that these effects largely depend on its activity. Of note, the stimulation of human endothelial cells with low doses of the NO donor DETA NONOate activates the endothelial cells to upregulate adhesion molecules, indicating that in response to the combination therapy, iNOS-derived NO directly activates tumour endothelial cells, thereby promoting T cell infiltration and tumour immune rejection.

Moreover, adoptive transfer of low dose irradiated peritoneal macrophages into unirradiated RIP1-TAg5 mice prior to adoptive T cell transfer resulted in effects corresponding to the combination treatment, which highlights the role of macrophages in this mechanism. Whole transcriptome analysis of the irradiated peritoneal macrophages revealed that LDI causes gene expression and functional changes in these cells. Specifically, LDI activated interferon signalling and induced the upregulation of interferon regulated genes. This effect is likely due to the detection of danger signals released from damaged cells, which primes macrophages and induces a shift in their polarization state. Signal transduction and amplification of

interferon responses is mediated by interferon regulatory factors like IRF7. These transcription factors induce the expression of proinflammatory genes such as *Nos2*. *Irf7* but also *Nos2* and various proinflammatory genes like tumour necrosis factor (*Tnf*) were upregulated in response to LDI. Since NO and TNF-α are mediators of endothelial activation, this finding represents the link between LDI and macrophage-mediated activation of the tumour endothelium.

In conclusion, the presented thesis demonstrates that macrophages with proinflammatory phenotypes are required for the activation of tumour endothelial cells, which in turn is critical for the infiltration of immune effector cells and, thereby, for tumour immune destruction. Therefore these findings are of great importance for future immunotherapeutic approaches in the treatment of cancer patients.

ZUSAMMENFASSUNG

Die Erkennung maligne entarteter Zellen durch das Immunsystem löst spontane Immunantworten aus, um die entarteten Zellen zu eliminieren. Während der Krebsentstehung entwickeln die Tumorzellen jedoch Eigenschaften, die es ihnen ermöglichen sich der Erkennung durch das Immunsystem zu entziehen. Krebsimmuntherapien haben zum Ziel diese Prozesse umzukehren und das Immunsystem sowohl zu aktivieren als auch gegen Tumorzellen zu richten. Allerdings beeinträchtigen verschiedene Resistenzmechanismen der Tumorzellen die Wirkung vieler immuntherapeutischer Ansätze. Dabei stellen die funktionell und morphologisch veränderten Tumorgefäße ein Hindernis für die Einwanderung von Immuneffektorzellen dar. Die Funktion der Immuneffektorzellen wird zudem durch das immunsuppressive Tumormikromilieu eingeschränkt. Um dem entgegenzuwirken, werden effektivere therapeutische Strategien entwickelt. Die Kombination von Immuntherapie mit Behandlungsmodalitäten, die das Tumormikromilieu umprogrammieren, kann die Wirksamkeit der Behandlung optimieren und somit klinische Resultate verbessern. Verschiedene präklinische Tumormodelle zeigten eine erhöhte Wirksamkeit von adoptiven T-Zell Therapien durch Kombination mit Strahlentherapie. Unsere Gruppe hat in RIP1-TAg5 Mäusen, welche spontan Insulinome entwickeln, gezeigt, dass der Transfer von *in vitro*-aktivierten tumor-spezifischen T-Zellen sowohl die Einwanderung von T-Zellen in den Tumor induziert als auch das Langzeitüberleben fördert, unter der Voraussetzung, dass der adoptive Transfer mit neoadjuvanter lokaler Niedrigdosisbestrahlung kombiniert wird. Weiterhin konnte gezeigt werden, dass die Effekte der Behandlung durch $iNOS^+$ Makrophagen vermittelt werden.

In der vorliegenden Arbeit haben wir die Mechanismen untersucht, die der erhöhten T-Zell Infiltration und dem verlängerten Überleben nach der Therapie mit lokaler Niedrigdosisbestrahlung und adoptivem T-Zell Transfer zu Grunde liegen. Wir zeigten, dass diese Kombinationstherapie zu einer Normalisierung der abnormalen Tumorvaskulatur, sowie zur Endothelaktivierung führt. Außerdem wurde eine Vermehrung intratumoraler Makrophagen, eine Reduktion intratumoraler myeloider Suppressorzellen und der Rückgang etablierter Tumore beobachtet. Diese Untersuchungsergebnisse weisen darauf hin, dass diese Behandlung die Immunsuppression durch die Tumorzellen hemmt und gleichzeitig, mittels der Gefäßnormalisierung, die Infiltration von Immuneffektorzellen in den Tumor fördert. Zusammen führt dies zur Abstoßung der Tumore durch das Immunsystem. Eine Hemmung der induzierbaren Stickstoffmonoxid (NO) Synthase (iNOS) zeigte, dass die Behandlungseffekte entscheidend von deren Aktivität abhängen. Zudem führte die Stimulation humaner Endothelzellen mit niedrigen Konzentrationen des NO-Donors DETA NONOat zu einer erhöhten Expression von Adhäsionsmolekülen. Diese Ergebnisse deuten darauf hin, dass die Kombinationstherapie zur erhöhten NO Produktion durch iNOS führt. NO aktiviert die Tumorendothelzellen und fördert damit die Einwanderung von T-Zellen, was letztlich zur Abstoßung der Tumore führt.

Darüber hinaus wurden bei einem Transfer peritonealer Makrophagen aus Niedrigdosis bestrahlten wildtyp Mäusen in unbestrahlte RIP1-TAg5 Mäuse, gefolgt von einem adoptiven T-Zell Transfer, Effekte beobachtet, die denen nach Kombinationstherapie entsprechen, wodurch die Bedeutung der Makrophagen in dem Mechanismus verdeutlicht wird. Genomweite Transkriptomanalysen bestrahlter peritonealer Makrophagen ermöglichte die Untersuchung genetischer und funktioneller Veränderungen, die durch die Niedrigdosisbestrahlung hervorgerufen wurden. Demnach zeigen bestrahlte Makrophagen eine Aktivierung des Interferon Signalwegs, sowie eine erhöhte Expression interferon-regulierter Gene. Durch Strahlung geschädigte und gestresste Zellen setzen so genannte „danger“ Signalmoleküle frei, die von Makrophagen erkannt werden. Die Detektion dieser Moleküle führt zur Aktivierung der Makrophagen und schließlich zu einer Interferonantwort. Transkriptionsfaktoren wie die Interferon regulatorischen Faktoren (IRF), darunter IRF7, spielen bei der Signaltransduktion und -amplifikation von Interferonantworten eine zentrale Rolle. Diese Transkriptionsfaktoren induzieren unter anderem die Expression von *Nos2.* Die Expression von *Irf7* sowie *Nos2* und von verschiedenen profinflammatorischen Genen wie Tumor-Nekrose-Faktor-α (*Tnfa*) waren nach Niedrigdosisbestrahlung in den peritonealen Zellen erhöht. Da NO und TNF-α die Endothelaktivierung auslösen können, stellt diese Beobachtung eine Verbindung zwischen Niedrigdosisbestrahlung und der Makrophagen-vermittelten Aktivierung des Tumorendothels dar.

Diese Arbeit verdeutlicht die Rolle proinflammatorischer Makrophagen bei der Aktivierung von Tumorendothelzellen, welche für die Infiltration von Immuneffektorzellen und somit für die Tumorimmunabwehr essentiell ist. Die Erkenntnisse aus dieser Arbeit sind daher von großer Bedeutung für zukünftige immuntherapeutische Ansätze bei der Behandlung von Krebspatienten.

TABLE OF CONTENTS

LIST OF ABBREVIATIONS

A

ACK	Ammonium chloride potassium phosphate
AF488	Alexa Fluor® 488
AF647	Alexa Fluor® 647
AIM2	Absent in melanoma 2
ALR	AIM2-like receptor
APC	Allophycocyanin
APC-Cy7	Allophycocyanin/cyanine7
APCs	Antigen presenting cells

B

bFGF	basic fibroblast growth factor
BSA	Bovine serum albumin
BV510	Brilliant Violet™ 510

C

C3H	C3HeB/Fe
CAR	Chimeric antigen receptor
CCL	Chemokine C-C motif ligand
CD	Cluster of Differentiation
cDNA	complementary DNA
CIT	Cancer Immunotherapy
CpG	Cytosine-phosphorothioate-Guanine
CPM	Counts Per Million
CTL	Cytotoxic T cell
CTLA-4	Cytotoxic T-lymphocyte-associated protein 4
Cx3cr1	Chemokine (C-X3-C motif) receptor 1
CXCL	Chemokine C-X-C motif ligand

D

DAI	DNA-dependent activator of IRFs
DAMP	Danger associated molecular pattern
DAPI	4',6-diamidino-2-phenylindole
DC	Dendritic cell
ddH_2O	double distilled water
DDR	DNA-damage response
Ddx58	DEAD (Asp-Glu-Ala-Asp) box polypeptide 58
DEG	Differentially expressed gene
Dhx58	DEXH (Asp-Glu-X-His) box polypeptide 58
DKFZ	Deutsches Krebsforschungszentrum
DMEM	Dulbecco's Modified Eagle's Medium
DMSO	Dimethyl sulfoxide
DNA	Deoxyribonucleic acid
DNase	Deoxyribonuclease
DR	Death receptors

E

e.g.	exempli gratia
EDTA	Ethylenediaminetetraacetic acid
EGF	Epidermal growth factor
ER	Endoplasmic reticulum
E-selectin	Endothelial selectin
et al.	et alii

F

FACS	Fluorescence-activated cell sorting
FBS	Fetal bovine serum
FBS	Fetal bovine serum
FC	Fold Change
Fcrls	Fc receptor-like S, scavenger receptor
FCS	Fetal calf serum
FDA	Food and Drug Administration
FDR	False Discovery Rate
FGF-2	Fibroblast growth factor-2
FITC	Fluorescein isothiocyanate
Fizz-1	Found in inflammatory zone
Flt1	FMS-like tyrosine kinase 1
FMO	Fluorescence minus one
FoxP3	Forkhead-Box-Protein P3

G

GC	Glucocorticoids
GO	Gene Ontology
GPCF	DKFZ Genomics & Proteomics Core Facility
Gy	Gray

H

HEPES	N-(2-Hydroxyethyl)piperazine-N'-(2-ethanesulfonic acid)
HIF-1	Hypoxia-inducible factor 1
HMGB1	High-mobility group box 1
Hprt	Hypoxanthine guanine phosphoribosyl transferase
HSN	Hybridoma supernatant
Hsp70	Heat shock protein 70
HUVEC	Human umbilical vein endothelial cells

I

i.e.	id est
i.p.	intraperitoneal
i.v.	intravenous
Ic	immune complexes
ICAM-1	Intercellular adhesion molecule 1
IDO	Indoleamine-pyrrole 2,3-dioxygenase
IF	Immunofluorescence
IFI	Interferon gamma inducible protein
Ifih1	Interferon induced with helicase C domain 1
Ifit	Interferon-induced protein with tetratricopeptide repeats
IFN	Interferon
Ig	Immunoglobulin
Igigp	Interferon inducible GTPase
IL	Interleukin
iNOS	inducible nitric oxide synthase
IPA	Ingenuity Pathway analysis
IRF	Interferon regulatory factor
IRG	Interferon regulated gene
irr	irradiated
Isg15	Interferon-stimulated gene 15

L

LDI	Low dose irradiation
LPS	Lipopolysaccharide

M

MA	Minus-Average
mAb	monoclonal antibody
MAVS	Mitochondrial antiviral signalling protein
MCA	3'-methylcholanthrene
MDA5	Melanoma differentiation gene 5
MDSC	Myeloid-derived suppressor cell
MHC	Major histocompatibility complex
mRNA	messenger Ribonucleic acid
Msr2	Macrophage scavenger receptor
MyD88	Myeloid differentiation primary response 88

N

NCT	Nationales Centrum für Tumorerkrankungen
NF-κB	Nuclear factor 'κ-light-chain-enhancer' of activated B-cells
NK	Natural Killer
NO	Nitric oxide
Nos2	Nitric oxide synthase 2 (inducible)

O

Oas	2'-5'-oligoadenylate synthetase 3, 100kDa

P

PAMP	Pathogen associated molecular pattern
PB	Pacific Blue™
PBS	Phosphate buffered saline
PCA	Principal-Component-Analysis
PD-1	Programmed cell death protein 1
PDGF	Platelet-derived growth factor
PD-L1	Programmed cell death 1 ligand
PE	Phycoerythrin
PECs	Peritoneal exudate cells
PE-Cy7	Phycoerythrin/cyanine7
Pen	Penicillin
PerCP	Peridinin Chlorophyll
PGF	placental growth factor
poly I:C	Polyinosinic:polycytidylic acid
PRR	Pattern recognition receptor

R

R3-IGF-1	Insulin-like growth factor-1
Rb	Retinoblastoma protein
RetnIa	Resistin like alpha
RIG-I	Retinoic acid-inducible gene-I

RIN	RNA integrity number
RIP1	Rat insulin promotor-1
RLR	RIG-I like receptor
RNA	Ribonucleic acid
RNS	Reactive nitrogen species
ROS	Reactive oxygen species
RPMI	Roswell Park Memorial Institute medium
RT	Radiotherapy
RT5	RIP1-TAg5
RT-qPCR	Reverse Transcription–Quantitative real-time Polymerase Chain Reaction

S

SDF-1	Stromal cell-derived factor 1
SEM	Standard error of the mean
STAT	Signal transducer and activator of tran-Scription
Strep	Streptomycin
SV40TAg	Simian Virus 40 large T-Antigen

T

TAA	Tumour-associated antigen
TAM	Tumour associated macrophage
Tap1	Transporter associated with Antigen Processing 1
TBI	Total body irradiation
Tbk1	TANK-binding kinase 1
TC	T cell
TCR	T cell receptor
TCR8	TCRtg/TCRCD8
TCR8	TCRtg/TCRCD8
TCRtg	TCR transgenic
TGF	Transforming growth factor
T_H	T helper cell
TIL	Tumour infiltrating lymphocyte
TIRAP	TIR-containing adaptor protein
TLR	Toll-like receptor
TNF	Tumour necrosis factor
TRAIL	TNF-related apoptosis-inducing ligand
T_{reg}	regulatory T cell

U

unirr	unirradiated
VCAM-1	Vascular cell adhesion protein 1
VEGF	Vascular-endothelial growth factor

W

wt	Wildtype

Z

Zbp-1	Z-DNA binding protein

1. INTRODUCTION

1.1. Cancer and the tumour microenvironment

Carcinogenesis is a multistep and often multifactorial process during which initially normal cells acquire genetic and epigenetic alterations, such as somatic point mutations in tumour suppressor genes and oncogenes, which provide them with growth and survival advantages over their neighbouring cells. In cells undergoing malignant transformation multiple genetic alterations accumulate that provide characteristics necessary for the development of cancer. Six crucial capabilities of tumour cells have been described in 2000 by Hanahan and Weinberg, the so-called hallmarks of cancer: 'sustained proliferative signalling', 'evading growth suppression', 'resisting cell death', 'enabling replicative immortality', 'inducing angiogenesis' and 'activating invasion and metastasis' (Hanahan and Weinberg, 2000). In 2011 two emerging hallmarks ('deregulating cellular energetics', 'avoiding immune destruction') and two enabling characteristics ('genome instability and mutation', 'tumour-promoting inflammation') were added (Hanahan and Weinberg, 2011). For a long time, the focus of cancer research has been laid on the cancer cells themselves, despite the fact that tumours are complex tissues with malignant cells embedded in a connective tissue framework. The tumour stroma is a conjunction of extracellular matrix-producing stromal cells (cancer associated fibroblasts and fat cells), immune cells and the tumour vasculature (endothelial cells, pericytes). The complex of cancer cells and tumour stroma is called the tumour microenvironment. The importance of the tumour microenvironment in cancer is stressed by the observations that it affects tumour progression (Hanahan and Weinberg, 2011), disease prognosis (Chen et al., 2015) and treatment outcome (Klemm and Joyce, 2015). Although the tumour stroma can have protective properties by restricting tumour growth (Burnet, 1967; Ozdemir et al., 2014; Proia and Kuperwasser, 2005; Quail and Joyce, 2013), it has mainly been described to promote tumour progression and impair treatment outcome (Hanahan and Coussens, 2012; Mueller and Fusenig, 2004). In the course of tumour development, the cancer cells modulate the tumour microenvironment to sustain tumour progression and to support invasion and metastasis. In addition, some tumours are capable of recruiting cells that support their growth, invasion and metastasis (Hanahan and Coussens, 2012). In the next chapters I will focus on two components of the tumour microenvironment that are relevant in the context of this study: 1) The immune cells and 2) the tumour vasculature.

1.1.1. Tumour immunity

Leukocyte infiltrates were found in tumours as early as 1863 by Rudolf Virchow, who hypothesised that chronic inflammation leads to tumourigenesis (Balkwill and Mantovani, 2001). In the following decades the study of the interactions between the immune system and cancer has become a rapidly advancing field and provided a better understanding of the

complex cellular and molecular mechanisms involved. The ever-increasing knowledge is applied in the discovery of new cancer therapies which aim to harness the immune system to fight cancer.

1.1.1.1. T cells

For many years, it was unclear and has been a matter of controversial debate whether transformed cells can be recognised by the immune system. Since tumour cells are derived from self, it was argued that recognition is suppressed by the immune system's regulatory mechanisms. The first indication of the existence of tumour-specific antigens was found in 1953 by Foley et al., who showed that mice cured of carcinogen-induced cancers resisted rechallenge with the same tumour cells (Foley, 1953). However, it took five decades until it was unequivocally shown that the immune system can recognise transformed cells and that it is able to elicit an antitumour immune response (Parish, 2003). It is now commonly accepted that antitumour immune responses involve cells of the innate immune system, as well as cells of the adaptive immune system (Gajewski et al., 2013). For instance, many tumours have been shown to be infiltrated by T cells, which can be associated with a better clinical outcome, depending on the specific type of T cells. In ovarian, colorectal and breast cancer, as well as in renal cell carcinoma, melanoma and gastrointestinal stromal tumours, increased numbers of $CD8^+$ cytotoxic T cells (CTLs) correlate with improved survival (Azimi et al., 2012; Galon et al., 2006; Kreike et al., 2007; Mahmoud et al., 2011; Rusakiewicz et al., 2013; Zhang et al., 2003) Interestingly, CTLs are not only present, they have been shown to be tumour-specific since they recognise tumour-specific antigens and mediate spontaneous antitumour immune responses (Bonertz et al., 2009; Nagorsen et al., 2003; Schmitz-Winnenthal et al., 2005). In the case of $CD4^+$ T cell infiltration, the data regarding its prognostic value is controversial. Unlike $CD8^+$ T cells, $CD4^+$ T cells differentiate into diverse T helper (T_H) cell lineages (T_H1, T_H2, T_H17 and T_{reg}) upon antigen recognition, depending on the cytokines they encounter during antigen exposure. T_H1 cells are induced by interferon (IFN)-γ and interleukin (IL)-12, while T_H2 cells are induced by IL-4. Differentiation into T_H17 cells and regulatory T cells (T_{reg}) is triggered by transforming growth factor (TGF)-β with IL-6, IL-21 and IL-23 or IL-2, respectively. Upon differentiation, the T helper cell lineages exert distinct functions which are mediated by cytokine secretion. T_H1 cells secrete IFN-γ, IL-12, as well as tumour necrosis factor (TNF)-α, and thereby mediate macrophage activation and elimination of intracellular pathogens. T_H2 cells, on the other hand, produce IL-4, IL-5, IL-10 and IL-13. They are involved in the clearance of extracellular parasites, antibody-mediated immunity and allergic diseases. They also counteract T_H1 responses. T_H17 cells are characterized by the production of IL-17. T_{reg} express FoxP3 (Forkhead-Box-Protein P3), secrete TGF-β, IL-35 and IL-10 and regulate immune responses by maintaining immunogenic tolerance (Luckheeram et al., 2012). The diverse functions (pro- and anti-inflammatory) of the distinct $CD4^+$ T cell subsets could explain the controversial study reports on the prognostic value of intratumoural $CD4^+$ T cells. High T_{reg} infiltrates are associated with poor prognosis in many cancer types (breast (Bates et al., 2006), ovarian (Curiel et al., 2004), hepatocellular (Gao et al., 2007), lung (Petersen et al., 2006), gastric (Perrone et al., 2008) and cervical cancer (Shah et

al., 2011)). On the other hand, a high $CD8^+/T_{reg}$ ratio is associated with improved clinical outcome (Shang et al., 2015), highlighting the essential role of $CD8^+$ T cells in tumour elimination.

1.1.1.2. Macrophages

A major component of tumour-infiltrating leukocytes are macrophages (mononuclear phagocytes), which can make up 50 % of the tumour mass (Kelly et al., 1988; Tu et al., 2014; Van Overmeire et al., 2014). The literature concerning the prognostic value of intratumoural macrophages is controversial. Some studies report a correlation between high numbers of intratumoural macrophages and good prognosis (colorectal (Forssell et al., 2007) gastric (Ohno et al., 2003) endometrial (Ohno et al., 2004) non-small cell lung cancer (Kawai et al., 2008; Kim et al., 2008; Welsh et al., 2005), prostate (Shimura et al., 2000)), whereas others showed either no effect of macrophage infiltration on prognosis (breast cancer (Kelly et al., 1988)) or revealed an association with reduced survival (gastric, urogenital and head and neck cancer (Zhang et al., 2012)). This controversy might be due to differences in the tumour entities and tumour stages but it might also be attributed to distinct functional states of intratumoural macrophages. Macrophages display large functional diversity and high plasticity meaning they are able to quickly adapt to changes in their environment by altering their functional phenotype. Of note, these phenotypical changes are reversible. As part of the first line of the host defence, tissue-resident macrophages constantly monitor their surroundings for pathogen infection and tissue damage. They detect pathogen and danger associated molecular patterns (PAMPs, DAMPs), which are displayed by microorganisms or released by infected and damaged cells, through pattern recognition receptors (PRRs). Membrane-bound PRRs like the Toll-like receptors (TLRs) allow for the detection of extracellular pathogens such as gram-negative bacteria by the stimulation of TLR4 with lipopolysaccharide (LPS) but also intracellular microbial ligands such as double- or single-stranded RNA which activate TLR3 or TLR7/8, respectively. Cytosolic PRRs such as the RIG-I like receptors (RLRs) and AIM2-like receptors (ALRs) identify intracellular microbial ligands such as foreign nucleic acids. The RLRs, RIG-I (retinoic acid-inducible gene-I) and MDA5 (melanoma differentiation gene 5), detect cytosolic RNAs, while the ALRs, AIM2 (absent in melanoma 2) and IFI (interferon gamma inducible protein) 16, detect intracellular DNA. PRR engagement leads the activation of enzymatic cascades via adaptor molecules, such as MyD88 (myeloid differentiation primary response 88) and TIRAP (TIR-containing adaptor protein) for TLRs, as well as MAVS (mitochondrial antiviral signalling protein) for RLRs, subsequently leading to the activation of NF-κB and/or other transcription factors such as interferon regulatory factors (IRFs), which induce the transcription of IFNs (Akira et al., 2001; Kawai and Akira, 2010; Loo and Gale Jr, 2011). Overall, PRR signalling activates macrophages to initiate an inflammatory response. Activated macrophages produce proinflammatory cytokines like TNF-α and IL-1 that subsequently activate endothelial cells in surrounding blood vessels leading to the upregulation of adhesion molecules and thereby promoting leukocyte extravasation. By secretion of chemoattractants (e.g. chemokines), activated macrophages can also recruit other immune cells to the site of inflammation, first neutrophils and monocytes, later, when the stimuli persist,

eosinophils and lymphocytes. Additional cytokines such as IL-6, IL-12, IFNs and co-stimulatory molecules are also upregulated in response to the above mentioned stimuli. This leads to the activation of different types of immune cells and the initiation of an adaptive immune response. In addition, macrophages are capable of directly killing pathogens by phagocytosis and the production of reactive oxygen and nitrogen species (ROS, RNS). Phagocytosis, as well as other non-transcriptional responses, can also be initiated by PRR signalling (Brubaker et al., 2015). After the infection is cleared, the macrophages are involved in the resolution of the inflammatory response and in the repair of the damaged tissue. To prevent secondary necrosis, macrophages phagocytose debris and apoptotic cells, especially neutrophils, which are abundant in early wounds as they are involved in pathogen clearance. It has been suggested that phagocytosis of neutrophils induces the transition from pro- to anti-inflammatory, reparative macrophages (Ortega-Gómez et al., 2013). By producing anti-inflammatory cytokines, such as IL-10 and IL-1Ra (interleukin-1 receptor antagonist), macrophages attenuate the inflammatory response. In addition, macrophages, as well as other cell types, produce growth factors to initiate and support the repair of tissue damage which was induced during inflammation by oxidative stress and protease degradation. The vascular-endothelial growth factor (VEGF), a proangiogenic molecule, promotes revascularization (angiogenesis), while TGF-β and platelet-derived growth factor (PDGF) induce fibroblasts to differentiate, proliferate and produce extracellular matrix components (Koh and DiPietro, 2011; Mantovani et al., 2013; Murray and Wynn, 2011). This shows that macrophages are able to exert a variety of functions during immune responses, which can be very specific depending on the immunological context.

The functional diversity of macrophages is reflected in their phenotypes. In the literature, macrophage phenotypes are classified using the M1/M2 polarization model. In analogy to the T_H nomenclature, M1 macrophages describe inflammatory subtypes which are involved in pathogen clearance, whereas M2 macrophages, which are involved in immune regulation and wound healing, are associated with anti-inflammatory characteristics. However, it was soon recognized that this classification is oversimplified and does not cover the full extent of different activation states that were reported in related literature (Gordon, 2003; Mosser, 2003). A standardized classification system was recently recommended by a consortium of macrophage biologists, in which the activation stimulus is reflected in the nomenclature, i.e. macrophages stimulated with IFN-γ or IL-4 are termed M(IFN-γ) and M(IL-4), respectively (Murray et al., 2014). In the new model, the different macrophage phenotypes are assigned to a spectrum of activation states with macrophages activated by IFN-γ, IFN-γ + LPS or LPS at the “M1” end of the spectrum and macrophages stimulated with IL-4, immune complexes (Ic), IL-10, glucocorticoids (GC) or TGF-β at the “M2” end, representing the fluent transition between the different phenotypes.

Classical activation of macrophages with IFN-γ alone or in combination with microbial stimuli (e.g. LPS) or cytokines induces the M(IFN-γ) or M(LPS + IFN-γ) phenotype, formerly known as the M1 phenotype. This phenotype is characterised by high expression of IL-12 and IL-23.

Through their production of the T_H1 chemokines CCL5, CXCL9, CXCL10 and CXCL11 they recruit T cells, as well as monocytes, eosinophils and dendritic cells to the site of infection. These macrophages show increased expression of co-stimulatory molecules and production of inflammatory cytokines such as IL-1β, TNF-α and IL-6 thereby orchestrating T_H1 (and T_H17) responses. They also produce effector molecules such as reactive oxygen and nitrogen intermediates to clear microorganisms (Martinez and Gordon, 2014; Murray et al., 2014). An additional M1 phenotype was observed after activation through microbial stimuli (such as LPS) that signal via PRRs. In contrast to the classical activation with T_H1 -derived IFN-γ, this activation is T cell-independent and antigen non-specific. This 'Innate activation' leads to the production of ROS, nitric oxide (NO) and type I IFNs. Thus activated cells display increased phagocytic and endocytic properties and show enhanced expression of co-stimulatory molecules (Gordon, 2003; Martinez et al., 2008).

Activation stimuli that shift macrophages to the 'M2' end of the spectrum induce a diversity of phenotypes that can be discriminated based on their cytokine, chemokine and receptor expression, as well as their effector functions. M2-like macrophages have in common that they are involved in attenuating inflammatory processes, while promoting anti-parasite immunity and T_H2 responses. They scavenge debris, promote tissue remodelling and repair, in addition to supporting angiogenesis. For their phagocytic activities, they express mannose and galactose receptors such as CD163 and CD206. Furthermore, some secrete large amounts of IL-10 and TGF-β. The specific phenotypes can be divided as follows: stimulation with the T_H2 derived cytokine IL-4 (and IL-13), formally known as 'alternative activation', leads to the production of CCL17, CCL18, CCL24 and CCL22, which attract T_{reg} and T_H2 cells. Stimulation with IL-10 or TGF-β and GC induces the secretion of CCL24, CLCL10, CXCL11 and CCL5. This shows that the different phenotypes attract distinct cell populations. M(Ic) macrophages express *Nos2* (nitric oxide synthase 2) and produce high levels of IL-10 but low levels of IL-12. They recruit eosinophils, T_{reg} and T_H2 cells via CCL1 and mediate T_H2 polarization of $CD4^+$ T cells. In comparison to other M2 phenotypes, the arginase pathway does not dominate in M(Ic) macrophages (Murray et al., 2014).

It has to be taken into account that this classification system is predominantly based on findings from *in vitro* studies that do not reflect the situation in complex organ systems as in inflammation or cancer where multiple stimuli simultaneously act on macrophages making the identification of distinct phenotypes challenging. Furthermore, the transition from one phenotype to another can be fluent and can even result in macrophages with mixed M1-and M2-like characteristics (Martinez and Gordon, 2014). In malignant tumours, macrophages are usually classified as M2-like macrophages since they mostly harbour tumour promoting properties. But, as in other situations like infection, tumour associated macrophages (TAM) can have dual effects. Apart from promoting tumour growth, invasion and immunosuppression, they are capable of killing tumour cells and induce antitumour immune responses. Whether they support or inhibit tumour growth largely depends on the signals they receive from their surroundings, the tumour microenvironment, and can differ depending on the

location in the tumour but also on the type and stage of the tumour (Van Overmeire et al., 2014). It has been shown that especially in early carcinogenesis TAMs play a role in anti-tumour resistance (O'Sullivan et al., 2012). In established tumours, on the other hand, TAMs usually display M2-like phenotypes and harbour tumour promoting characteristics (Mantovani and Locati, 2013).

1.1.1.3. Immunoediting

Tumours are infiltrated by various immune cell subsets which are capable of eliciting anti-tumour immune responses. Although immune cells are able to recognise and eliminate transformed cells, cancer is diagnosed in approximately 39 % of all people at some point throughout their life (Howlader, 1975-2013), indicating that antitumour immune responses are insufficient and cannot fully eradicate tumours. At the same time, distinct immune cell subsets have been shown to promote tumour development. This dichotomy is illustrated by the two apparently opposing hallmarks of cancer 'avoiding immune destruction' and 'tumour-promoting inflammation' (Hanahan and Weinberg, 2011) and can be explained by the 'Immunoediting hypothesis', which describes the switch from initial antitumour immune responses towards tumour-promoting environments in three major steps (Figure 1).

The **Elimination** phase is based on the 'cancer immunosurveillance theory' proposed in the 1960s by Burnett & Thomas. This theory states that one of the immune system's functions is the elimination of potentially dangerous mutant cells to protect the organism from carcinogenesis (Burnet, 1970; Burnet, 1957; Thomas, 1982). This theory was later supported by the observation that wildtype (wt) mice are less prone to spontaneous and carcinogen-induced tumours than immunodeficient mice (Kaplan et al., 1998; Shankaran et al., 2001) but also by further evidence generated over the last years (reviewed in (Corthay, 2014)). The processes involved in the elimination of transformed cells are very similar to those observed during pathogen clearance and require the cooperation of the innate and the adaptive immune response. In early tumours, malignant cells produce stress-induced ligands and danger signals, such as calreticulin, that can be detected by cells of the innate immune system via PRRs. Upon ligand-binding to the PRRs, innate immune cells become activated and induce a tumour-specific immune response (Schreiber et al., 2011). These early tumour cells also express tumour antigens presented by major histocompatibility complex (MHC) class I molecules, which are recognised by tumour-specific $CD8^+$ T effector cells. Together, these effector cells produce proinflammatory cytokines, type I and type II IFNs and co-stimulatory molecules (CD28, CD137, OX-40), that further activate adjacent immune cells. Effector molecules like granzymes and perforin secreted by T cells can directly kill transformed cells. Another mechanism of T cell-induced apoptosis of tumour cells acts via activation of death receptors on tumour cells. The process of antitumour immunity also involves macrophages that secrete proinflammatory cytokines (TNF-α, IL-1, IL-12) and produce ROS and RNS. The elimination phase ends when all transformed cells are eliminated and tumour formation is prevented. However, if the elimination is incomplete and few tumour cell clones survive elimination, the tumour progresses to the equilibrium phase.

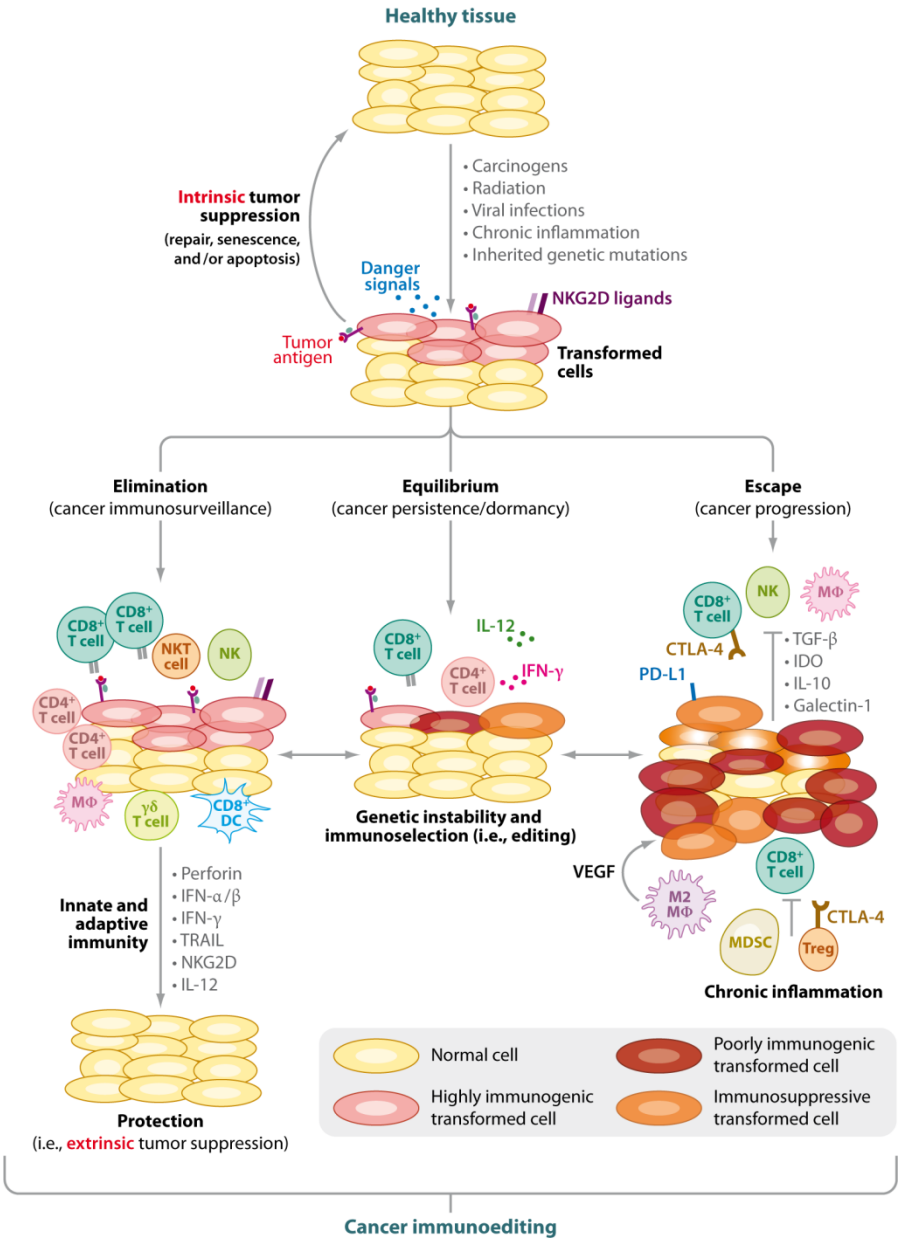

Figure 1 The three phases of Cancer immunoediting.
When intrinsic mechanisms have failed to suppress tumour formation, the immune system, as an extrinsic tumour suppressing mechanism, can eliminate tumours or prevent their outgrowth. During the first phase (Elimination/Cancer Immunosurveillance), innate and adaptive immune cells cooperate to eliminate developing tumours. Tumour cells that survive enter the equilibrium phase, where immune control is in balance with tumour growth and tumours appear dormant. When the balance tips and the immune system can no longer control the tumour cells the cancer progresses to clinically detectable malignancies. This figure is taken from (Vesely et al., 2011).

During the **Equilibrium** phase, the surviving tumour cells are under constant selection pressure induced by the ongoing immune response. Tumour cells that undergo unrestricted cell division continuously accumulate genetic modifications fostered by their genetic instability. This process leads to the positive selection of mutations by which tumour cells develop resistances to immune recognition and elimination. In this way the immune system selects tumour variants that show reduced immunogenicity thereby supporting tumour progression

(Darwinian selection). As long as the immune control mechanisms are able to balance tumour growth promoting mechanisms, the tumour appears dormant; a condition which can last for decades (Aguirre-Ghiso, 2007). It was found that in mice that did not develop progressively growing tumours in response to a low dose of the chemical carcinogen MCA (3'-methylcholanthrene), depletion of $CD8^+$ T cells, IFN-γ or IL-12 led to the outgrowth of occult cancer cells (Koebel et al., 2007), demonstrating that the adaptive immune system controls tumour growth and maintains dormancy.

The **Escape** phase is defined by a dominance of immunosuppressive stimuli over proinflammatory signals and is characterized by re-expanding tumour cells that are no longer constrained by the immune system. When the immune system fails to eliminate or control cancerous cells, tumours grow out, resulting in clinically detectable disease. Many different escape mechanisms contribute to the evasion of tumour cells from the immune system: in response to immune pressure, tumour cells display reduced immune recognition and increased resistance to immune-cytotoxicity. However, the tumours also change the immune system through immunosuppression. The diverse escape mechanisms will be discussed in the next chapter.

1.1.1.4. Tumour immune evasion

Successful antitumour immune responses require the interaction between innate and adaptive immune components. Dendritic cells (DCs) and macrophages are activated in early tumours by danger signals and cellular stress. DCs take up tumour-associated antigens (TAA), migrate to draining lymph nodes and present the TAAs to T cells, thereby priming and activating them. These activated, tumour-specific T cells migrate to the tumour site where they eliminate tumour cells. However, tumours develop multiple mechanisms to circumvent these processes. Selected mechanisms that are relevant for the understanding of this research project are listed below.

Evading immune recognition and elimination. Tumour cells have been shown to avoid recognition and elimination by CTLs (Khong and Restifo, 2002). Reduced recognition can be caused by loss or downregulation of TAAs, by acquired defects in the antigen processing and loading mechanism or by the downregulation of MHC class I molecules (Vinay et al., 2015). A reduced response to IFN-γ by tumour cells can also lead to impaired TAA presentation, since antigen processing and presentation is regulated by IFNs. Furthermore, a lack or reduction of co-stimulatory molecules can impair tumour cell detection by CTLs (Ahmad et al., 2004). Tumour cells avoid elimination by increased resistance to immune-cytotoxicity mechanisms. Decreased expression of death receptors (Stewart and Abrams, 2008) or upregulation of anti-apoptotic molecules facilitates escape from T cell-mediated apoptosis (Vesely et al., 2011). Another way of evading recognition and elimination by immune cells is the expression of "don't eat me" signals, which inhibit phagocytosis of tumour cells by macrophages (Willingham et al., 2012).

Immunosuppression. Immunosuppressive cytokines like TGF-β and IL-10 which are present in the tumour microenvironment impede with effector functions of antitumouricidal immune cells (Khong and Restifo, 2002). TGF-β acts on innate and adaptive immune cells by

affecting the differentiation, maturation and activation of macrophages, DCs and effector T cells. In CTLs for example TGF-β inhibits the production of perforin, granzymes, Fas ligand and IFN-γ, thereby suppressing their cytotoxic effects on tumour cells (Thomas and Massagué, 2005). In $CD4^+$ T cells, TGF-β was shown to promote T_H2 phenotypes and inhibit T_H1 T cell responses (Maeda and Shiraishi, 1996). On the other hand, TGF-β induces the differentiation and proliferation of T_{reg} (Tu et al., 2014). Upon stimulation with TGF-β, macrophages were shown to adopt an anti-inflammatory phenotype with reduced TLR signalling. These macrophages lose the ability to produce proinflammatory cytokines in response to danger signals (Tu et al., 2014). IL-10 also suppresses DC differentiation, maturation and function. It inhibits antigen presentation and IL-12 production, thereby suppressing IL-12-induced T_H1 responses and skewing the T cell response towards T_H2 (Sato et al., 2011). Furthermore, it activates macrophages towards an anti-inflammatory phenotype. Tumour cells can further inhibit T cell function by the upregulation of PD-L1 (Programmed cell death 1 ligand), an immunoinhibitory molecule which limits T cell activity, and by the recruitment, as well as the activation, of immunosuppressive cells such as T_{reg} or myeloid-derived suppressor cells (MDSCs). T_{reg} mainly inhibit CTL functions by producing IL-10 and TGF-β, but also other mechanisms have been suggested such as T_{reg}-induced effector cell death (Schmidt et al., 2012; Zou, 2006). Tumours recruit MDSCs, induce their expansion and polarize TAMs to an M2-like phenotype by the secretion of various anti-inflammatory cytokines and effector molecules (e.g. TGF-β, IL-10, Indoleamine-pyrrole 2,3-dioxygenase (IDO), VEGF). MDSCs are immunosuppressive immature myeloid cells that form a heterogeneous population including granulocytic and monocytic cells. In addition, TAMs stimulated with anti-inflammatory cytokines are also able to adopt immunosuppressive phenotypes. Those cells produce immunosuppressive cytokines, such as IL-10 and TGF-β, thereby further contributing to the generation of an immunosuppressive tumour microenvironment. Increased expression of arginase 1 and IDO suppresses T cell function and proliferation (Munn et al., 1999; Rodriguez et al., 2004). By secretion of VEGF, they promote angiogenesis and by degrading the extracellular matrix, they stimulate tumour cell migration and metastasis (Engblom et al., 2016).

Prevention of effector cell infiltration. Another way for tumours to escape immune responses is by restricting the access of immune effector cells to the tumour site. Tumours can generate a non-permissive microenvironment by specific chemokine profiles that favour infiltration of immunosuppressive cells rather than immune effector cells (Viola et al., 2012) and by an abnormal vasculature with reduced expression of adhesion molecules.

1.1.2. Tumour vasculature

As part of the tumour microenvironment, the tumour vasculature also affects tumour progression and treatment efficacies (Jain, 2013; Tanigawa et al., 1997). Tumour cells require large amounts of nutrients and oxygen for their uncontrolled proliferation. During tumour growth, hypoxic areas develop due to a lack of blood vessels. In response, tumour cells and stromal cells produce high levels of VEGF and other growth factors such as basic fibroblast

growth factor (bFGF), placental growth factor (PGF), TGF-α and PDGF (Baeriswyl and Christofori, 2009; Nagy et al., 2009; Weis and Cheresh, 2011). These growth factors induce angiogenesis by stimulating endothelial cells to proliferate, migrate and form new branches (sprouting of existing vessels). In tumours, production of VEGF is chronically upregulated and aberrantly high since it is not only induced by hypoxia but also by oncogene activation (Carmeliet, 2005). Prolonged and imbalanced angiogenesis leads to the formation of abnormal blood vessels, which are tortuous and leaky and display erratic diameters with largely dilated segments. The leakiness is caused by oversized pores in the vessel wall formed by gaps in the endothelial barrier, low or lacking pericyte coverage and abnormal basement membranes. This allows plasma and erythrocytes to escape into the stroma. Microhaemorrhages (intratumoural blood lakes), haemoconcentration (increased concentration of cellular components in the blood) and increased interstitial pressure are the consequence (Baluk et al., 2005). The haemoconcentration, high interstitial pressure (by compression of vessels) and the heterogeneous spatial distribution of tumour blood vessels leads to a slow and irregular blood flow. The reduced tumour perfusion not only impairs access of immune effector cells to the tumour site (Jain, 2013) but also causes hypoxia and an accumulation of metabolic waste which leads to the release of more proangiogenic factors, creating a vicious cycle. Additionally, the endothelium of tumour blood vessels shows reduced expression of adhesion molecules in response to VEGF and bFGF stimulation (Griffioen et al., 1996). This further inhibits tumour immunity since the expression of adhesion molecules on endothelial cells is required for the extravasation of T cells and other immune effector cells. Reduced expression of adhesion molecules leads to reduced leukocyte-endothelium interaction, as well as reduced adherence and diapedesis (Dirkx et al., 2003; Schmidt et al., 1999; Wu et al., 1992). Consequently, the tumour vasculature forms a physical barrier to effector cell infiltration.

1.2. Cancer immunotherapy

The idea to treat cancer by directing and activating the immune system against tumours is not novel. About 110 years ago William Coley made the first attempts at cancer immunotherapy (CIT) by injecting streptococci into cancer patients with inoperable sarcoma. In over 10 % of the cases, this treatment led to tumour regression (Parish, 2003). Today, the injection of mycobacteria (Bacillus Calmette-Guerin) is still successfully being used for the treatment of superficial bladder cancer (Baselli and Greenberg, 2000). A lot has happened since then, especially in the last decades where several immunotherapeutics have been approved by the FDA as cancer therapies. Among them the most prominent is the use of monoclonal antibodies (mAb) directed against the immune-checkpoint inhibitors CTLA-4 (cytotoxic T-lymphocyte-associated protein 4) and PD-1 (programmed cell death protein 1), which enhance endogenous antitumour T cell responses (Pardoll, 2012; Sharma and Allison, 2015). With the advent of these two inhibitors, CIT established itself among the main pillars of cancer therapy: surgery, chemotherapy and radiotherapy. As described before, clinically detect-

able tumours are the ones that escaped immune surveillance and are either not immunogenic or have developed a tumour microenvironment which is not permissive for immune effector cells. Cancer immunotherapy aims to reverse the process of immunoediting by antagonizing immunosuppressive processes in the tumour microenvironment and potentiating antitumour immune responses. The various immunotherapeutic approaches include cytokine and interferon therapies (high-dose IL-2, IFN-α), TLR agonists (Imiquimod, Resiquimod), therapeutic mAb that are directed against targets expressed on tumour cells (Rituximab, Trastuzumab) or against immune checkpoint molecules (Ipilimumab, Nivolumab), cancer vaccines (recombinant viruses, bacteria, vector-DNA, peptides, whole tumour vaccines or DC based vaccines) and cellular immunotherapies such as the adoptive transfer of tumour-specific T cells (Kazemi et al., 2016).

1.2.1. Adoptive T cell therapy

The adoptive transfer of T cells is a cell-based immunotherapy. Here, tumour infiltrating lymphocytes (TILs) are isolated from resected tumours and expanded *ex vivo* in very high concentrations of IL-2. This generates a mixed population of T cells that can be tested *in vitro* for tumour recognition. Selection and further expansion of tumour-specific TIL cultures, is followed by reinjection into the patient (Rosenberg and Restifo, 2015; Rosenberg et al., 2008) (Figure 2). Initial studies in metastatic melanoma showed that the adoptive transfer of naturally occurring TILs led to objective tumour regression in metastatic melanoma patients with an overall response rate of 34 %, including some cases with complete response (Rosenberg et al., 1994). This treatment was combined with systemic high dose IL-2, which supports TIL survival and promotes TIL expansion *in vivo* (Rosenberg et al., 1988). The treatment effects observed in these early studies could be further improved by lymphodepletion prior to cell transfer. Nonmyeloablative chemotherapy with or without total body irradiation (2 or 12 Gy (gray) TBI) improved the persistence of transferred T cells from days to months, which can be explained by the fact that transferred cells do not need to compete with host T cells for homeostatic cytokines like IL-7 and IL-15 (Wu et al., 2012). Furthermore, the duration and incidence of clinical responses was strongly increased. Combining nonmyeloablative chemotherapy and 12 Gy TBI as a preparative regimen for adoptive T cell transfer in metastatic melanoma showed the best response rate with complete and durable responses of around 20 % (Dudley, 2011; Rosenberg et al., 2011). However, due to the high toxicity, this pre-conditioning regimen is not widely applied.

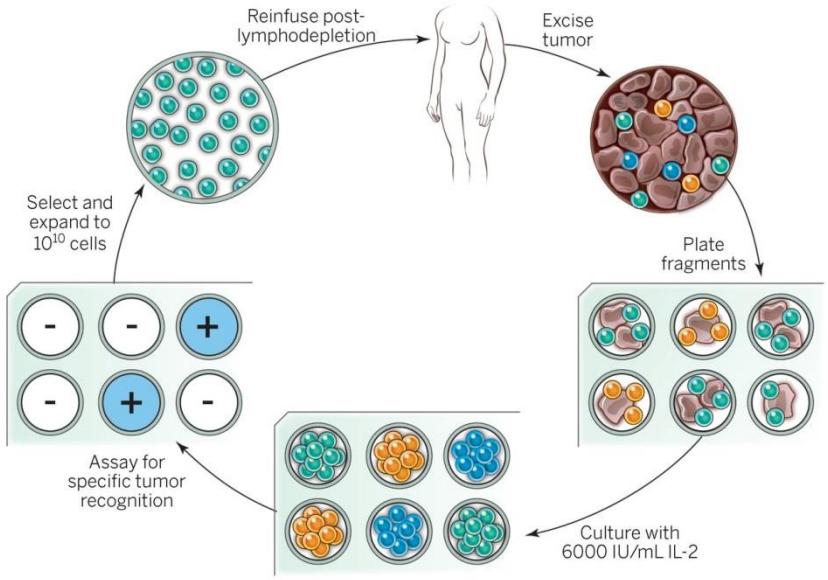

Figure 2 Adoptive T cell therapy using autologous TILs in melanoma.
Following tumour excision, the melanoma sample is divided into fragments which are cultured individually with with 6000 IU/ml IL-2. After 2-3 weeks, the tumour cells are destroyed and the pure lymphocyte cultures can be assayed for tumour reactivity. Only cultures that display high antitumour reactivity are rapidly expanded for 3 weeks producing up to 10^{11} lymphocytes that are reinjected into the lymphodepleted cancer patient. This figure is taken from (Rosenberg and Restifo, 2015).

TIL isolation and expansion from other cancer entities, though successful, rarely resulted in specific antitumour immune responses, since the TILs did not display antigen-specificity and did not specifically lyse autologous tumour cells (Yannelli et al., 1996). In order to overcome this obstacle and achieve application across other tumour entities, T cells, isolated from peripheral blood of cancer patients, were genetically engineered to express T cell receptors (TCR), that display high affinity for tumour antigens, or to express chimeric antigen receptors (CARs). CARs are recombinant proteins spanning the cell membrane with an extracellular antibody-derived single variable fragment for antigen recognition and an intracellular TCR-derived signalling chain optionally modified with co-stimulatory domains (Dai et al., 2016). CARs enable the recognition of a wide range of unprocessed antigens which is independent of MHC restriction. The antibody variable fragment detects 3-dimensional structures, including proteins and carbohydrates. Genetic modification of T cells for adoptive transfer allowed the expansion of the treatment to tumour entities other than melanoma: clinical responses were observed in colorectal cancer, multiple myeloma and synovial sarcoma trials with genetically engineered TCR T cells, but also in studies testing CAR therapies in leukaemia and lymphoma, as well as in colorectal and prostate cancer (Houot et al., 2015; Kershaw et al., 2013; Rosenberg and Restifo, 2015).
Overall, these clinical studies showed impressive responses in some patients, however complete clinical responses were found only in a subset of patients after adoptive T cell therapy (Lanitis et al., 2015; Melero et al., 2014). The limited success of adoptive T cell transfers in non-responders could be explained by therapy-induced immunoediting, functional suppression or restricted access of the transferred cells to the tumour site. Therapy-induced immu-

noediting leads to the development of resistances to the treatment by the tumours (Holzel et al., 2013). Functional suppression or restricted access to the tumour site is mediated by an immunosuppressive tumour microenvironment, which is able to inhibit the functionality of the transferred T cells by providing “off signals” to T cells, or to prevent T cell infiltration due to an immunosuppressive chemokine milieu and an abnormal tumour vasculature (Lanitis et al., 2015; Wu et al., 2012).

1.3. Radiotherapy

In cancerous diseases radiotherapy (RT) is one of the most common treatments. It is based on the fact that ionizing radiation induces cell death in rapidly dividing cells and therefore primarily targets cancer cells. Direct damage caused by ionization of cellular macromolecules such as DNA, proteins and lipids is rare. The indirect, but more common way of radiation-induced damage is by hydrolysis (radiolysis) of water (and other molecules) which leads to the formation of reactive oxygen and nitrogen species. The free radicals oxidize structural and functional proteins leading to impaired integrity of the cell membrane and impaired function of enzymes and cell cycle regulators (Corre et al., 2010; Daly, 2012; Mishra, 2004). Oxidation of DNA can induce double- and single-strand breaks (Desouky et al., 2015). The DNA breaks are sensed within seconds after the damaging event and initiate the DNA-damage response (DDR) pathway resulting either in apoptosis or enforced cell cycle arrest (Ciccia and Elledge, 2010). Cell cycle arrest provides time for damage assessment and DNA repair. p53 plays a major role in the DDR by directly activating DNA repair mechanisms and regulators of cell-cycle, apoptosis or senescence depending on the extent of DNA damage (Ciccia and Elledge, 2010; Lauber et al., 2012). Other mechanisms induced by DDR include the activation of immune surveillance (Ciccia and Elledge, 2010). The effects of RT are not restricted to tumour cells, however. Ionizing radiation also affects untransformed cells within the tumour microenvironment, like the cells of the immune system. Although, RT has initially been described to be immunosuppressive (Cole, 1986; James et al., 1989; Wasserman et al., 1989), today many reports describe its immunostimulatory effects. One of the major side effects in RT-treated patients is radiation-induced inflammation (Schaue et al., 2015). Moreover, the local (bystander effect) and distant (abscopal effect) out of field effects were found to be mediated by systemic antitumour immune responses (Demaria et al., 2004; Ehlers and Fridman, 1973; Ohba et al., 1998; Wersall et al., 2006).

As part of the RT-induced DDR pathway, NF-κB signalling is activated (Wu and Miyamoto, 2007), which leads to the expression of proinflammatory cytokines such as IL-1α, IL-1β, IL-6 and TNF-α (Weichselbaum et al., 2012). Tumour endothelial cells have been shown to respond to these cytokines by upregulation of cell adhesion molecules in the context of RT. This in turn promotes leukocyte extravasation and infiltration of the tumour, leading to RT-mediated antitumour immunity (Hallahan et al., 1996; Handschel et al., 1999). In addition, radiation/ROS-induced cellular stress leads to immunogenic cell death which is characterized

by the exposure of danger signals that activate innate immune cells such as macrophages in the tumour microenvironment (Barker et al., 2015). Danger signals associated with irradiated cells include calreticulin, a chaperone from the endoplasmic reticulum (ER), which is exposed on the cell surface of dying cells due to ER stress; HMGB1 (high-mobility group box 1), a chromatin protein that is passively released from dying cells (Apetoh et al., 2007); HSP70 (heat shock protein 70), a chaperone and member of the stress-induced heat shock proteins; as well as nucleotides such as adenosine and uridine triphosphate (ATP, UTP), which are actively secreted by dying cells (Bezu et al., 2015; Derer et al., 2016; Frey et al., 2014). The nucleotides act as chemoattractants for antigen presenting cells (APCs)(Elliott et al., 2009) and induce proinflammatory responses like phagocytosis, chemotaxis and the production of IL-1β (Di Virgilio et al., 1996; Weisman et al., 1998). HMGB1 is detected by TLR4 and HSP70 binds to TLR2/4 on APCs, while both induce the upregulation of co-stimulatory molecules and the secretion of proinflammatory chemokines and cytokines (Asea, 2008; Klune et al., 2008). Binding of calreticulin to lipoprotein receptor-related protein 1 (LRP1) promotes antigen uptake by APCs (Bezu et al., 2015; Vandenberk et al., 2015). Together, the interplay of cytokines, chemokines, and co-stimulatory molecules triggers an adaptive immune response. Since RT provides tumour antigen presentation and co-stimulatory signalling at the same time, it has been referred to as an *in situ* antitumour vaccine (Demaria et al., 2014). In RT-induced immune responses, danger signals trigger IFN responses in APCs, which are characterized by type I IFN production, thereby forming an additional link between the innate and adaptive immune response (Deng et al.). Besides type I, also type II IFNs are induced by RT and together they enhance the cytolytic activity of CTLs (Lim et al., 2014). Through IFNs and chemokines, such as CXCL9 and CXCL10, as well as CXCL16, RT further promotes the recruitment of circulating immune cells as demonstrated by the enhanced T cell infiltration in various tumour mouse models (Draghiciu et al., 2014; Lim et al., 2014; Lugade et al., 2005). In tumour cells, radiation enhances the presentation of TAAs by an increased protein translation rate and by increased surface expression of MHC class I molecules, induced by type I and type II IFNs, as well as TNF-α. Increased TAA presentation enables tumour cell recognition by CTLs (Barker et al., 2015; Kalbasi et al., 2013; Soukup and Wang, 2015). Upregulation of death receptors by tumour cells, in response to RT, further exposes them to T cell-mediated elimination (Chakraborty et al., 2003; Chakraborty et al., 2004).

In contrast to the large amount of data supporting proinflammatory effects of RT, some reports show that RT can also promote immune suppression: increased numbers of intratumoural T_{reg} were observed in a preclinical setting after high doses of irradiation (Schaue et al., 2012), as well as in colorectal and oesophageal cancer after radio-chemotherapy (Schaue et al., 2008; Vacchelli et al., 2015), which might be caused by a higher radioresistance displayed by T_{reg}. Following high dose irradiation also an increase in PD-L1 expression was observed on immune cells isolated from tumours of a mouse transplantation model (Deng et al.). Conversely, irradiation doses <1 Gy are commonly described to be immunosuppressive. Due to their anti-inflammatory and analgesic effects, these very low irradiation doses are used for the treatment of inflammatory diseases (Leroi et al., 2016). These data suggest a

window of radiation doses between 2 and 14 Gy that induce immunostimulatory rather than immunosuppressive effects.

As a consequence of the nonspecific working mechanism of RT, one also has to consider RT-induced modulation of other tumour microenvironment components such as fibroblasts and vascular cells. The majority of studies analysing the influence of RT on the tumour microenvironment report effects in favour of tumour resistance and disease recurrence (Barker et al., 2015). In several studies (Baker and Krochak, 1989; Langley et al., 1997; Paris et al., 2001), it was demonstrated that conventional radiotherapy doses (>8 Gy) do not only kill tumour cells, but also induce apoptosis in endothelial cells thereby reducing blood vessel density and aggravating the hypoxic conditions within the tumour. Hypoxia leads to the activation of HIF-1 (Hypoxia-inducible factor 1), which is followed by increased levels of SDF-1 (stromal cell-derived factor 1; CXCL12) which cause the recruitment of $CD11b^+$ myeloid cells and endothelial progenitor cells to the tumour site. The $CD11b^+$ myeloid cells can either differentiate into macrophages or into endothelial cells which, together with the endothelial progenitor cells, reconstruct the tumour vasculature by *de novo* vessel formation (vasculogenesis). It has been demonstrated that this process promotes tumour recurrence and leads to the development of radioresistance (Brown, 2014; Leroi et al., 2016; Russell and Brown, 2013). On the other hand, RT has been described to cause vascular normalization. Increased secretion of the antiangiogenic factors CXCL9 and CXCL10, in response to RT, promotes the remodelling of vessels and induces the expression of VCAM-1 (Ganss et al., 2002), as well as the infiltration of T cells and tumour regression.

RT has effects on the tumour microenvironment that can support but also inhibit tumour growth. Even though the heterogeneity of study procedures (applied RT doses and fractionation, as well as distinct tumour entities) complicates the interpretation of the study results, regarding RT-induced effects on the tumour microenvironment, the majority of studies report that RT induces immunostimulatory environments. Still, RT is not suitable to induce long-lasting immune response and tumour elimination due to therapy-induced resistance and cancer immunoediting. It has therefore been suggested to combine RT with CIT to take advantage of the inhibitory, but to prevent the stimulatory effects of RT on tumour growth and recurrence (Burnette and Weichselbaum, 2013; Derer et al., 2016; Frey et al., 2014; Kalbasi et al., 2013; Kershaw et al., 2013; Kwilas et al., 2012; Soukup and Wang, 2015).

1.4. RIP1-TAg5 tumour mouse model and previous work

Cancer immunotherapy, in particular adoptive transfer of tumour-specific T cells, has been shown to result in complete clinical responses in only a minority of patients. Radiotherapy has been shown to induce an initial but not long-lasting immune response. Therefore, the combination of CIT and RT has been proposed to achieve enhanced clinical response rates. In our group, the RIP1-TAg5 (RT5) tumour mouse model was used to study the effects of local

low dose irradiation in combination with adoptive T cell transfer on tumour progression. The RT5 mouse model is a genetically engineered mouse model of spontaneous and autochthonous tumour growth. It was selected, as it very closely reflects the clinical situation of human tumour growth. In contrast to transplantation models, which tend to grow fast, are usually not orthotopically implanted and do not undergo the multistep process of tumourigenesis with the simultaneous development of a tumour microenvironment, mouse models with spontaneous tumours more closely resemble slower growing human tumours. Moreover, the study of cancer therapies in transplantation models has been suspected to be one cause of the increase in clinical trial failures, as treatment is frequently initiated at low tumour burdens or even simultaneously with tumour inoculation (Budhu et al., 2014; Denayer et al., 2014; Fox et al., 2011; Talmadge et al., 2007). This is in contrast to the clinical setting where, at the time of diagnosis and treatment decision, cancers are fully established or even metastasized, representing a condition where they have already escaped immune surveillance mechanisms.

RT5 mice are transgenic for the hybrid RIP1-TAg gene. Expression of the oncogene *SV40TAg* (Simian Virus 40 large T-Antigen) starts at 10-12 weeks of age controlled by the rat insulin promotor-1 (RIP1) and is therefore restricted to β-cells in pancreatic islets. The oncoprotein SV40TAg binds to and inhibits the tumour suppressors p53 and Rb (retinoblastoma protein), thereby inducing β-cell transformation and hyperproliferation (Ahuja et al., 2005; Casanovas et al., 2005). In the early hyperplastic islets, before tumour formation, VEGF-mediated angiogenesis leads to the formation of angiogenic islets that progress to invasive, insulin-producing pancreatic islet carcinomas by 18-20 weeks. These insulinomas are highly vascularized and display an abnormal vasculature which is characterized by an increased vessel density and heterogeneity, as well as irregular vessel diameters and increased leakiness of the tumour vessels. The leaky vessels lead to the formation of intratumoural haemorrhages, which are caused by extravascular erythrocytes (Ryschich et al., 2002). Due to the delayed onset of oncogene expression, SV40TAg is not recognized as 'self' by the immune system (Adams et al., 1987). Consequently, its expression elicits an immune response against the transformed cells (Grant et al., 1990), which is followed by the infiltration of B cells, macrophages and TAg-specific cytotoxic ($CD8^+$) and helper ($CD4^+$) T cells into premalignant hyperplastic islets (Förster et al., 1995; Skowronski et al., 1990). However, antitumour immunity does not lead to complete elimination of the tumour causing some hyperplastic islets to progress to insulin-secreting carcinomas. If left untreated RT5 mice die from hypoglycaemia at 30-35 weeks of age (Ganss and Hanahan, 1998). Of note, in the fully established tumours no infiltrating lymphocytes were observed indicating that the tumours evade the immune system by restricting the access of T cells. It has been shown that the angiogenic switch correlates with reduced leucocyte adhesion (Ryschich et al., 2002), suggesting that the aberrant vasculature forms a barrier for immune effector cell infiltration and thereby promotes a non-permissive tumour microenvironment that allows these tumours to escape immune surveillance. The RT5 mouse model is therefore a suitable model to study the interactions between the immune system and cancer progression, as well as cancer therapies that target the tu-

mour microenvironment, besides the tumour cells, since it resembles human tumours with regard to the abnormal tumour vasculature and tumour immune escape.

The RT5 model was previously used to study adoptive T cell transfers (Ganss et al., 2002; Garbi et al., 2004; Klug et al., 2013; Sektioglu et al., 2016). However, these studies showed that the transfer of *in vitro*-activated tumour-specific T cells alone is unable to reject established tumours. Combined with irradiation or systemic application of CpG (cytosine-phosphorothioate-guanine), a TLR9 agonist, the same treatment could overcome the tumours' resistance of immune elimination. In our group it was found that the combination of adoptive T cell transfer with local low dose irradiation led to a massive infiltration of T cells into the tumours and long-term survival. A dose of 2 Gy was identified as most beneficial, as it induced the highest intratumoural CTL/T_{reg} ratio (Klug et al., 2013). Both, the T cell infiltration and the prolonged survival, were dependent on macrophages as their depletion attenuated the treatment effects. This was further supported by macrophage transfer experiments, where peritoneal exudate cells from irradiated syngeneic wt mice were transferred into otherwise untreated 24-week old RT5 mice. In combination with adoptive T cell transfer this also led to increased numbers of intratumoural $CD11b^+$ cells and T cells. It was further shown that the treatment-induced T cell infiltration was dependent on the activity of the inducible nitric oxide synthase (iNOS), which was expressed by intratumoural $CD11b^+$ cells (Klug et al., 2013).

1.5. Aim of the study

A major challenge in cancer immunology is the development of new strategies to overcome tumour immune evasion and therapeutic resistance, the two main factors which limit the efficacy of cancer immunotherapies (CIT). The combination of CIT with specific treatment modalities that alter the tumour suppressive environment offers a promising approach to address these challenges. Radiation therapy has been shown to enhance the effects of CIT (Burnette and Weichselbaum, 2013). In our group, low dose irradiation was therefore combined with the adoptive transfer of tumour-specific T cells in the treatment of RT5 tumours. The resulting increase in tumour infiltration of T cells turned out to be dependent on the activity of iNOS and macrophages, but the precise mechanism of T cell infiltration and the exact role of the macrophages and iNOS remain unclear.

This thesis aims to investigate the therapeutic effects of low dose irradiation and adoptive T cell transfer and to elucidate the underlying molecular mechanisms.

In the first part, the effects of low dose irradiation (LDI) and adoptive T cell therapy on tumour regression and the tumour microenvironment will be investigated. In order to identify the cellular and molecular mechanisms, which lead to the increased T cell infiltration after combination therapy, the status of the tumour vasculature will be evaluated and the intratumoural myeloid cell populations will be characterized. Furthermore, the influence of macrophage depletion on tumour regression and survival in untreated mice will be examined.

The second part will present a detailed analysis of the mediators of the therapeutic effects, namely, the peritoneal cells that were used for the transfer experiments. First, the distribution of the transferred cells in RT5 mice will be assessed, to identify possible site-specific accumulations. Next, the effects of LDI on global gene expression alterations in peritoneal cells will be investigated to explore LDI-induced functional changes. Finally, a characterization of the polarization state of peritoneal macrophages will provide information on the specific macrophage phenotype that is stimulated by LDI.

2. RESULTS

Studies in spontaneous and xenograft tumour mouse models demonstrate that adoptive T cell therapy alone is insufficient to cause full rejection of established tumours, while the combination of T cell transfer with irradiation (Ganss et al., 2002; Klug et al., 2013) or immunostimulatory agents, such as CpG (Garbi et al., 2004; Sektioglu et al., 2016), can cure mice from established tumours. Combined local LDI (2 Gy) and CD8 T cell transfer was shown to induce massive T cell infiltration in solid tumours, resulting in long-term survival. These effects were dependent on macrophages and the activity of iNOS (Klug et al., 2013). However, the precise mechanism underlying increased T cell infiltration is not fully understood. Therefore, the aim of this study is to investigate the molecular mechanisms that drive the tumour modifications, which lead to a more permissive environment for increased T cell infiltration.

2.1. Tumour-suppressive effects of LDI and adoptive T cell transfer

For a detailed investigation of the effects of LDI in combination with adoptive T cell transfer on the tumour microenvironment, RT5 mice were treated as previously described (Klug et al., 2013). Briefly, 24-week old RT5 mice were irradiated locally with a single dose of 2 Gy. After 10 days, they received $5x10^6$ *in vitro*-activated tumour-specific $CD8^+$ T cells from TCR transgenic (TCRtg) TCR8 mice. On day 17, the tumours were excised for analysis (Figure 3 A). iNOS was described to be necessary for T cell infiltration after combination therapy. To investigate how iNOS facilitates T cell infiltration and to assess the influence of iNOS on the tumour microenvironment, in connection with the treatment effects, the enzyme was selectively inhibited with the iNOS inhibitor 1400w. Systemic iNOS inhibition was achieved by subcutaneously implanting an osmotic pump, containing 1400w, one day before local LDI. The inhibitor was slowly released from the pump over 2 weeks. Since the treatment effects of local LDI and adoptive T cell transfer were demonstrated to be dependent on macrophages, their role was examined more closely by performing macrophage transfer experiments. Here, unirradiated RT5 mice received thioglycolate-elicited peritoneal exudate cells (PECs) from C3HeB/Fe (C3H) wt mice that had been subjected to 2 Gy total body irradiation, instead of local LDI. On day 10, the RT5 mice also received tumour-specific $CD8^+$ T cells and tumours were excised for analysis one week later (Figure 3 B).

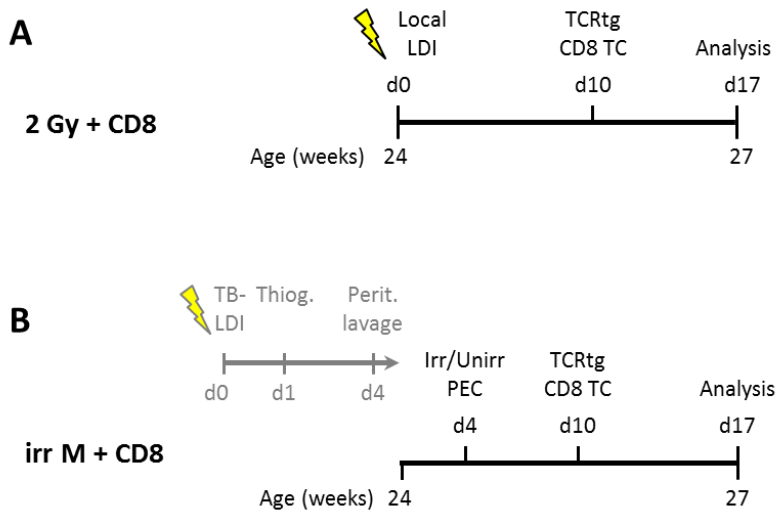

Figure 3 Schematic representation of experimental design
Tumour development in RT5 mice after adoptive T cell transfer of *in vitro*-activated TCRtg $CD8^+$ T cells combined either with local LDI (A) or with adoptive transfer of irradiated PECs (B). A) 2 Gy + CD8: the pancreatic region of 24-week old RT5 mice was irradiated locally with a single dose of 2 Gy, followed by adoptive transfer of $5x10^6$ $CD8^+$ T cells 10 days later. On day 17, the tumours were excised and analysed. B) irr M + CD8: 24-week old RT5 mice received $5x10^6$ thioglycolate-elicited peritoneal cells from C3H wt mice, that were subjected to 2 Gy TBI. This was followed by adoptive transfer of $5x10^6$ $CD8^+$ T cells 6 days later. On day 17 the tumours were excised and analysed. (irradiated (irr) unirradiated (unirr)).

2.1.1. Composition of peritoneal exudate cells

Thioglycolate is widely used to elicit naïve tissue resident macrophages in the peritoneum for macrophage research (Gallily et al., 1964). More recent studies demonstrated that thioglycolate elicits multiple populations of leukocytes in the peritoneal cavity (Ghosn et al., 2010; Schleicher et al., 2005). To ascertain the composition of the thioglycolate-elicited PECs from irradiated and unirradiated C3H wt mice, the cells were analysed by flow cytometry. The results show that 60-80 % of the freshly isolated PECs are macrophages ($CD11b^{hi}$ $F4/80^+$). It further shows minute numbers of T cells in the exudate; less than 1 % of the PECs are positive for $CD3^+$. Between 5.8 and 10.5 % of the cells are positive for CD11c, indicating the presence of dendritic cells. Also $Gr\text{-}1^+$ cells were observed; 7 % in the PECs from unirradiated mice and 20.3 % in the PECs from irradiated mice (Figure 4). The results demonstrate that a high percentage of the freshly isolated PECs are macrophages, however it has to be taken into account that the contaminating cell populations also affect the studied processes.

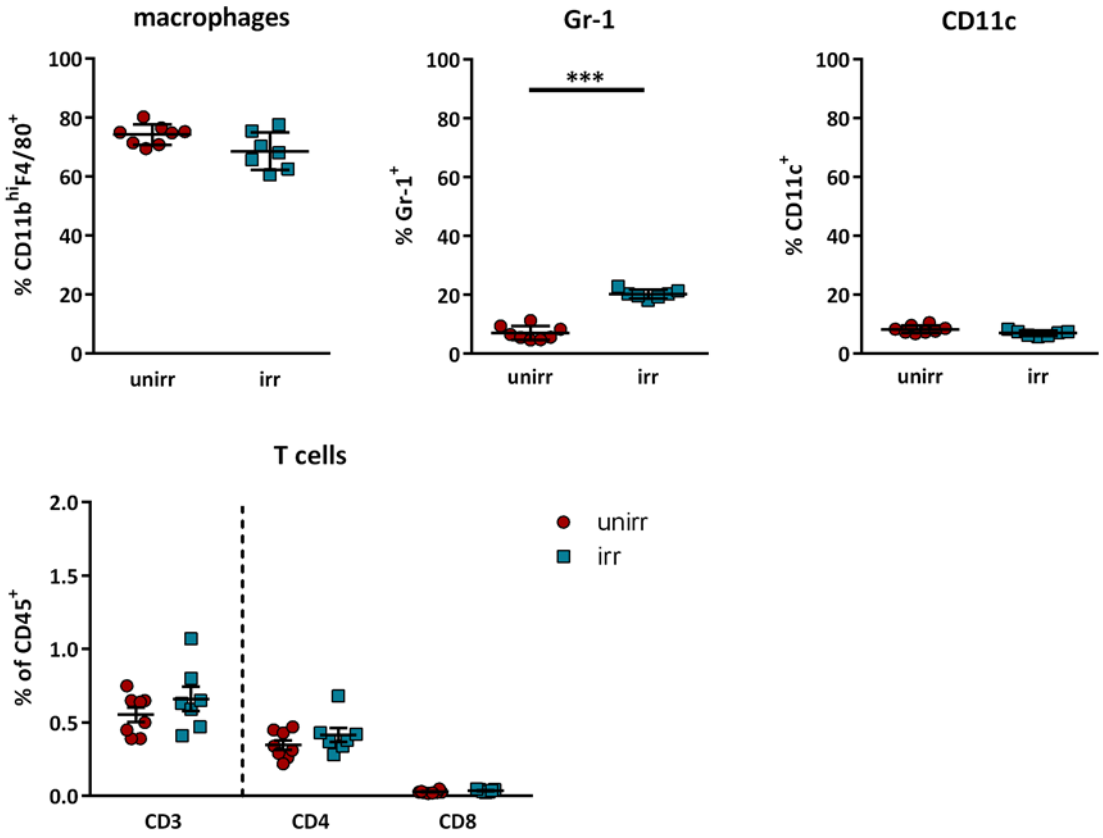

Figure 4 Immune cell composition of PECs after *in vivo* irradiation
Flow cytometric analysis of thioglycolate-elicited PECs from unirradiated C3H wt mice or C3H wt mice subjected to 2 Gy TBI. Shown are the percentages of macrophages ($CD11b^{hi}$ $F4/80^{+}$), $CD11c^{+}$, $Gr\text{-}1^{+}$ cells and T cells. Only single, viable cells were included in the analysis. Data shown as mean ± SEM (n=8 mice per group; two-tailed Mann-Whitney test).

2.1.2. *in vitro* activation of TCRtg T cells

For adoptive T cell transfer, splenocytes from TCRtg TCR8 mice were cultured with IL-2 and SV40TAg peptide for 72 hrs, to activate and expand the $CD8^{+}$ T cells. $5x10^{6}$ activated tumour-specific T cells were subsequently injected into RT5 mice. The activation state of the T cells was confirmed by detection of IFN-γ production using flow cytometry. IFN-γ secretion was assessed in T cells stimulated with IL-2, SV40TAg peptide, or a combination of both. As a control, splenocytes were cultured in medium only. This experiment was carried out by L. Nögel and was published in his master thesis. Activation with IL-2 and the SV40TAg peptide or the peptide alone resulted in increased IFN-γ secretion by 50 % of the T cell population, while less than 10 % of the T cells showed an increased IFN-γ secretion upon stimulation with IL-2 alone. IFN-γ secretion was not detected in unstimulated control T cells (Figure 5). These results indicate that the $CD8^{+}$ T cells that were used for transfer into RT5 mice are highly activated.

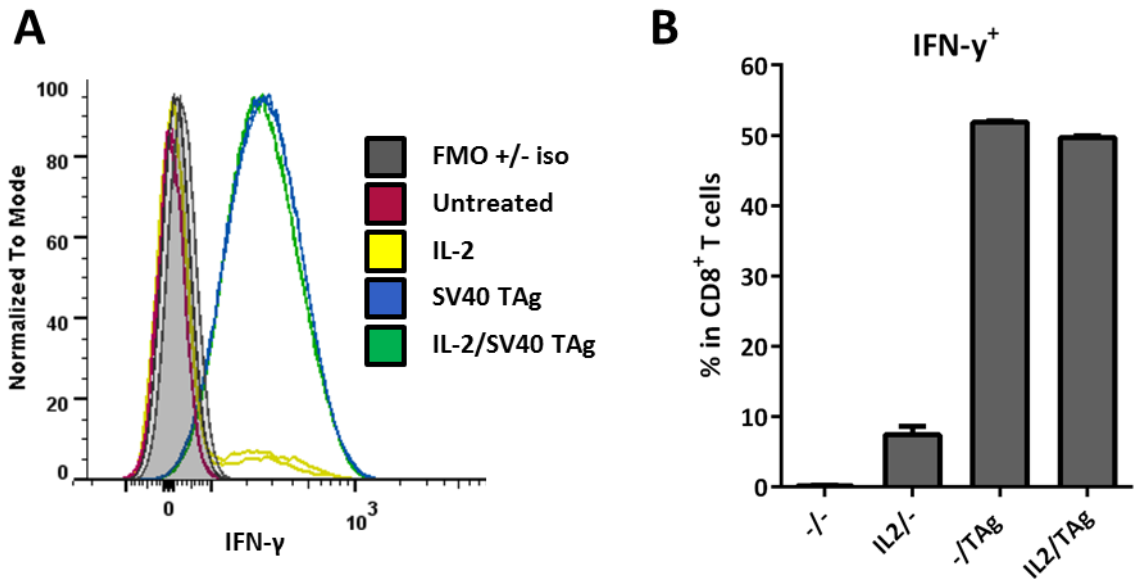

Figure 5 Increased IFN-γ production by CD8$^+$ T cells upon antigen-specific activation *in vitro*
Splenocytes from TCR8 mice were activated *in vitro* with IL-2, SV40TAg peptide or IL-2 and SV40TAg peptide. Control cells were cultured in medium only. After 72 hrs in culture, IFN-γ secretion of CD8$^+$ T cells was analysed by flow cytometry. Only single, viable, CD11c$^-$, CD3$^+$ cells were included in the analysis. A) Histogram showing the level of IFN-γ secretion by CD8$^+$ T cells after stimulation. B) Quantification of IFN-γ$^+$ T cells. Data shown as mean + SEM (n=2). The experiment was performed by L. Nögel, figure published in L. Nögel`s master thesis.

2.1.3. The combination of LDI and adoptive T cell transfer leads to tumour immune rejection

Local LDI combined with adoptive T cell transfer led to long-term survival in RT5 mice (Klug et al., 2013). This suggests that the treatment causes tumour regression. To test if the combination therapy affects tumour development, RT5 tumours were excised and inspected macroscopically. Insulinomas from untreated RT5 mice appear dark red with a granular surface. In contrast, tumours from RT5 mice treated with local LDI and CD8 T cell transfer, as well as the tumours treated with irradiated PECs and CD8 T cell transfer, are smaller in size and milky white with a smooth even surface (Figure 6 A).
The dark red appearance of the untreated tumours is caused by haemorrhages resulting from leaky tumour blood vessels, a characteristic of an abnormal tumour vasculature (Jain, 2013). Therefore, tumour haemorrhages are an indicator of an abnormal tumour vasculature. Relative quantification of non-haemorrhagic tumours between treated and untreated mice reveals a significant increase of non-haemorrhagic tumours in treated mice (Figure 6 B), suggesting a normalization of the aberrant tumour vasculature after combination therapy. Tumour diameters ranged between 1.0 and 2.8 mm in mice treated with local LDI or transfer of irradiated PECs combined with CD8 T cell transfer, displaying a more than 2-fold size reduction compared to tumour diameters of 1.7 to 8.3 mm in untreated RT5 mice. Interestingly, iNOS inhibition in mice treated with local LDI and tumour-specific T cells suppressed the treatment-specific effect on tumour size (Figure 6 C).

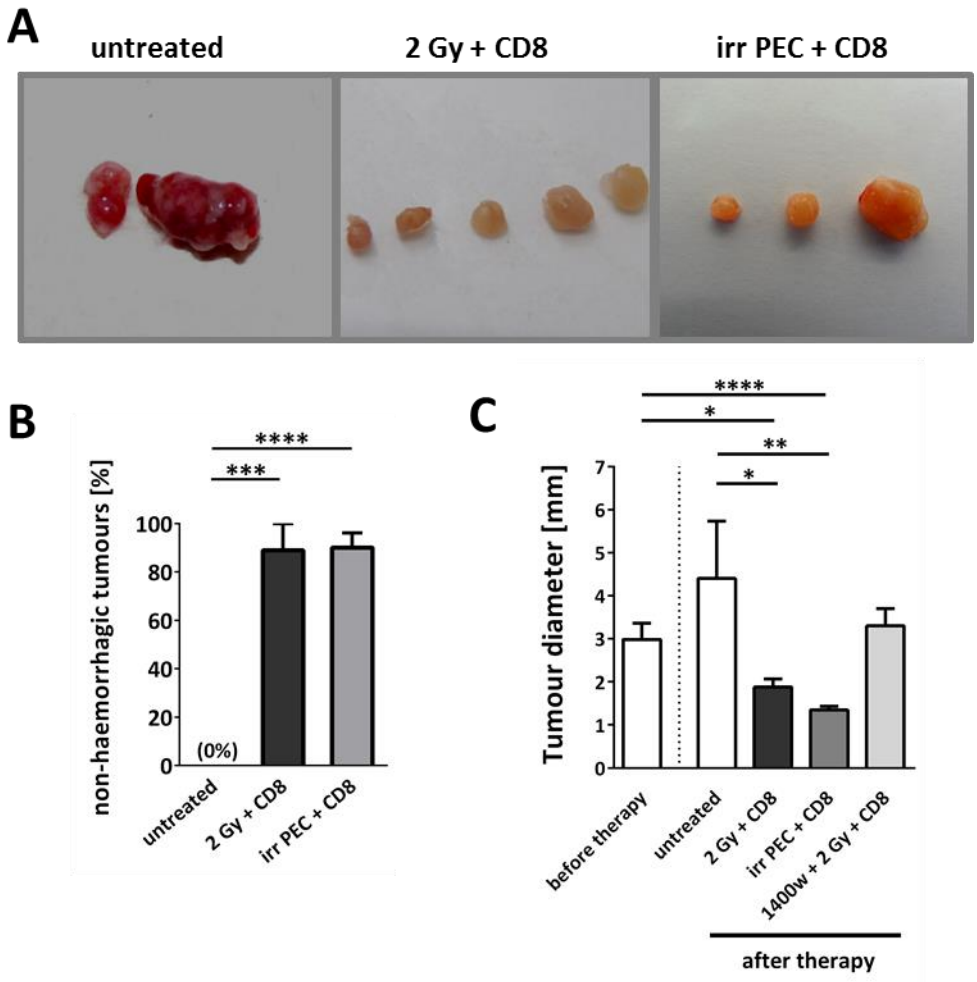

Figure 6 The impact of combined LDI and adoptive T cell transfer on tumour size and phenotype in RT5 mice
A) Representative RT5 tumours from untreated mice, mice treated with local LDI (2 Gy) and $CD8^+$ T cells or with irradiated PECs and $CD8^+$ T cells. B) Percentage of non-haemorrhagic tumours in the different treatment groups. (n=3-4 mice per group). C) Tumour diameter before therapy (24-week old) or after therapy (27-week old) of untreated mice and of mice treated with local LDI (2 Gy) and $CD8^+$ T cells, with irradiated PECs and $CD8^+$ T cells or with local LDI (2 Gy), $CD8^+$ T cells and 1400w (iNOS inhibitor) (n=2-11 tumours per group, with 2-3 mice per group). Data is shown as mean + SEM; * $p<0.05$; ** $p<0.01$; *** $p<0.001$; **** $p<0.0001$ (unpaired two-tailed Student's t-test)

Taken together, these results confirm that the combination of local LDI and adoptive T cell transfer leads to the rejection of established tumours in an iNOS-dependent manner. They further suggest that the treatment leads to a normalization of the tumour vasculature.

2.2. Vessel normalization after combination therapy

2.2.1. Normalization of vessel morphology

In the previous section, it was shown that local LDI and T cell transfer induce changes in the macroscopic characteristics of the tumour, suggesting a normalization of the tumour vasculature after combination therapy. Abnormal tumour vasculature is characterised by uncontrolled and chaotic outgrowth of existing blood vessels, resulting in irregularly enlarged and tortuous blood vessels (Jain, 2013). To test whether the aberrant tumour vasculature of RT5 mice is affected by the treatment with local LDI and tumour-specific $CD8^+$ T cells, the tumour vessel morphology was analysed at a microscopic level. Tumour sections were stained for the endothelial cell marker CD31 and for SV40TAg, which labels tumour cells. Subsequently, the sections were evaluated by immunofluorescence (IF) microscopy. The IF microscopy images show that tumour vessels of untreated RT5 mice are enlarged and dilated. In contrast, the tumour vasculature of mice that received local LDI and $CD8^+$ T cells, is characterized by smaller and less dilated vessels (Figure 7 A). Quantitative analysis of the tumour sections revealed that the average vessel size is significantly decreased after combination therapy, as is the total vessel area (Figure 7 B).
Similar effects on the tumour vasculature were observed when adoptive T cell transfer was combined with the transfer of irradiated PECs instead of local LDI, as the average vessel size and total vessel area were significantly reduced. In mice in which iNOS activity was inhibited, the average vessel size remained unchanged after local LDI and CD8 T cell transfer. The total vessel area on the other hand was increased in comparison to mice with normal iNOS activity, but it was still lower than in the untreated group, suggesting that the changes in vessel morphology, induced by combination therapy, are not solely dependent on the activity of iNOS.

2.2.2. Endothelial activation caused by combination therapy is dependent on iNOS

In addition to abnormal morphological features, the aberrant tumour vasculature is further characterised by low expression levels of adhesion molecules thereby forming a barrier to lymphocyte infiltration (Griffioen, 2008). Normalization of aberrant tumour vasculature is accompanied by the activation of the endothelium, which is characterised by the upregulation of adhesion molecules such as VCAM-1 (vascular cell adhesion protein 1) and ICAM-1 (intercellular adhesion molecule 1)(Lanitis et al., 2015).

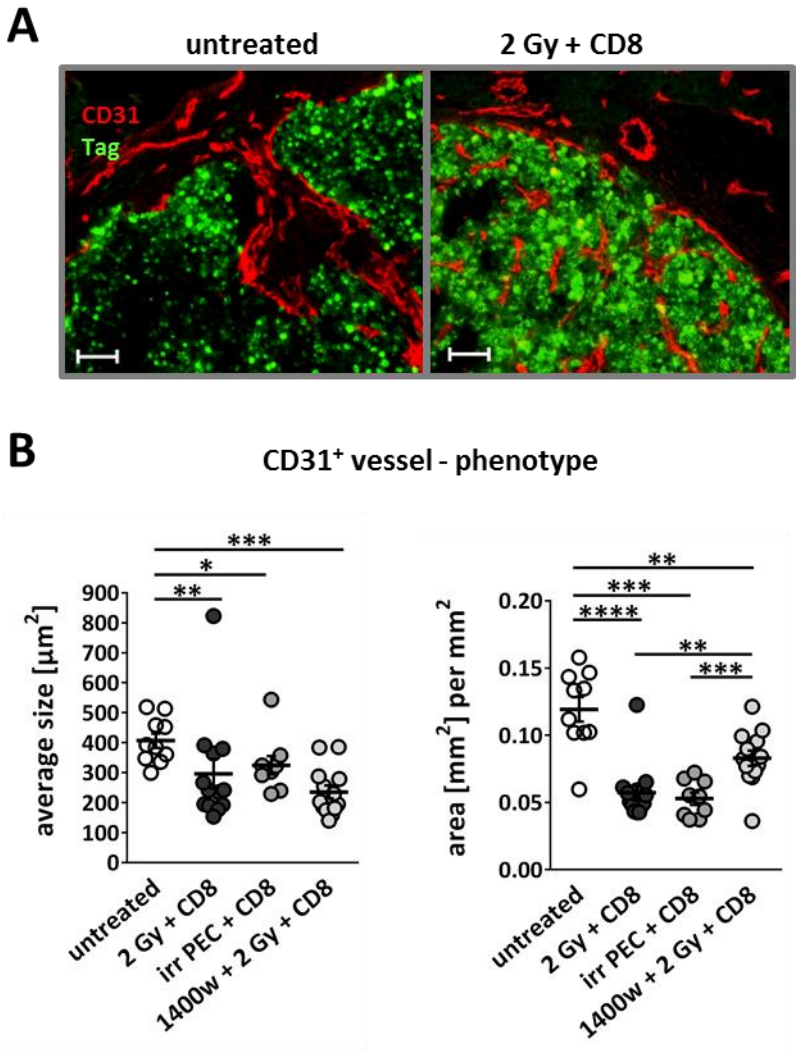

Figure 7 Normalized tumour vasculature after low dose irradiation combined with adoptive T cell transfer Morphological characteristics (average vessel size, total vessel area) of the tumour vasculature in untreated RT5 mice compared to mice treated with adoptive T cell transfer following local LDI or adoptive transfer of irradiated PECs. A) Representative IF microscopy images of RT5 tumours from untreated mice or mice treated with local LDI (2 Gy) and $CD8^+$ T cells, showing blood vessels in red (anti-CD31, marking endothelial cells) and tumour cells in green (anti-SV40TAg). Scale bar, 50 µm. B) Quantitative analysis of the tumour vasculature: average vessel size and $CD31^+$ area $[mm^2]/mm^2$ in RT5 mice treated with local LDI (2 Gy) and $CD8^+$ T cells, with irradiated PECs and $CD8^+$ T cells or with local LDI (2 Gy), $CD8^+$ T cells and 1400w (iNOS inhibitor). Data shown as mean ± SEM; * p<0.05; ** p<0.01; *** p<0.001; **** p<0.0001 (n=5-9 tumours per group of 3-5 mice; two-tailed Mann-Whitney test).

To assess if the tumour endothelium of RT5 mice was activated after combination therapy, tumour sections were stained for CD31 and VCAM-1 and analysed for endothelial cells that expressed VCAM-1. Tumour vessels in untreated RT5 mice show no or very low levels of VCAM-1 expression (Figure 8 A). Conversely, in mice treated with local LDI and adoptive T cell transfer, VCAM-1 expression on endothelial cells is strongly increased. An average of 47.1 % (range 17 to 73 %) of the $CD31^+$ area was positive for VCAM-1. When treated with irradiated PECs instead of local LDI, the level of colocalized VCAM-1 and CD31 expression in RT5 tumours even further increased to 81 % on average (range 65 to 92 %)(Figure 8 B). This

demonstrates that the transfer of irradiated PECs in combination with tumour-specific T cells has a greater effect on endothelial activation than local LDI and $CD8^+$ T cells. Interestingly, iNOS inhibition almost completely abrogates the effect of combination therapy on endothelial activation. VCAM-1 expression was greatly reduced with an average of 15 % colocalized area (Figure 8). Yet, the levels are not as low as in untreated tumours, suggesting that iNOS activity is not the only factor responsible for endothelial activity after combination therapy.

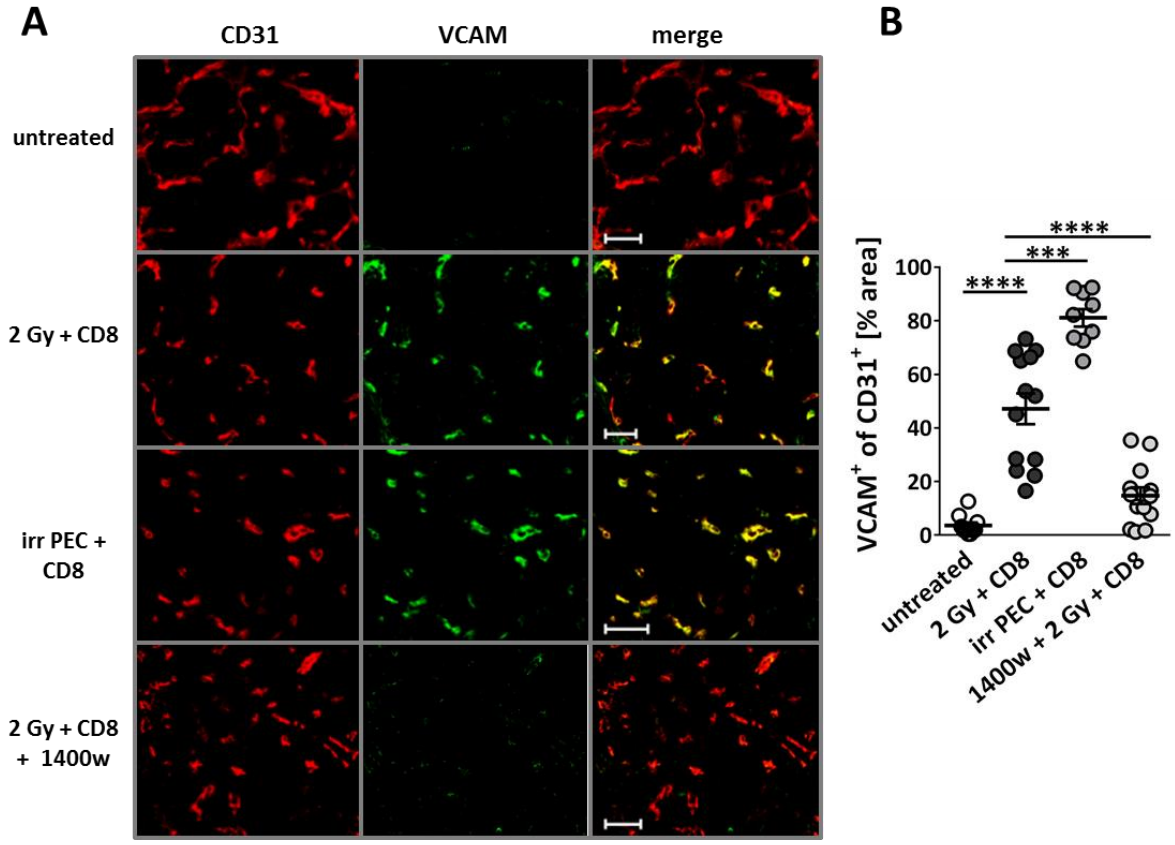

Figure 8 Endothelial activation in RT5 tumours after combination therapy
Adhesion molecule (VCAM-1) expression on tumour endothelial cells in untreated RT5 tumours compared to tumours after treatment with local LDI or adoptive transfer of irradiated PECs prior to adoptive T cell transfer, or local LDI combined with adoptive T cell transfer under iNOS inhibition. A) Representative IF images of RT5 tumour sections from untreated mice, mice treated with local LDI (2 Gy) and $CD8^+$ T cells, with irradiated PECs and $CD8^+$ T cells or with local LDI (2 Gy), $CD8^+$ T cells and 1400w (iNOS inhibitor), were immunolablelled with antibodies against CD31 (red) marking endothelial cells and VCAM-1 (green). The colocalized areas (yellow) show activated endothelium. Scale bar, 50 µm. B) Quantitative analysis of the $VCAM\text{-}1^+/CD31^+$ colocalized area for the indicated treatment groups. Data shown as mean ± SEM; *** $p<0.001$; **** $p<0.0001$ (n=9-13 tumours of 2 mice per group; two-tailed Mann-Whitney test).

Taken together, these results demonstrate that combination therapy leads to vessel normalization in RT5 tumours which is partly dependent on the enzymatic activity of iNOS. Since iNOS produces NO it can be hypothesized that NO might be one of the factors responsible for endothelial activation in this setting.

2.2.3. Direct endothelial activation by nitric oxide

In RT5 tumours we could show that the upregulation of adhesion molecules on endothelial cells is partly dependent on the activity of iNOS. However its product NO has been predominantly described to inhibit cytokine-induced expression of adhesion molecules. Khan et al. showed that the NO donor DETA-NO (=DETA NONOate) decreases ICAM-1 and VCAM-1 levels on HUVECs (human umbilical vein endothelial cells) at concentrations between 50 µM to 1000 µM. Of note, 10 µM induced a slight but not significant increase of VCAM-1 and ICAM-1 levels and lower concentrations of DETA-NO were not tested (Khan et al., 1996). We hypothesized that NO concentrations below 10 µM might have a different effect on endothelial cells. To investigate the effects of NO on endothelial activation, the expression of distinct adhesion molecules was assessed on HUVECs treated with DETA NONOate (in cooperation with I. Sektioglu). Therefore, HUVECs were incubated for 18 hrs with different concentrations (0.098 µM to 50 µM) of DETA NONOate and subsequently analysed by flow cytometry. Levels of VCAM-1 and ICAM-1 increased at a concentration of 0.195 µM, showing a peak at 3.125 µM. Increasing levels of E-selectin expression were observed at 0.781 µM of DETA NONOate, reaching a peak at 3.125 µM. Higher concentrations than 3.125 µM did not further increase the expression levels of the adhesion molecules. Interestingly, higher doses seemed to block adhesion molecule expression completely, as MFIs for VCAM-1, ICAM-1 and E-selecting were as low as in untreated HUVECs (Figure 9 A).

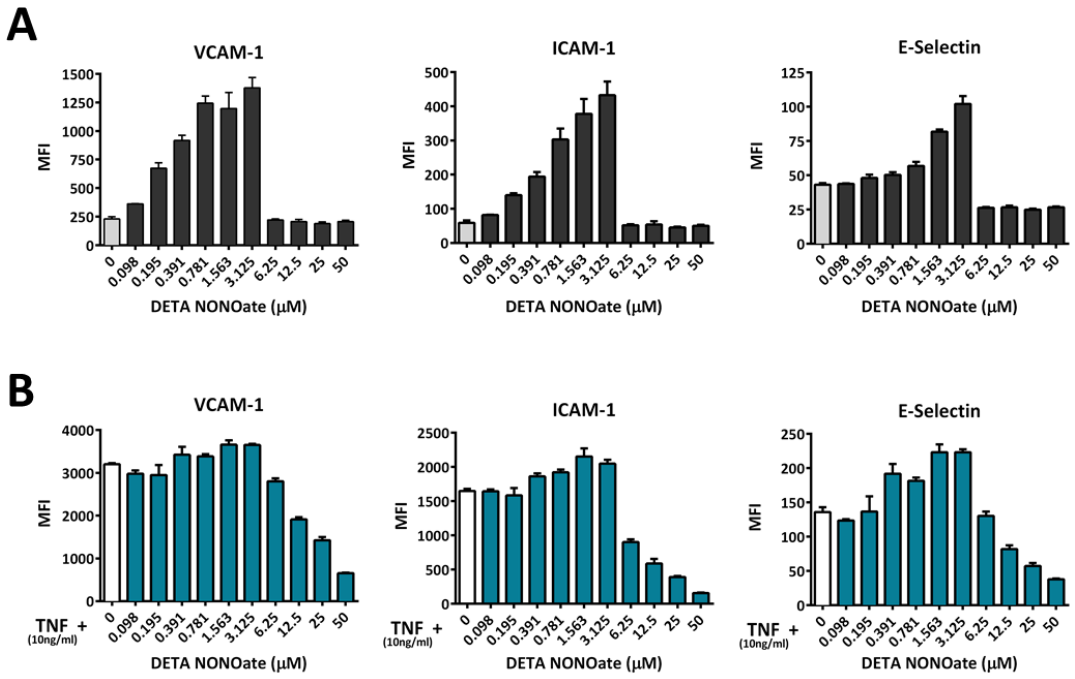

Figure 9 Dose-dependent induction of adhesion molecules on HUVECs stimulated with NO
Surface expression of adhesion molecules on HUVECs treated with the NO donor, DETA NONOate, with or without TNF-α. HUVECs were analysed by flow cytometry after 18 hrs culture with the indicated concentrations of A) DETA NONOate alone or B) DETA NONOate with 10 ng/ml TNF-α. Quantification of VCAM-1, ICAM-1 and E-Selectin surface expression (mean fluorescent intensity (MFI)) in $CD31^+$ single, viable HUVECs. Data is shown as mean + SEM of triplicate wells from two independent experiments. The experiment was performed in cooperation with I. Sektioglu.

A well described inducer of adhesion molecules on vascular endothelial cells is TNF-α (Bernot et al., 2005; Dhawan et al., 1997; Mattila et al., 1992; Xia et al., 1998). To test whether TNF-α and low concentrations of NO can synergistically enhance the expression levels of the selected adhesion molecules, HUVECs were treated with 10 ng/ml TNF-α and increasing concentrations of DETA NONOate (0.098 µM to 50 µM). TNF-α-induced expression levels of E-selectin and to a lesser extent ICAM-1 are further increased by low concentrations of DETA NONOate. Furthermore, we observed that concentrations of DETA NONOate, higher than 3.125 µM supress TNF-α induced expression of the three adhesion molecules (Figure 9 B). Together these findings show that low concentrations of NO are able to induce expression of the adhesion molecules VCAM-1, ICAM-1, and E-selectin in HUVECs, while high concentrations lead to a reduction of their expression, even when induced by TNF-α.

2.3. iNOS dependent macrophage infiltration induced by combination therapy

Previous work has demonstrated that local LDI in combination with CD8 T cell transfer leads to the infiltration of T cells into RT5 tumours, as well as to the infiltration of $CD11b^+$ cells, which are thought to migrate from the periphery into tumour tissue (Klug et al., 2013). However, the infiltration of macrophages can be reduced in large tumours (Zhang et al., 1997), suggesting that the tumour size can affect the infiltration of macrophages. To analyse whether infiltration of $CD11b^+$ cells is reduced in larger tumours, the number of intratumoural $CD11b^+$ cells was analysed with respect to the size of the corresponding tumour. In untreated RT5 mice, as well as in RT5 mice treated with local LDI and tumour-specific T cells, the number of intratumoural $CD11b^+$ cells negatively correlates with tumour size (Figure 10 A). Of note, mice receiving the combination therapy depict a higher absolute number of intratumoural $CD11b^+$ cells, irrespective of the cell/size ratio, confirming that local LDI combined with tumour-specific CD8 T cell transfer leads to the infiltration of $CD11b^+$ cells regardless of the tumour size.

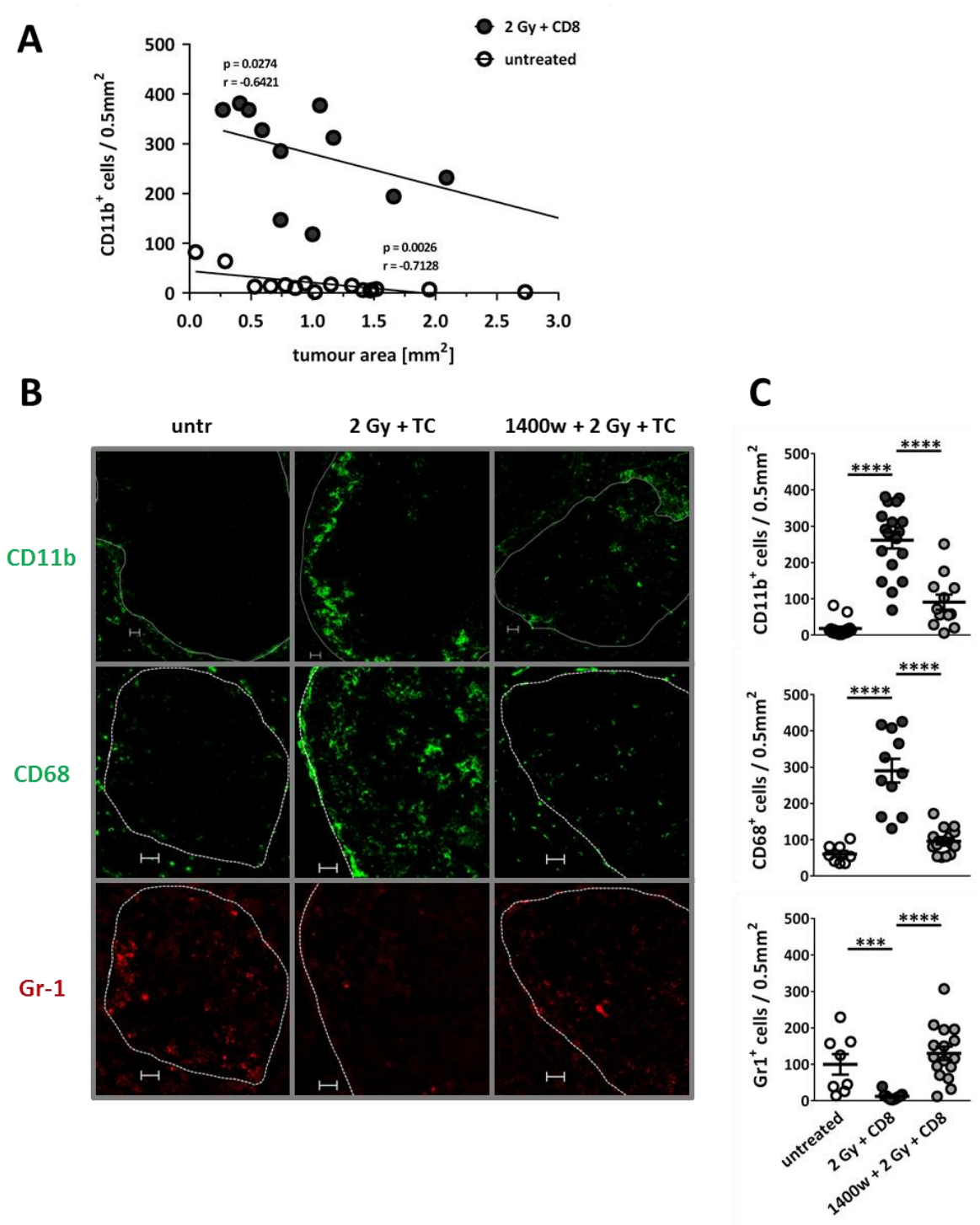

Figure 10 Combination therapy affects myeloid cell populations in insulinomas
Intratumoural myeloid cell populations ($CD11b^+$, $CD68^+$, $Gr\text{-}1^+$ cells) in untreated RT5 mice or after treatment with local LDI and adoptive T cell transfer with or without iNOS inhibition. A) Number of $CD11b^+$ cells/0.5mm^2 in RT5 tumours of untreated mice or mice treated with local LDI (2 Gy) and $CD8^+$ T cells in relation to the total tumour area (n=12-16 tumours per group with 2 mice per group; Spearman´s rank correlation coefficient test). B, C) IF analysis of myeloid cell markers in RT5 tumours from untreated mice, mice treated with local LDI (2 Gy) and $CD8^+$ T cells or local LDI (2 Gy), $CD8^+$ T cells and 1400w. B) Representative IF microscopy images of RT5 tumour sections from the indicated treatment groups, stained for CD11b (green), CD68 (green) or Gr-1 (red). Outlined are tumour areas. Scale bar, 50 µm. C) Quantitative analysis of IF microscopy images: number of $CD11b^+$, $CD68^+$ or $Gr\text{-}1^+$ cells per 0.5mm^2 for the indicated treatment groups. Data shown as mean ± SEM; *** p<0.001; **** p<0.0001 (n=8-16 tumours of 2 mice per group; two-tailed Mann-Whitney test).

Since CD11b has been shown to be expressed on various myeloid cells, including MDSCs and granulocytes (Murdoch et al., 2008), the intratumoural myeloid cell population was further characterised by IF microscopy analysis. RT5 tumour sections were stained for CD11b, as well as for CD68, a macrophage marker (Murray and Wynn, 2011), and Gr-1 which is expressed on MDSCs (Youn and Gabrilovich, 2010) and granulocytes (Murdoch et al., 2008). Here we show that in response to local LDI and CD8 T cell transfer, the tumour infiltrating myeloid cell population in RT5 tumours consists mainly of macrophages. Representative IF microscopy images (Figure 10 B) and quantitative analysis (Figure 10 C) show, that combination therapy leads to an increased number of $CD11b^+$ and $CD68^+$ cells and a decrease in $Gr\text{-}1^+$ cells in the tumour tissue. Of note, the inhibition of iNOS suppresses macrophage infiltration. Mice treated with 1400w in addition to local LDI and $CD8^+$ T cells show reduced numbers of $CD11b^+$ and $CD68^+$ cells in the tumour, the number of $Gr\text{-}1^+$ cells, on the other hand, was higher under iNOS inhibition. These findings demonstrate that macrophage accumulation in insulinomas after local LDI and CD8 T cell transfer is dependent on the activity of iNOS.

2.4. Macrophages are essential for the effects of local LDI and T cell transfer

2.4.1. Clodrosome depletes intratumoural macrophages

Tumour associated macrophages are known to promote tumour progression (Noy and Pollard, 2014). The observed increase of intratumoural macrophages after combination therapy led to the question whether these macrophages influenced the treatment outcome. To study the function of macrophages in RT5 tumours, they were depleted by intraperitoneal (i.p.) injections of clodronate disodium salt encapsulated in liposomes (Clodrosome; 5 mg/ml). These liposomes are recognised and taken up by macrophages. The toxic clodronate is released into the macrophages' cytosol causing their death. Flow cytometric analysis of RT5 tumours and pancreata revealed a considerably reduced number of macrophages ($CD11b^{hi}$ $F4/80^+$ cells) in pancreatic (3-fold decrease) and tumour tissues (6-fold decrease) of mice treated with Clodrosome over 3 weeks compared to untreated mice (Figure 11). The dot plots show that not only $CD11b^{hi}$ $F4/80^+$ cells were considerably reduced, but all $CD11b^+$ and all $F4/80^+$ cells.

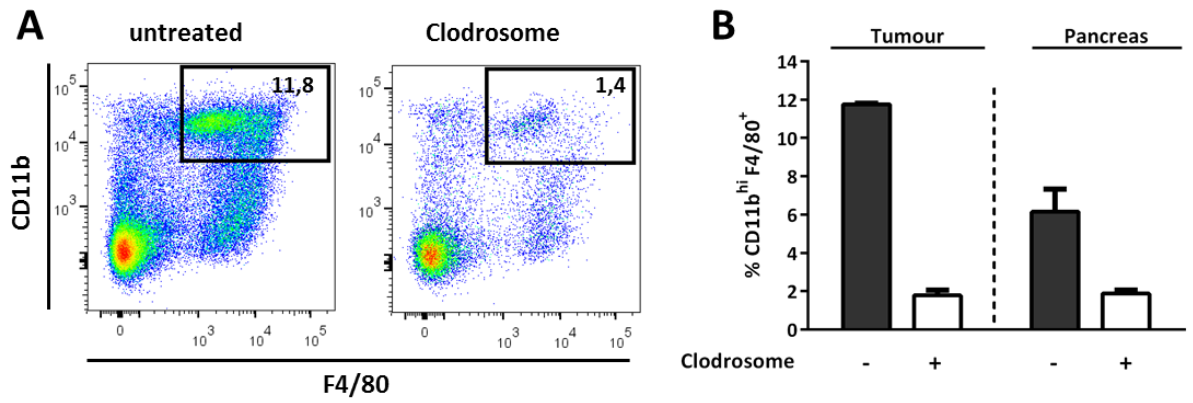

Figure 11 Macrophage depletion in tumour and pancreatic tissue following Clodrosome treatment
Flow cytometric analysis of tumours and pancreata from untreated RT5 mice or after a 3 week Clodrosome treatment (100 µl of 5 mg/ml i.p injections every 5 days, with an initial injection of 200 µl).
A) Representative dot plots showing intratumoural macrophages ($CD11b^{hi}$ $F4/80^{+}$) in untreated or Clodrosome-treated mice. B) Quantitative analysis: results presented are % $CD11b^{hi}$ $F4/80^{+}$ of viable, single, $CD45^{+}$ cells in tumour or pancreatic tissue of untreated or Clodrosome treated mice. Data shown as mean + SEM (from 2 independent experiments; n=2-5 mice per group).

2.4.2. Macrophage depletion affects survival or tumour rejection only after combination therapy

After macrophage depletion, RT5 tumours exhibit a similar phenotype compared to tumours from untreated mice, characterised by a dark red appearance and a tumour size that is comparable to untreated control tumours (Figure 12 A). Based on cumulative data, the percentage of non-haemorrhagic tumours is only marginally higher (5 % compared to 0 %) and the size only slightly decreased (3.3 mm compared to 4.3 mm) (Figure 12 B, C). Furthermore, depletion of macrophages in RT5 mice that were otherwise untreated had no beneficial or detrimental effect on survival (Figure 12 D). These results indicate that the depletion of macrophages in untreated mice does not affect tumour rejection, vascular normalization or improve their survival. It further shows that Clodrosome is not systemically toxic since the survival of the RT5 mice is not impaired by Clodrosome alone.
As has been shown before (Klug et al., 2013; Seibel, 2010), depletion of macrophages in treated RT5 mice significantly attenuates their survival. Mice treated with Clodrosome in addition to 2 Gy local LDI and repeated CD8 T cell transfers showed a median survival of 40 weeks. In comparison, mice that received Encapsome (empty liposomes) depicted long-term survival, showing that prolonged survival in response to combination therapy is impaired by macrophage depletion (Figure 12 D). Furthermore, macrophage depletion by Clodrosome treatment was previously shown to impair T cell infiltration into RT5 tumours (Klug et al., 2013). Overall, these results demonstrate that macrophages are required for the treatment effects of combination therapy (Klug et al., 2013).

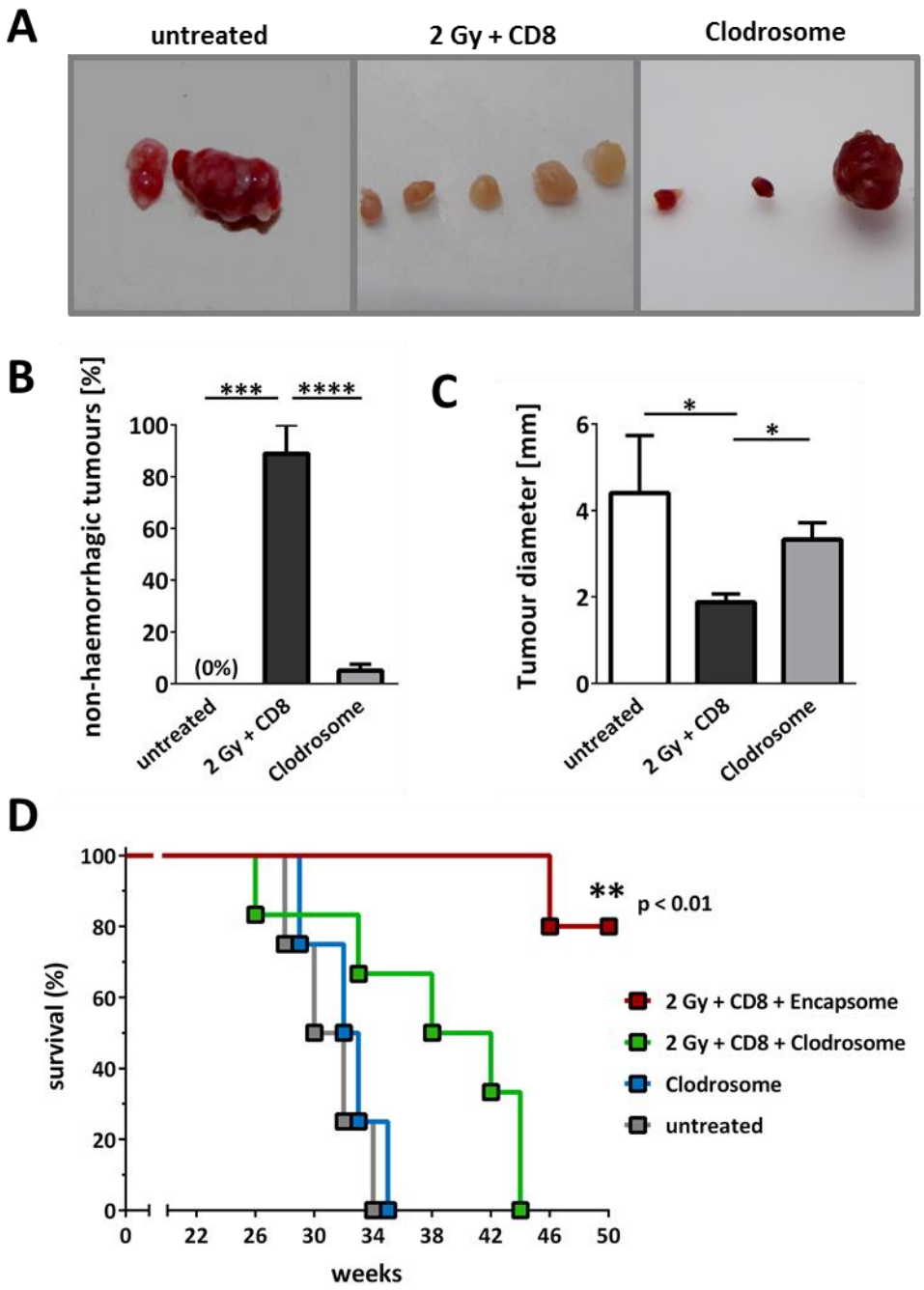

Figure 12 Effects of macrophage depletion on tumour rejection and survival

A, B, C) Haemorrhagic phenotype and size of RT5 tumours from untreated mice, mice treated with LDI (2 Gy) and $CD8^+$ T cells or mice treated with Clodrosome. A) Representative images of RT5 tumours B) Percentage of non-haemorrhagic tumours in the different treatment groups (n=3-8 mice per group). C) Tumour diameter in the different treatment groups (n=5-15 tumours per group with 3-8 mice). Data is shown as mean + SEM; * $p<0.05$; *** $p<0.001$; **** $p<0.0001$ (unpaired two-tailed t-test) D) Survival of RT5 mice after macrophage depletion: 24-week old RT5 mice were treated with a single dose of local LDI (2 Gy) combined with CD8 T cell transfers starting on day 10 (weekly during the first 5 weeks, then biweekly). In addition, they received clodronate loaded or empty liposomes (Clodrosome/Encapsome) every 5 days, starting one week before irradiation. Control mice were untreated or received Clodrosome. ** $p<0.01$ for survival in the 2 Gy + CD8 + Encapsome group compared to the untreated or the 2 Gy + CD8 + Clodrosome group (n=4-6 mice per group; Mantel-Cox test). Experiments were performed together with F. Klug.

2.5. More macrophages but fewer MDSCs infiltrate RT5 tumours after transfer of irradiated PECs

As demonstrated in chapter 2.3, combination treatment of RT5 mice leads to the infiltration of macrophages but not MDSCs into tumour tissue (Figure 10 B, C). Klug et al. further showed that the number of intratumoural CD11b$^+$ cells is increased after transfer of irradiated PECs when combined with CD8 T cell transfer (Klug et al., 2013).
To ascertain the identity of these CD11b$^+$ myeloid cells, tumour sections of RT5 mice that received no, irradiated or unirradiated PECs prior to a CD8 T cell transfer were stained for F4/80 or Gr-1 (Figure 13). After the transfer of irradiated PECs and CD8$^+$ T cells, the number of F4/80$^+$ cells in RT5 tumours was increased indicating an increased number of intratumoural macrophages. This effect could not be observed in tumours of mice that received no or unirradiated PECs in combination with T cell transfer. Notably, only few Gr-1$^+$ cells were found in RT5 tumours after transfer of irradiated PECs, but they were abundant when the mice only received CD8$^+$ T cells or unirradiated PECs and CD8$^+$ T cells. These findings imply that the transfer of irradiated PECs in combination with CD8$^+$ T cells leads to an increase in macrophages and a reduction of MDSCs in the tumour tissue.

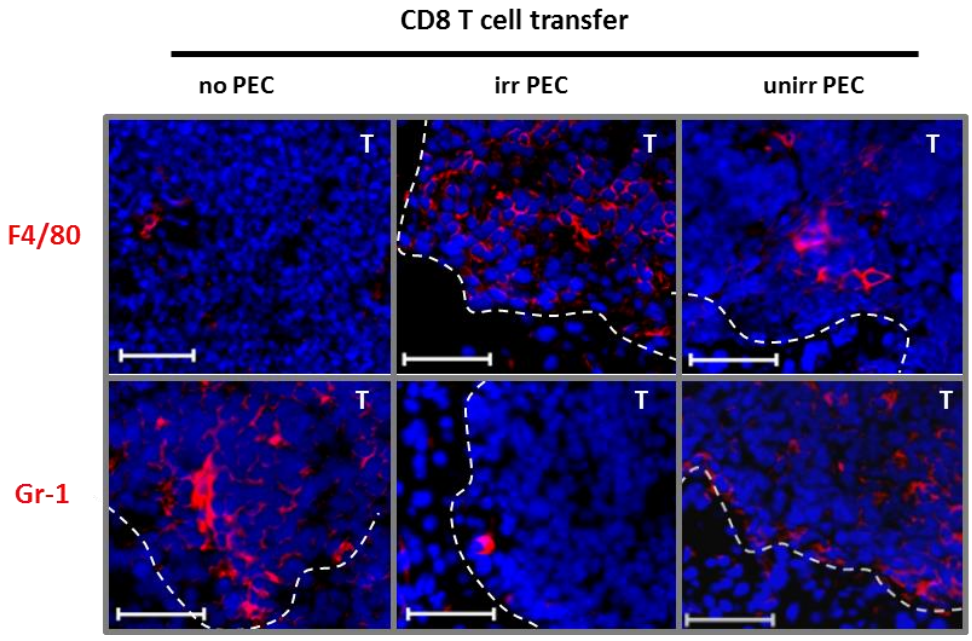

Figure 13 The impact of adoptively transferred irradiated PECs on myeloid cell infiltration into RT5 tumours
Intratumoural myeloid cell populations in RT5 mice after adoptive transfer of PECs from unirradiated or irradiated wt mice combined with adoptive T cell transfer. IF microscopy images of RT5 tumours from mice that received no, irradiated (irr) or unirradiated (unirr) PECs and CD8$^+$ T cells, showing macrophages (F4/80$^+$) or MDSCs/Granulocytes (Gr-1$^+$) in red and nuclei in blue. Outlined are tumour areas (T). Scale bar, 50 µm.

2.6. Transferred macrophages infiltrate RT5 tumours

In the next step, we wanted to identify the origin of the macrophages observed after the transfer of irradiated PECs and $CD8^+$ T cells in RT5 tumours. The intratumoural macrophages either stem from the wt donor mice or they originate from the host and are recruited into the tumour tissue. To ascertain the source of the intratumoural macrophages, PECs were labelled with PKH26 before they were transferred into tumour bearing RT5 mice. The establishment of the staining protocol was performed by L. Nögel in the course of his master thesis and is published therein. Briefly, after isolating the thioglycolate-elicited PECs from irradiated (2 Gy TBI) or unirradiated C3H wt mice, they were labelled *ex vivo* with micro-aggregates of PKH26. These aggregates are selectively taken up by phagocytes. $5x10^6$ labelled cells were then transferred into otherwise untreated, 24-week old RT5 mice. On day 10, some of the mice received $CD8^+$ T cells. On day 10 and on day 17 after the PEC transfer, tumours and additional organs (lung, pancreas, tumour, peritoneum and spleen) were analysed by flow cytometry to study the visceral distribution of PECs after transfer in RT5 mice.
The analysis revealed that the transferred PECs do migrate into RT5 tumours, as $PKH26^+$ cells were detectable in tumour tissue on day 10, as well as on day 17 after the transfer (Figure 14 A). In the lung, tumour and spleen, more $PKH26^+$ cells were detected on day 10 in mice that received irradiated PECs compared to mice that received unirradiated PECs (lung: 0.106 % vs. 0.050 %; tumour 0.010 % vs. 0.003 %; spleen 0.216 % vs. 0.126 %). On day 17 however, fewer $PKH26^+$ cells were found in these organs after transfer of irradiated cells when combined with CD8 T cell transfer (lung: 0.022 % vs. 0.046 %; tumour 0.001 % vs. 0.018 %; spleen 0.020 % vs. 0.049 %). Without the transfer of $CD8^+$ T cells, the percentages of $PKH26^+$ cells were also lower after transfer of irradiated cells but only in the tumour and spleen (tumour 0.002 % vs. 0.008 %; spleen 0.103 % vs. 0.220 %). On day 10, the percentages of $PKH26^+$ cells in the pancreas and peritoneum do not differ between the two treatment groups. For the pancreatic tissue the same observation was made on day 17. In the peritoneum, the number of $PKH26^+$ cells in mice treated with irradiated PECs was reduced (0.053 vs. 0.081 %), compared to unirradiated PECs. However, an increased number (0.114 %) of $PKH26^+$ cells were detected in mice that received $CD8^+$ T cells in addition to irradiated macrophages (vs. 0.072 % in the unirr PEC+TC group) (Figure 14 B). The differences between the treatment groups are not consistent over time, indicating that LDI does not affect the distribution of $PKH26^+$ cells in RT5 mice. Furthermore, the numbers of intratumoural $PKH26^+$ cells are very low. Therefore, the transfer of irradiated PECs does not contribute greatly to the massive accumulation of macrophages in tumour tissue after the combination of irradiated PECs and $CD8^+$ T cells. However, the results do show that a small fraction of irradiated PECs infiltrate the tumour tissue, suggesting that irradiated PECs affect macrophage accumulation by alternative mechanisms.

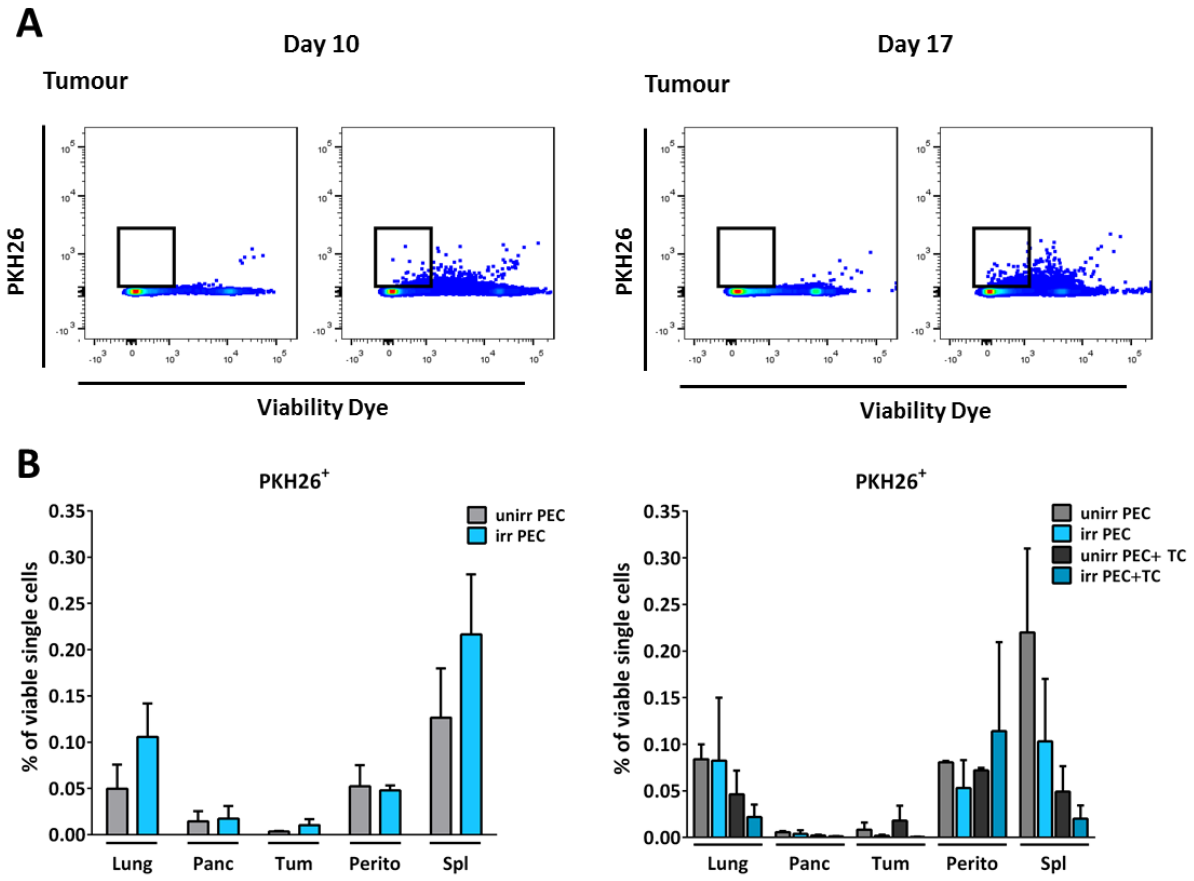

Figure 14 Distribution and tumour infiltration of transferred PECs in RT5 mice
24-week old RT5 mice received 5x10^6 PKH26 labelled PECs from total body irradiated (2 Gy) or unirradiated C3H wt mice. 7 days later (d10) mice in the indicated groups received TCRtg CD8$^+$ T cells. Flow cytometric analysis was performed on day 10 (left) and day 17 (right). A) Representative dot plots showing viable PKH26$^+$ cells in RT5 tumours after transfer with unlabelled or labelled PECs. B) Percentage of PKH26$^+$ cells in the lung, pancreas, tumour, peritoneum or spleen of RT5 mice after transfer of unirradiated or irradiated PECs with or without T cell transfer (TC). Results presented are % PKH26$^+$ of single, viable cells as means + SEM (n=2-4 mice per group, from 2 independent experiments). The experiments were performed by L. Nögel and N. Bender.

2.7. Low dose irradiation causes transcriptomic changes in PECs

2.7.1. Whole transcriptome analysis of peritoneal macrophages reveals effects of LDI on gene expression

Macrophages can be considered as a crucial component in the mechanisms underlying the effects of the combination therapy, demonstrated by the fact that macrophage depletion supressed these effects. This is further supported by the transfer of peritoneal cells from irradiated wt donor mice into unirradiated RT5 mice combined with a T cell transfer which has equivalent effects on vascular normalization, T cell and macrophage infiltration as the application of the combination therapy. Since no difference in the relative number of intratumoural PKH26$^+$ cells could be observed after transfer of irradiated and unirradiated cells, we hypothesized that the treatment effects are likely due to functional changes induced by low dose irradiation.

To investigate LDI-induced global gene expression changes, whole transcriptome analysis (RNA sequencing) of PECs from low dose irradiated as well as from unirradiated control mice was performed. PECs were either irradiated *in vivo* or *ex vivo*, to examine whether LDI either directly affects the gene expression profile in macrophages or indirectly causes changes in macrophages through damaged and apoptotic tissue cells. For *in vivo* irradiation, C3H wt mice were subjected to 2 Gy TBI on day 0, followed by thioglycolate injection on the next day. 72 hrs later, PECs were collected by peritoneal lavage for RNA isolation. For *in vitro* irradiation, thioglycolate-elicited PECs from C3H wt mice were isolated by peritoneal lavage on day 0, irradiated *ex vivo* on the same day and kept in culture for 72 hrs before RNA isolation. RNA sequencing of the isolated RNA from unirradiated, *in vivo* or *in vitro* irradiated PECs was followed by count-based differential gene expression analysis (Anders et al., 2013) which was performed by T. Michels (Figure 15).

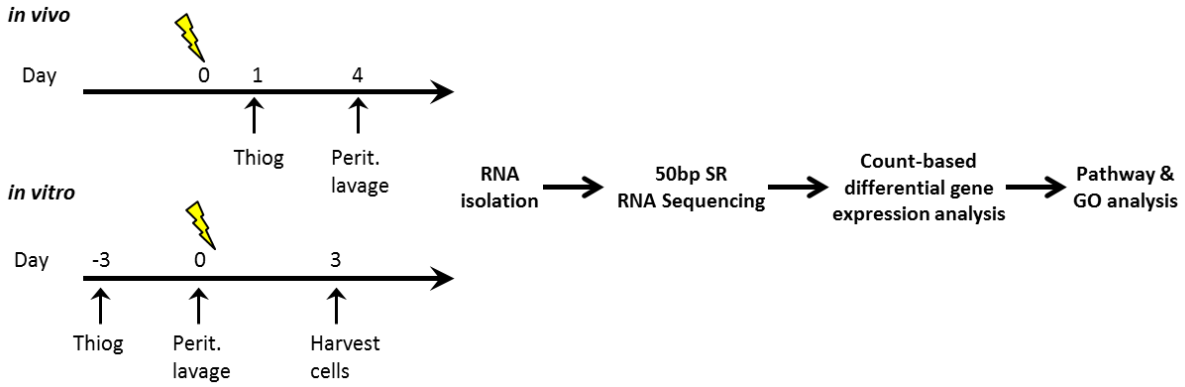

Figure 15 Schematic overview of experimental design and RNA sequencing workflow
Whole transcriptome analysis of thioglycolate-elicited PECs after *in vitro* or *in vivo* irradiation. For *in vivo* irradiation, C3H wt mice received 2 Gy TBI on day 0, followed by thioglycolate injection on the next day. 3 days later, PECs were collected by peritoneal lavage. For *in vitro* irradiation, thioglycolate-elicited PECs from C3H wt mice were isolated by peritoneal lavage on day 0, irradiated *ex vivo* on the same day and cultured for 72 hrs at 37°C. The isolated RNA from unirradiated, *in vivo* or *in vivo* irradiated PECs was submitted to the DKFZ GPCF or GATC Biotech for RNA sequencing. Count-based differential gene expression analysis (Anders et al., 2013) of the raw data, performed by T. Michels, was followed by pathway and Gene Ontology (GO) analysis of the differentially expressed genes (DEGs) (n=4 mice per group).

The PECs used for the RNA Sequencing were either freshly isolated (*in vivo*) or cultured following irradiation (*in vitro*). Since culturing thioglycolate-elicited peritoneal cells causes an enrichment of macrophage populations (Zhang et al., 2001), the *in vivo* and *in vitro* irradiated PECs were analysed by flow cytometry for macrophage content. The freshly isolated PECs contained 60-80 % macrophages (Figure 16 A) whereas 90-96 % of the cultured PECs were found to be macrophages which did not change over time in culture. Of note, LDI slightly increased the amount of macrophages by 1-2 % (Figure 16 B). The difference in macrophage content in *in vivo* versus *in vitro* irradiated PECs might affect downstream analyses.

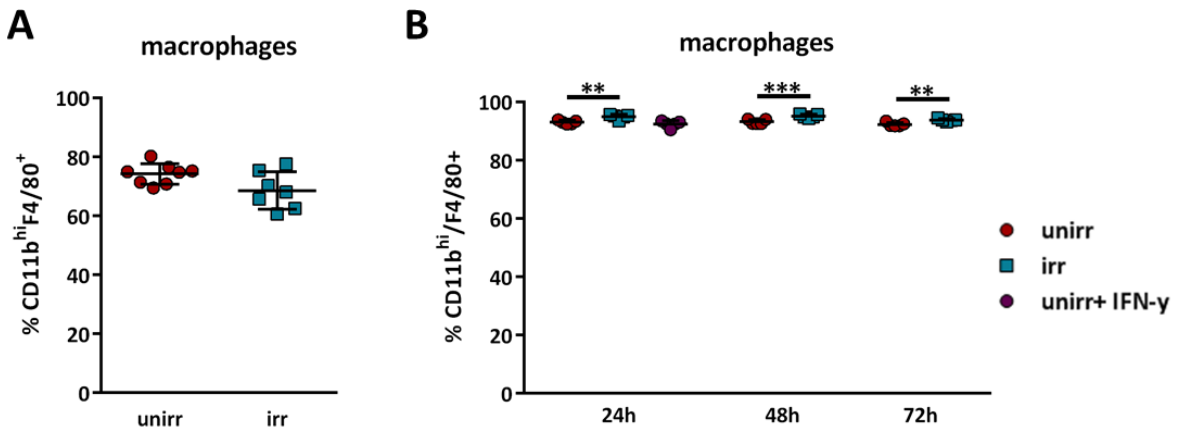

Figure 16 Adherence-mediated macrophage enrichment in PECs
Flow cytometric analysis of *in vivo* (A) or *in vitro* (B) irradiated thioglycolate-elicited PECs showing the percentage of macrophages ($CD11b^{hi}$ $F4/80^{+}$) in all single, viable cells. A) % $CD11b^{hi}$ $F4/80^{+}$ in PECs from unirradiated C3H wt mice or C3H wt mice subjected to 2 Gy TBI (n=8 mice per group; two-tailed Mann-Whitney test). B) % $CD11b^{hi}$ $F4/80^{+}$in PECs from C3H wt mice that were irradiated *ex vivo* with 2 Gy. Flow cytometric analysis was performed after 24, 48 and 72 hrs in culture. Data shown as mean ± SEM; ** $p<0.01$; *** $p<0.001$ (n=5; with cells pooled from 2 mice per sample; Paired two-tailed t-test (SAS)).

The whole transcriptome analysis of *in vivo* and *in vitro* irradiated PECs produced large and complex datasets. To generate an overview of the gene expression changes induced by LDI, the count-based differential gene expression analysis workflow included a `Principal-Component-Analysis´ (PCA) and produced a `Minus-Average´ (MA) plot, to visualize the gene expression data. The PCA examines the variance of gene expression between the samples and identifies subgroups that display similar gene expression patterns. This is illustrated in the PCA plot (Figure 17 A). *In vivo*: in the first principal component, a high similarity was observed between the control samples and between the irradiated samples, respectively. Furthermore, the PCA plot illustrates that the sex of the mice has an effect on the gene expression similarity of the samples. PECs from sex-matched mice show similarity with respect to the second principal component. This, however, is unlikely to affect downstream analyses since the first principal component accounts for the largest part of the variance in the dataset (Jolliffe, 2014). The second principal component only accounts for the second largest part of the variance. Moreover, the differences resulting from different sexes were not observed in the hierarchical clustering analysis (Figure 18) and were therefore not considered in subsequent analyses. For the *in vitro* studies only female animals were used to prevent influences of the sex. Here, the unirradiated (CTL) samples form a cluster, displaying high similarities regarding the first and second principal component, demonstrating their high similarity in gene expression. The irradiated samples are scattered in the PCA plot. Samples 1 and 4 and samples 2 and 3 display similarities with regard to the first principal component, respectively. Samples 2 and 3 show a higher similarity to the unirradiated samples than to the other irradiated samples (1 and 4).

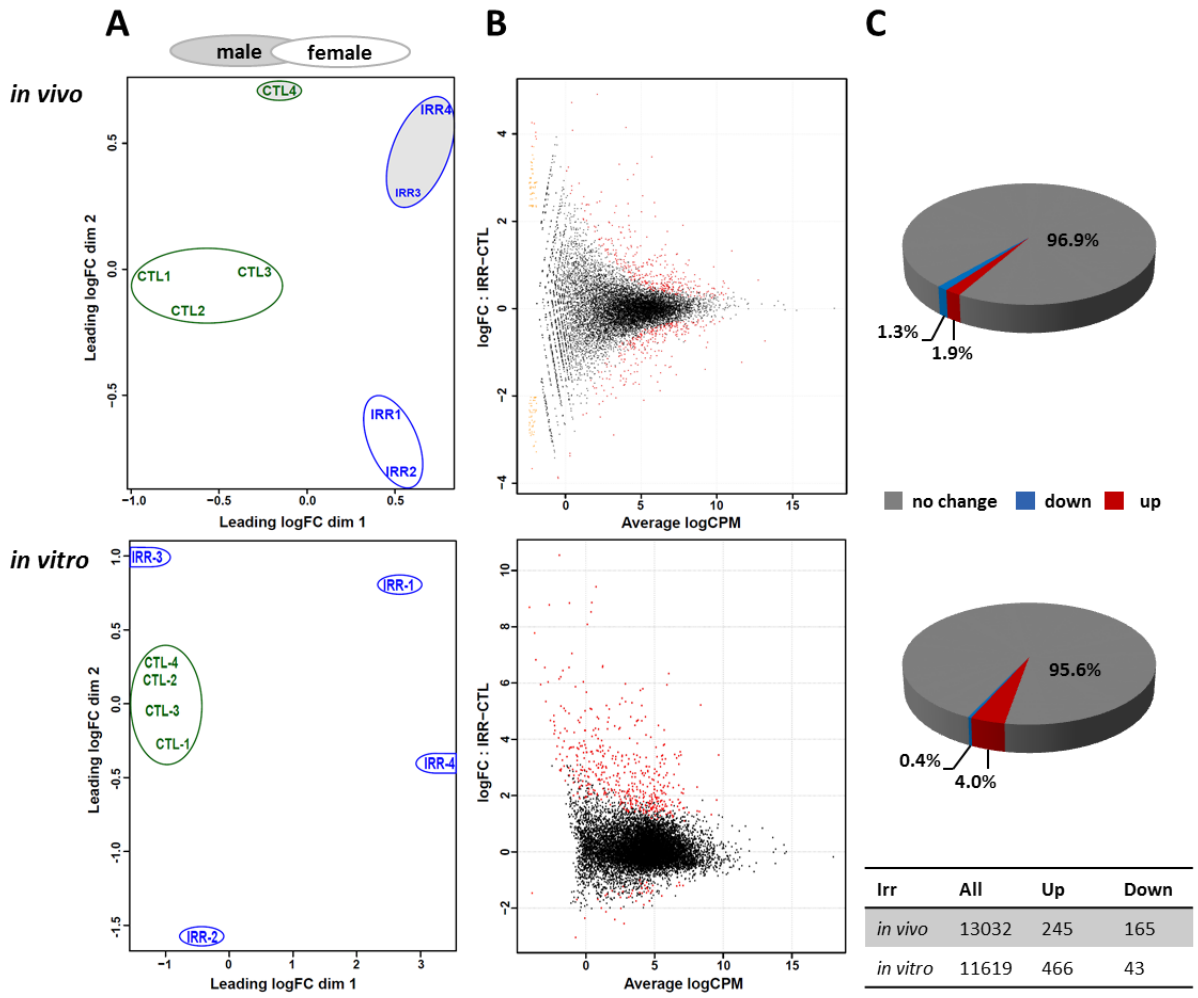

Irr	All	Up	Down
in vivo	13032	245	165
in vitro	11619	466	43

Figure 17 Overview of LDI-mediated gene expression changes in PECs
Transcriptomic data of *in vivo* (upper panel) and *in vitro* (lower panel) irradiated PECs in comparison to unirradiated control PECs, visualized by PCA plots (A), MA plots (B) and pie charts (C). A) PCA plots illustrate the relations among all samples of each dataset. Irradiated samples (IRR) are shown in blue, unirradiated control samples (CTL) in green. B) The MA plots show the distribution of all sequenced genes regarding their log2 fold change values (irradiated vs. unirradiated) plotted against the average standardized read counts, displayed as Average log10 counts per million (CPM). Each dot represents a gene; in red, genes with an FDR<0.05; in orange, condition-unique points C) Pie charts present the percentage of up- (red) and downregulated (blue) DEGs (defined as, FDR <0.05, FC ≥ |1.5|) of all sequenced transcripts in the *in vivo* and *in vitro* dataset. (n=4 mice per group)

2.7.2. Identification of DEGs

The MA-plots in Figure 17 B display all transcripts determined by the RNA sequencing analysis. The log2 fold change value of each identified transcript (gene) is plotted against the average read counts (Average logCPM), thereby visualizing the level of expression and the level of regulation after LDI of each transcript. The plots show the significantly up- or downregulated genes in red. Significance is defined by a False Discovery Rate (FDR) < 0.05. Many of the genes with low average counts display FDR values below 0.05, even with high fold change values. Of the significantly regulated genes those with a Fold Change (FC) ≥ |1.5| were se-

lected for subsequent analyses and herein referred to as differentially expressed genes (DEGs). Shown in orange are the genes with no detectable reads in a large proportion of samples in one or both conditions; the so called condition-unique points. They were not included in downstream analyses. In the *in vivo* dataset significantly up- and downregulated genes seem to be equally distributed. 165 (1.3 %) of all transcripts were significantly downregulated and 245 (1.9 %) were significantly upregulated. After *in vitro* irradiation, only 43 genes were significantly downregulated (0.4 %) while 466 of the DEGs were upregulated (4.0 %) (Figure 17 C). For closer examination of this bias, the DEGs were analysed by hierarchical clustering, illustrated in heat maps (Figure 18). Clusters are grouped together based on similarity of gene expression, thereby revealing two main clusters. One encompasses the genes that show decreased expression and the other includes all genes with increased expression after LDI. After *in vitro* irradiation, the majority of the DEGs are upregulated, while in the *in vivo* dataset almost two thirds of the DEGs are upregulated, thereby confirming the results from Figure 17.
The heat maps also show dendrograms visualizing the unsupervised hierarchical clustering of the samples (above the heat map). The height of the branches indicates the similarity between 2 samples, thus larger distances represent larger dissimilarities. *In vivo*: the control samples and the irradiated samples respectively form clusters. This analysis did not reveal differences in gene expression related to the sex of the mice, as seen in the PCA plot (Figure 17 A). *In vitro*: the control samples show high similarities in gene expression, shown by the small distances of the dendrogram branches. The irradiated samples 2 and 3 form a cluster with the unirradiated samples, while the irradiated samples 1 and 4 form a separate cluster. This confirms the results of the PCA plot. Together, these results demonstrate that low dose irradiation (*in vivo,* as well as *in vitro*) leads to gene expression changes in PECs.

For a more detailed analysis, the top 25 DEGs up- or downregulated after *in vivo* or *in vitro* LDI were explored. This revealed that several genes, whose expression is associated with M2-like macrophages, were downregulated in response to LDI: *Retnla* (resistin like alpha; synonym Found in inflammatory zone (Fizz)-1) (Murray et al., 2014), *CD163* (Martinez and Gordon, 2014), *CD163l1*, *Fcrls* (Fc receptor-like S, scavenger receptor; synonym macrophage scavenger receptor (Msr)2 (Cai et al., 2012), *Cx3cr1* (chemokine (C-X3-C motif) receptor 1) (Lee et al., 2013)) (Table 2, Table 4). In contrast, *Flt1* (FMS-like tyrosine kinase 1) which is associated with M1-like macrophages (Lee et al., 2013) and *Nos2* an important M1 marker (Martinez and Gordon, 2014; Murray et al., 2014) are among the top 25 DEGs upregulated after *in vivo* and *in vitro* LDI, respectively. Furthermore, several IFN-associated genes were upregulated after LDI: *Igigp* (interferon inducible GTPase) *1*, *Ifit* (interferon-induced protein with tetratricopeptide repeats) *1*, *Ifit1bl*, *Ifit2* and *Ifit3*, as well as *Oas* (2'-5'-oligoadenylate synthetase 3, 100kDa) *3* (Table 1, Table 3). These observations suggest an LDI-mediated M2 to M1 shift in peritoneal macrophages and an involvement of IFN signalling.

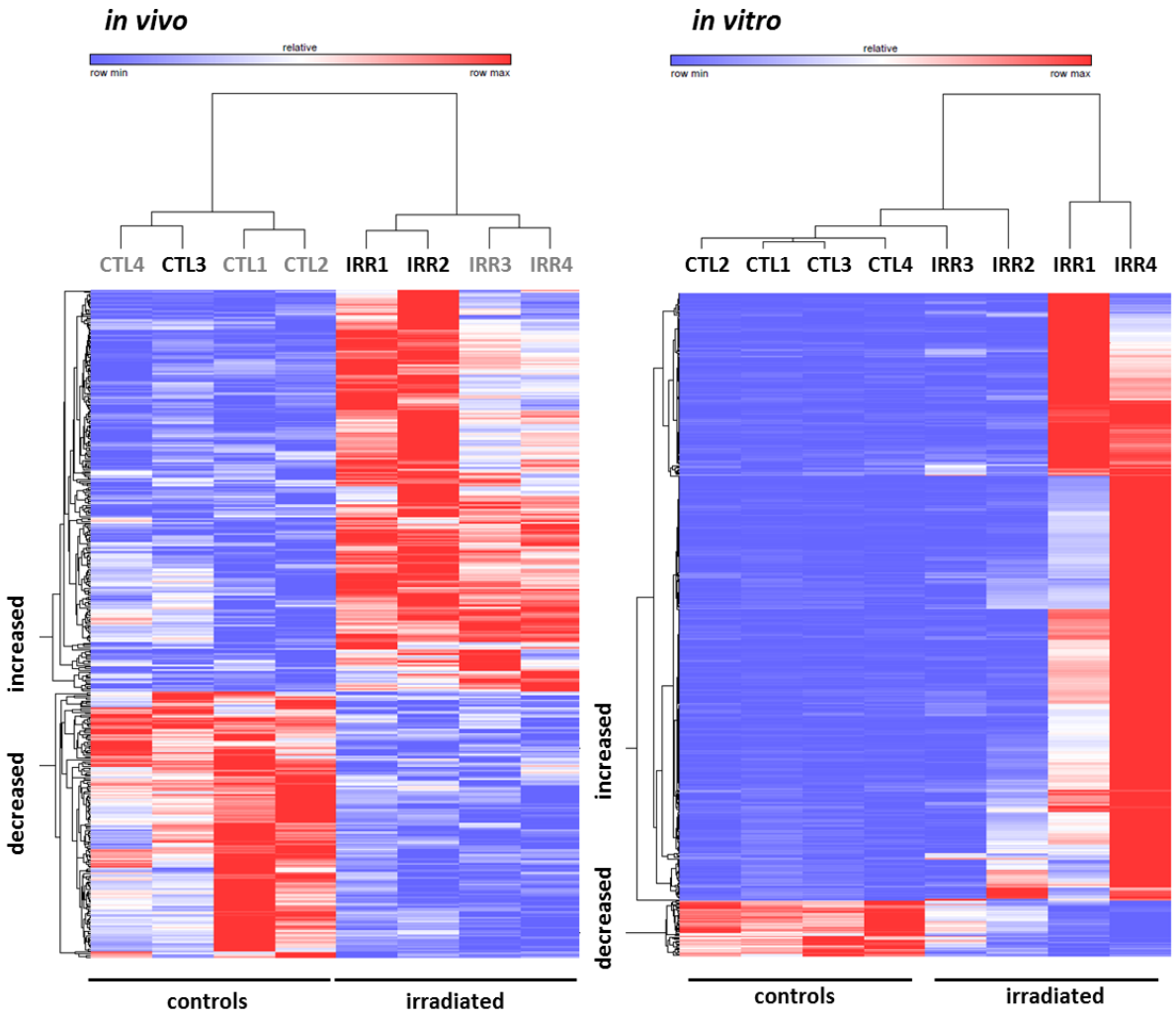

Figure 18 Effects of LDI on gene expression of PECs

Heat maps and unsupervised hierarchical clustering of all DEGs from the A) *in vivo* or B) *in vitro* dataset. The columns represent the samples: irradiated PECs (IRR 1-4) compared to unirradiated control PECs (CTL 1-4) (male; female). Each row represents one DEG and depicts the expression level for each sample. The colour intensity indicates the level of gene expression (normalized read counts as CPM) with tones of red representing high and tones of blue low expression values within a row. The up- and downregulated DEGs are clustered (increased; decreased, respectively) FDR <0.05, FC ≥ |1.5|. Heat maps were generated and clustering of DEGs was performed by Gene-e.

Table 1 Top 25 DEGs significantly upregulated after *in vivo* irradiation.

Gene	FC	FDR	Description
Pou3f1	32.45	0.0034	POU domain, class 3, transcription factor 1
Stfa2l1	30.76	0.0145	stefin A2
Ifit3	27.57	0.0000	interferon-induced protein with tetratricopeptide repeats 3
Pdgfrb	26.19	0.0154	platelet-derived growth factor receptor, beta polypeptide
Tnc	25.58	0.0336	tenascin C
Rarres1	24.74	0.0297	retinoic acid receptor responder (tazarotene induced) 1
Gzmb	24.50	0.0001	granzyme B
Wwc1	22.01	0.0418	WW and C2 domain containing 1
Ifit2	17.44	0.0000	interferon-induced protein with tetratricopeptide repeats 2
Ifit1bl1	12.59	0.0020	interferon-induced protein with tetratricopeptide repeats 1
Ccl2	10.79	0.0000	chemokine (C-C motif) ligand 2

Ifit1	10.03	0.0000	interferon-induced protein with tetratricopeptide repeats 1B
Ccl7	9.69	0.0000	chemokine (C-C motif) ligand 7
Ly6c2	8.06	0.0000	lymphocyte antigen 6 complex, locus A
Samd3	7.62	0.0200	sterile alpha motif domain containing 3
Ly6c1	7.52	0.0000	lymphocyte antigen 6 complex, locus A
Iigp1	7.17	0.0356	interferon inducible GTPase 1
Rab15	6.18	0.0031	RAB15, member RAS oncogene family
Spire2	6.13	0.0000	spire-type actin nucleation factor 2
Rsad2	5.97	0.0000	radical S-adenosyl methionine domain containing 2
Klrb1f	5.74	0.0191	killer cell lectin-like receptor subfamily B member 1F
Flt1	5.61	0.0128	fms-related tyrosine kinase 1
Oas3	5.37	0.0000	2'-5'-oligoadenylate synthetase 3, 100kDa
Usp18	5.33	0.0000	ubiquitin specific peptidase 18
Ccl24	5.22	0.0143	chemokine (C-C motif) ligand 24

Table 2 Top 25 DEGs significantly downregulated after *in vivo* irradiation.

Gene	FC	FDR	Description
Sult1a1	-21.99	0.0250	sulfotransferase family 1A, phenol-preferring, member 1
Igha	-8.94	0.0250	immunoglobulin heavy constant alpha
Pkmyt1	-7.90	0.0051	protein kinase, membrane associated tyrosine/threonine 1
Slc36a2	-7.53	0.0083	solute carrier family 36 (proton/amino acid symporter), member 2
Blk	-6.87	0.0000	BLK proto-oncogene, Src family tyrosine kinase
Fcrls	-5.22	0.0027	Fc receptor-like S, scavenger receptor
Klrg2	-4.73	0.0074	killer cell lectin-like receptor subfamily G, member 2
Cd163	-4.40	0.0038	CD163 molecule
Rltpr	-4.36	0.0379	RGD motif, leucine rich repeats, tropomodulin domain and proline-rich containing
Retnla	-4.18	0.0000	resistin like alpha
St8sia6	-4.10	0.0062	ST8 alpha-N-acetyl-neuraminide alpha-2,8-sialyltransferase 6
Cd163l1	-3.87	0.0120	CD163 molecule-like 1
Cd209a	-3.87	0.0001	C-type lectin domain family 4, member M
Ighd	-3.72	0.0000	immunoglobulin heavy constant delta
C1qb	-3.63	0.0000	complement component 1, q subcomponent, B chain
Mgl2	-3.62	0.0242	C-type lectin domain family 10, member A
Fcrla	-3.50	0.0003	Fc receptor-like A
Siglech	-3.41	0.0175	sialic acid binding Ig-like lectin H
H2-Ob	-3.30	0.0000	major histocompatibility complex, class II, DO beta
Fcmr	-3.25	0.0191	Fc fragment of IgM receptor
Rcn3	-3.25	0.0000	reticulocalbin 3, EF-hand calcium binding domain
Tmem176a	-3.24	0.0108	transmembrane protein 176A
Nynrin	-3.22	0.0105	NYN domain and retroviral integrase containing
C1qc	-3.18	0.0000	complement component 1, q subcomponent, C chain
Pou2af1	-3.15	0.0000	POU class 2 associating factor 1

Table 3 Top 25 DEGs significantly upregulated after *in vitro* irradiation.

Gene	FC	FDR	Description
Serpina3f	1050.60	0.0008	serine (or cysteine) peptidase inhibitor, clade A, member 3G
Ubd	869.47	0.0008	ubiquitin D
Lcn2	651.67	0.0008	lipocalin 2
Iigp1	448.20	0.0015	interferon inducible GTPase 1
Htr7	429.35	0.0008	5-hydroxytryptamine (serotonin) receptor 7, adenylate cyclase-coupled

Gm4951	405.34	0.0008	predicted gene 4951
Ly6i	355.08	0.0015	lymphocyte antigen 6 complex, locus A
Gbp8	334.30	0.0015	guanylate-binding protein 8
Cxcl3	265.03	0.0015	chemokine (C-X-C motif) ligand 3
Ly6a	121.26	0.0008	lymphocyte antigen 6 complex, locus A
Gbp4	96.80	0.0008	guanylate binding protein family, member 6
Cfb	93.64	0.0010	complement factor B
Il23r	87.49	0.0027	interleukin 23 receptor
Ly6c1	87.12	0.0015	lymphocyte antigen 6 complex, locus A
Marco	80.90	0.0009	macrophage receptor with collagenous structure
Spon1	80.62	0.0062	spondin 1, extracellular matrix protein
U90926	76.16	0.0043	cDNA sequence U90926
Ly6c2	64.58	0.0023	lymphocyte antigen 6 complex, locus A
Fpr1	62.55	0.0015	formyl peptide receptor 1
Irg1	61.35	0.0010	immunoresponsive 1 homolog (mouse)
Trim30c	57.44	0.0010	tripartite motif-containing 30C
Nos2	55.56	0.0011	nitric oxide synthase 2, inducible
Fpr2	53.41	0.0008	formyl peptide receptor 2
Tnfaip8l3	50.18	0.0071	tumor necrosis factor, alpha-induced protein 8-like 3
Ctgf	49.80	0.0079	connective tissue growth factor

Table 4 Top 25 DEGs significantly downregulated after *in vitro* irradiation.

Gene	FC	FDR	Description
Cyp2s1	-8.62	0.0008	cytochrome P450, family 2, subfamily S, polypeptide 1
Cx3cr1	-5.95	0.0008	chemokine (C-X3-C motif) receptor 1
Fcrls	-5.47	0.0110	Fc receptor-like S, scavenger receptor
Cited4	-5.25	0.0008	Cbp/p300-interacting transactivator, with Glu/Asp-rich carboxy-terminal domain, 4
Apln	-5.10	0.0026	apelin
Cdkn3	-4.39	0.0375	cyclin-dependent kinase inhibitor 3
Fads2	-4.05	0.0008	fatty acid desaturase 2
H1fx	-3.91	0.0083	H1 histone family, member X
Ube2c	-3.69	0.0380	ubiquitin-conjugating enzyme E2C
Cd200r3	-3.38	0.0458	CD200 receptor 3
Cdc20	-3.36	0.0425	cell division cycle 20
Cdca3	-3.36	0.0424	cell division cycle associated 3
Cd34	-3.27	0.0377	CD34 molecule
Gpr183	-3.08	0.0083	G protein-coupled receptor 183
Acap1	-3.06	0.0084	ArfGAP with coiled-coil, ankyrin repeat and PH domains 1
Kif2c	-2.99	0.0488	kinesin family member 2C
Tsc22d1	-2.96	0.0010	TSC22 domain family, member 1
Rasal1	-2.95	0.0495	RAS protein activator like 1 (GAP1 like)
Atg9b	-2.83	0.0194	autophagy related 9B
Traip	-2.82	0.0313	TRAF interacting protein
Pttg1	-2.78	0.0467	pituitary tumor-transforming 1
Dlgap5	-2.78	0.0450	discs, large (Drosophila) homolog-associated protein 5
Lmnb1	-2.74	0.0231	lamin B1
Ncapd2	-2.74	0.0269	non-SMC condensin I complex, subunit D2
Kif22	-2.73	0.0334	kinesin family member 22

2.7.3. Overlapping DEGs after *in vivo* and *in vitro* irradiation

The whole transcriptome analysis was performed on *in vivo* and *in vitro* irradiated PECs with the aim to discern whether LDI exerts its effects directly on macrophages or whether the effects are indirectly induced through surrounding damaged tissues. To assess whether *in vivo* and *in vitro* irradiation cause similar effects on gene expression in PECs, the DEGs from the two datasets were compared and genes unique to, as well as genes shared by, the two datasets were identified (Figure 19). Transcriptome analysis of irradiated and unirradiated PECs identified a total of 410 (*in vivo*) and 509 (*in vitro*) DEGs. Ninety-eight (11.9 %) of these DEGs are found in both datasets (Figure 19 A). In order to account for the direction of altered gene expression, up- and downregulated genes of the *in vivo* and *in vitro* datasets were analysed separately, thereby revealing genes which are commonly up- or downregulated and genes which are conversely regulated. After *in vivo* irradiation 245 genes and after *in vitro* irradiation 466 genes were upregulated. Of note, the upregulated genes showed an overlap of 92 genes (14.9 %) between *in vivo* and *in vitro* irradiation, indicating that transcriptional modulation of these commonly regulated genes is a direct effect of LDI. Hence, these genes were included in further analyses. Surprisingly, only two genes were commonly downregulated after *in vivo* and *in vitro* irradiation (*Cx3cr1* and *Fcrls*) (Figure 19 A).
A small fraction of genes was inversely regulated, as depicted by the lower Venn diagrams in Figure 19 B. There was no overlap between the 245 upregulated genes of the *in vivo* dataset and the 43 downregulated genes of the *in vitro* dataset which further supports the specific upregulation of the above identified set of 92 genes by LDI. Furthermore, only 4 genes were found to be downregulated after *in vivo* and upregulated after *in vitro* irradiation. The identified DEGs of the *in vivo* (n=410) and the *in vitro* (n=509) data sets, as well as the 92 commonly upregulated genes in both datasets, were further studied by Gene Ontology and pathway analyses.

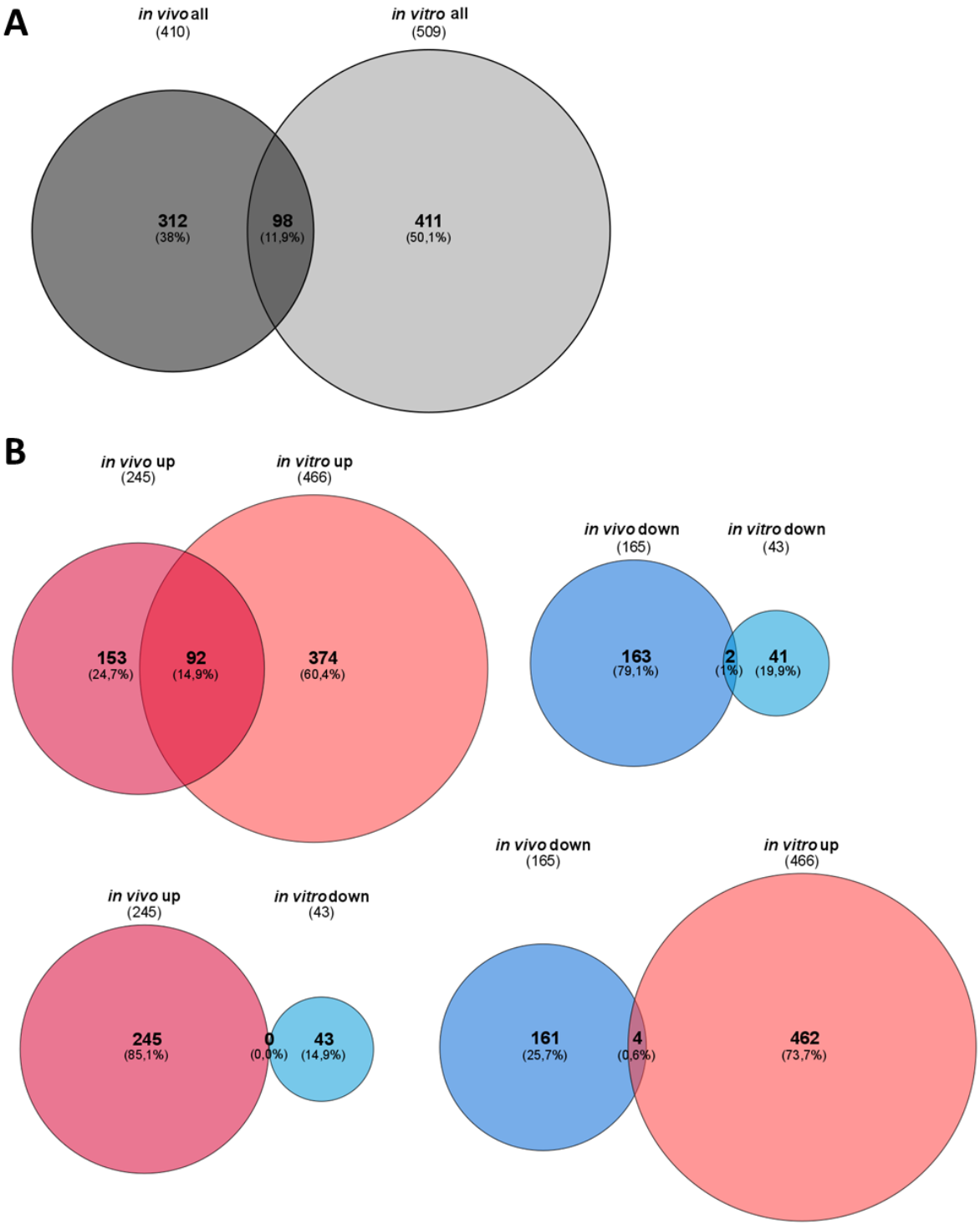

Figure 19 Overlap of differentially expressed genes in PECs upon *in vivo* versus *in vitro* LDI

Overlap between the *in vivo* and *in vitro* dataset of upregulated and/or downregulated genes. Scaled Venn diagrams identifying shared DEGs after *in vivo* and *in vitro* irradiation: A) Comparison of all DEGs from the *in vivo* and *in vitro* dataset. B) Comparison of genes upregulated (red) or downregulated (blue) by *in vivo* or *in vitro* irradiation: upper Venn diagrams depict shared upregulated (left) or shared downregulated (right) DEGs. Lower Venn diagrams show overlap in DEGs which are inversely regulated after *in vivo* and *in vitro* irradiation.

2.7.4. DEGs are associated with immune system processes

The previous experiments demonstrated that LDI induces gene expression changes in PECs. To analyse their implications on macrophage characteristics, the downstream effects of these transcriptional changes, as well as the biological functions and processes associated with the DEGs, were identified by linking the gene lists of DEGs to gene ontologies using the databases of the online annotation tool STRING 10.0 and the Ingenuity® Pathway Analysis software (IPA®, QIAGEN, Redwood City). The STRING Gene Ontology (GO) enrichment analysis allows for the functional interpretation of the transcriptomic data, since the GO terms describe gene product (protein) properties. Analysis of genes up- or downregulated after *in vivo* or *in vitro* irradiation, revealed GO terms that were overrepresented to a significant degree in the respective gene sets. Genes upregulated after *in vivo* irradiation are associated with the biological processes of 'Immune response', 'Response to other organism', 'Innate immune response', 'Defence response' and 'Immune system process' (Table 5). Genes downregulated after *in vivo* irradiation are associated with 'Antigen processing and presentation of exogenous peptide antigen via MHC class II', 'Immune system process', 'Regulation of immune system process', 'Regulation of immune response' and 'Antigen processing and presentation' (Table 5). Overall, the GO terms, associated with altered gene expression after *in vivo* irradiation, are related to processes of the immune system, suggesting that *in vivo* irradiation affects immune responses.

Table 5 Top 5 overrepresented GO biological process terms (*in vivo* up (red) and down (blue))

Biological Process	observed gene count	FDR	Biological Process	observed gene count	FDR
Immune response	43	1.14e-17	Ag processing and presentation of exogenous peptide Ag via MHC class II	7	7.65e-09
Response to other organism	40	2.16e-17	Immune system process	33	4.28e-07
Innate immune response	32	4.94e-17	Regulation of immune system process	27	7.1e-07
Defence response	44	5.22e-16	Regulation of immune response	17	5.7e-06
Immune system process	54	1.64e-14	Ag processing and presentation	8	1.44e-05

GO biological processes significantly overrepresented in the up- (red) and downregulated (blue) gene sets after *in vivo* irradiation, generated with the STRING database.

Biological processes associated with genes upregulated after *in vitro* irradiation are analogous to the terms overrepresented after *in vivo* irradiation: 'Immune response', 'Immune system process', 'Defence response', 'Innate immune response' and 'Response to cytokine' (Table 6), indicating that *in vitro* irradiation affects immune responses as well. STRING analysis of the 43 genes downregulated after *in vitro* irradiation revealed alterations of cell cycle functions, as was evident from the top 5 GO terms shown in Table 6. It has to be considered that this analysis does not take into account which effect (activating or inhibiting) a single

gene has on the associated biological process, therefore this analysis does not show whether low dose irradiation suppresses or stimulates immune responses.

Table 6 Top 5 overrepresented GO biological process terms (*in vitro* up (red) and down (blue))

Biological Process	observed gene count	FDR	Biological Process	observed gene count	FDR
Immune response	86	2.71e-41	Nuclear division	11	1.12e-06
Immune system process	114	3.74e-38	Cell cycle	15	1.12e-06
Defence response	83	1.98e-32	Mitotic nuclear division	10	1.12e-06
Innate immune response	56	1.79e-30	Cell cycle process	13	1.5e-06
Response to cytokine	59	6.78e-27	Mitotic cell cycle process	11	2.64e-06

GO biological processes significantly overrepresented in the up- (red) and downregulated (blue) gene sets after *in vitro* irradiation, generated with the STRING database.

To further assess the impact of LDI on immune responses, the list of 92 genes, commonly upregulated after *in vivo* and *in vitro* irradiation, was also analysed using STRING. Indeed, the top 10 GO biological processes significantly overrepresented in this gene set included 'Innate immune response', 'Immune response', 'Defence response', 'Response to other organism', 'Defence response to other organism', 'Defence response to virus', 'Immune effector process', 'Response to interferon-beta', 'Immune system process', and 'Response to cytokine' as summarised in Table 7.

Table 7 Top 10 overrepresented GO biological process terms (in vivo and in vitro up)

Biological Process	observed gene count	FDR
Innate immune response	22	3.01e-16
Immune response	26	2.9e-15
Defence response	27	2.02e-14
Response to other organism	23	1.92e-13
Defence response to other organism	18	5.69e-13
Defence response to virus	13	2.43e-12
Immune effector process	16	9.1e-11
Response to interferon-beta	7	7.45e-09
Immune system process	26	8.17e-09
Response to cytokine	16	4.9e-08

GO biological processes associated with the 92 genes upregulated after *in vivo* and *in vitro* irradiation, generated with the STRING database.

STRING analysis further generated a protein interaction network showing the proteins encoded by the 92 genes upregulated by *in vivo* and *in vitro* irradiation (Figure 20). This over-

view visualizes the relations between the 92 proteins. The network comprises a significant enrichment of interactions, as calculated by STRING, signifying the functional linkage of these proteins. Using the MCL (Markov Cluster Algorithm) cluster function, protein clusters were associated to GO terms. The yellow shaded area highlights the proteins in cluster A, which are mainly associated with the GO term 'Innate immune response'. Proteins in cluster B (green shaded area) are mainly associated with the biological process term 'Cell migration'. The specific proteins forming cluster A and B, respectively, are shown in the supplemental Figure S33.

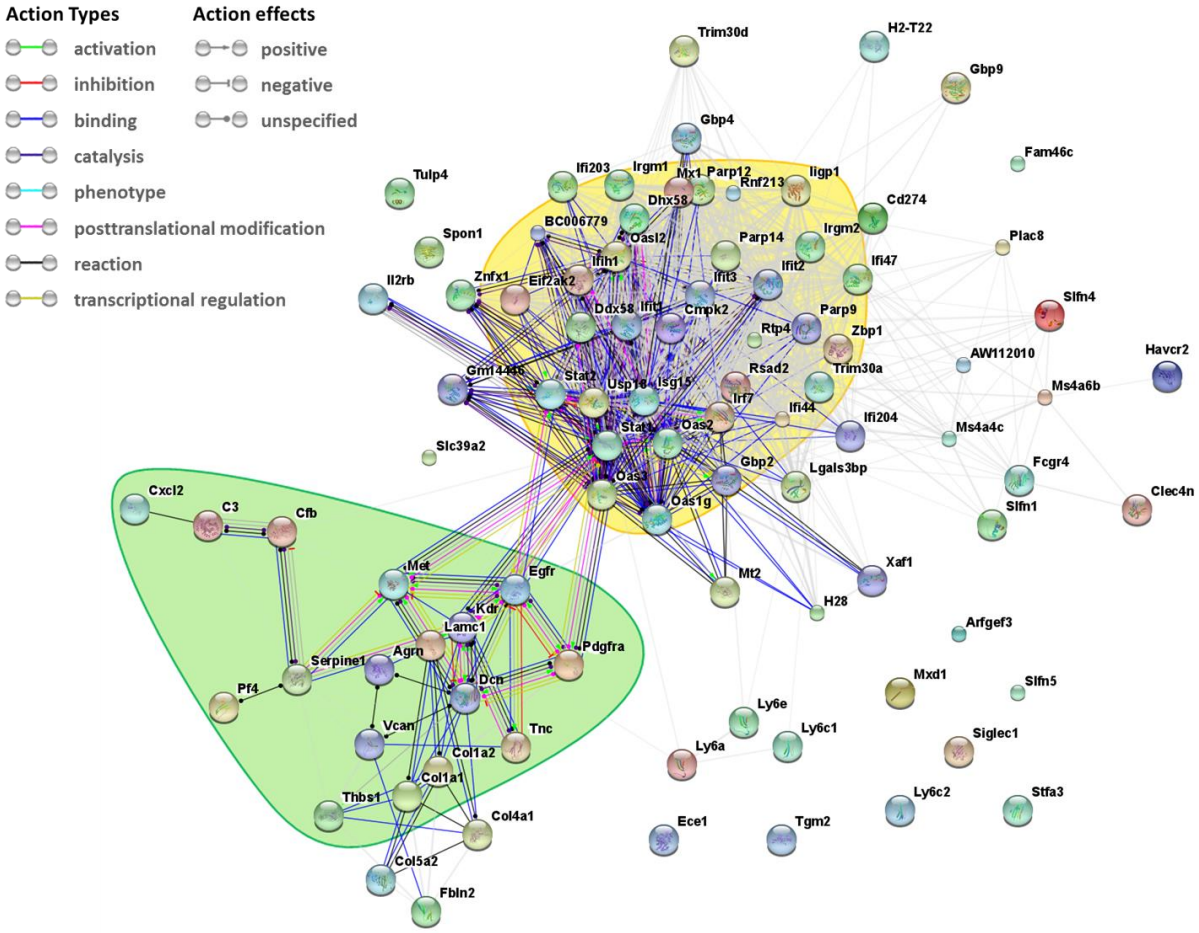

Figure 20 Protein interaction network of genes upregulated in PECs in response to LDI
Protein-protein interactions of the proteins encoded by the 92 genes upregulated after both *in vivo* and *in vitro* irradiation, visualized by STRING. The nodes represent proteins, the edges (841) represent physical and functional connections between the proteins, with the line colour indicating the action type and the line shape indicating the action effect (detailed description, see legend). The coloured areas highlight protein clusters which predominantly comprise proteins involved in an innate immune response (yellow) or cell migration (green).

As an additional finding, the dataset of commonly upregulated genes (n=92), as well as the *in vivo* and *in vitro* dataset, revealed a statistical enrichment for the GO term 'Response to stress' (Table 8). Figure 21shows the 92 genes upregulated after *in vivo* and *in vitro* irradiation with the 31 genes associated with the GO term 'Response to stress' highlighted in red.

In summary, these results suggest that *in vivo* and *in vitro* LDI lead to a stress response in PECs, to an increase in cell migration and an innate immune response of these cells.

Table 8 GO biological process term 'Response to Stress'

Response to stress	observed gene count	FDR
***In vivo* up**	**68**	**1.61e-11**
***In vitro* up**	**123**	**6.27e-21**
***In vivo* & *in vitro* up**	**31**	**1.05e-06**

Enrichment of the GO term 'Response to Stress' in genes upregulated after *in vivo* and/or *in vitro* irradiation, generated with the STRING database. Shown is the number of genes annotated with the (GO) Biological process term 'Response to Stress' in the indicated gene sets.

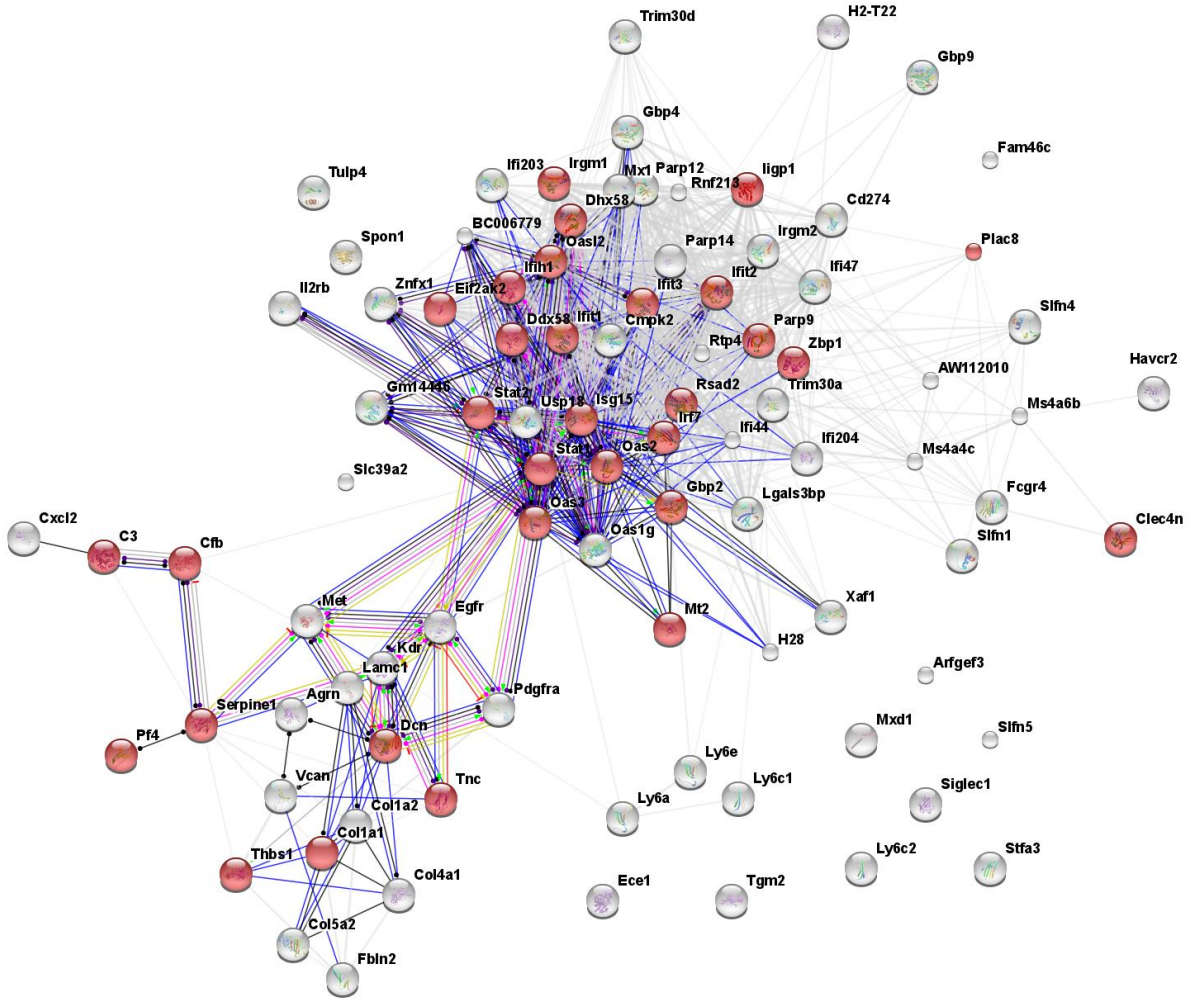

Figure 21 Network of stress response-associated proteins induced in PECs upon LDI
STRING protein interaction network of the 92 genes upregulated after *in vivo* and *in vitro* irradiation with proteins associated with a stress response highlighted in red. The nodes represent proteins, the edges represent physical and functional associations between the proteins, with the line colour indicating the action type and the line shape indicating the action effect.

Subsequently, the *in vivo* and *in vitro* datasets were analysed with the Ingenuity® Pathway Analysis software. Only significantly regulated genes with an FDR <0.05 and FC values ≥ |1.5|

were included in the analysis (*in vivo* n=410; *in vitro* n=509). The software mapped the datasets to the Ingenuity® Knowledge Base, thereby creating causal networks, identifying upstream regulators, as well as overrepresented biological functions and canonical pathways. In these analyses, the direction of change, that is whether a gene is up- or downregulated, is taken into account.

Table 9 IPA Diseases and biological functions

Diseases and Bio Functions	activation z-score *in vivo*	activation z-score *in vitro*
Innate immune response	**1.94**	**3.44**
Activation of leukocytes	**2.76**	**4.42**
Activation of myeloid cells	1.39	**4.24**
Activation of phagocytes	1.17	**3.56**
Activation of macrophages	0.74	**3.77**
Cell movement	**2.32**	**6.25**
Cell movement of myeloid cells	**2.26**	**3.92**
Cell movement of phagocytes	1.97	**4.01**
Cell movement of macrophages	1.09	**2.90**
Viral Infection	**-2.39**	**-2.50**

Diseases and functions predicted by IPA to be increased (red) or decreased (blue) after *in vivo* or *in vitro* irradiation. Activation z-score ≥ |2|; p-value <0.0001 considered significant. Insignificant values shown in black. Table 29 lists the DEGs of the two datasets for each Disease and biological function.

The IPA Downstream Effects Analysis identified which downstream biological processes were predicted to be increased or decreased after *in vivo* or *in vitro* irradiation. Several biological functions in the categories 'Cellular Movement', 'Inflammatory Response' as well as in other categories were predicted to be activated; a selection is listed in Table 9. The sub functions 'Innate immune response' and 'Activation of leukocytes' of the category 'Inflammatory Response' were predicted to increase after LDI. 'Activation of myeloid cells, phagocytes and macrophages' were predicted to be activated after *in vitro* but not after *in vivo* irradiation. 'Cell movement' in general, and 'Cell movement of myeloid cells, phagocytes or macrophages' in particular, were all predicted to be increased after *in vitro* irradiation; the first two also after *in vivo* irradiation. In the category 'Infectious Diseases', 'Viral infection' was one of the diseases predicted to decrease after *in vivo* and *in vitro* LDI. The IPA Downstream Effects Analysis confirmed the results of the GO enrichment analysis generated by STRING. Moreover, it gives additional information about the activity of the biological functions signifying whether the gene expression changes lead to an activation or inhibition of the process. In summary, LDI seems to activate the peritoneal macrophages, stimulate their migration and promote an (innate) immune response.

As described above, IPA also identified enriched canonical signalling pathways in the *in vivo* and *in vitro* gene sets. To determine which pathways are affected by a certain gene set, IPA calculates whether the overlap between the genes in the pathway and the DEGs of the dataset is statistically significant. This is described by the overlap p-value (-log(p-value)). On the basis of the expression data, IPA additionally ascertains the activation state of the affected pathway. IPA Pathway analysis of the targets that were differentially regulated by *in vivo* or *in vitro* irradiation revealed that 'Interferon Signalling', 'Activation of IRF by Cytosolic Pattern Recognition Receptors' and 'Role of Pattern Recognition Receptors in Recognition of Bacteria and Viruses' are predicted to be activated by both, *in vivo* and *in vitro* irradiation (Figure 22 A, B).

Due to its role in the mechanism of combination therapy-induced endothelial activation and T cell infiltration, we were interested in the expression of iNOS in peritoneal macrophages after LDI. Also, it is known that iNOS can be induced by IFN stimulation (Blanchette et al., 2003). Therefore, the subsequent analyses focussed on the IFN signalling pathway. In short, the pathway is initiated by the binding of type I (IFN-α/IFN-β) or type II (IFN-γ) interferons to their respective receptors. This induces the activation of the Jak/Stat signalling pathway and leads to the expression of interferon regulated genes (IRGs). After *in vivo* irradiation *Stat1* (signal transducer and activator of transcription 1) is significantly upregulated, as well as the interferon regulated genes *Ifit1bl1*, *Oas1a*, *Isg15* and *Ifit3* (Der et al., 1998; Fensterl and Sen, 2015; Pulit-Penaloza et al., 2012; Zhang and Zhang, 2011) (Figure 22 C). *In vitro* irradiation leads to an upregulation of *Stat1*, *Stat2*, *Irf1* and the interferon regulated genes *Tap1*, *Ifit1bl1*, *Oas1a*, *Isg15* and *Ifit3* (Min et al., 1998) (Figure 22 D). The canonical signalling pathways are designed by IPA on the basis of literature findings. However, they do not cover all interactions of each molecule but rather show a selection of well-described interactions. Therefore, not all genes which are regulated by IFNs are displayed in this figure. But since the results indicate that LDI activates the IFN signalling pathway and induces IRG expression, the identification of IRGs in the *in vivo* and *in vitro* datasets was subject of the following analyses.

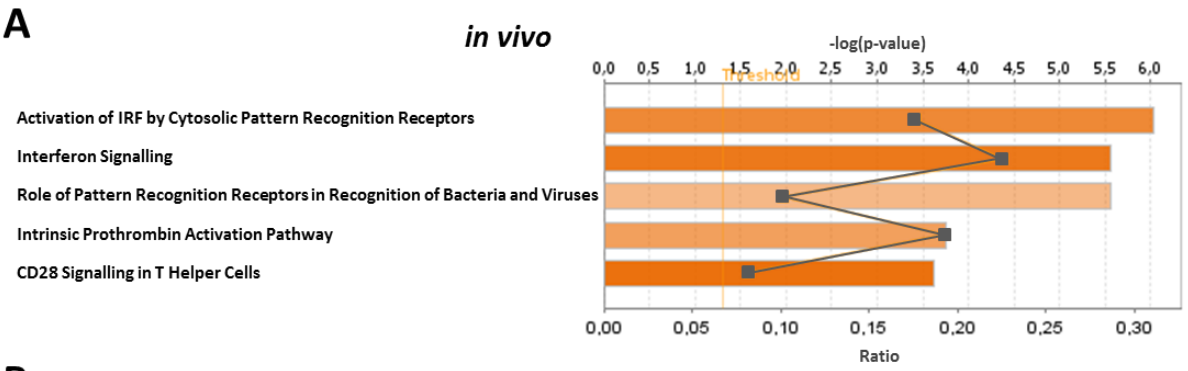

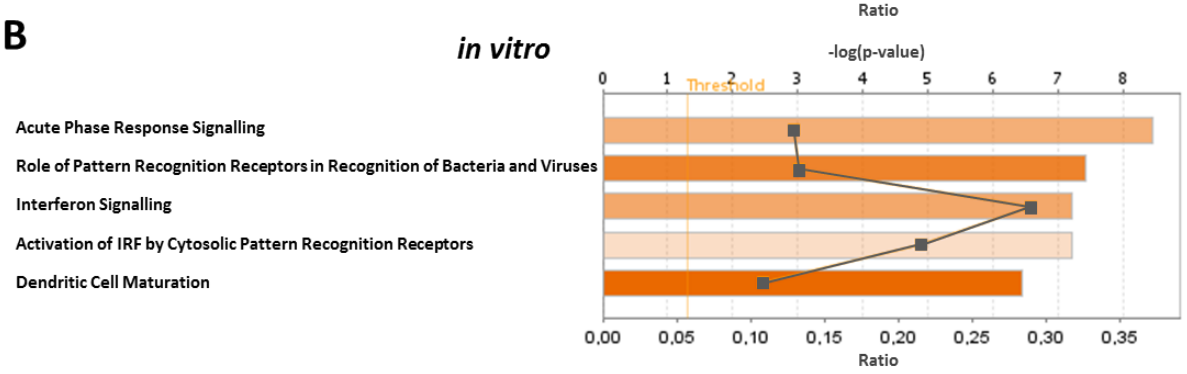

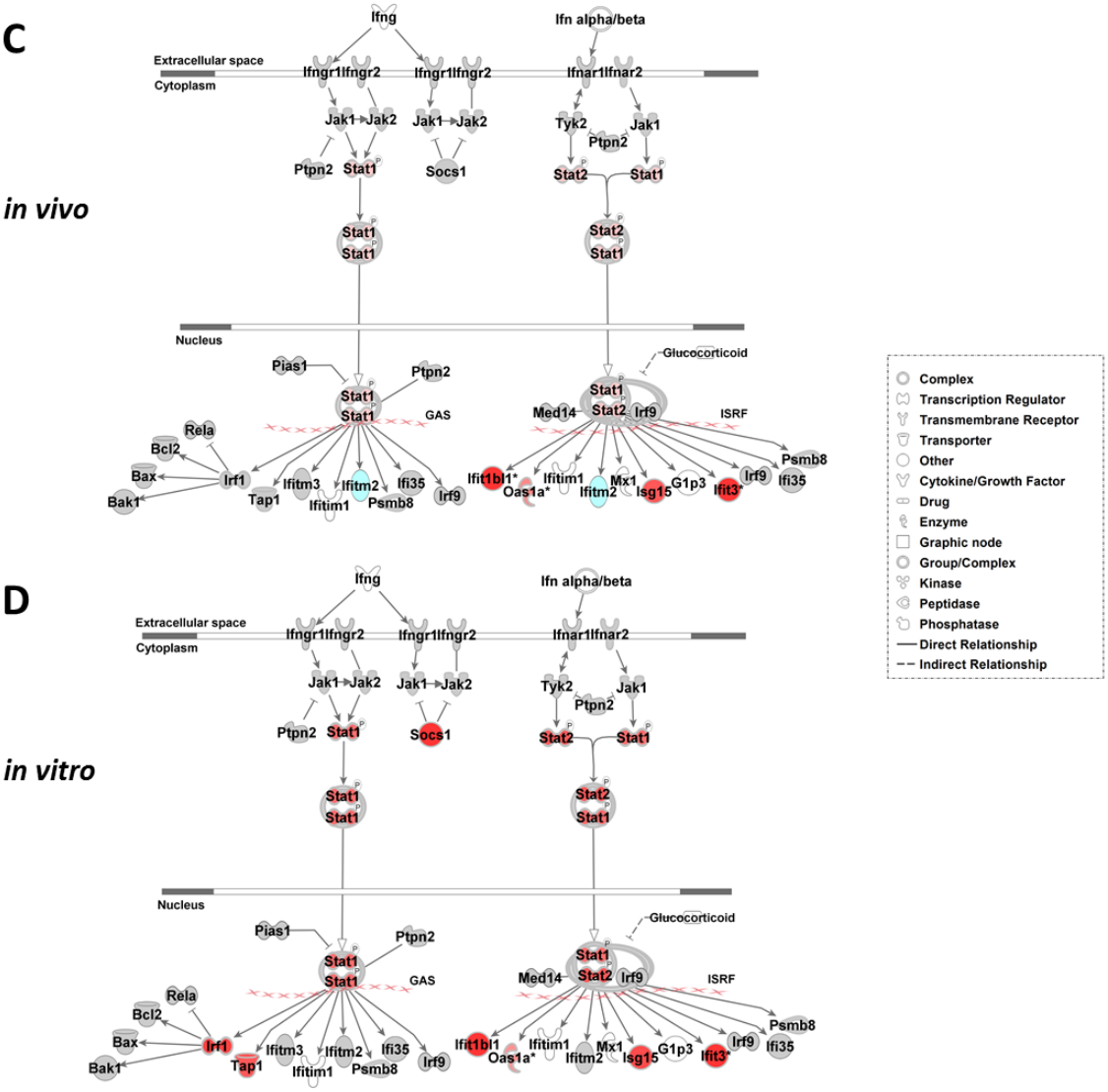

Figure legend on the next page

Figure 22 Canonical pathways predicted to be activated by LDI
Top 5 canonical pathways, predicted to be activated by A) *in vivo* or B) *in vitro* irradiation with an activation z-score ≥ 0.9 and an overlap p-value <0.001. The colour intensity of the bars indicates the activation z-score (0.9 - 4); the height of the bars represents the overlap p-value (upper axis; -log(p-value)) which was calculated by IPA using the right-tailed Fisher`s Exact test. The threshold line represents the p-value cut-off set at 0.05. (IPA default setting); the second line represents the ratio between the DEGs from the dataset that map to the pathway and the total number of genes in the pathway (lower axis labelled; 'Ratio'). C, D) Interferon signalling pathway with DEGs from the C) *in vivo* or D) *in vitro* dataset highlighted by coloured fillings. The colour intensity indicates the level of gene expression, with tones of red representing increased and tones of blue decreased gene expression (FC values). In grey, genes that did not pass the threshold of FDR <0.05, FC ≥ |1.5|; in white, genes that were not present in the dataset. Relationships between molecules are denoted by solid (direct) or dashed lines (indirect); Molecule types are described in the legend. A-D) Generated by analysis of all DEGs using IPA.

2.7.5. Effect of LDI on the expression of IRGs

Pathway analysis of the DEGs revealed a role of IFN signalling in irradiated peritoneal macrophages. This indicates that LDI induces the expression of IRGs. To identify IRGs in the *in vivo* and *in vitro* dataset, the Interferome database was employed. Interferome is a searchable database, containing published datasets with expression data of genes differentially expressed after treatment with different types and concentrations of IFNs allowing the retrieval and comparison of IFN-specific transcriptional modulation. To obtain further information about the direction of gene expression regulation in the *in vivo* and *in vitro* dataset, up- and downregulated genes were analysed separately (Figure 23). Comparison analysis with the Interferome database aimed to identify genes that are commonly regulated by IFN as well as by *in vivo* and/or *in vitro* irradiation. Therefore, the database was searched for the genes up (Figure 23 A) or downregulated (Figure 23 B) after *in vivo* and/or *in vitro* irradiation.
Of the 245 genes significantly upregulated after *in vivo* irradiation, more than half (54.7 %) were identified as IRGs. 48.2 % were reported to be upregulated by IFN treatment according to the Interferome database, revealing a high consistency between IFN stimulation and *in vivo* irradiation. Similarly, of the genes significantly upregulated after *in vitro* irradiation (n=466), 48.7 % have been identified as IRGs, and 42.3 % are positively regulated by IFN. The overlap between IFN-induced gene expression and *in vivo* or *in vitro* irradiation-induced gene expression was even higher in the commonly upregulated gene set. Here, 72.8 % of the 92 genes were identified as IRGs, the majority (71.7 %) being upregulated by IFN. Less than a third (27.2 %) of the shared upregulated genes is not regulated by IFNs. The proportion of IRGs in the genes downregulated after *in vivo* or *in vitro* irradiation is lower compared to the relative number of IRGs found in the upregulated gene sets. 35.8 % of the genes downregulated by *in vivo* irradiation are considered IRGs, according to the Interferome database. 27.9 % are reported to be downregulated by IFNs, while 7.9 % are upregulated by IFNs. *In vitro* irradiation led to 43 significantly downregulated genes (Figure 23 B), the vast majority of which (76.7 %) are not affected by IFN treatment. 6.98 % of these genes show higher and 16.3 % lower expression after IFN treatment. In summary, many genes were identified that are transcriptionally regulated in the same direction by LDI and IFN stimulation with a very high target overlap between LDI and IFN treatment, demonstrating that LDI and IFNs similar-

ly affect gene expression. This strongly suggests that LDI-induced gene expression changes in macrophages are (at least in part) mediated through IFN signalling.

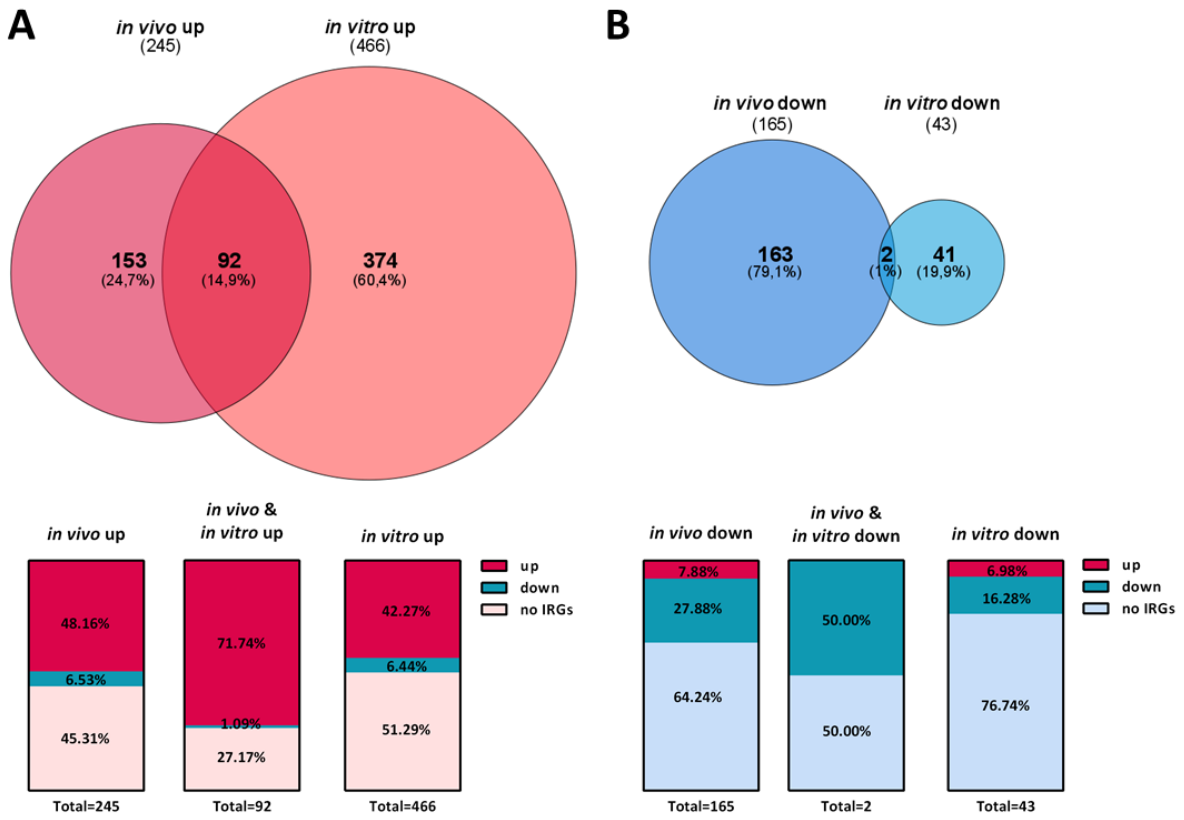

Figure 23 LDI-mediated increase in interferon regulated genes among the DEGs in PECs
Identification of interferon regulated genes (IRGs) in *in vivo* or *in vitro* up- or downregulated DEGs using the Interferome database. Upper panel: Venn diagrams showing the overlap in A) upregulated B) downregulated genes after *in vivo* and *in vitro* irradiation. Lower panel: A) Percentages of IRGs in genes upregulated after *in vivo*, after *in vivo* and *in vitro*, after *in vitro* irradiation (from left to right). B) Percentage of IRGs in all DEGs downregulated after *in vivo*, after *in vivo* and *in vitro*, after *in vitro* irradiation (from left to right). The light red/blue shaded segments represent genes not regulated by interferons. The dark red/blue segments show the percentage of genes identified as IRGs. In dark red, genes upregulated and in dark blue, genes downregulated after IFN treatment. FC ≥ |1.5|, FDR <0.05

2.7.6. Activation of the iNOS signalling pathway in irradiated PECs

As shown previously, iNOS activity is essential for endothelial activation, T cell and macrophage infiltration, as well as tumour rejection in RT5 mice following local LDI and adoptive T cell transfer. It is further known that the expression of *Nos2*, the gene encoding iNOS, is upregulated in macrophages by type I or type II IFNs (Diefenbach et al., 1998; Farlik et al., 2010) through Jak/Stat-mediated upregulation of *Irf1,* a transcription factor that induces *Nos2* expression (Figure 24) (Kamijo et al., 1994). Based on the findings that several of the genes upregulated by LDI could be linked to an activated IFN signalling pathway (Figure 24) and since IFN signalling can induce *Nos2* gene expression it was assumed that irradiation could also affect expression levels of *Nos2.* Analysis of the transcriptome data further strength-

ened this hypothesis. A 55.6-fold upregulation of *Nos2* was observed after *in vitro* irradiation. Additional evidence was provided by significant upregulation of the IFN signalling-associated genes: *Jak1* (FC: 1.8) and *Jak2* (FC: 2.3) (FDR>0.05), as well as *Stat1* (FC: 4.1), *Stat2* (FC: 4.99) and *Irf1* (FC: 6.2). After *in vivo* irradiation *Stat1* (FC: 1.6) and *Stat2* (FC: 1.7) were significantly upregulated (Table 10). Figure 24 shows the iNOS signalling pathway with the DEGs from the *in vivo* (A) and the *in vitro* (B) dataset highlighted in red.

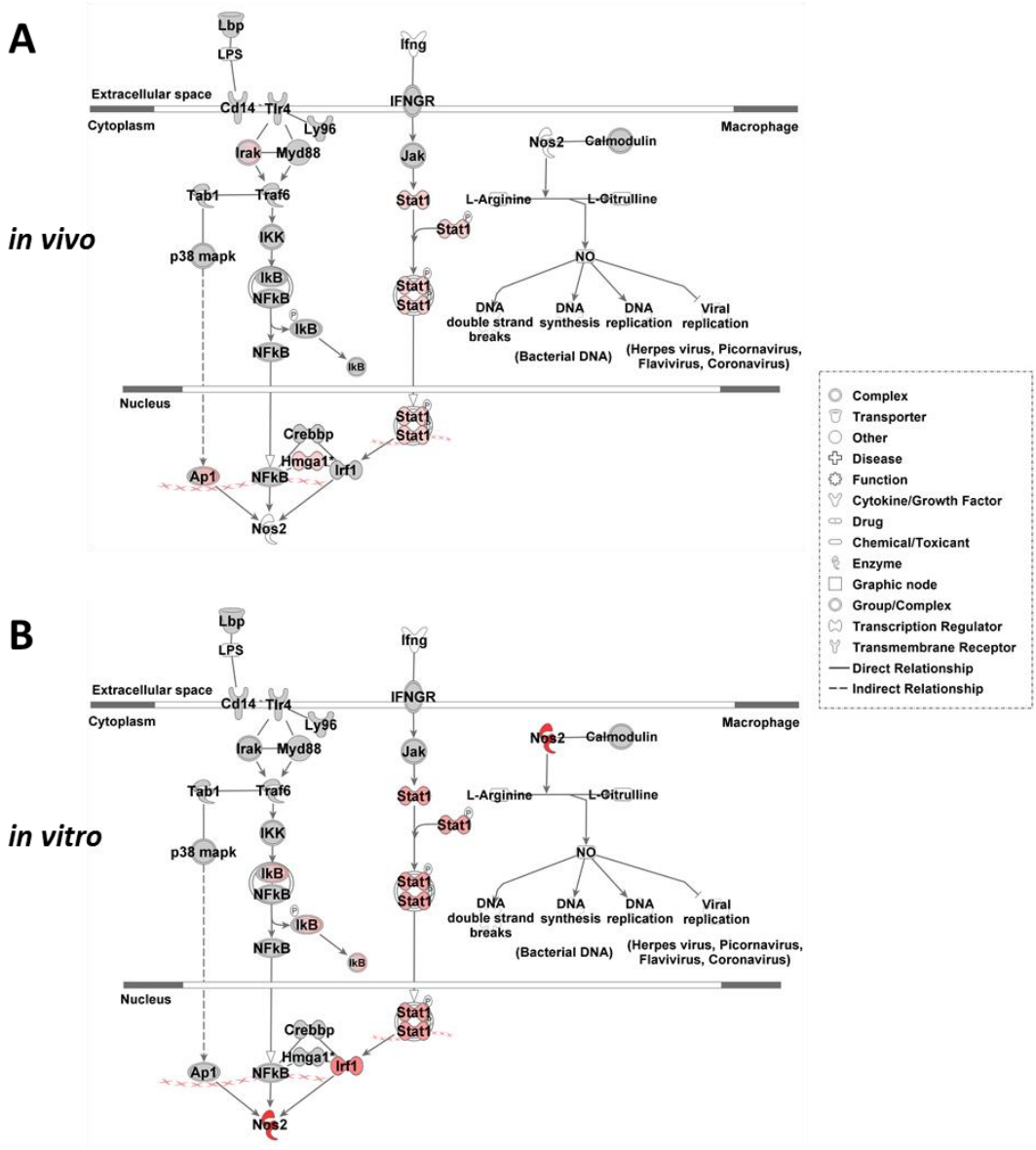

Figure 24 LDI-induced upregulation of iNOS signalling pathway- associated genes in PECs
iNOS signalling pathway, with genes highlighted in red that were significantly upregulated after A) *in vivo* or B) *in vitro* irradiation. The colour intensity corresponds to the degree of differential expression. In grey, genes that did not pass the threshold of FDR <0.05, FC ≥ |1.5|; in white, genes that were not present in the dataset. Relationships between molecules are represented by solid (direct) or dashed lines (indirect); Molecule types and functions are described in the legend. Generated by analysis of all DEGs using IPA.

Table 10 LDI-induced expression changes in iNOS signalling-associated genes.

Gene Symbol	FC (*in vivo*)	FDR (*in vivo*)	FC (*in vitro*)	FDR (*in vitro*)	Description
Ifng	**NA**	**NA**	**NA**	**NA**	**Interferon gamma**
Jak1	**1.078**	**0.701**	**1.778**	**0.172**	**Janus kinase 1**
Jak2	**1.069**	**0.951**	**2.302**	**0.089**	**Janus kinase 2**
Stat1	**1.628**	**0.043**	**4.073**	**0.009**	**signal transducer and activator of transcription 1**
Stat2	**1.715**	**0.000**	**4.993**	**0.008**	**signal transducer and activator of transcription 2**
Irf1	**1.357**	**0.367**	**6.229**	**0.011**	**interferon regulatory factor 1**
Nos2	**NA**	**NA**	**55.561**	**0.001**	**nitric oxide synthase 2, inducible**

Presented are the FC and FDR values from the *in vivo* and *in vitro* dataset. Significantly upregulated genes (FDR <0.05, FC ≥ |1.5|) are highlighted in tones of red, with the colour intensity indicating the level of gene expression.

To further examine the role of LDI in the activation of the IFN-γ signalling pathway and subsequent induction of *Nos2* gene expression, mRNA expression levels of *Ifng*, *Jak1*, *Stat1*, *Irf1* and *Nos2* were analysed by RT-qPCR in PECs from C3H mice that received the same treatment protocol as in previous experiments (Figure 15). Briefly, C3H wt mice received 2 Gy TBI on day 0, followed by thioglycolate injection on the next day. 3 days later, PECs were collected by peritoneal lavage (*in vivo*). Thioglycolate-elicited PECs from C3H wt mice were isolated by peritoneal lavage on day 0, irradiated *ex vivo* on the same day and cultured for 72 hrs at 37°C (*in vitro*). RNA was isolated from the collected PECs and analysed by RT-qPCR. Though it was not detected by RNA Sequencing, *Ifng* was included in the following experiments, as RNA sequencing can be less sensitive compared to RT-qPCR, especially at low read depths (Consortium, 2014). *Ifng*, *Stat1* and *Nos2* were significantly upregulated after *in vivo* and *in vitro* irradiation. *Irf1* was found to be upregulated only after *in vitro* irradiation, but not after *in vivo* irradiation, whereas *Jak1* expression levels were not affected by LDI (Figure 25 B). Together, these results confirm that LDI leads to the upregulation of *Nos2* gene expression and suggest that this is mediated by IFN-γ signalling.

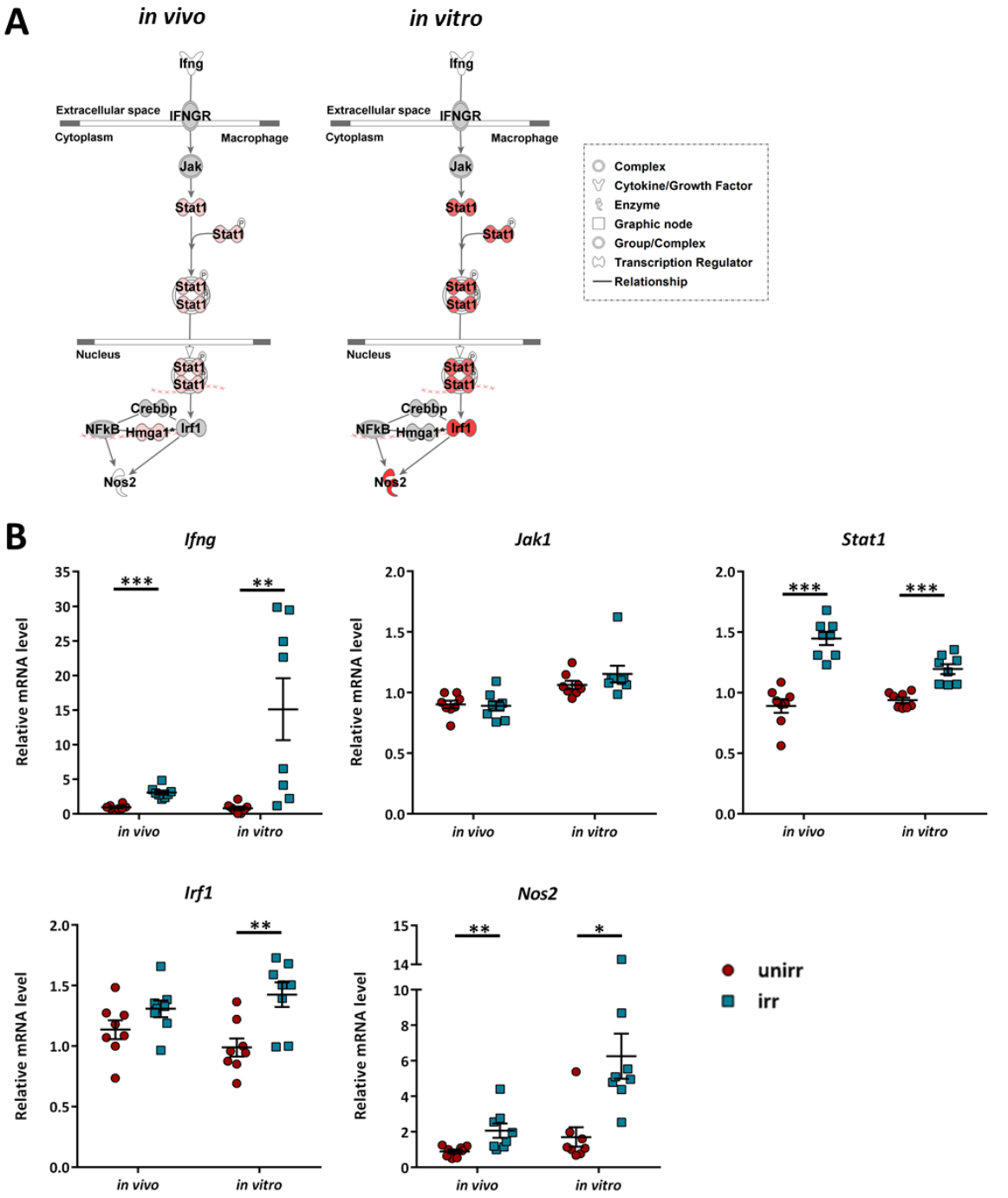

Figure 25 The effect of LDI on the expression of IFN-γ/iNOS signalling pathway-genes

A) IFN-γ/iNOS signalling pathway, with genes that were significantly upregulated after *in vivo* or *in vitro* LDI highlighted in red, as determined by RNA Sequencing. B) RT-qPCR validation of selected genes from the IFN-γ/iNOS signalling pathway. *In vivo*: thioglycolate-elicited PECs were derived from C3H mice that were subjected to 2 Gy TBI. *In vitro*: thioglycolate-elicited PECs were irradiated *ex vivo* with 2 Gy and cultured for 72 hrs. RNA isolated from the peritoneal cells was analysed by RT-qPCR. The graphs show *Ifng*, *Jak1*, *Stat1*, *Irf1* and *Nos2* gene expression levels, relative to an unirradiated control sample. The gene expression values were normalized to a reference gene (*Hprt* (hypoxanthine guanine phosphoribosyl transferase)) according to the $\Delta\Delta C_t$ method. Data is shown as mean ± SEM; * p<0.05; ** p<0.01; *** p<0.001 (n=8 mice per group; *in vivo*: two-tailed Mann-Whitney test; *in vitro*: paired, two-tailed t-test (SAS))

To assess whether the underlying mechanism of LDI-induced *Nos2* expression is dependent on IFN-γ signalling, *Nos2* mRNA levels were measured in *ex vivo* irradiated PECs under IFN-γ blockage (Figure 26 A). Since *Nos2* gene expression can also be induced by type I IFNs (Mattner et al., 2000), the effect of blocking IFN-β alone or in combination with IFN-γ inhibition on LDI-induced gene expression was analysed as well. PECs from C3H wt mice were irradiated *ex vivo* in medium containing neutralizing antibodies against IFN-γ, IFN-β or both. After culture for 48 or 72 hrs, the samples were analysed for *Ifng*, *Jak1*, *Stat1*, *Irf1* and *Nos2* gene expression (Figure 26 A). As a positive control, unirradiated PECs were treated with 20 ng/ml IFN-γ. *Ifng*, *Irf1* and *Nos2* mRNA levels were found to be increased by LDI after 48 hrs and 72 hrs. *Stat1* expression was also induced by LDI after 72 hrs and inhibition by anti-IFN-γ or anti-IFN-β clearly attenuated the effect of LDI as compared to the unirradiated control. *Jak1* gene expression was neither affected by LDI, the neutralizing antibodies or IFN-γ stimulation, indicating that it is regulated at a translational rather than the transcriptional level (Figure 26 C). Together, these results demonstrate that LDI-induced gene regulation of *Ifng*, *Jak1*, *Stat1*, *Irf1* and *Nos2* in peritoneal macrophages is dependent on IFN signalling. This indicates that the effects of LDI on peritoneal macrophages are (at least partly) mediated by IFNs.

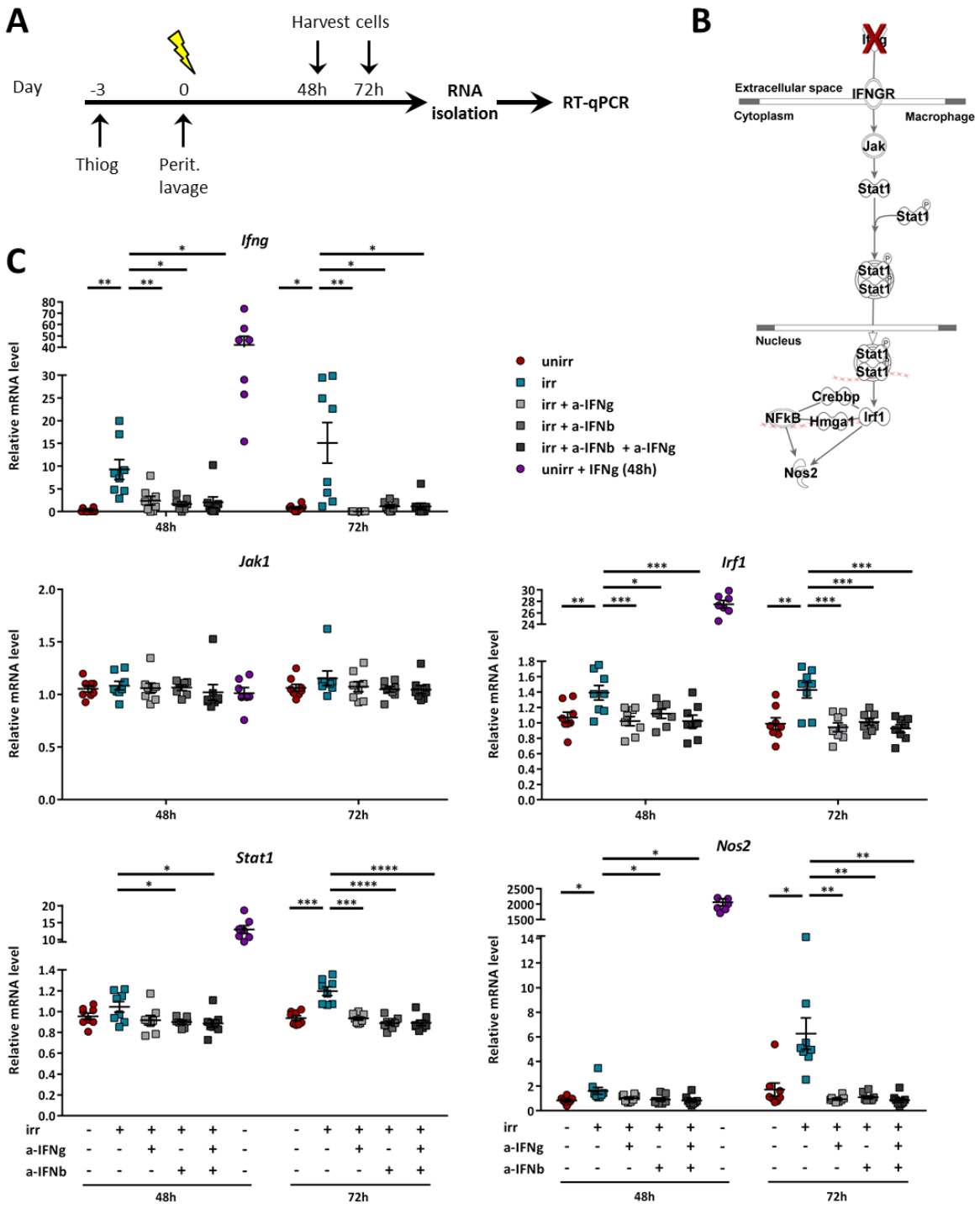

Figure 26 The impact of IFN signalling blockade on gene expression in low dose irradiated PECs
Gene expression in *in vivo* or *in vitro* irradiated PECs under blockade of IFN-γ or IFN-β. A) Experimental setup: thioglycolate-elicited PECs were collected from C3H wt mice by peritoneal lavage, irradiated *ex vivo* and cultured at 37°C in medium only, in medium containing anti-IFN-γ mAb, anti-IFN-β mAb or both for the indicated times. Control samples were not irradiated and cultured in medium only or medium containing IFN-γ (20 ng/ml). RNA was isolated for RT-qPCR analysis. B) Proposed effect: antibody neutralization of IFN-γ is expected to inhibit LDI-induced upregulation of genes in the IFN-γ/iNOS signalling pathway. C) RT-qPCR analysis of genes in the IFN-γ/iNOS signalling pathway: *Ifng*, *Jak1*, *Stat1*, *Irf1* and *Nos2* gene expression levels, relative to an unirradiated control sample. The gene expression values are normalized to *Hprt*, according to the $\Delta\Delta C_t$ method. Data shown as mean ± SEM; * p<0.05; ** p<0.01; *** p<0.001; **** p<0.0001 (n=8 mice per group; Paired, two-tailed t-test (SAS))

2.7.7. LDI affects macrophage polarization

Since *Nos2* expression is induced by LDI, it seemed likely that iNOS protein levels were increased as well. To examine whether the upregulation in gene expression is accompanied by an increase in iNOS protein levels, *in vivo* and *in vitro* irradiated PECs were analysed for iNOS by flow cytometry. As reviewed in the introduction, M1-like macrophages have been shown to exert antitumouricidal effects while M2-like macrophages are capable to promote tumour progression. To ascertain the effect of LDI on the polarization state of the peritoneal macrophages, which were used for the transfer experiments, PECs were stained for the polarization markers iNOS, MHC class II, and CD206. iNOS and MHC class II have been described to be M1 and CD206 has been describe to be an M2 marker (Lawrence and Natoli, 2011). As before, *in vivo* irradiated PECs were derived from C3H wt mice subjected to 2 Gy TBI. *In vitro* irradiated PECs were derived from unirradiated C3H wt mice, irradiated *ex vivo* and cultured for 24, 48 or 72 hrs (Figure 27 A).

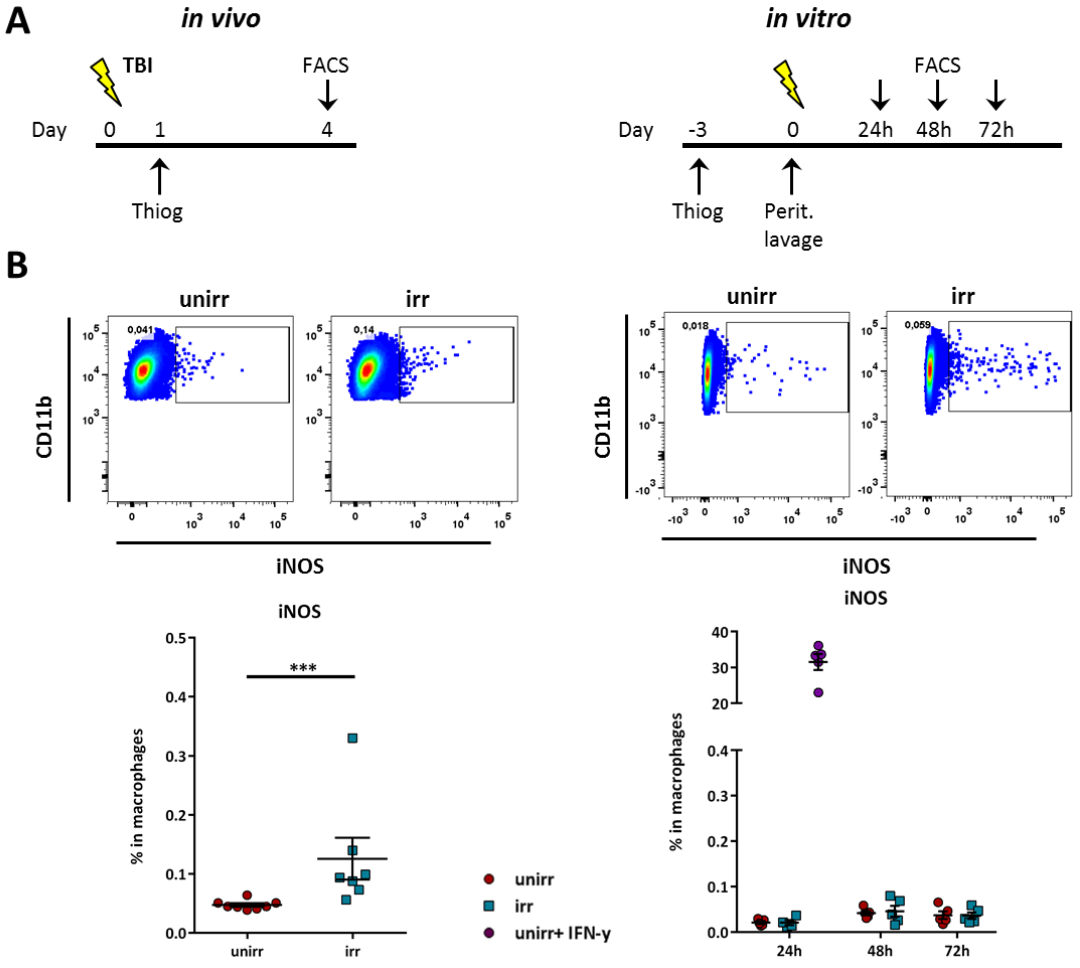

Figure continues on the next page

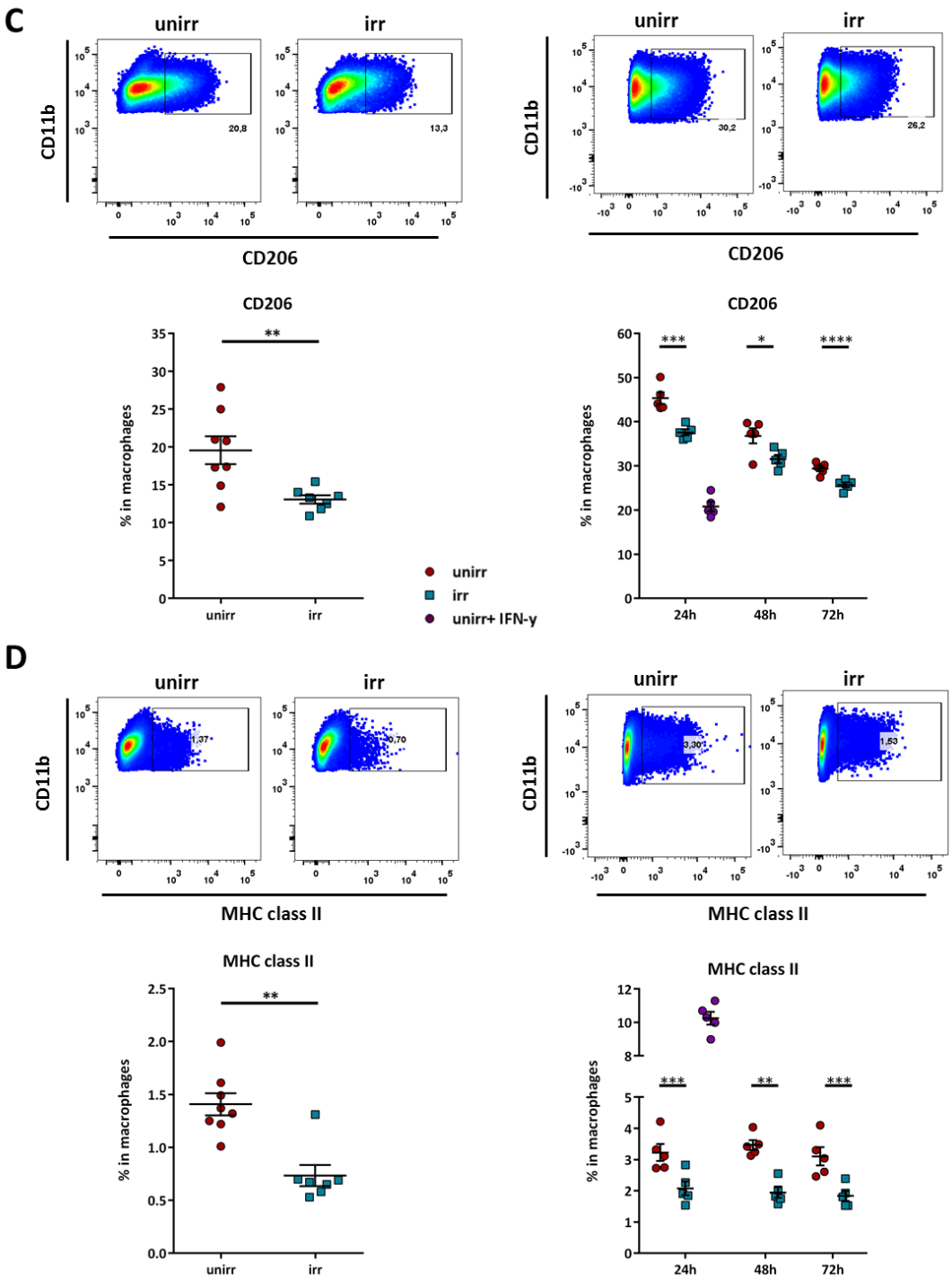

Figure 27 Effects of LDI on macrophage polarization

Flow cytometric analysis of *in vivo* or *in vitro* irradiated peritoneal macrophages for macrophage polarization markers (iNOS, MHC class II, CD206). A) Experimental setup *In vivo*: thioglycolate-elicited peritoneal macrophages from unirradiated C3H wt mice or C3H wt mice, subjected to 2 Gy TBI, were collected for flow cytometry on day 4 by peritoneal lavage. *In vitro*: thioglycolate-elicited peritoneal macrophages from C3H wt mice were harvested on day 0 by peritoneal lavage, irradiated *ex vivo* with 2 Gy and analysed after 24, 48 and 72 hrs in culture. Unirradiated PECs were cultured in medium only or in medium containing 20 ng/ml IFN-γ. Representative dot plots and quantitative analysis of B) iNOS^{+}, C) CD206^{+} and D) MHC class II^{+} macrophages (CD11b^{hi}F4/80^{+}). Only single, viable cells were included in the analysis. Data shown as mean ± SEM; * p<0.05; ** p<0.01; *** p<0.001; **** p<0.0001 (*in vivo*: n=8 mice per group, two-tailed Mann-Whitney test; *in vitro*: n=5 with cells pooled from 2 mice per sample, Paired two-tailed t-test (SAS)).

After *in vivo* irradiation, a significantly increased number of macrophages was positive for iNOS (0.05 versus 1.3 %), representing a 2.6-fold increase in irradiated PECs (Figure 27 B). *In vitro* irradiation did not lead to an increase in iNOS$^+$ macrophages. However, IFN-γ stimulation of unirradiated PECs strongly induced iNOS expression in macrophages demonstrating that peritoneal macrophages are capable of iNOS expression by direct IFN-γ stimulation (Figure 27 B). Flow cytometric analysis of CD206 expression revealed a significantly smaller fraction of CD206$^+$ (M2-like) macrophages after *in vivo* irradiation (13 % versus 20 %). *In vitro* irradiation reduced the number of CD206$^+$ cells already after 24 hrs (45 % versus 37 %), and further after 48 hrs (37 % versus 31 %). This effect was further sustained throughout 72 hrs (29 % versus 26 %) in culture, but the relative difference in CD206 protein expression decreased. IFN-γ stimulation also reduced CD206 expression (20 % CD206$^+$ macrophages). Overall, the levels of CD206 in cultured PECs are higher compared to freshly isolated PECs (Figure 27 C), but irrespective of the treatment conditions, LDI consistently reduced CD206 expression on peritoneal macrophages.

Interestingly, the MHC class II expression level on macrophages was slightly but significantly reduced after *in vivo* (1.4 % versus 0.7 %) and *in vitro* irradiation (3 % versus 2 %) (Figure 27 D). IFN-γ stimulation, on the other hand, induced the expression of MHC class II which is in agreement with the literature (Giroux et al., 2003). Also, at the mRNA level it was observed that LDI causes the downregulation of MHC class II genes. RNA sequencing results revealed that most MHC class II genes were significantly downregulated in peritoneal cells after *in vivo* irradiation (Table 11). *In vitro* irradiation did not induce significant gene expression changes of MHC class II genes. All in all, these results indicate that LDI does affect macrophage polarization. However, it does not induce a clear shift towards an M1 or M2-like phenotype.

Table 11 Gene expression changes of MHC class II genes after *in vivo* or *in vitro* irradiation.

Gene Symbol	FC (in vivo)	FDR (in vivo)	FC (in vitro)	FDR (in vitro)	Description
H2-Aa	-2.84	0.000	1.03	0.984	histocompatibility 2, class II antigen A, alpha
H2-Ab1	-2.45	0.000	1.99	0.465	histocompatibility 2, class II antigen A, beta 1
H2-Ea-ps	-2.41	0.000	1.77	0.564	histocompatibility 2, class II antigen E alpha, pseudogene
H2-Eb1	-2.49	0.000	1.10	0.934	histocompatibility 2, class II antigen E beta
H2-Eb2	-2.75	0.777	NA	NA	histocompatibility 2, class II antigen E beta2
H2-DMa	-2.01	0.000	1.83	0.390	histocompatibility 2, class II, locus Dma
H2-DMb1	-1.71	0.005	1.31	0.638	histocompatibility 2, class II, locus Mb1
H2-DMb2	-1.68	0.045	1.32	0.654	histocompatibility 2, class II, locus Mb2
H2-Oa	-2.07	0.421	5.18	0.148	histocompatibility 2, O region alpha locus
H2-Ob	-3.30	0.000	NA	NA	histocompatibility 2, O region beta locus
Ciita	-1.81	0.027	4.51	0.169	class II transactivator

Presented are the FC and FDR values from the *in vivo* and *in vitro* dataset. Significantly downregulated genes (FDR <0.05, FC ≥ |1.5|) are highlighted in tones of blue, with the colour intensity indicating the level of gene expression.

2.7.8. IFN-dependent upregulation of *Tnf* after LDI

One major factor responsible for failure of adoptive T cell therapy is the aberrant tumour vasculature. Although normalization of the tumour blood vessels in RT5 tumours after combination therapy was partly dependent on iNOS activity (Figure 7, Figure 8), it is unclear which additional factors might be involved. TNF-α is a known activator of endothelial cells (McHale et al., 1999) and it is produced by activated macrophages (Flynn et al., 1995) and $CD8^+$ T cells (Vassalli, 1992). According to the RNA sequencing results, *in vivo* irradiation led to a 2.43-fold increase in *Tnf* gene expression, while *in vitro* irradiation resulted in a 1.45-fold increase. These changes were not considered to be significant, since the FDR values were >0.05. Nevertheless, this trend was further investigated, because RT-qPCR is can be more sensitive than RNA sequencing. A 1.7-fold increase in *Tnf* mRNA levels was observed after *in vivo* irradiation (Figure 28 A). *In vitro* irradiation, as well as IFN-γ stimulation, also induced *Tnf* expression. Here, the upregulation of *Tnf* was more pronounced 48 hrs after irradiation compared to 72 hrs. Furthermore, blocking IFN-γ, IFN-β or both abrogates the upregulation of *Tnf* induced by LDI after 48 hrs, demonstrating that LDI induces *Tnf* expression in an IFN-dependent manner (Figure 28 B). These results suggest that TNF-α, together with NO, mediates LDI-induced endothelial activation in RT5 tumours.

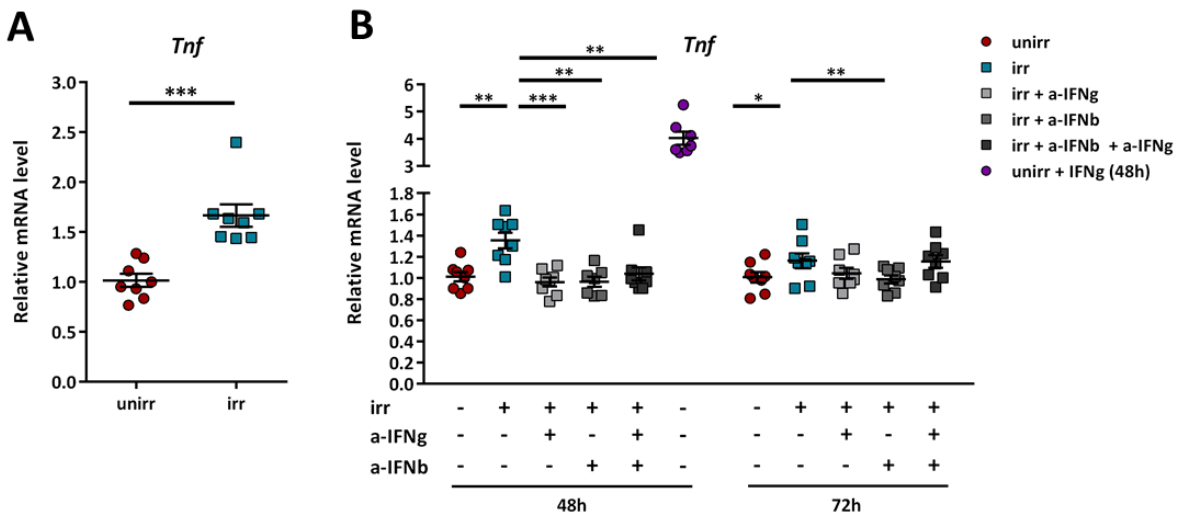

Figure 28 The role of IFNs on LDI-induced *Tnf* gene expression in PECs
Tnf gene expression in PECs after A) *in vivo* irradiation or B) *in vitro* irradiation under blockade of IFN-γ, IFN-β or both (experimental setup, see Figure 26 A) based on RT-qPCR analysis. The graphs show *Tnf* gene expression levels for the indicated treatment groups, relative to the respective unirradiated control samples. The gene expression values were normalized to *Hprt*, according to the $\Delta\Delta C_t$ method. Data shown as mean ± SEM; * p<0.05; ** p<0.01; *** p<0.001 (n=8 mice per group; *in vivo* (A): two-tailed Mann-Whitney test; *in vitro* (B): Paired, two-tailed t-test (SAS)).

2.7.9. Upstream regulators of low dose irradiation in PECs

After assessing the downstream processes induced by LDI, next we wanted to investigate the factors which are responsible for the gene expression changes following LDI, to further elucidate the underlying mechanisms. To this end, the Upstream Regulator Analysis by IPA was employed. By calculating the overlap between all the target genes regulated by a particular molecule and the genes of a dataset, IPA identifies potential upstream regulators (IPA). Based on the expression data, IPA additionally predicts the activation state of the transcriptional regulators, indicated by the activation z-score. Upstream regulators predicted to be activated by *in vivo* and *in vitro* LDI included IFN-associated proteins and proteins involved in the detection of danger signals, as well as their ligands (Table 12, Table 13, Table 14)

2.7.9.1. IFN-response molecules predicted to be upstream regulators

Corresponding to the finding that the effects of LDI are mediated by IFN signalling, the Upstream Regulator Analysis by IPA identified several proteins which are associated with IFN signalling to be upstream regulators, including type I (IFN-α and IFN-β1) and type II (IFN-γ) interferons, as well as the IFN regulating factors IRF3, 5 and 7 and STAT1 (Table 12). To visualize the relationships between the upstream regulator and the downstream target genes, IPA generates interaction networks. As an example, Figure 29 displays the upstream regulator network of IRF7. Some of the upstream regulators, like IRF7 and STAT1, were identified to be upregulated in PECs after LDI by RNA Sequencing. *Irf7* expression was 3.76-fold increased after *in vivo* irradiation and 14.1-fold after *in vitro* irradiation. Independent RT-qPCR experiments confirmed LDI-mediated upregulation of *Stat1* (Figure 25) and *Irf7* (Figure 30). *Irf7* expression was strongly induced by *in vivo* irradiation, with a fold change of 3.5, while the effects of *in vitro* irradiation on *Irf7* expression were less pronounced with a modest upregulation after 72 hrs. Inhibition of IFN-γ, IFN-β or both suppressed the upregulation of *Irf7* expression induced by LDI after 72 hrs, showing that the increased *Irf7* expression in PECs after LDI is dependent on IFNs. Taken together, these results further support previous observations that LDI induces IFN-responses and thereby exerts its effects.

Table 12 IPA Upstream regulators (IFN signalling)

Upstream regulator	*in vivo*	*in vitro*
IRF3	**5.63**	**6.01**
IRF7	**5.47**	**5.73**
IRF5	**4.17**	**3.93**
IFN-γ	**4.09**	**7.67**
IFN-α	**4.95**	**5.88**
IFN-β1	**3.76**	**5.16**
STAT1	**3.50**	**4.47**

Upstream regulators, associated with IFN signalling, predicted by IPA to be activated in PECs after *in vivo* or *in vitro* LDI. Activation z-score ≥ |2|; p-value <0.0001 considered significant.Table 29 lists the DEGs of the two datasets for each Upstream regulator.

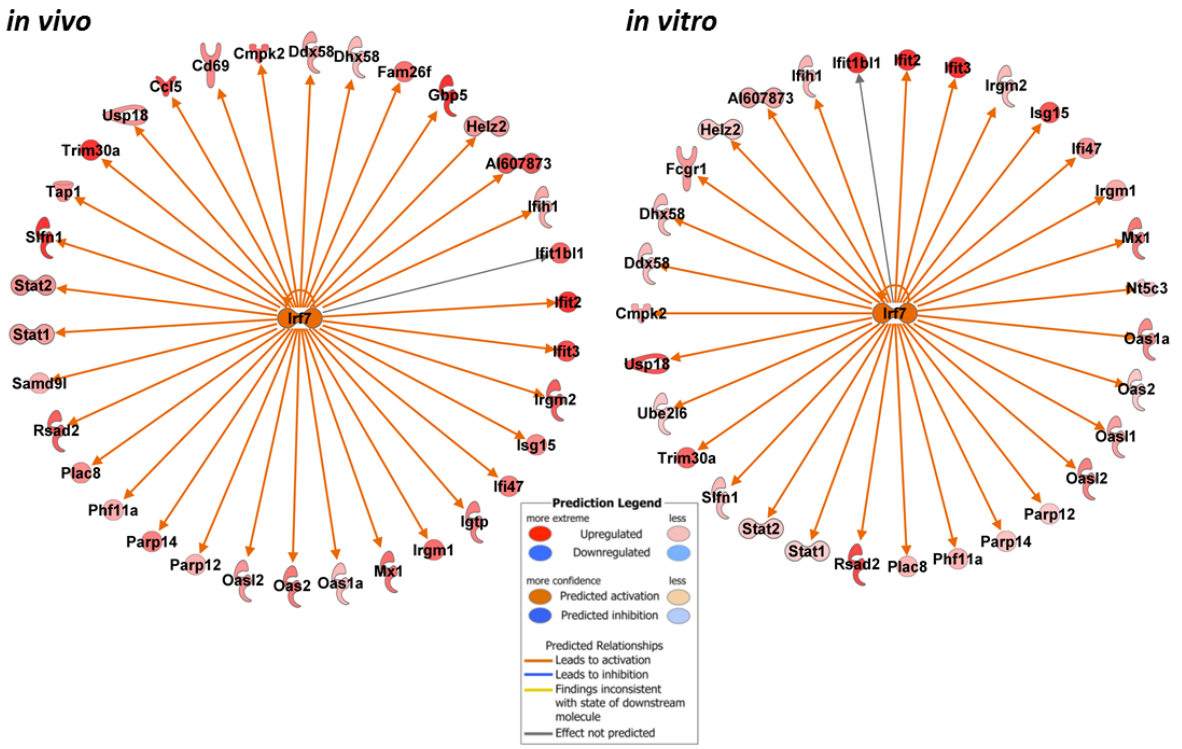

Figure 29 IRF7 – Upstream regulator network of DEGs

Interaction network displaying IRF7 with its downstream target genes from the A) *in vivo* or B) *in vitro* irradiation dataset. Upregulated DEGs are highlighted in tones of red with the colour intensity corresponding to the degree of differential expression. Relationships between molecules are represented by solid lines (direct) with the colour indicating the predicted action: orange - activation; grey -not predicted. Networks generated by IPA.

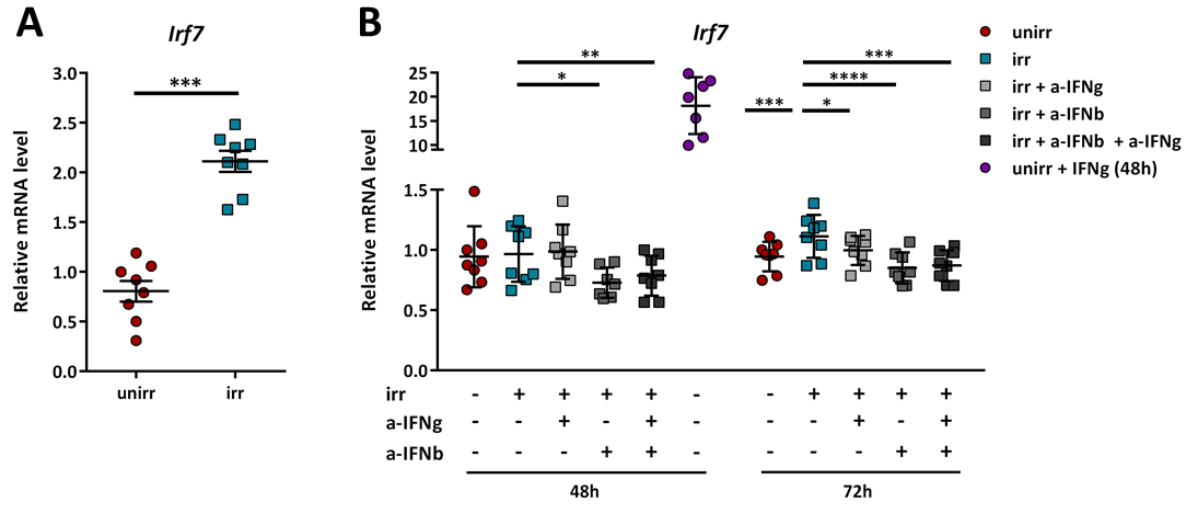

Figure 30 IFN-dependent upregulation of *Irf7* expression in low dose irradiated PECs

Irf7 gene expression in PECs after A) *in vivo* irradiation or B) *in vitro* irradiation under blockade of IFN-γ, IFN-β or both (experimental setup, see Figure 26 A) based on RT-qPCR analysis. All graphs show *Irf7* gene expression levels for the indicated treatment groups, relative to the respective unirradiated control samples. The gene expression values are normalized to *Hprt*, according to the $\Delta\Delta C_t$ method. Data shown as mean ± SEM; * p<0.05; ** p<0.01; *** p<0.001; **** p<0.0001 (n=8 mice per group; *in vivo* (A): two-tailed Mann-Whitney test; *in vitro* (B): paired, two-tailed t-test (SAS)).

2.7.9.2. DNA damage response molecules predicted to be upstream regulators

Besides the upstream regulators associated with IFN signalling, two other groups of upstream regulators were prominent. Table 13 shows TLR agonists like LPS, poly I:C (Polyinosinic:polycytidylic acid), CpG oligonucleotides and Resiquimod, which were identified to be potential upstream activators. In line with that, the upstream regulators shown in Table 14 are proteins involved in the detection of danger and pattern associated molecular patterns (DAMPs and PAMPs) like the Toll-like receptors (TLR) 3, 7 and 9 which are sensors of endosomal nucleic acids. But also other pattern recognition receptors like the RLRs DDX58 (DEAD (Asp-Glu-Ala-Asp) box polypeptide 58; synonym RIG-1), IFIH1 (interferon induced with helicase C domain 1; synonym MDA5) and their adaptor molecules MAVS, TBK1 (TANK-binding kinase 1) and MYD88 were predicted to be transcriptional activators (Table 14). These results show that many of the predicted upstream regulators are involved in sensing cytosolic nucleic acids. Further analysis of the *in vivo* and *in vitro* datasets revealed that genes coding for sensors of cytosolic RNA or DNA are significantly upregulated after low dose irradiation: *Ifi204* (synonym *Ifi16*), *Zbp-1* (Z-DNA binding protein; synonym *Dai* (DNA-dependent activator of IRFs), *Dhx58* (DEXH (Asp-Glu-X-His) box polypeptide 58), *Ddx58*, *Ifih1*, *Ifit1bl1* (IFN-induced protein with tetratricpeptide repeats 1B like 1) a sensor of viral ssRNAs, and *Ifit3b* (adapter bridging TBK1 and MAVS) (Table 15).

Table 13 IPA Upstream regulators (TLR agonists)

Upstream regulator	*in vivo*	*in vitro*
LPS	**6.31**	**9.65**
poly I:C	**5.65**	**7.02**
CpG oligonucleotide	**1.24**	**4.45**
Resiquimod	**1.83**	**3.39**

TLR agonist upstream regulators predicted by IPA to be activated in PECs after *in vivo* or *in vitro* LDI. Activation z-score ≥ |2|; p-value <0.0001 considered significant. Grey shaded values are below the threshold. Table 31lists the DEGs of the two datasets for each Upstream regulator.

Table 14 IPA Upstream regulators (PRR signalling)

Upstream regulator	*in vivo*	*in vitro*
DDX58	**3.05**	**4.02**
MAVS	**4.23**	**4.07**
TBK1	**2.81**	**4.08**
IFIH1	**2.75**	**2.76**
TLR3	**4.94**	**6.16**
TLR7	**2.22**	**3.13**
TLR9	**4.53**	**6.01**
MYD88	**4.16**	**6.80**
TICAM1	**4.41**	**6.48**

Upstream regulators, associated with PRR signalling, predicted by IPA to be activated in PECs after *in vivo* or *in vitro* LDI. Activation z-score ≥ |2|; p-value <0.0001 considered significant. Table 32 lists the DEGs of the two datasets for each Upstream regulator.

Of note, IPA analysis predicted an activation of the canonical pathways 'Activation of IRF by Cytosolic Pattern Recognition Receptors' and 'Role of Pattern Recognition Receptors in Recognition of Bacteria and Viruses' by LDI (Figure 22 A). Together, these results strongly suggest that LDI leads to IFN signalling via the activation of Pattern Recognition Receptors.

Table 15 LDI-induced expression changes in PRR signalling-associated genes

Gene Symbol	FC (*in vivo*)	FDR (*in vivo*)	FC (*in vitro*)	FDR (*in vitro*)	Description
Ddx58	**1.970**	**0.000**	**4.263**	**0.009**	**DEAD (Asp-Glu-Ala-Asp) box polypeptide 58**
Dhx58	**2.097**	**0.000**	**2.860**	**0.050**	**DEXH (Asp-Glu-X-His) box polypeptide 58**
Ifi204	**2.382**	**0.000**	**3.792**	**0.013**	**interferon activated gene 204**
Ifih1	**2.081**	**0.000**	**3.620**	**0.013**	**interferon induced with helicase C domain 1**
Ifit1bl1	**12.588**	**0.002**	**10.021**	**0.027**	**IFN induced protein with tetratricpeptide repeats 1B like 1**
Ifit3b	**9.553**	**0.072**	**13.473**	**0.001**	**IFN-induced protein with tetratricopeptide repeats 3B**
Zbp1	**4.569**	**0.000**	**25.246**	**0.001**	**Z-DNA binding protein 1**

Presented are the FC and FDR values from the *in vivo* and *in vitro* dataset. Significantly upregulated genes (FDR <0.05, FC ≥ |1.5|) are highlighted in tones of red, with the colour intensity indicating the level of gene expression.

3. DISCUSSION

The efficacy of cancer immunotherapies is inhibited by the immunosuppressive characteristics of the tumour microenvironment. In therapies based on the adoptive transfer of T cells, complete responses are restricted to a subset of patients. The limited success of adoptive T cell therapy can be attributed to a non-permissive tumour microenvironment that restricts their access to the tumour site but also impairs T cell function. The process of T cell extravasation requires an activated endothelium which shows high expression levels of adhesion molecules. In many tumour entities, however, the vasculature is abnormal regarding its structure and function. For example, tumour endothelial cells express low levels of adhesion molecules, thereby forming a physical barrier to effector cell infiltration. On the other hand, the normalization of the tumour vasculature has been shown to enhance T cell infiltration (Huang et al., 2013) and, consequently, the efficacy of adoptive T cell therapy (Hamzah et al., 2008; Johansson et al., 2012). On this basis, it was suggested to combine adoptive T cell therapy with additional treatment modalities that reprogram the tumour microenvironment and overcome the tumour's intrinsic resistance mechanisms that interfere with T cell infiltration and function. Among them, radiotherapy represents a suitable candidate, as it stimulates antitumour immune responses, is capable of breaking the endothelial barrier and reduces immunosuppressive processes within tumours (Burnette and Weichselbaum, 2013; Soukup and Wang, 2015). The combination of irradiation with various cancer immunotherapies has already shown promising results in preclinical, as well as clinical studies (Kalbasi et al., 2013; Kwilas et al., 2012).

Previous work has investigated the combinatorial effects of radiotherapy and adoptive T cell transfer in the RT5 tumour mouse model, as the transfer of tumour-specific, *in vitro*-activated T cells alone was revealed to be insufficient to induce tumour immune rejection (Ganss et al., 2002; Klug et al., 2013). Moreover, adoptive T cell therapy may even reinforce immunosuppression as it was shown to induce intratumoural T_H2 cytokines when it was not combined with irradiation (Klug et al., 2013). On the other hand, in this, but also in other tumour mouse models, radiation was shown to enhance the efficacy of adoptively transferred T cells to reject solid tumours (Chakraborty et al., 2003; Ganss et al., 2002; Reits et al., 2006; Zhang et al., 2007). The doses used in these studies, however, were high (8-10 Gy) rendering the translation into a clinical setting problematic, since high radiation doses cause organ toxicities and, in severe cases, require bone marrow transplantation. As published by our group, low dose irradiation (2 Gy; LDI) combined with adoptive T cell therapy induced massive T cell infiltration and resulted in long-term survival in RT5 mice (Klug et al., 2013), suggesting that LDI offers a better approach for clinical translation as a neoadjuvant therapy prior to adoptive T cell transfer. This study presents an analysis of the underlying mechanisms of increased T cell infiltration following LDI in combination with adoptive T cell transfer and focusses on the cross-talk between LDI and the tumour microenvironment.

3.1. Combination therapy reprograms the tumour microenvironment

The first part of this work demonstrated that the combination of local LDI and adoptive T cell transfer leads to a normalization of the aberrant tumour vasculature, to an increase in intratumoural macrophages and a reduction in intratumoural MDSCs, which is indicative of a less immunosuppressive tumour microenvironment after treatment. This is further supported by Klug et al. who showed that combination therapy promotes a shift of the tumours' cytokine profile in favour of a T_H1 cytokine response (Klug et al., 2013). The less immunosuppressive tumour microenvironment, together with the normalized tumour vasculature and activated endothelium, renders tumours more accessible to the infiltration of T cells and supports their antitumour functions, thereby enhancing the rejection of established RT5 insulinomas. Tumour rejection induced by combination therapy was demonstrated by the reduction in tumour size but also by normalized blood glucose levels, which indicate tumour regression (Klug et al., 2013; Seibel, 2010). Insulinomas are pancreatic islet carcinomas, which constantly produce insulin and thus cause chronically reduced blood glucose levels (hypoglycaemia). Therefore, blood glucose levels provide an indirect measurement of the tumour burden in RT5 mice. Notably, tumour growth could merely be delayed in mice that received a single injection of $CD8^+$ T cells, while repetitive T cell transfers, following a single low dose of radiation, were able to provoke complete macroscopic regression of established tumours and led to long-term survival (Klug et al., 2013). Since highly activated T cells display only a short lifespan of approximately 7-20 days after *in vivo* expansion (Ganss et al., 2002; Nayar et al., 2015), repeated transfers guarantee consistently high levels of tumour-specific T cells, in contrast to a single infusion.

In 2008, Quezada et al. published similar findings in a transplantable melanoma mouse model. They combined 4.5 Gy irradiation with the transfer of tumour antigen-reactive T cells and found that this treatment leads to the infiltration of T cells, delayed tumour growth and prolonged survival, as well as an upregulation of VCAM-1 and ICAM-1 on tumour endothelial cells (Quezada et al., 2008). In their study, as in our model, LDI alone did not cause vessel normalization, endothelial activation or T cell infiltration. Moreover, T cell transfer alone had only minor effects on vessel normalization and slightly increased T cell infiltration (Klug et al., 2013; Quezada et al., 2008)(data not shown). This demonstrates that full vascular normalization requires the synergy of LDI and T cell transfer, indicating that the *in vitro*-activated transferred T cells substantially contribute to endothelial activation and vessel normalization.

The massive infiltration of macrophages into RT5 tumours after combination therapy raised the question of their role in the treatment effects. Systemic depletion of macrophages prevented treatment-induced T cell infiltration and reduced the prolonged survival (Klug et al., 2013; Seibel, 2010). In this study, clodrosome-mediated depletion of TAMs in otherwise untreated RT5 mice did not suppress tumour growth, nor did it affect the aberrant tumour vasculature or survival compared to untreated control mice. Together these findings demon-

strate that macrophages are necessary for the effects of LDI and adoptive T cell transfer. They further suggest that these macrophages exert proinflammatory functions as they are required to overcome the immunosuppressive tumour microenvironment and enable tumour immune rejection. An important characteristic of proinflammatory macrophages is the production of iNOS. Expression of *Nos2*, the gene encoding iNOS, can be induced in response to various inflammatory stimuli during pathogenic infections, but also during radiation-induced inflammation (Lorimore et al., 2001). In RT5 tumours, iNOS was shown to be expressed by macrophages after combination therapy (Klug et al., 2013), demonstrating their proinflammatory phenotype. On the other hand, iNOS can also be associated with tumour immune suppression. The enzyme is expressed by intratumoural MDSCs and its product NO has been shown to inhibit T cell function by nitrating T cell receptors, CD8 molecules and various proteins involved in TCR signalling (Monu and Frey, 2012). Here we show that the inhibition of iNOS in RT5 mice, treated with local LDI and adoptive T cell transfer, prevents tumour rejection. These findings suggest that in our setting, T cell function is not impaired by iNOS and that iNOS promotes tumour immune rejection in response to the treatment. Treatment-mediated activation of the tumour endothelium, as well as increased T cell and macrophage infiltration were dependent on the enzymatic activity of iNOS. As iNOS synthesizes NO, these findings further imply that NO is directly involved in the activation of the tumour endothelium. We tested this assumption by treating HUVECs with increasing doses of the NO donor DETA NONOate, which revealed a dose-dependent dichotomy in the functions of NO: high doses of NO inhibited the expression of adhesion molecules on endothelial cells, even after cytokine stimulation, whereas low concentrations of NO activated the HUVECs to upregulate adhesion molecules. These results also explain the frequently reported finding that NO suppresses the expression of VCAM-1 and other adhesion molecules on endothelial cells, since these studies used high concentrations of NO (De Caterina et al., 1995; Khan et al., 1996). Interestingly, it was recently shown that the endothelial upregulation of adhesion molecules, mediated by low doses of NO, is dependent on NF-κB signalling (Sektioglu et al., 2016). Together, these data demonstrate that by inducing iNOS activity in macrophages, the combination of local LDI and adoptive T cell transfer leads to the activation of tumour endothelial cells, which upregulate adhesion molecules and thereby promote tumour infiltration of T cells and macrophages. Our findings, thus, confirm the observations of an *in vitro* study in which irradiated macrophages were shown to induce VCAM-1 expression in HUVECs in an iNOS/NO dependent manner (Xiao et al., 2014). Since iNOS inhibition did not fully abrogate the effects of combination therapy on the vessel phenotype or adhesion molecule expression, we presume that additional factors are involved in regulating the vessel characteristics in response to the treatment.

Radiation is used as a localized therapy for solid tumours. As abscopal effects, where distant metastases are affected by the treatment, are rare (Demaria and Formenti, 2016), radiation therapy is not suitable for the treatment of disseminated disease, thereby limiting its range of application considerably. Since we found that the combination of local LDI and adoptive T cell transfer is mediated by iNOS-producing macrophages, we examined whether the trans-

fer of peritoneal macrophages from irradiated wt donor mice, together with adoptive T cell transfer, had similar effects. The combined transfers would allow the treatment of metastasized cancer patients and haematological malignancies. Peritoneal macrophages were therefore elicited by thioglycolate-induced sterile peritonitis, followed by isolation of peritoneal exudate cells (PECs), a protocol widely used in macrophage research (Gallily et al., 1964; Li et al., 1997). Analysis of freshly isolated PECs revealed that the majority were macrophages (60-80 %), while very few T cells, some dendritic and granulocytic cells were also detected. In agreement with these findings, it was recently shown that thioglycolate-elicited peritoneal exudates comprise a heterogeneous mix of several cell types including B and T lymphocytes, as well as NK cells, DCs, neutrophils, eosinophils and macrophages, which make up the majority of PECs (Misharin et al., 2012). *In vivo* LDI of peritoneal cells led to an increase in Gr-1$^+$ cells. Gr-1 can be expressed by granulocytes (neutrophils, eosinophils (Ghosn et al., 2010; Misharin et al., 2012)), monocytes (Geissmann et al., 2003) and by rare subsets of peritoneal macrophages (Ghosn et al., 2010). Gr-1 expression is therefore not suitable for the discrimination between different types of myeloid cells and a more detailed analysis is required. Granulocytes, accounted for the largest fraction of non-macrophages in the peritoneal exudate, which is in line with the literature where eosinophils are described to be a major source of contamination in thioglycolate-elicited macrophages (Carretero et al., 2015; Misharin et al., 2012). Of note, in transplantable tumour mouse models, activated eosinophils have recently been shown to enhance T cell infiltration into tumours by modulating the tumour microenvironment. The eosinophils induced the normalization of the aberrant tumour vasculature and the polarization of TAMs to an M1-like phenotype (Carretero et al., 2015). Neutrophils were also reported to exhibit antitumour potential and to suppress tumour growth (Di Carlo et al., 2001; Noffz et al., 1998; Sionov et al., 2015). Furthermore, eosinophils and neutrophils become activated by danger signals released after irradiation (Dalal et al., 1992; Lorimore et al., 2001; Takeshima et al., 2016). Therefore, the eosinophils and neutrophils could further support the treatment effects on RT5 tumours by skewing peritoneal macrophages to M1-like phenotypes, thereby further promoting the reprogramming of the tumour microenvironment.

Following the transfer of irradiated PECs and CD8$^+$ T cells, the aberrant tumour vasculature was normalized and the endothelium was activated, thereby facilitating leukocyte infiltration. During tumour development, abnormally high levels of intratumoural VEGF result in uncontrolled angiogenesis and the development of an aberrant tumour vasculature. Tumour vessels are characterized by reduced perfusion, which aggravates hypoxia and further promotes the production of VEGF. Anti-angiogenic therapies can break this vicious cycle and, by targeting VEGF, transiently normalize the vasculature which can improve the efficacy of anticancer therapies (Jain, 2013). Similarly, the transfer of irradiated PECs combined with adoptive T cell transfer reduced intratumoural VEGF levels that were increased after LDI or transfer of CD8$^+$ T cells alone (Klug et al., 2013). The vascular normalization, as well as the endothelial upregulation of adhesion molecules, can be explained by a combination therapy-induced shift from M2-like TAMs, which are characterized by the production of high levels of VEGF

and other proangiogenic factors, to M1-like macrophages that generate NO via increased expression of iNOS. The reduced levels of the proangiogenic factors may account for vascular normalization, while NO-mediated activation may result in the upregulation of adhesion molecules on the endothelium. Of note, endothelial activation in RT5 tumours was even more pronounced after transfer of irradiated PECs and $CD8^+$ T cells compared with local LDI and T cell transfer, indicating that the transfer of irradiated macrophages has a stronger effect on endothelial activation than local LDI. Possibly, fewer macrophages are stimulated by local LDI, due to the restricted field of radiation, compared to the number of macrophages stimulated by TBI in wt mice, which are transferred to RT5 mice. Hence, the transfer of irradiated macrophages may provide more stimulatory factors for endothelial cells in RT5 tumours, causing a stronger activation and upregulation of adhesion molecules. Alternatively, macrophage phenotypes might be part of the cause. Macrophages in RT5 tumours are influenced by the immunosuppressive microenvironment and may therefore be polarized towards M2-like phenotypes, whereas macrophages which are transferred from wt mice were not exposed to pro- or anti-inflammatory stimuli and might therefore display a more naïve phenotype. The effects of radiation on the distinct phenotypes could differ and induce stronger activation towards M1-like phenotypes in the more naïve macrophages. Of course, further investigations are required to clarify the observations.

The normalization of the tumour vasculature and the activation of the tumour endothelium correlated with an increased number of intratumoural T cells and macrophages, as well as with a reduced tumour size, suggesting that the transferred tumour-specific T cells, which were enabled to infiltrate the tumour tissue by the normalized tumour vasculature, exert their antitumour functions, thereby mediating tumour immune rejection. After transfer of irradiated but not unirradiated PECs, T cell infiltration was accompanied by the infiltration of macrophages, indicating that the transferred PECs migrate to the tumour site and accumulate therein. However, only few endogenous intratumoural macrophages were observed in untreated RT5 mice, suggesting that macrophages, just like T cells, are hindered from infiltrating the tumour tissue by the tumour endothelial barrier. Consequently, the aberrant tumour vasculature may impair tumour infiltration by irradiated PECs which are injected into untreated RT5 mice. Furthermore, PEC infiltration may be influenced by the yet undefined mechanisms of tumour vasculature normalization induced by adoptive T cell transfer. To investigate whether the transferred irradiated PECs are capable of infiltrating untreated tumours, labelled PECs were tracked *in vivo* and RT5 tumours were analysed for labelled PECs before and after T cell transfer (day 10). Transferred PECs could be detected on day 10 and day 17 following PEC injection, demonstrating that macrophages are able to infiltrate RT5 tumours with or without T cell transfer and that the infiltration was not affected by the aberrant tumour vasculature. This implies that macrophages can overcome the endothelial barrier or circumvent it and migrate into tumours via surrounding tissues (Dandekar et al., 2011; Lamagna et al., 2006). Of note, macrophage migration is not a directed process, as the majority of transferred PECs drained in the lung, liver, and spleen and only a small number of peritoneal macrophages reached the tumour site. The numbers of labelled PECs within tu-

mours were too low to account for the vast accumulation of intratumoural macrophages observed after the transfer of irradiated PECs and T cells. An alternative explanation for the increased number of TAMs after treatment could be the recruitment of endogenous macrophages to the tumour site from the surrounding tissues (Klug et al., 2013) or from the blood but also the proliferation of intratumoural macrophages (Campbell et al., 2011; Tymoszuk et al., 2014; Van Overmeire et al., 2014). However, it remains unclear how the irradiated PECs instigate the reprogramming of the tumour microenvironment. As no treatment-specific differences in PEC infiltration were observed, we assumed that LDI affects PEC effector functions rather than the migration to and infiltration into RT5 tumours.

3.2. LDI primes peritoneal macrophages

Ionizing radiation can induce macrophage activation through the release of danger signals from damaged tissues (Schaue et al., 2015). To gain insight in gene expression and functional changes induced by LDI in peritoneal macrophages, whole transcriptome analysis was performed of *in vivo* and *in vitro* irradiated PECs. RNA sequencing revealed that *in vivo,* as well as *in vitro* (*ex vivo*), LDI affects gene expression in PECs. After *in vivo* and *in vitro* irradiation, 410 and 509 genes, respectively, were significantly differentially expressed. By unsupervised hierarchical clustering, the samples of the *in vivo* dataset clustered together according to their treatment. In the *in vitro* dataset however, two of the irradiated samples displayed a higher similarity to the controls than to the other irradiated samples, which showed distinct expression patterns compared to the unirradiated samples. Since independent experiments with *in vitro* irradiated PECs clearly showed that irradiated samples differed from control samples in their gene expression, we assume that irradiation might have failed in the two unresponsive samples of the first experiment.

Comparison of the datasets revealed that 94 of the differentially expressed genes (DEGs) were commonly regulated after *in vivo* and *in vitro* irradiation, demonstrating a strong overlap between the different experimental setups. It was presumed that these DEGs represent the genes whose expression is directly affected by LDI. Due to the different experimental conditions, however, it was expected that the majority of DEGs shows no overlap between *in vivo* and *in vitro* treatment. In the *in vivo* setting, wt mice received total body irradiation and so whole tissues were affected, resulting in cell damage and stress responses in immune cells, as well as non-immune cells, causing the release of various factors that activate components of the immune system. *In vitro* irradiation, on the other hand, affects only cells in the peritoneal exudate, thereby restricting the effects to immune cells. Furthermore, in this setting the cells were cultured after isolation, which affects the composition of the different cell subsets. As described earlier, freshly isolated, thioglycolate-elicited PECs are a heterogeneous mix of many cell types with the majority (60-80 %) being macrophages. Culturing the PECs led to an enrichment of macrophages (90-95 %). Misharin et al. described that adherence considerably reduces the contamination with dead cells, lymphocytes, dendritic cells, neutrophils and, although to a lesser extent, eosinophils (Misharin et al., 2012). In addition,

isolation procedures and culture conditions can influence the functional phenotype of macrophages (Chiang et al., 2008). But despite the differences between the two setups, the DEGs of both datasets were associated with similar biological functions, namely immune system processes, cell migration and stress response. GO enrichment analysis indicated that LDI increases the migration of PECs and promotes PEC-induced cell movement of other cells. The former is supported by changes in chemokine receptor or adhesion molecule expression (*Cx3cr1*; integrins) and the latter by the upregulation of chemokines such as *Ccl2*, *Ccl7* and *Cxcl2* in response to *in vivo* LDI and *Ccl5*, *Ccl6*, *Ccl12*, *Cxcl1*, *Cxcl2*, *Cxcl3* and *Cxcl16* after *in vitro* LDI, as well as other chemoattractive proteins, such as components of the complement system. These changes enable irradiated PECs to migrate and infiltrate various organs, including tumours, and to recruit other leukocytes to their location, such as T cells or macrophages to the tumour site after their infiltration. Furthermore, 'innate immune response' was identified as a GO term enriched in the datasets, and leukocytes, such as myeloid cells, phagocytes and macrophages were predicted to be activated by LDI. Interestingly, the IFN signalling pathway was enriched and a high abundance of IFN regulated genes (IRGs) was identified among the DEGs, demonstrating that LDI leads to the upregulation of IRGs through the activation of IFN signalling. It is well described that type I but also type II IFNs are produced in response to irradiation, thereby initiating IFN signalling (Deng et al., 2014; Lim et al., 2014; Lugade et al., 2005; Sugihara et al., 2011). Type I IFNs have been shown to be upregulated in tumours early after radiation and subsequently induced the production of IFN-γ (Lim et al., 2014).

During viral infections, the presence of foreign nucleic acids initiates an innate immune response through the activation of the interferon regulatory factors, IRF3 and IRF7, which induce the transcription of type I IFNs. Secreted IFN-α and β bind to type I IFN receptors in an autocrine and paracrine manner and thereby induce the transcription of IRGs, including *Irf7*. This initiates a positive feedback loop which amplifies the signal and ensures a quick response to infectious viruses (Honda and Taniguchi, 2006). Here we show that LDI induces the upregulation of *Irf7* in PECs, which was dependent on type I and type II IFNs, suggesting that LDI activates processes similar to the ones induced by viral infections. Using IPA, IRF7 was identified as an upstream regulator of the DEGs. Through the amplification of IFN signalling, IRF7 promotes the upregulation of IRGs, suggesting that LDI acts via the IRF7 and IFN amplification loop to mediate its effects. Prior to that, IRF7 becomes activated by cytosolic nucleic acids, danger signals that are generated during viral infections, but also during cellular stress which can be induced by irradiation-generated radicals. Cytosolic DNA, as well as certain cytosolic RNAs, are sensed by PRRs which activate signalling cascades that lead to the expression of effector genes, thereby shifting the irradiated cells to an activated (anti-viral) state. In the *in vivo* and *in vitro* dataset, PRRs that sense cytosolic DNA, as well as their ligands and adaptor molecules, were identified as upstream regulators. Furthermore, the signalling pathways 'Activation of IRF by Cytosolic Pattern Recognition Receptors' and 'Role of Pattern Recognition Receptors in Recognition of Bacteria and Viruses' were predicted to be activated. In this line, genes encoding sensors of cytosolic nucleic acids were highly upregu-

lated after LDI. The DExH/D box helicases encoded by *Ddx58* and *Ifih1* detect ds and ssRNA and signal via the adaptor protein MAVS. MAVS activates TBK-1 and IKK (IκB kinase), thereby initiating IRF3/IRF7 and NF-κB signalling, which culminates in the expression of type I and type II IFNs and IRGs, as well as proinflammatory cytokines (Brubaker et al., 2015). IFIT1bl1 is a sensor of viral ssRNAs and IFIT3b is an adaptor bridging TBK1 and MAVS. IFI204, is induced by IFN signalling and an inducer of *Ifnb* transcription. Its human homolog IFI16 is involved in the DNA damage response. ZBP-1, also called DAI, activates IRF3 and NF-κB upon sensing cytosolic DNA (Unterholzner, 2013). In summary, the genes *Ddx58, Dhx58, Ifi204, Ifih1, Ifit1bl1, Ifit3b* and *Zbp1* were upregulated after LDI and together, this demonstrates that LDI leads to a stress response in PECs and, through the detection of cytosolic nucleic acids, induces IFN signalling.

In peritoneal macrophages, LDI leads to the activation of IFN signalling and to the expression of *Irf7* which both strongly upregulate the expression of *Irf1* (Sgarbanti et al., 2007). IRF1 is a transcription factor and direct inducer of *Nos2* expression (Kamijo et al., 1994). In accordance, LDI led to the upregulation of *Nos2* in PECs which was dependent on IFN-γ and IFN-β. Moreover, the IFN-γ signalling pathway genes *Ifng,* as well as *Stat1* and *Irf1*, displayed increased expression levels after LDI, which was also dependent on IFN-γ and IFN-β. We thereby show that LDI leads to the upregulation of iNOS through the induction of an IFN response. The release of NO from $iNOS^+$ macrophages can then induce the expression of adhesion molecules on tumour endothelial cells, thereby promoting leukocyte infiltration.

TNF-α and IL-1β are the most important mediators of endothelial activation during inflammation. They stimulate increased expression of adhesion molecules on endothelial cells (Mako et al., 2010) and have been shown to be upregulated in macrophages in response to irradiation (Iwamoto and McBride, 1994; Nemoto et al., 1995; Ray et al., 2013). In this study, gene expression analysis of irradiated PECs revealed that *Tnfa* was upregulated after LDI in an IFN-γ- and IFN-β-dependent manner, suggesting that it synergizes with NO in the activation of endothelial cells in RT5 tumours. *IL-1ß* was also strongly upregulated after *in vitro* LDI as determined by RNA Sequencing and might contribute to endothelial activation, in addition to NO and TNF-α.

Taken together, the results obtained in the course of this study point to an LDI-induced M2 to M1 shift in the peritoneal macrophages. The literature reports contradictory findings regarding the effects of radiation on the polarization of macrophages. Intramuscular or intracranial murine tumours treated with 25 or 8 Gy, respectively, developed hypoxic areas that were associated with an accumulation of M2 macrophages. Another study showed that phenotypic changes following irradiation were dependent on the mouse strain: murine-derived BMDMs from CBA/Ca and C57/BL/6 mice displayed M1- and M2-like phenotypes, respectively, after *in vivo,* as well as *in vitro* irradiation, with 4 Gy (Coates et al., 2008). A recent study describes a shift towards pro-inflammatory M1-like phenotypes in human blood monocyte-derived macrophages after ionizing radiation (5x2 Gy), however, these macrophages re-

tained some tumour promoting abilities (Teresa Pinto et al., 2016). In 2007 Shan et al. showed that 2 Gy TBI induced the production of proinfilammatory cytokines in murine peritoneal macrophages (Shan et al., 2007). In the present study, gene expression analysis of irradiated peritoneal macrophages revealed that several genes, associated with M2-like phenotypes were downregulated (i.e. *Cd163*, *Retnla*, *Fcrls*), whereas genes associated with M1-like phenotypes were upregulated (*Nos2, Isg15, Ifi44, Ifit1*) (Jablonski et al., 2015). Furthermore, the surface expression of the M2 marker CD206 (Chávez-Galán et al., 2015; Martinez et al., 2008) was decreased after *in vivo* and *in vitro* irradiation. Surprisingly, gene expression of MHC class II, which is generally described to be an M1 marker (Biswas and Mantovani, 2010), was downregulated after *in vivo* irradiation. Also the number of MHC class II^+ macrophages was decreased after *in vivo* as well as *in vitro* LDI. Stimulation with IFN-γ (but not LPS), on the other hand, induced the upregulation of MHC class II surface expression on peritoneal macrophages (Figure S34). Interestingly, IFN-γ-induced MHC class II expression can be suppressed by the TLR9 and 7 ligands CpG ODN and Resiquimod (Celhar et al., 2016; Chu et al., 1999), by TNF-α (Watanabe and Jacob, 1991) and by type I IFNs (Heise et al., 1998), all of which are proinflammatory stimuli that skew macrophages towards M1- rather than M2-like phenotypes (Kratochvill et al., 2015; Lee et al., 2014; Sica and Mantovani, 2012; Wang et al., 2015; Wu et al., 2016; Xie et al., 2016). As described earlier, irradiation mediates its effects via type I IFN responses. Therefore, we assume that irradiation inhibits MHC class II expression by means of type I IFN induction. Overall, MHC class II might not be the ideal M1 marker, as it is also expressed on M2 macrophages (Martinez and Gordon, 2014) and therefore does not clearly characterize macrophage polarization states. iNOS, on the other hand, is an established marker of M1-like macrophages (Murray et al., 2014) and in our setting *Nos2* expression was upregulated after *in vivo* and *in vitro* LDI. However, flow cytometric evaluation of iNOS protein levels revealed only low expression intensities on peritoneal macrophages and *in vivo* but not *in vitro* irradiation led to a slight increase in $iNOS^+$ macrophages. The reported controversy in the literature regarding macrophage polarization in response to irradiation might be attributable to divergent effects of different doses and dose fractionations. However, another reason might be that the macrophage polarization paradigm, which is applied, is oversimplified. The M1/M2 polarization model describes isolated *in vitro* activation of macrophages with a limited number of stimuli and does not take into account the complex networks of pro- and anti-inflammatory factors that are present in inflammatory or tumour tissues. These -often conflicting- stimuli influence the activation state of macrophages and produce mixed populations including different polarization states where M1 and M2 represent the extremes in a spectrum of phenotypes (Martinez and Gordon, 2014; Murray et al., 2014). Therefore, it is unlikely that macrophages isolated from tissues of living organisms display a clear-cut activation status as it is described by the M1/M2 paradigm. According to the newly proposed nomenclature by Murray et al, the irradiated peritoneal macrophages in our setting most closely resemble M(LPS) macrophages, which express low levels of *Nos2* and are not fully activated unless they receive additional stimuli, such as IFN-γ. In addition, the thioglycolate-induced PECs might also comprise macrophages that are not fully differentiated and still display monocytic features, such as lower

surface expression of MHC class II. In monocytes, MHC class II molecules are retained in endosomal compartments until macrophages become fully activated (Roche and Furuta, 2015). In contrast, the macrophages observed in RT5 tumours after the treatment with either LDI or irradiated PECs in combination with adoptive T cell transfer display a more fully activated phenotype, as they express higher levels of iNOS (Klug et al., 2013). A possible explanation may be that these macrophages are exposed to the adoptively transferred T cells, which infiltrate the tumour and produce IFN-γ, which can fully activate the macrophages to a proinflammatory M1 phenotype.

3.3. Conclusion

Combining cancer immunotherapies with treatment modalities that break tumour-induced immune suppression can synergistically potentiate their efficacy and enhance clinical responses (Drake, 2012; Kalbasi et al., 2013). However, the complex interactions between the different therapeutic approaches are not well understood. The present study demonstrates how low dose irradiation in combination with adoptive T cell transfer augments tumour immune rejection through the manipulation of the tumour microenvironment. It thereby contributes to the understanding of the interactions between radiation therapy, the immune system and cancer. Based on the findings of this study we propose the following model of the mechanism of action:
LDI, locally applied to the tumour tissue or systemically applied to wt mice, primes macrophages through the induction of DNA damage and the release of danger signals, which are sensed by macrophages through PRRs. PRR signalling then induces IFN responses that lead to the expression of IRGs, amongst others, *Nos2* and *Tnfa*. Primed macrophages produce low levels of iNOS and TNF-α, which lead to an initial and modest activation of endothelial cells in tumour tissues. The upregulation of adhesion molecules allows the infiltration of small numbers of leukocytes, including *in vitro*-activated IFN-γ producing T cells that are injected into tumour-bearing mice, as adoptive T cell therapy. The T cell-derived IFN-γ provides the required stimulus to fully activate intratumoural, primed macrophages which in turn increase their production of iNOS and other proinflammatory cytokines, as well as chemokines, and become fully activated. The increased expression of iNOS and TNF-α further activates the endothelium and the secreted proinflammatory cytokines and chemokines reprogram the tumour microenvironment. Together, this leads to the recruitment and the infiltration of increasing numbers of immune effector cells. The initiated positive feedback loop can be maintained by repeated T cell transfers. Finally, the infiltrating, tumour-specific T cells exert their antitumour functions and mediate tumour eradication, leading to long-term survival (Figure 31).

The present study demonstrates the benefits of the combination of adoptive T cell therapy with neoadjuvant local low dose irradiation over the monotherapy. It further implies the

huge potential of this treatment strategy in clinical settings. We therefore suggest that these findings should be tested in a clinical trial.

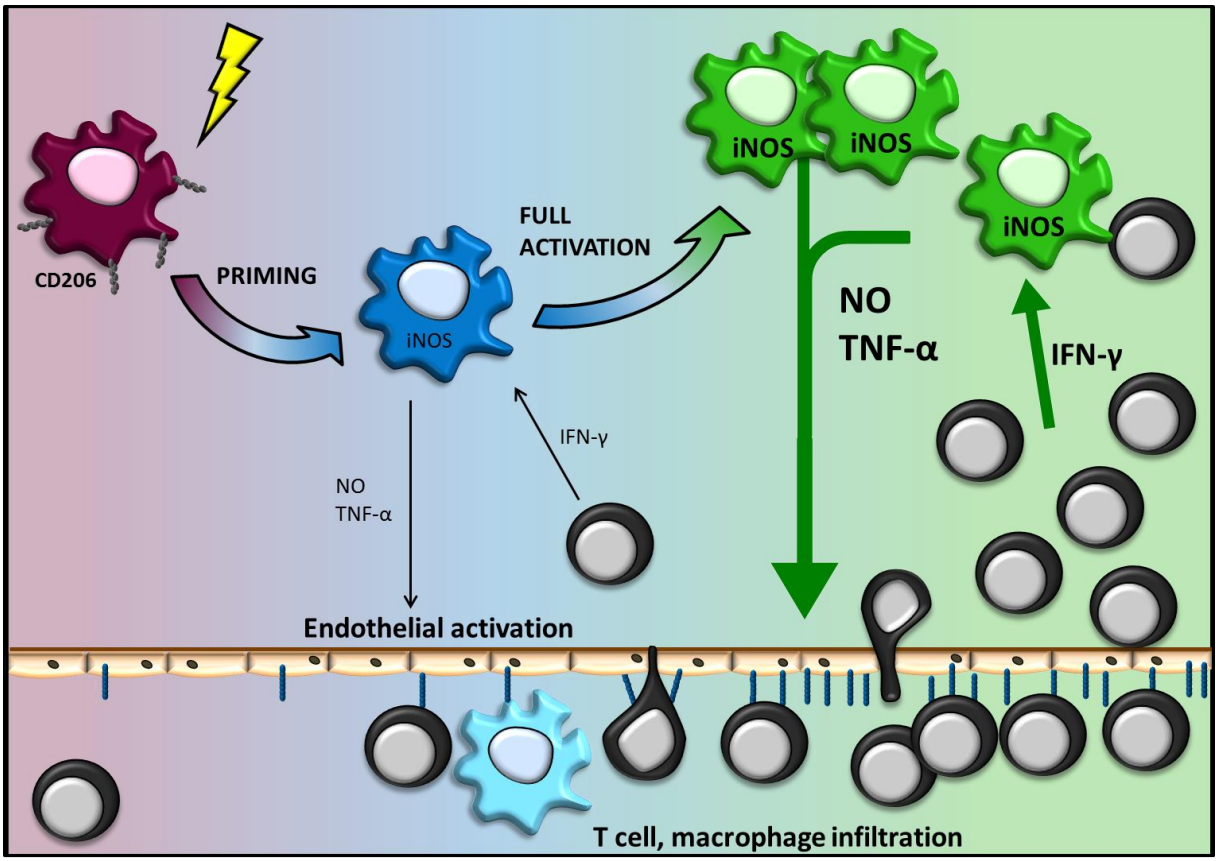

Figure 31 Proposed mechanism of action
LDI primes TAMs through the generation of danger signals in irradiated tissues. Primed macrophages downregulate M2-markers and induce low levels of iNOS and TNF-α, which modestly activate the tumour endothelium. Infiltrating *in vitro*-activated, IFN-γ producing T cells further activate the primed macrophages through IFN-γ, thereby increasing the expression of iNOS, TNF-α and initiating a positive feedback response. Similar models have been proposed by (Lee and Biswas, 2016; Sektioglu et al., 2016).

4. MATERIALS AND METHODS

4.1. Materials

4.1.1. Assay kits

Product	Supplier
Agilent RNA 6000 Nano Kit	Agilent Technologies
ArC™ Amine Reactive Compensation Bead Kit	Molecular Probes, Invitrogen
Clodrosome Macrophage Depletion Kit	Encapsula NanoSciences
Foxp3/Transcription Factor Staining Buffer Set	eBioscience
LIVE/DEAD® Fixable Yellow Dead Cell Staining Kit	Molecular Probes, Invitrogen
Mouse IFN-γ Secretion Assay - Detection Kit (PE)	Miltenyi Biotec
Mouse IL-2 Secretion Assay - Detection Kit (APC)	Miltenyi Biotec
PKH26 Red Fluorescent Cell Linker Kit for Phagocytic Cell Labelling	Sigma-Aldrich
RevertAid H Minus First Strand cDNA Synthesis Kit	Thermo Scientific
RNase-Free DNase Set (50)	QIAGEN
RNeasy Mini Kit (50)	QIAGEN
Zombie NIR™ Fixable Viability Kit	Biolegend

4.1.2. Antibodies

4.1.2.1. Flow Cytometry

Antibodies for flow cytometry directed against human epitopes

Specificity	Conjugation	Species	Isotype	Clone	Supplier
CD31	BV421	Mouse	IgG1,κ	WM59	Biolegend
ICAM-1 (CD54)	FITC	Mouse	IgG1	O1	Sino Biological
VCAM-1 (CD106)	APC	Mouse	IgG1,κ	STA	Biolegend
E-Selectin (CD62E)	PE	Mouse	IgG2a,κ	HCD62E	Biolegend

Antibodies for flow cytometry directed against murine epitopes

Specificity	Conjugation	Species	Isotype	Clone	Supplier
CD11b	BV510	Rat	IgG2b,κ	M1/70	Biolegend
	PerCP	Rat	IgG2b,κ	M1/70	Biolegend
	PE-Cy7	Rat	IgG2b,κ	M1/70	ebioscience

	APC-Cy7	Rat	IgG2b,κ	M1/70	BD Biosciences
CD11c	PerCP	Armenian Hamster	IgG	N418	Biolegend
	PE-Cy7	Armenian Hamster	IgG1, λ2	HL3	BD Biosciences
CD206 (MMR)	FITC	Rat	IgG2a,κ	C068C2	Biolegend
CD3e	APC	Armenian Hamster	IgG1,κ	145-2C11	BD Biosciences
CD4	APC-Cy7	Rat	IgG2b,κ	GK1.5	BD Biosciences
	FITC	rat	IgG2a,κ	RM4-5	BD Biosciences
CD45	V450	Rat	IgG2b,κ	30-F11	BD Biosciences
	V500	Rat	IgG2b,κ	30-F11	BD Biosciences
	FITC	Rat	IgG2b,κ	30-F11	BD Biosciences
CD8a	PerCP	Rat	IgG2a,κ	53-6.7	BD Biosciences
	PB	Rat	IgG2a,κ	53-6.7	BD Biosciences
F4/80	AF647	Rat	IgG2b	Cl:A3-1	AbD Serotec
	AF488	Rat	IgG2b	Cl:A3-1	AbD Serotec
	APC	Rat	IgG2a,κ	BM8	ebioscience
	PE	Rat	IgG2a,κ	BM8	ebioscience
I-A/I-E (MHC class II)	PB	Rat	IgG2b,κ	M5/114.15.2	Biolegend
Ly-6G/Ly-6C (Gr-1)	PerCP	Rat	IgG2b, κ	RB6-8C5	Biolegend
	APC	Rat	IgG2b,κ	RB6-8C5	BD Biosciences
NOS2	PE	Rat	IgG2a,κ	CXNFT	eBioscience
	AF488	Rat	IgG2a,κ	CXNFT	eBioscience

APC (Allophycocyanin), BV510 (Brilliant Violet™ 510), FITC (Fluorescein isothiocyanate), PE (Phycoerythrin), PerCP, (Peridinin Chlorophyll), PE/Cy7 (Phycoerythrin/cyanine7), AF647 (Alexa Fluor® 647), AF488 (Alexa Fluor® 488), APC/Cy7 (Allophycocyanin/cyanine7), PB (Pacific Blue™).

4.1.2.2. Antibodies for Immunofluorescence

Primary antibodies

Specificity	Reactivity	Host	Clonality	Supplier
CD31	mouse	hamster	2H8	AbD serotec
SV40TAg	Simian Virus 40	rabbit	poly	Santa Cruz
VCAM-1 (CD106)	mouse	rat	429	BD Pharmingen
Gr-1 (Ly6G and Ly6C)	mouse	rat	CRB6-8C5	BD Biosciences
F4/80	mouse	rat	Cl:A3-1	AbD serotec
CD11b	mouse	rat	M1/70	BD Biosciences
CD68	mouse	rabbit	poly	Abcam

CD3	mouse	goat	poly	Santa Cruz
CD4	mouse	rat	H129.19	BD Biosciences
CD8	mouse	rat	YTS105.18	AbD serotec

Secondary antibodies

Specificity	Conjugation	Host	Supplier
anti-goat	Alexa Fluor® 488	chicken	Invitrogen
anti-rat	Alexa Fluor® 594	chicken	Invitrogen
	Alexa Fluor® 488	chicken	Invitrogen
anti-rabbit	Alexa Fluor® 488	chicken	Invitrogen
anti-hamster	Alexa Fluor® 594	goat	Invitrogen

4.1.3. Chemicals and Biological Reagents

Product	Supplier
2.4G2 HSN (Hybridoma Supernatant)	Kindly provided by Prof. Dr. Cherwenka
Accutase solution	SIGMA-Aldrich
Acetone	SIGMA-Aldrich
Aqua ad injectibilita	B. Braun
BD™ CompBead Compensation Particles Anti-rat/hamster Ig, k	BD Biosciences
BD™ CompBead Compensation Particles Anti-mouse Ig, k	BD Biosciences
BD™ Cytometer Setup & Tracking beads	BD Biosciences
Bovine Serum Albumin (BSA)	SIGMA-Aldrich
Collagenase D	Roche
Dispase® I (neutral protease, grade I)	Roche
Dimethyl sulfoxide (DMSO)	Sigma-Aldrich
Deoxyribonuclease I from bovine pancreas (DNase I)	SIGMA-Aldrich
Dulbecco's Phosphate Buffered Saline (PBS)	SIGMA-Aldrich
Ethylenediaminetetraacetic acid EDTA (Versen) 1 % w/v in PBS w/o Ca2+/Mg2+	Biochrom AG
Ethanol, Absolute	SIGMA-Aldrich
Ethanol, Absolute (200proof) Molecular Biology Grade	Fisher BioReagents
FACS Clean Solution	BD Biosciences
FACS Flow Sheath Solution	BD Biosciences
FACS Shutdown Solution	BD Biosciences
Fluoromount-G™, with DAPI	eBioscience
Griess reagent (modified)	Sigma-Aldrich
N-(2-Hydroxyethyl)piperazine-N'-(2-ethanesulfonic acid) (HEPES) Solution	SIGMA-Aldrich

IgG aus Maus (polyklonal)-unkonj	Dianova
Isopropanol	SIGMA-Aldrich
Ketanest S (25 mg/ml)	Pfizer
NaCl 0.9 %	B. Braun
Nuclease Free Water	Ambion
Protein Block, Serum-Free	DAKO
RNaseZap®	Ambion
Rompun, 2 %	Bayer-Schering
Sandoglobulin (human IgG)	CSL Behring
Sera (Chicken, Goat)	Santa Cruz
Sodium Azide (NaN3)	Gbiosciences
Spitacid	Ecolab
SYTOX® Blue Dead Cell Stain	Life Technologies
TaqMan® Gene Expression Assay GAPDH Mm99999915_g1	Applied Biosystems
TaqMan® Gene Expression Assay HPRT1 Mm03024075_m1	Applied Biosystems
TaqMan® Gene Expression Assay IFNg Mm00801778_m1	Applied Biosystems
TaqMan® Gene Expression Assay IFNg Mm01168134_m1	Applied Biosystems
TaqMan® Gene Expression Assay iNOS Mm00440502_m1	Applied Biosystems
TaqMan® Gene Expression Assay IRF1 Mm01288580_m1	Applied Biosystems
TaqMan® Gene Expression Assay IRF7 Mm00516793_g1	Applied Biosystems
TaqMan® Gene Expression Assay JAK1 Mm00600614_m1	Applied Biosystems
TaqMan® Gene Expression Assay STAT1 Mm00439531_m1	Applied Biosystems
TaqMan® Universal Master Mix II, with UNG	Applied Biosystems
Thioglycolate Medium (Powder)	Applichem, Germany
Tissue-Tek® O.C.T. Compound	Sakura, Finetek
Trypan Blue (0.4 %)	SIGMA-Aldrich
Trypsin-EDTA Solution (1x)	SIGMA-Aldrich
Universal Mouse Reference RNA	Agilent Technologies
2-Mercaptoethanol	SERVA Electrophoresis

4.1.4. Cell Culture Media and Supplements

Product	Supplier
Dulbecco's Modified Eagle's Medium (DMEM)	SIGMA-Aldrich
RPMI-1640 Medium	SIGMA-Aldrich
Fetal calf serum (FCS)	Biochrom AG
Penicillin-Streptomycin (10 000 U/ml, 10 000 µg/ml) (Pen-Strep)	Gibco
L-Glutamine (200 mM)	Gibco
2-Mercaptoethanol (50 mM)	Gibco

neutralizing IFN-γ antibody (R4-6A2 Hybridoma Supernatant)	kindly provided by Prof. Dr. Rainer Zawatzky
neutralizing IFN-β antibody (7F-D3 Hybridoma Supernatant)	kindly provided by Prof. Dr. Rainer Zawatzky
Murine IL-2	eBioscience
Murine IFN-γ	CellSystems
SV-40 TAg peptide 560–568 (SEFLLEKRI)	DKFZ core facility for peptide synthesis
Lipopolysaccharide (LPS) from E. coli 0111:B4	SigBayerma
Endopan-3 kit with 9 supplements	PAN-BioTech
Recombinant Human TNF-α	PeproTech
DETA NONOate	Enzo
Human Umbilical Vein Endothelial Cells (HUVECs), pooled	PromoCell

4.1.5. Buffers, Solutions and Cell Culture Media

Thioglycolate	Components	Volumes
	Thioglycolate medium	3 % (w/v)
	ddH_2O	

ACK buffer	Components	Volumes
	NH_4Cl	150 mM
	$KHCO_3$	10 mM
	$(Na_2)EDTA$	100 µM
	ddH_2O	

Trypan blue solution	Components	Volumes
	PBS	1x
	Trypan blue 0.4 %	1:3 (v/v)

Macrophage medium	Components	Volumes
	DMEM	1x
	FCS	10 % (v/v)
	Pen Strep	100 U/ml, 100 µg/ml
	L-Glutamine	2 mM
	β-mercaptoethanol	0.05 mM

T cell medium	Components	Volumes

	RPMI	1x
	FCS	10 % (v/v)
	Pen Strep	100 U/ml, 100 µg/ml
	L-Glutamine	2 mM
	β-mercaptoethanol	0.05 mM

HUVEC medium	Components	Volumes
	Endopan 3	1x
	EGF (epidermal growth factor)	0.1 %
	FGF-2 (fibroblast growth factor-2)	0.1 %
	VEGF (vascular endothelial growth factor)	0.1 %
	Ascorbic Acid phosphate	0.1 %
	R3-IGF-1 (insulin-like growth factor-1)	0.1 %
	FBS (fetal bovine serum)	3 %
	Gentamycin/Amphotericin	0.12 %
	Hydrocortison	0.02 %
	Heparin	0.1 %

Digestion solution	Components	Volumes
	PBS	1x
	Collagenase D	0.2 mg/ml
	Dispase I	0.08 mg/ml
	DNase I	25 µg/ml

Pancreas digestion mix	Components	Volumes
	PBS	1x
	Collagenase D	0.2 mg/ml
	DNase I	25 µg/ml

Complete medium	Components	Volumes
	RPMI	1x
	FCS	10 % (v/v)

FACS buffer	Components	Volumes
	PBS	1x
	FCS	3 % (v/v)
	EDTA	1.5 mM
	2.4G2 HSN	20 % (v/v)

FACS blocking solution	Components	Volumes
	FACS buffer	1x
	IgG aus Maus (polyklonal)-unkonj	1:20 (v/v)

SYTOX Blue solution	Components	Volumes
	SYTOX Blue Dead Cell Stain	1 µl
	FACS buffer	15 ml

IF-staining buffer	Components	Volumes
	PBS	1x
	BSA	1 % (w/v)
	serum (goat/chicken)	10 % (v/v)

4.1.6. Consumables

Product	Supplier
Cell Scraper	TPP
Cell strainer (40 µm, 100 µm)	BD Falcon
Cell-culture dishes, non-tissue culture treated (Optilux, 100 x 20 mm)	BD Falcon
Cell-culture dishes, tissue-culture treated (100 x 20mm, 150 x 20 mm)	TPP
Cell-culture flasks – tissue-culture treated with filtercap	TPP
Cryomolds®	Sakura, Finetek
Cyrovials with screw cap (2 ml)	Greiner Bio-One
Bepanthen® eye and nose ointment	Bayer
PAP Pen	Dako
Disposable needles – 20 G x 1 1/2 ’’, 0.9 x 40 mm (Sterican)	B. Braun
Disposable needles – 27 G x ¾’’, 0.4 x 20 mm (Neolus 100)	Terumo
Disposable scalpels	Feather
DNA LoBind Tubes (0.5 ml, 1.5ml)	Eppendorf
Falcon conical centrifuge tubes (15 and 50ml)	BD Falcon
LightCycler 480 multiwell plates 384, white	Roche
LightCycler 480 Sealing Foil	Roche
Microscopical glass cover slips	R. Langenbrinck
Multiwell plates, non-tissue culture treated (6-,12-, 24-, 48-, 96-well (round bottom))	BD Corning
Multiwell plates, tissue-culture treated (6-,12-, 24-, 48-, 96-well	TPP

(round or flatbottom))	
Parafilm M®	Bemis NA
Pasteur pipettes	Corning
PCR tube (0.1 ml) and cap strips, domed	Eppendorf
Pipette filter tips (10 µl, 20 µl, 100 µl, 200 µl, 1000 µl)	Starlab
Pipette tips (10 µl, 200 µl, 1000 µl)	Gilson
Pipette tips (200 µl) for multi-channel pipettes	Rainin
Plastic serum pipettes (2 ml)	Greiner Bio-One
Polypropylene round bottom tubes (5 ml)	BD Falcon
Polystyrene round-bottom tube with cell-strainer cap (5 ml)	BD Falcon
Reagent reservoir, sterile (50 ml)	Corning
Safe-lock tubes (0.5 ml, 1.5 ml, 2.0 ml and 5.0 ml)	Eppendorf
Serological pipettes (2ml, 5 ml, 10 ml, 25 ml, 50 ml)	BD Falcon
Sterile syringe driven filter (0.22 µm)	Millipore
Superfrost™ Ultra Plus Adhesion Slides	Thermo Scientific
Syringe, Norm-Ject tuberkulin (1 ml)	Henke Sass Wolf
Syringes with luer lock tip (1, 5, 10, 30 and 50 ml)	Terumo
T cell dishes (60, 100), suspension	Sarstedt
Warming pad	

4.1.7. Technical Laboratory Equipment

Product	Supplier
^{137}Cs irradiation unit (OB. 58/902-1; FA)	Buchler GmbH
Agilent2100 Bioanalyzer	Agilent Technologies
Analytical Balance (AE163)	Mettler Toledo
Digital calliper gauge	Carl Roth
Cell culture incubator (Heracell 240i)	Thermo Scientific
Cell Sorter (FACSAria™ III)	BD Biosciences
Centrifuge (Heraeus™ Multifuge™ X3 FR)	Thermo Scientific
Centrifuge (Megafuge 2.0R)	Heraeus
Cryotome (CM3050S)	Leica
Dissecting Instruments	Fine Science Tools
Flow Cytometer (FACSCanto™ II)	BD Biosciences
Fluorescence Mircroscope (AxioObserver Z1)	Carl Zeiss
Freezer (-20°C)	Liebherr
Freezer (-80°C)	Thermo Fisher Scientific
Fridge (4°C)	Liebherr
Gammacell 1000 D (^{137}Cs)	Best Theratronics
Gammatron Cobalt 60 device	Siemens

Glassware	Schott
Heatblock (Thermo mixer comfort)	Eppendorf
Ice Machine	Hoshizaki
Liquid Nitrogen Tank (Cryosystem 6000)	MVE
Magnetic stirrer (heatable)	Heidolph Instruments
Micro pipettes (2-1000 µl)	Gilson
Microcentrifuge (Heraeus™ Fresco™ 17)	Thermo Scientific
Microplate Reader (Infinite M200)	Tecan
Microscope (AxioVert A1)	Carl Zeiss
Microwave	Bosch
Milli-Q® Integral Water Purification System	Millipore
Multichannel pipettes (200 µl; 8, 12 channels)	Rainin
Neubauer haemocytometer	Brand
PCR Machine (PTC-225)	MJ Research™ Inc.
Pipetboy (accu-jet® pro)	Brand
Real-time PCR Machine (LightCycler® 480 II)	Roche
Roller-Mixer (RM5)	Karl Hecht
Spectrophotometer (NanoDrop 2000c)	PEQLAB Biotechnology
Sterile Laminar Flow cabinet (Herasafe KSP)	Thermo Scientific
Vacuum Pump	neoLab
Vortexer (Reax 2000)	Heidolph Instruments
Water Bath (SW21)	Julabo

4.1.8. Software

Name	Company
Office 2010	Microsoft Cooperation
EndNote X7.5	Thomson Reuters
FACSDiva software v.6.1.3	BD Biosciences
FlowJo software v.X.06	Tree Star, Inc.
AxioVision LE Rel. 4.8	Carl Zeiss Imaging Solutions GmbH
ZEN 2012 blue edition	Carl Zeiss Microscopy GmbH
Fiji (Fiji is just ImageJ)	LOCI, University of Wisconsin-Madison
Incscape v.0.91	Freeware
GraphPad Prism 6	GraphPad Software, Inc.
Ingenuity® Pathway Analysis (IPA®)	QIAGEN
Gene-E v.3.0.204	Broad Institute, Inc.
Venny 2.1.0	BioinfoGP, CNB-CSIC
InteractiVenn	VICG, ICMC, USP

Interferome v.2.01	Monash University
STRING v.10.0	String Consortium
LightCycler® 480 SW 1.5	Roche
Tierbase Client v.2009.8.0	4D

4.2. Methods

4.2.1. Murine studies

4.2.1.1. Mouse strains

All mice were bred and housed in the central animal core facility of the German Cancer Research Center (DKFZ) under specific pathogen-free conditions. The animal experiments were performed according to governmental and institutional guidelines (based on the German Animal Welfare Act) and were authorized by local regulatory authorities (Regierungspräsidium Karlsruhe, Germany). Table 16 lists the strains used in this work.

Table 16. Mouse strains

Strain	Description	Origin
C3HeB/Fe (C3H)	C3H substrain not carrying the mouse mammary tumour virus (MMTV)	Charles River
RIP1-TAg5 (RT5) (C3HeB/Fe background)	SV40TAg expression, controlled by the rat insulin promotor 1 (RIP1) leads to spontaneous development of insulinoma in β-islets	D. Hanahan
TCRtg/TCRCD8 (TCR8) (C3HeB/Fe background)	Transgenic for an MHC class I-restricted (H2-Kk), SV40TAg-specific TCR	T. Geiger, R. Flavell

4.2.1.2. Preparation of murine tissue

Mice, euthanized with CO_2, were disinfected using 70 % ethanol and dissected under the laminar flow. The organs of interest were harvested under sterile conditions: spleen, pancreas and/or lung were removed and kept in PBS on ice until further use. Tumours were separated from the pancreatic tissue with the use of a scalpel and forceps; their size (diameter) was measured with a calliper before they were either collected in PBS on ice or were placed in cryomolds and embedded in OCT-compound. The embedded tissue was gradually frozen in an isopropanol-filled freezing container and subsequently stored at -80°C for immunohistochemistry.

4.2.1.3. Anaesthesia

A mixture of Rompun 2 % (20 mg/ml xylazine) and Ketanest S (25 mg/ml ketamine) was prepared in PBS with a final concentration of 2 mg/ml xylazine and 10 mg/ml ketamine. Mice were injected intraperitoneally (i.p.) with 66 µl of the mixture per 10 g body weight, which provided a 20-30 min duration of anaesthesia. Anaesthetized mice were treated with ophthalmic ointment (Bepanthen® eye and nose ointment) and kept warm using a warming pad, to prevent desiccation-induced blindness and hypothermia. Pedal and eye blink reflexes were monitored every 10 min during anaesthesia, to determine the depth of anaesthesia.

4.2.1.4. Animal irradiation

Local low dose irradiation (local LDI)

Prior to local irradiation, 24-week old RT5 mice were anaesthetized and placed on a warming pad in the Gammatron Cobalt 60 therapy unit (Siemens), an open γ-irradiation device. 2 Gy were applied to the pancreas by focussing the radiation beam on the abdominal region. To reduce stray radiation the caudal and cranial areas were covered with 3 mm lead shields (Figure 32).

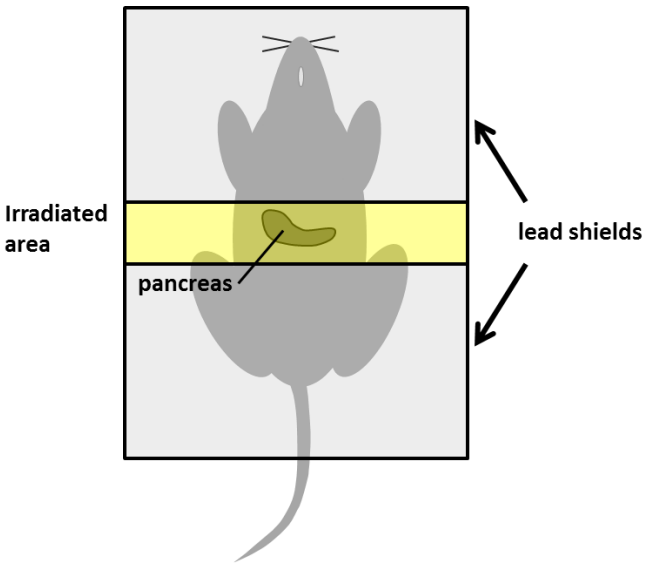

Figure 32 Schematic representation of mouse local irradiation.
Anaesthetized RT5 mice were placed back down on warming pads in the Gammatron therapy unit. The irradiation beam was focussed on the abdominal region (yellow shaded area) and the caudal and cranial areas were shielded with lead plates (grey shaded areas).

Total body irradiation (TBI)

8-12-week old C3H wt mice were placed in mouse pie cages and transferred to the animal irradiation unit OB.58/902-1 (^{137}Cs source, Buchler) where they were subjected to 2 Gy total body irradiation (TBI).

4.2.1.5. Adoptive T cell transfer

Spleens from TCR8 mice were washed twice with sterile, ice-cold PBS and cut into pieces using a scalpel. These fragments were minced through 100 µm cell strainers using the plunger of a syringe, while continuously rinsing the fragments with ice-cold RPMI, to obtain a single-cell suspension. After centrifugation of the cell suspension at 400 g and 4°C for 7 min, the supernatant was discarded and the cells were resuspended in 3 ml ACK (ammonium chloride potassium phosphate) buffer per spleen to lyse all erythrocytes. After 60 sec at room temperature, 10 ml RPMI were added to stop the lysis. The splenocytes were centrifuged as before. Following centrifugation, the supernatant was discarded and the cell pellet was resuspended in mouse medium complemented with 10 U/ml mIL-2 and 25 nM TAg peptide 560-568. To remove residual cell debris, derived from erythrocyte lysis, the cell suspension was passed through a 40 µm cell strainer. The number of living cells was determined by counting

trypan blue stained cells using a Neubauer haemocytometer. $1.5x10^7$ viable cells were distributed evenly in a tissue culture treated six-well plate and cultured in mouse medium containing mIL-2 and the TAg peptide 560-568.
After 72 hrs, the activated and expanded SV40TAg-specific $CD8^+$ T cells were collected, centrifuged and resuspended in PBS. The cell number was adjusted to $25x10^6$ cells/ml and 200 µl ($5x10^6$) of the cell suspension were injected i.p. into RT5 mice.

4.2.1.6. Elicitation of peritoneal macrophages & peritoneal lavage

Recruitment of macrophages into the peritoneal cavity can be induced by aged thioglycolate medium which causes sterile peritonitis (Li et al., 1997). A 3 % thioglycolate solution was prepared from thioglycolate medium powder (AppliChem). For sterilization the solution was autoclaved and passed through a 0.22 µm filter. Before use, the solution was kept at room temperature for at least 6 weeks to age. C3H wt mice were injected i.p. with 1 ml of the aged solution, to induce the recruitment of macrophages into the peritoneal cavity. 72 hrs after injection the peritoneal exudate cells (PECs) were harvested by peritoneal lavage. For that, the mice were sacrificed with CO_2, disinfected using 70 % ethanol and transferred to a laminar flow. Without opening the peritoneal cavity, the ventral skin was removed. To collect the peritoneal cells, 10 ml of ice-cold DMEM were injected into the peritoneal cavity with a 27 G needle. By withdrawing and reinjecting the medium, the peritoneal cavity was washed and the cells were removed. Additionally, the abdomen was gently massaged to loosen attached cells before the medium, which contained the PECs, was withdrawn and transferred to a centrifugation tube. The cells were kept on ice until further use.

4.2.1.7. PEC transfer

For the transfer of PECs into RT5 mice, the thioglycolate-elicited PECs, which were collected from C3H wt mice by peritoneal lavage, were centrifuged at 400 g and 4°C for 8 min. After centrifugation, the supernatant was discarded and the cells were resuspended in PBS. The cell suspension was passed through a 100 µM cell strainer before the cell number was determined. The cell number was adjusted to $5x10^6$ cells per 150 µl which were injected intravenously (i.v.) into 24-week old RT5 mice.

4.2.1.8. PKH26 labelling of peritoneal macrophages

To track transferred PECs in RT5 mice, the cells were labelled with PKH26 before the transfer. To selectively label macrophages, the 'PKH26 Red Fluorescent Cell Linker Kit for Phagocytic Cell Labelling' (Sigma) was used. The establishment of a protocol to detect transferred peritoneal macrophages was part of L. Nögel's master thesis; therefore this method was already published therein. The experiments were conducted by L. Nögel under my supervision. The thioglycolate-elicited PECs were stained with PKH26 according to the manufacturers protocol ('PKH26 Red Fluorescent Cell Linker Kit for General Cell Membrane Labelling' with Diluent B instead of Diluent C). All steps were performed at room temperature. In detail, the thioglycolate-elicited peritoneal cells were centrifuged (400 g for 8 min). Afterwards, the supernatant was removed and the cells were resuspended in PBS. The cell suspension was passed

through a 100 µm cell strainer before the cell number was determined. $2x10^7$ cells were centrifuged at 400 g for 5 min, the supernatant was removed and the cells were resuspended in 1 ml Diluent B. A 2x dye solution was prepared by adding 16 µl of the PKH26 dye stock to 1 ml Diluent B obtaining a concentration of 16 µM PKH26. 1 ml of the 2x dye solution were added directly to the cell suspension and immediately mixed well by pipetting. The staining was stopped after 1-5 min by adding 2 ml FCS. 5 ml complete medium were added to the tube after 1 min incubation, and the cells were centrifuged (10 min, 400 g). After centrifugation, the supernatant was removed and the cells were resuspended in 10 ml complete medium. The cell suspension was transferred to a new tube and washed another 2 times with complete medium before the cells were resuspended in PBS. The cell number was assessed by counting in a Neubauer haemocytometer. $5x10^6$ cells in 150 µl PBS were injected intravenously (i.v.) into 24-week old RT5 mice.

4.2.1.9. Macrophage depletion

Macrophages were depleted from RT5 mice by administration of Clodrosome. Clodrosome is a suspension of liposomes in PBS. The liposomes contain clodronate disodium salt (5 mg/ml) which is cytotoxic. RT5 mice received an initial injection of 200 µl, followed by injections of 100 µl every 5 days over the course of 3 weeks or for the duration of the experiment. Control liposomes (Encapsome) did not contain clodronate disodium salt.

4.2.1.10. iNOS inhibition

iNOS inhibition in RT5 mice was accomplished by administration of 1400w ((N-[[3-(Aminomethyl) phenyl]methyl]-ethanimidamide), a selective iNOS inhibitor. To ensure continuous dosing, 200 µl of the inhibitor at a concentration of 240 µg/µl were filled into slow release mini-osmotic pumps which were implanted into RT5 mice. This provided a dose of 144 mg/kg/d over 2 weeks. Implantation of the mini-osmotic pumps was performed by T. Seibel and the procedure is described in his doctoral thesis (Seibel, 2010). Briefly, in a sterile environment, ALZET mini-osmotic pumps, containing 1400w or PBS were inserted into a 25 mm long pocket under the dorsal skin of anesthetized RT5 mice. Afterwards, the wound was closed using Ethicon Mersilene 3-0 suture.

4.2.2. Cell culture methods

All cells were cultured in cell culture plates, dishes or flasks under sterile conditions at 37°C and 5 % CO_2 (v/v).

4.2.2.1. Determination of cell number and viability

To quantify viable cells in a cell suspension, a 10 µl aliquot of each sample was diluted 1:10 in trypan blue solution and applied to a Neubauer haemocytometer. Trypan blue stains dead cells, therefore unstained (live) cells were counted in the four large squares of the counting chamber with a hand tally counter. The cell number per ml was calculated using this formula:

$$\text{Nr of cells/ml} = \frac{\text{Nr of counted cells}}{\text{Nr of counted squares (4)}} \text{ x dilution factor (10) x chamber factor } (10^4)$$

4.2.2.2. Irradiation of cells

Thioglycolate-elicited peritoneal cells collected from C3H wt mice by peritoneal lavage were centrifuged at 400 g and 4 °C for 8 min. After centrifugation, the supernatant was discarded and the cells were resuspended in macrophage medium. The cell suspension was passed through a 100 µM cell strainer before the cell concentration was determined. The samples were transported on ice to the Gammacell 1000 D, where they were irradiated with 2 Gy. After irradiation, the cells were transferred to suspension culture dishes (TC dishes; Sarstedt) with $5x10^5$ cells/ml. The cells were incubated at 37°C and 5 % CO_2 for the indicated times.

4.2.2.3. IFN-γ blockade

For *ex vivo* irradiation of PECs under IFN blockade, the macrophage medium was supplemented with R4-6A2 (Abrams et al., 1992) and/or 7F-D3 (Belardelli et al., 1987) hybridoma supernatant (HSN) which was kindly provided by Prof. Rainer Zawatzky. These supernatants contain monoclonal antibodies directed against murine IFN-γ (R4-6A2) or IFN-β (7F-D3) and have been tested to neutralize 20 IU of the respective interferon at a dilution of 1:3632 (R4-6A2 HSN) or 1:6700 (7F-D3 HSN). A final concentration of 1:50 was used to provide a surplus of neutralizing antibodies, to completely block IFN-γ and IFN-β in culture.
The thioglycolate-elicited peritoneal cells collected from C3H wt mice were centrifuged (400 g, 4 °C, 8 min), the supernatant was discarded and the cells were resuspended in macrophage medium. Each cell suspension was divided into 5 samples, according to the 5 treatment groups listed in the following table. The samples of the unirradiated and irradiated group were not treated with neutralizing antibodies. The samples of the Irr + α-IFN-γ group and the samples of the Irr + α-IFN-β group were resuspended in macrophage medium containing R4-6A2 HSN or 7F-D3 HSN, respectively. The samples of the Irr + α-IFN-γ/α-IFN-β group were resuspended in macrophage medium containing both HSNs.

Treatment group
unirr
Irr
Irr + α-IFN-γ
Irr + α-IFN-β
Irr + α-IFN-γ/α-IFN-β

The samples of the indicated groups were then irradiated with 2 Gy at the Gammacell 1000 D. Following irradiation, the cells were transferred to non-tissue culture-treated 6 well plates with $1x10^6$ cells per well in 3 ml medium as indicated. As a positive control, unirradiated

PECs were stimulated with 20 ng/ml mIFN-γ. The cells were incubated at 37°C and 5 % CO_2 for the specified times.

4.2.2.4. HUVEC Culture and Stimulation

HUVECs were thawed and cultured according to the manufacturer's instructions. In detail, frozen HUVECs, pooled from up to four donors, were commercially acquired (PromoCell) and stored in a cryovial in liquid nitrogen. For the experiment, the cells were thawed by placing the cryovial in a water bath for 2 min at 37°C. Before opening the vial under the laminar flow, it was disinfected with 70 % ethanol. The cells were transferred to a 75 cm^2 tissue culture flask containing 20 ml pre-warmed HUVEC medium, a basal medium for endothelial cells, supplemented with 3 % FBS, 0.1 % FGF-2, 0.1 % VEGF, 0.1 % R3-IGF-1, 0.1 % ascorbic acid, 0.1 % heparin, 0.12 % gentamicin sulfate amphotericin B and 0.02 % hydrocortisone (PanBiotech). After 24 hrs, the cells had attached to the culture flask and the medium was replaced. The cells reached 70-90 % confluency after 2-4 days in culture and were subcultured: the supernatant was removed and the cells were rinsed with PBS containing 2 % HEPES solution (v/v) and 2 % EDTA (v/v; Versen). To detach the cells, 4 ml pre-warmed 1x Trypsin/EDTA solution were added to the flask and incubated for 5-10 min at RT. When the cells detached, 5 ml FCS were added to stop the enzymatic activity of trypsin and the cell suspension was transferred to a centrifugation tube. The cells were centrifuged at 220 g for 3 min and the supernatant was discarded. After resuspending the cells in HUVEC medium, the cell number and viability was determined.
For activation with the NO donor DETA NONOate, HUVECs were seeded in 6-well plates with $1x10^5$ cells per well in 3 ml HUVEC medium. When the cells were confluent, the medium was replaced by HUVEC medium containing the indicated concentrations of DETA NONOate and/or 10 ng/ml hTNF-α. The cells were stimulated for 18 hrs.

4.2.3. Cell biology methods

4.2.3.1. Flow Cytometry

Preparation of single-cell suspensions:
From RT5 tissues: tumours, lungs and spleens, isolated from RT5 mice, were transferred to 1.5 ml eppendorf tubes and homogenized with small scissors. Subsequently, the tissue was incubated at 37°C in 1 ml digestion solution. Every 10 min the samples were resuspended. After 30 min, the cell suspensions were passed through 100 µm cell strainers and any undigested tissue was mashed through with the plunger of a syringe, while the strainer was continuously rinsed with ice-cold complete medium to stop the enzymatic digestion. Pancreata from RT5 mice were incubated at 37 °C in 5 ml pancreas digestion mix for 10 min. They, too, were passed through cell strainers. After centrifugation at 400 g and 4 °C for 8 min, the cells were resuspended in FACS buffer.
Freshly isolated PECs: thioglycolate-elicited peritoneal cells collected from C3H wt mice were centrifuged (400 g, 4°C, 8 min); the supernatant was discarded and the cells were re-

suspended in FACS buffer. Subsequently, the cell suspension was passed through a 100 µM cell strainer.

Cultured PECs, HUVECs: the medium was removed and the cells were washed once with PBS. To detach the cells, they were incubated for 5 min with 500 µl Accutase solution per well. When the cells detached, 1 ml FCS were added and the cell suspension was transferred to a centrifugation tube. After centrifugation at (400 g, 4 °C, 8 min), the cells were resuspended in FACS buffer.

The single-cell suspensions were transferred to non-tissue culture treated round bottom 96-well plates (BD falcon) with $5x10^5$ to $5x10^6$ cells per well.

Staining: all incubation steps were performed on ice, in the dark. The plates were centrifuged (400 g, 4°C, 5 min) and the supernatant was discarded. The murine cells were resuspended in 100 µl FACS blocking solution, to saturate Fc receptors. HUVECs were blocked using FACS buffer supplemented with 1.5 mg/ml Sandoglobulin. After 20 min incubation, 100 µl FACS buffer were added and the cells were spun down. This was followed by the viability staining with the Zombie NIR™ Fixable Viability Kit or the LIVE/DEAD® Fixable Yellow Dead Cell Stain Kit: 100 µl of DMSO were added to one vial Zombie NIR™ dye and 50 µl of DMSO were added to one vial LIVE/DEAD® Yellow Stain, to reconstitute the lyophilized dyes. The Zombie NIR™ stock solution was diluted 1:1000 and the LIVE/DEAD® Yellow Stain stock solution was diluted 1:500 in PBS for the staining. The cells were resuspended in 200 µl of the respective diluted viability dye and incubated for 20 min on ice. Subsequently, the cells were centrifuged and washed twice with 200 µl FACS buffer to remove unbound dye molecules. For the surface staining, the cells were incubated for 20 min with the antibody mixes as defined in Tables 17-20. After the surface staining, the cells were washed twice with 200 µl FACS buffer and transferred to 5 ml round bottom tubes for acquisition with the FACS Canto II.

Table 17 HUVEC adhesion molecule staining

Antibody	Conjugation	Dilution
CD31	BV421	1:100
ICAM-1 (CD54)	FITC	1:100
VCAM-1 (CD106)	APC	1:100
E-Selectin (CD62E)	PE	1:100
FACS buffer		Ad 100 µl

Table 18 T cell surface antigen staining

Antibody	Conjugation	Dilution
CD45	V450	1:500
CD3e	APC	1:100

CD4	APC-Cy7	1:100
CD8a	PerCP	1:100
FACS buffer		Ad 100 µl

Table 19 Macrophage phenotype staining

Antibody	Conjugation	Dilution
CD11b	PerCP	1:100
F4/80	APC	1:100
CD206 (MMR)	FITC	1:100
I-A/I-E (MHC class II)	PB	1:100
FACS buffer		Ad 100 µl

Table 20 Myeloid cell population staining

Antibody	Conjugation	Dilution
CD45-V450	V450	1:500
CD11b	PE-Cy7	1:100
F480	AF488	1:50
CD11c	PerCP	1:100
CD14	ApC-Cy7	1:100
CD86	PE	1:100
Ly-6G/Ly-6C (Gr-1)	APC	1:100
FACS buffer		Ad 100 µl

For flow cytometric analysis of PKH26 positive cells in RT5 mice, the single cell suspensions of RT5 tissues were not stained with antibodies against surface antigens and cell viability was assessed by adding one volume of SYTOX blue solution to the cells shortly before acquisition of the samples at the FACS Canto II.

Intracellular Staining: the cells that were to be stained for iNOS were fixed and permeabilized using the FoxP3/Transcription Factor Staining Buffer Set (eBiocscience), according to the manufacturer's instructions: after the surface antigen staining, the cells were washed twice with FACS buffer, followed by resuspension in 200 µl Fixation/Permeabilization Solution (Fixation/Permeabilization Concentrate 1:4 in Fixation/Permeabilization Diluent) and incubation on ice, in the dark for at least 30 min. The cells were washed twice in 200 µl 1x Permeabilization buffer (Permeabilization Buffer (10X) 1:10 in ddH_2O). For intracellular staining, the cells were resuspended and incubated for 30 min with the iNOS antibody (diluted 1:200 in 1x Permeabilization buffer). The cells were then washed twice with 200 µl 1x Per-

meabilization buffer and once with 200 µl FACS buffer. Afterwards, the samples were resuspended in 100 µl FACS buffer and were transferred to 5 ml round bottom tubes, for acquisition at the FACS Canto II.

Acquisition: compensation of spectral overlaps was performed using compensation beads or cells stained with the single antibodies used for the respective staining. The compensation beads were stained on the same plate as the samples to guarantee identical staining conditions. Furthermore, cells left unstained and cells stained only with the viability dye were used as reference samples in the compensation calculations. Compensation was calculated automatically by the BD FACS Diva software and was manually verified. The obtained data was analysed using the FlowJo Software. The gates were set according to the fluorescence minus one (FMO) controls.

IFN-γ secretion assay: to assess the activation state of *in vitro* stimulated T cells, a flow cytometry based IFN-γ secretion assay was performed by L. Nögel, as described in his master thesis. Splenocytes from TCR8 mice were isolated and cultured as described before (Chapter 4.2.1.5). The cells were collected, centrifuged at 400 g and 4°C for 8 min and resuspended in FACS buffer. The cells were distributed to a non-tissue culture treated round bottom 96 well plate (BD falcon) with $5x10^5$ cells per well. After Fc receptor blocking, the cells were incubated with 100 µl IFN-γ catch reagent (1:20 in mouse medium) for 20 min on ice. To remove unbound catch reagent, the cells were centrifuged and resuspended in 200 µl pre-warmed mouse medium. For cytokine secretion, the cells were incubated at 37 °C and 5 % CO_2 for 30 min. Afterwards the cells were washed with FACS buffer and viability staining with the LIVE/DEAD® Fixable Yellow Dead Cell Stain Kit was performed as described before. This was followed by surface marker staining (Table 18) including the IFN-γ detection antibody for 20 min on ice. After washing the cells, they were resuspended in FACS buffer and the samples were acquired with the FACS Canto II.

4.2.3.2. Immunofluorescence

5-7 µm cryosections of frozen tissue samples, embedded in OCT compound, were mounted on Superfrost Ultra Plus Adhesion Slides. The sections were air-dried at room temperature (RT) before they were fixed for 10 min in ice-cold acetone. When the acetone was evaporated, the sections were encircled with a PAP pen creating a hydrophobic barrier around the sections. The slides were then transferred to a lightproof humidity chamber for immunostaining. First the sections were rehydrated for 20 min using a serum-free protein-block solution which blocks Fc receptors. Subsequently, the sections were stained with the first primary antibody: 100 µl of the respective antibody diluted 1:50 in IF staining buffer were pipetted onto the sections and left at RT for one hour or at 4 °C over night. The slides were rinsed with PBS to remove excess antibody and washed three times for 5 min in PBS. The highly cross absorbed secondary antibodies were diluted 1:200 in IF staining buffer and centrifuged for 10 min at 13000 g to precipitate antibody aggregates. The sections were then

incubated at RT for one hour with 200 µl of the first secondary antibody. Again the slides were rinsed with PBS after the incubation and washed three times for 5 min in PBS. Staining of the second primary and secondary antibodies was performed in the same manner. Finally a coverslip was sealed to the slide using Fluoromount G, a mounting medium containing DAPI (4',6-diamidino-2-phenylindole) to counterstain nuclei.
For analysis immunofluorescence (IF) images of the sections were taken at the AxioObserver Z1 (Zeiss). The images were processed using the AxioVision or Zen blue software (Zeiss) and analysed with Fiji software.

4.2.4. Molecular biology methods

4.2.4.1. RNA isolation & quality assessment

For RNA works, the workplace and all required equipment was wiped with RNaseZAP® to prevent RNase contamination. Moreover, only nuclease and RNase free eppendorf tubes, reagents and filter tips were used.

RNA was isolated from freshly isolated or cultured thioglycolate-elicited peritoneal cells. The freshly isolated PECs were centrifuged at 400 g and 4 °C for 8 min. After centrifugation, the supernatant was discarded and the cells were resuspended in PBS. The cell suspensions were passed through 100 µM cell strainers and the cell numbers were determined using a Neubauer haemocytometer. Up to $1x10^7$ cells were transferred to 1.5 ml eppendorf tubes, centrifuged (400 g, 4°C, 8 min) and the supernatant was discarded. The cells were resuspended in 100 µl RLT lysis buffer containing 2-Mercaptoethanol and were homogenized by vigorous pipetting and vortexing. The lysates were stored at -80 °C over night or until RNA isolation. Cultured PECs were lysed directly in the plate: after removing the supernatant, the attached cells were rinsed with PBS. Then 600 µl RLT buffer containing 2-Mercaptoethanol were added to the well and the cells were homogenised by pipetting. Finally the lysates were transferred to 1.5 ml eppendorf tubes which were vortexed and stored at -80 °C over night or until RNA isolation.

RNA from PEC lysates was isolated using the RNeasy Mini Kit (QIAGEN), following the protocol 'Purification of Total RNA from Animal Cells using Spin Technology' by QIAGEN, including the on-column DNase digestion using the RNase-Free DNase Set (QIAGEN). RNA was eluted in 30 µl nuclease free water of which 5 µl were used for quality assessment The other 25 µl were stored at -80 °C until further use. RNA quantity and purity were determined using the NanoDrop 2000c spectrophotometer. RNA integrity was analysed with the Agilent RNA 6000 Nano Assay, according to the manufacturer`s protocol, on the Agilent 2100 Bioanalyzer. The resulting RNA integrity number (RIN) indicated whether RNA was degraded (RIN =1) or intact (RIN =10). Samples with RIN > 8 were accepted for downstream analyses.

4.2.4.2. RNA Sequencing

The RNA isolated from *in vivo* or *in vitro* irradiated PECs was diluted as to the requirements of the DKFZ Genomics & Proteomics Core Facility (GPCF) (55 µl with 40 ng/µl) or GATC Biotech (50 µl with 20 ng/µl). The samples were submitted on dry ice for RNA Sequencing. Each sample passed the quality control of the GPCF and GATC, respectively. The GPCF used the Illumina Hiseq2000 for sequencing with the 50 base pair single read sequencing type and the HCS 2.2.58 sequencing software, followed by a FastQC analysis (v. 0.10.0, performed by the GPCF) which confirmed successful sequencing of all samples. GATC Biotech used the Illumina HiSeq2500. They did not give further details regarding the run. For these samples, FastQC analysis (performed by T. Michels) showed contamination with adapter dimers. This however has no effect on downstream analyses, therefore the samples were used for downstream analyses.

4.2.4.3. RT-qPCR

Relative gene expression was analysed by reverse transcription quantitative real time PCR (RT-qPCR).
For the reverse transcription (RT) reactions, 800 ng of the RNA were transcribed to complementary DNA (cDNA) using the RevertAid First Strand cDNA Synthesis Kit (Thermo Scientific). Following the manufacturer`s protocol, the RNA template was mixed with 2 µl oligo$(dT)_{18}$ primers and incubated at 65°C for 5 min. The mixture was placed on ice and the following reagents were added (Table 21). A 'no reverse transcriptase control' (-RT) was included to determine genomic DNA contamination.

Table 21 RT reaction mix

Reagent	Volume
5X Reaction Buffer	4 µL
RiboLock RNase Inhibitor (20 U/µL)	1 µL
10 mM dNTP Mix	1 µL
RevertAid M-MuLV RT	1 µL

The reaction mix was then incubated at 60°C for 42 min for cDNA synthesis. Finally the cDNA was stored at -20°C.

Prior to quantitative real time PCR (qPCR) of these samples, all TaqMan assays were tested with regard to their amplification efficiency using universal mouse reference RNA. The RNA was prepared according to the manufacturer's instructions and transcribed into cDNA (as described above). A serial dilution provided solutions with known cDNA concentrations (from 16 ng/µl to 0.004 ng/µl). Following the TaqMan Universal Master Mix II protocol, the PCR reaction mix was prepared and plated out in a 384-well plate. Table 22 shows the mix for one well.

Table 22 qPCR reaction mix

Reagent	Volume
2x TaqMan Universal Master Mix II, with UNG	10 µL
Taqman assay	1 µL
Nuclease free water	4 µL

5 µl of the differently diluted cDNA, were added per well; each concentration in triplicates. A no template control (NTC) was included to monitor contamination of primer-dimer formation. The plate was sealed by LightCycler 480 Sealing Foil and loaded into the LightCycler® 480 II (Roche). The qPCR program which was applied is shown in Table 23.

Table 23 qPCR program

Cycle		Time	Temperature	cycles
UNG incubation		02:00	50 °C	1
Polymerase activation		10:00	95 °C	1
PCR	Denaturation	00:15	95 °C	40
	Annealing/Extension	01:00	60 °C	
Cooling		∞	10 °C	1

The efficiency was determined using the slope of the qPCR standard curve. With the exception of the *Ifng* TaqMan assay, all assays showed acceptable amplification efficiencies (Table 24).

Table 24 TaqMan assay amplification efficiencies

Genesymbol	AssayNr.	Slope	PCR Efficiency
Ifng	Mm01168134_m1	x	-
Ifng II	Mm00801778_m1	x	-
Jak1	Mm00600614_m1	-3.862	110
Stat1	Mm00439531_m1	-4.276	117
Irf1	Mm01288580_m1	-3.42	102
Irf7	Mm00516793_g1	-3.431	102
Nos2	Mm00440502_m1	-3.324	100
Tnf	Mm00443258_m1	-3.656	107
Gapdh	Mm99999915_g1	-3.525	104
Hprt1	Mm03024075_m1	-3.563	105

This was followed by qPCR analysis of the sample cDNA using the tested TaqMan assays and the TaqMan Universal Master Mix II protocol. 5 µl cDNA at a concentration of 4 ng/µl were added to a 384-well plate; each sample in triplicates. 15 µl of the PCR reaction mix were added to each well and the plate was analysed with the LightCycler® 480 II (Roche). The thereby generated gene expression values were normalized to a reference gene (*Hprt*) according to the $\Delta\Delta C_t$ method with a control sample as the calibrator.

4.2.5. Analysis of transcriptomic data

The transcriptomic data, in form of Fastq files, that was generated by RNA sequencing, was analysed by T. Michels using Bioconductor and R according to the 'Count-based differential expression analysis of RNA sequencing data' (Anders et al., 2013) Briefly, the sequenced reads were mapped to the annotated Ensembl mouse reference genome (GRCm38 (mm10)). Subsequently, the reads were summarized to the corresponding genes and normalized (tophat2). The normalized gene expression values were used for differential comparison which was computed using EdgeR. This resulted in differential gene expression data in form of Fold Change (FC) and False Discovery Rate (FDR) values for each gene. Thus differentially-expressed genes were further analysed by Gene-e, STRING, Venny, InteractiVenn, Ingenuity Pathway Analysis and Interferome:

Gene-e (www.broadinstitute.org/cancer/software/GENE-E/): Gene-e was employed to generate overview heat maps of the differentially expressed genes in the *in vivo* and *in vitro* dataset on the basis of the normalized read counts (CPM (counts per million)) per gene. The software was also used to perform unsupervised hierarchical clustering of the samples and the genes. Similar expression patterns between samples were clustered using the distance metric 'One minus Spearman rank correlation'. Expression patterns between genes were clustered with the 'One minus Pearson rank correlation' using an average linkage for both.

STRING (http://string-db.org/): For gene set enrichment analysis, gene sets of interest were uploaded to STRING. The database generated protein interaction networks showing known and predicted, direct (physical) and indirect (functional) associations between the proteins. Furthermore, the database tests the gene sets for Gene Ontology (GO) enrichments and pathway annotations (Szklarczyk et al., 2015).

Venn diagrams were generated using Venny 2.1 (http://bioinfogp.cnb.csic.es/tools/venny/) and InteractiVenn (http://www.interactivenn.net/)(Heberle et al., 2015; Oliveros, 2007-2015). The images were processed in Inkscape, to generate scaled Venn diagrams.

Ingenuity® Pathway Analysis (IPA®, QIAGEN Redwood City, www.qiagen.com/ingenuity): For the identification of pathways that are affected by low dose irradiation, the transcriptome data were analysed through the use of QIAGEN's Ingenuity Pathway analysis. The software maps datasets to the Ingenuity Knowledge Base. Thereby it creates causal networks, identifies upstream regulators, overrepresented biological functions and canonical pathways. The software also takes into account whether a gene is up- or downregulated which enables it to predict whether certain processes are activated or inhibited.

Table 25 IPA Analysis settings I

Selected Cut offs	
Cutoff before duplicate resolution	true
Resolve duplicate on	Expression logFC
Colour using	Expression logFC
Cutoff for logFC	0.585 and consider Both up/down regulated
Cutoff for p-value	0.05
Cutoff for q-value	0.05
Reference set	Ingenuity Knowledge Base (Genes Only)
Relationship to include	Direct and Indirect
Includes Endogenous Chemicals	Yes
Optional Analyses	My Pathways My List

Table 26 IPA Analysis settings II

Filter Summary	
Consider only molecules and/or relationships where	
species =	Mouse OR Uncategorized
confidence =	Experimentally Observed OR High (predicted))
tissues/cell lines =	Other NK cells OR Tissues and Primary Cells not otherwise specified OR CCRF-CEM OR Other Granulocytes OR Memory T lymphocytes not otherwise specified OR Monocytes not otherwise specified OR SR OR Other Organ Systems OR Myeloma Cell Lines not otherwise specified OR Spleen OR Mononuclear leukocytes not otherwise specified OR Central memory helper T cells OR PBMCs OR Other Memory T lymphocytes OR HMC-1 OR Eosinophils OR Intraepithelial T lymphocytes OR Jurkat OR Lymphocytes not otherwise specified OR Monocyte-derived dendritic cells not otherwise specified OR NK cells not otherwise specified OR Other Cell Line OR Cell Line not otherwise specified OR Leukemia Cell Lines not otherwise specified OR Macrophages not otherwise specified OR BA/F3 OR Other T lymphocytes OR Pre-B lymphocytes OR Memory B cells OR Peritoneal macrophages OR HL-60 OR U937 OR Peripheral blood monocytes OR Mature monocyte-derived dendritic cells OR Langerhans cells OR Vd2 Gamma-delta T cells OR Cytotoxic T cells OR Other Cells OR Peripheral blood leukocytes not otherwise specified OR Pro-B lymphocytes OR Vd1 Gamma-delta T cells OR Naive helper T cells OR RPMI-8266 OR Immune cell lines not otherwise specified OR Lymph node OR Other Myeloma Cell Lines OR Other Mononuclear leukocytes OR Activated CD56dim NK cells OR J-774A.1 OR Effector memory RA+ cytotoxic T cells OR Other Macrophages OR Other Macrophage Cancer Cell Lines OR Activated CD56bright NK cells OR Naive B cells OR Mast cells OR RBL-2H3 OR Splenocytes OR Effector memory cytotoxic T cells OR Other Dendritic cells OR Th17 cells OR Plasma cells OR Other Peripheral blood leukocytes OR Natural T-regulatory cells OR RAW 264.7 OR Activated helper T cells OR Other Immune cells OR Macrophage Cancer Cell Lines not otherwise specified OR Activated Vd1 Gamma-delta T cells OR Murine NKT cells OR Hematopoietic progenitor cells OR Other B lymphocytes OR K-562 OR U266 OR Th1 cells OR Neutrophils OR HEL OR Plasmacytoid dendritic cells OR Immature monocyte-derived dendritic cells OR Myeloid dendritic cells OR WEHI-231 OR Central memory cytotoxic T cells OR Other Lymphoma Cell Lines OR Activated Vd2 Gamma-delta T cells OR J774 OR MOLT-4 OR CD4+ T-lymphocytes OR Other Tissues and Primary Cells OR Bone marrow-derived macrophages OR BDCA-3+ dendritic cells OR B lymphocytes not otherwise specified OR Granulocytes not otherwise specified OR Bone marrow cells not otherwise specified OR Other Leukemia Cell Lines OR Megakaryocytes OR Other Lymphocytes OR Other Bone marrow cells OR Other Monocyte-derived dendritic cells OR Effector T cells OR Effector memory helper T cells OR CD56bright NK cells OR Other Immune cell lines OR Th2 cells OR Immune cells not otherwise specified OR THP-1 OR Organ Systems not otherwise specified OR BDCA-1+ dendritic

	cells OR T lymphocytes not otherwise specified OR CD56dim NK cells OR Dendritic cells not otherwise specified OR Other Monocytes OR Cells not otherwise specified OR NB4 OR Thymocytes OR Lymphoma Cell Lines not otherwise specified OR CD34+ cells OR Microglia OR Monocyte-derived macrophage OR Peripheral blood lymphocytes OR Bone marrow-derived dendritic cells)
mol. types =	biologic drug OR chemical - endogenous mammalian OR chemical - endogenous non-mammalian OR chemical - kinase inhibitor OR chemical - other OR chemical - protease inhibitor OR chemical drug OR chemical reagent OR chemical toxicant OR complex OR cytokine OR disease OR enzyme OR function OR G-protein coupled receptor OR group OR growth factor OR ion channel OR kinase OR ligand-dependent nuclear receptor OR mature microRNA OR microRNA OR other OR peptidase OR phosphatase OR transcription regulator OR translation regulator OR transmembrane receptor OR transporter)

Interferome (http://www.interferome.org/)**:** The Interferome database was searched to identify interferon (IFN) regulated genes (IRGs) in the *in vivo* and *in vitro* datasets (Rusinova et al., 2013). The following search conditions were applied:

Table 27 Interferome search conditions

Search Conditions	
Interferome Type	Any
Interferome SubType	Any
Treatment Concentration	Any
Treatment Time	Any
Vivo/Vitro	Any
Species	Mus musculus
System	Haemopoietic/Immune
Organ	Any
Cell	CD8+ DC; blood monocyte derived macrophages; monocyte derived macrophages; whole tissue; monocyte derived DCs; derived macrophages; peritoneal exudate cells
Cell Line	Any
Normal/Abnormal	Normal
Fold Change Up/Down	1.5

4.2.6. Statistical Analysis

All statistical analyses were performed using GraphPad Prism 6 software, except for the analyses of transcriptome data and data from the IFN blockade experiments. The two-sided (non-parametric) Mann-Whitney test or the two-sided, unpaired (parametric) t-test was used to assess differences between the compared groups. The correlation between the number of $CD11b^+$ cells and tumour size was calculated using the Spearman`s rank correlation coefficient test and the survival data was analysed with the Log-rank (Mantel-Cox) test. Differences between the treatment groups in the IFN blockade experiment were calculated

by Dr. Maria Pritsch using the paired, two-tailed t-test with the SAS software. Significant differences are represented by one or more asterisks: * $p<0.05$; ** $p<0.01$; *** $p<0.001$; **** $p<0.0001$.

Statistical analysis of transcriptome data was performed by T. Michels in the course of count-based differential gene expression analysis (Anders et al., 2013) of the raw data. To account for the multiple testing error occurring in such analyses, false discovery rate (FDR) values were computed for each result (gene). A p-value <0.05 indicates that 5 % of the results might be false positives. The FDR gives an estimation on how many of the significant results are false positives. By accepting results with FDR values <0.05, the possibility of false positive results is reduced to 5 %. Furthermore, analysis of the transcriptome data by IPA, String and Interferome generated p-values or FDRs, which were computed by the designated software or database. Insofar as it was known, the applied tests are stated in the figure legends.

5. REFERENCES

Abrams, J. S., Roncarolo, M.-G., Yssel, H., Andersson, U., Gleich, G. J., and Silver, J. E. (1992). Strategies of Anti-Cytokine Monoclonal Antibody Development: Immunoassay of IL-10 and IL-5 in Clinical Samples. Immunological Reviews *127*, 5-24.

Adams, T. E., Alpert, S., and Hanahan, D. (1987). Non-tolerance and autoantibodies to a transgenic self antigen expressed in pancreatic [beta] cells. Nature *325*, 223-228.

Aguirre-Ghiso, J. A. (2007). Models, mechanisms and clinical evidence for cancer dormancy. Nat Rev Cancer *7*, 834-846.

Ahmad, M., Rees, R. C., and Ali, S. A. (2004). Escape from immunotherapy: possible mechanisms that influence tumor regression/progression. Cancer immunology, immunotherapy : CII *53*, 844-854.

Ahuja, D., Saenz-Robles, M. T., and Pipas, J. M. (2005). SV40 large T antigen targets multiple cellular pathways to elicit cellular transformation. Oncogene *24*, 7729-7745.

Akira, S., Takeda, K., and Kaisho, T. (2001). Toll-like receptors: critical proteins linking innate and acquired immunity. Nat Immunol *2*, 675-680.

Anders, S., McCarthy, D. J., Chen, Y., Okoniewski, M., Smyth, G. K., Huber, W., and Robinson, M. D. (2013). Count-based differential expression analysis of RNA sequencing data using R and Bioconductor. Nat Protocols *8*, 1765-1786.

Apetoh, L., Ghiringhelli, F., Tesniere, A., Criollo, A., Ortiz, C., Lidereau, R., Mariette, C., Chaput, N., Mira, J. P., Delaloge, S.*, et al.* (2007). The interaction between HMGB1 and TLR4 dictates the outcome of anticancer chemotherapy and radiotherapy. Immunol Rev *220*, 47-59.

Asea, A. (2008). Heat shock proteins and toll-like receptors. Handbook of experimental pharmacology, 111-127.

Azimi, F., Scolyer, R. A., Rumcheva, P., Moncrieff, M., Murali, R., McCarthy, S. W., Saw, R. P., and Thompson, J. F. (2012). Tumor-Infiltrating Lymphocyte Grade Is an Independent Predictor of Sentinel Lymph Node Status and Survival in Patients With Cutaneous Melanoma. Journal of Clinical Oncology *30*, 2678-2683.

Baeriswyl, V., and Christofori, G. (2009). The angiogenic switch in carcinogenesis. Semin Cancer Biol *19*, 329-337.

Baker, D. G., and Krochak, R. J. (1989). The response of the microvascular system to radiation: a review. Cancer investigation *7*, 287-294.

Balkwill, F., and Mantovani, A. (2001). Inflammation and cancer: back to Virchow? The Lancet *357*, 539-545.

Baluk, P., Hashizume, H., and McDonald, D. M. (2005). Cellular abnormalities of blood vessels as targets in cancer. Current Opinion in Genetics & Development *15*, 102-111.

Barker, H. E., Paget, J. T. E., Khan, A. A., and Harrington, K. J. (2015). The tumour microenvironment after radiotherapy: mechanisms of resistance and recurrence. Nat Rev Cancer *15*, 409-425.

Baselli, E. C., and Greenberg, R. E. (2000). Intravesical therapy for superficial bladder cancer. Oncology (Williston Park, NY) *14*, 719-729; discussion 729-731, 734, 737.

Bates, G. J., Fox, S. B., Han, C., Leek, R. D., Garcia, J. F., Harris, A. L., and Banham, A. H. (2006). Quantification of Regulatory T Cells Enables the Identification of High-Risk Breast Cancer Patients and Those at Risk of Late Relapse. Journal of Clinical Oncology *24*, 5373-5380.

Belardelli, F., Gessani, S., Proietti, E., Locardi, C., Borghi, P., Watanabe, Y., Kawade, Y., and Gresser, I. (1987). Studies on the Expression of Spontaneous and Induced Interferons in Mouse Peritoneal Macrophages by Means of Monoclonal Antibodies to Mouse Interferons. Journal of General Virology *68*, 2203-2212.

Bernot, D., Peiretti, F., Canault, M., Juhan-Vague, I., and Nalbone, G. (2005). Upregulation of TNF-alpha-induced ICAM-1 surface expression by adenylate cyclase-dependent pathway in human endothelial cells. Journal of cellular physiology *202*, 434-441.

Bezu, L., Gomes-da-Silva, L. C., Dewitte, H., Breckpot, K., Fucikova, J., Spisek, R., Galluzzi, L., Kepp, O., and Kroemer, G. (2015). Combinatorial Strategies for the Induction of Immunogenic Cell Death. Frontiers in immunology *6*.

Biswas, S. K., and Mantovani, A. (2010). Macrophage plasticity and interaction with lymphocyte subsets: cancer as a paradigm. Nat Immunol *11*, 889-896.

Blanchette, J., Jaramillo, M., and Olivier, M. (2003). Signalling events involved in interferon-gamma-inducible macrophage nitric oxide generation. Immunology *108*, 513-522.

Bonertz, A., Weitz, J., Pietsch, D. H., Rahbari, N. N., Schlude, C., Ge, Y., Juenger, S., Vlodavsky, I., Khazaie, K., Jaeger, D.*, et al.* (2009). Antigen-specific Tregs control T cell responses against a limited repertoire of tumor antigens in patients with colorectal carcinoma. J Clin Invest *119*, 3311-3321.

Brown, J. M. (2014). Vasculogenesis: a crucial player in the resistance of solid tumours to radiotherapy. The British journal of radiology *87*, 20130686.

Brubaker, S. W., Bonham, K. S., Zanoni, I., and Kagan, J. C. (2015). Innate immune pattern recognition: a cell biological perspective. Annual review of immunology *33*, 257-290.

Budhu, S., Wolchok, J., and Merghoub, T. (2014). The importance of animal models in tumor immunity and immunotherapy. Current opinion in genetics & development *24*, 46-51.

Burnet, F. M. (1967). IMMUNOLOGICAL ASPECTS OF MALIGNANT DISEASE. The Lancet *289*, 1171-1174.

Burnet, F. M. (1970). The concept of immunological surveillance. Progress in experimental tumor research *13*, 1-27.

Burnet, M. (1957). Cancer—A Biological Approach: III. Viruses Associated with Neoplastic Conditions. IV. Practical Applications. British Medical Journal *1*, 841-847.

Burnette, B., and Weichselbaum, R. R. (2013). Radiation as an immune modulator. Semin Radiat Oncol *23*, 273-280.

Cai, X., Yin, Y., Li, N., Zhu, D., Zhang, J., Zhang, C.-Y., and Zen, K. (2012). Re-polarization of tumor-associated macrophages to pro-inflammatory M1 macrophages by microRNA-155. Journal of Molecular Cell Biology.

Campbell, M. J., Tonlaar, N. Y., Garwood, E. R., Huo, D., Moore, D. H., Khramtsov, A. I., Au, A., Baehner, F., Chen, Y., Malaka, D. O*., et al.* (2011). Proliferating macrophages associated with high grade, hormone receptor negative breast cancer and poor clinical outcome. Breast Cancer Research and Treatment *128*, 703-711.

Carmeliet, P. (2005). VEGF as a key mediator of angiogenesis in cancer. Oncology *69 Suppl 3*, 4-10.

Carretero, R., Sektioglu, I. M., Garbi, N., Salgado, O. C., Beckhove, P., and Hammerling, G. J. (2015). Eosinophils orchestrate cancer rejection by normalizing tumor vessels and enhancing infiltration of CD8(+) T cells. Nat Immunol *16*, 609-617.

Casanovas, O., Hager, J. H., Chun, M. G. H., and Hanahan, D. (2005). Incomplete inhibition of the Rb tumor suppressor pathway in the context of inactivated p53 is sufficient for pancreatic islet tumorigenesis. Oncogene *24*, 6597-6604.

Celhar, T., Pereira-Lopes, S., Thornhill, S. I., Lee, H. Y., Dhillon, M. K., Poidinger, M., Connolly, J. E., Lim, L. H. K., Biswas, S. K., and Fairhurst, A.-M. (2016). TLR7 and TLR9 ligands regulate antigen presentation by macrophages. International Immunology *28*, 223-232.

Chakraborty, M., Abrams, S. I., Camphausen, K., Liu, K., Scott, T., Coleman, C. N., and Hodge, J. W. (2003). Irradiation of Tumor Cells Up-Regulates Fas and Enhances CTL Lytic Activity and CTL Adoptive Immunotherapy. The Journal of Immunology *170*, 6338-6347.

Chakraborty, M., Abrams, S. I., Coleman, C. N., Camphausen, K., Schlom, J., and Hodge, J. W. (2004). External Beam Radiation of Tumors Alters Phenotype of Tumor Cells to Render Them Susceptible to Vaccine-Mediated T-Cell Killing. Cancer research *64*, 4328-4337.

Chávez-Galán, L., Olleros, M. L., Vesin, D., and Garcia, I. (2015). Much More than M1 and M2 Macrophages, There are also CD169(+) and TCR(+) Macrophages. Frontiers in immunology *6*, 263.

Chen, F., Zhuang, X., Lin, L., Yu, P., Wang, Y., Shi, Y., Hu, G., and Sun, Y. (2015). New horizons in tumor microenvironment biology: challenges and opportunities. BMC Medicine *13*, 1-14.

Chiang, C. S., Chen, F. H., Hong, J. H., Jiang, P. S., Huang, H. L., Wang, C. C., and McBride, W. H. (2008). Functional phenotype of macrophages depends on assay procedures. Int Immunol *20*, 215-222.

Chu, R. S., Askew, D., Noss, E. H., Tobian, A., Krieg, A. M., and Harding, C. V. (1999). CpG oligodeoxynucleotides down-regulate macrophage class II MHC antigen processing. Journal of immunology *163*, 1188-1194.

Ciccia, A., and Elledge, S. J. (2010). The DNA damage response: making it safe to play with knives. Molecular cell *40*, 179-204.

Coates, P. J., Rundle, J. K., Lorimore, S. A., and Wright, E. G. (2008). Indirect macrophage responses to ionizing radiation: implications for genotype-dependent bystander signaling. Cancer research *68*, 450-456.

Cole, S. (1986). Long-Term Effects of Local Ionizing Radiation Treatment on Langerhans Cells in Mouse Footpad Epidermis. Journal of Investigative Dermatology *87*, 608-612.

Consortium, S. M.-I. (2014). A comprehensive assessment of RNA-seq accuracy, reproducibility and information content by the Sequencing Quality Control Consortium. Nat Biotech *32*, 903-914.

Corre, I., Niaudet, C., and Paris, F. (2010). Plasma membrane signaling induced by ionizing radiation. Mutation Research/Reviews in Mutation Research *704*, 61-67.

Corthay, A. (2014). Does the Immune System Naturally Protect Against Cancer? Frontiers in immunology *5*, 197.

Curiel, T. J., Coukos, G., Zou, L., Alvarez, X., Cheng, P., Mottram, P., Evdemon-Hogan, M., Conejo-Garcia, J. R., Zhang, L., Burow, M.*, et al.* (2004). Specific recruitment of regulatory T cells in ovarian carcinoma fosters immune privilege and predicts reduced survival. Nat Med *10*, 942-949.

Dai, H., Wang, Y., Lu, X., and Han, W. (2016). Chimeric Antigen Receptors Modified T-Cells for Cancer Therapy. Journal of the National Cancer Institute *108*.

Dalal, B. I., Das, K. C., Dutta, T. K., and Malakar, K. (1992). Local and systemic eosinophilia in patients with carcinoma of the uterine cervix undergoing radiation therapy: correlation with radiation response. Clinical oncology (Royal College of Radiologists (Great Britain)) *4*, 18-21.

Daly, M. J. (2012). Death by protein damage in irradiated cells. DNA Repair *11*, 12-21.

Dandekar, R. C., Kingaonkar, A. V., and Dhabekar, G. S. (2011). Role of macrophages in malignancy. Annals of Maxillofacial Surgery *1*, 150-154.

De Caterina, R., Libby, P., Peng, H. B., Thannickal, V. J., Rajavashisth, T. B., Gimbrone, M. A., Jr., Shin, W. S., and Liao, J. K. (1995). Nitric oxide decreases cytokine-induced endothelial activation. Nitric oxide selectively reduces endothelial expression of adhesion molecules and proinflammatory cytokines. The Journal of Clinical Investigation *96*, 60-68.

Demaria, S., and Formenti, S. C. (2016). Can abscopal effects of local radiotherapy be predicted by modeling T cell trafficking? Journal for ImmunoTherapy of Cancer *4*, 29.

Demaria, S., Ng, B., Devitt, M. L., Babb, J. S., Kawashima, N., Liebes, L., and Formenti, S. C. (2004). Ionizing radiation inhibition of distant untreated tumors (abscopal effect) is immune mediated. International journal of radiation oncology, biology, physics *58*, 862-870.

Demaria, S., Pilones, K. A., Vanpouille-Box, C., Golden, E. B., and Formenti, S. C. (2014). The Optimal Partnership of Radiation and Immunotherapy: from Preclinical Studies to Clinical Translation. Radiation Research *182*, 170-181.

Denayer, T., Stöhr, T., and Van Roy, M. (2014). Animal models in translational medicine: Validation and prediction. New Horizons in Translational Medicine *2*, 5-11.

Deng, L., Liang, H., Burnette, B., Beckett, M., Darga, T., Weichselbaum, R. R., and Fu, Y.-X. Irradiation and anti–PD-L1 treatment synergistically promote antitumor immunity in mice. The Journal of Clinical Investigation *124*, 687-695.

Deng, L., Liang, H., Xu, M., Yang, X., Burnette, B., Arina, A., Li, X.-D., Mauceri, H., Beckett, M., Darga, T.*, et al.* STING-Dependent Cytosolic DNA Sensing Promotes Radiation-Induced Type I Interferon-Dependent Antitumor Immunity in Immunogenic Tumors. Immunity *41*, 843-852.

Deng, L., Liang, H., Xu, M., Yang, X., Burnette, B., Arina, A., Li, X. D., Mauceri, H., Beckett, M., Darga, T.*, et al.* (2014). STING-Dependent Cytosolic DNA Sensing Promotes Radiation-Induced Type I Interferon-Dependent Antitumor Immunity in Immunogenic Tumors. Immunity *41*, 843-852.

Der, S. D., Zhou, A., Williams, B. R. G., and Silverman, R. H. (1998). Identification of genes differentially regulated by interferon α, β, or γ using oligonucleotide arrays. Proceedings of the National Academy of Sciences of the United States of America *95*, 15623-15628.

Derer, A., Frey, B., Fietkau, R., and Gaipl, U. S. (2016). Immune-modulating properties of ionizing radiation: rationale for the treatment of cancer by combination radiotherapy and immune checkpoint inhibitors. Cancer Immunology, Immunotherapy *65*, 779-786.

Desouky, O., Ding, N., and Zhou, G. (2015). Targeted and non-targeted effects of ionizing radiation. Journal of Radiation Research and Applied Sciences *8*, 247-254.

Dhawan, S., Singh, S., and Aggarwal, B. B. (1997). Induction of endothelial cell surface adhesion molecules by tumor necrosis factor is blocked by protein tyrosine phosphatase inhibitors: role of the nuclear transcription factor NF-kappa B. Eur J Immunol *27*, 2172-2179.

Di Carlo, E., Forni, G., Lollini, P., Colombo, M. P., Modesti, A., and Musiani, P. (2001). The intriguing role of polymorphonuclear neutrophils in antitumor reactions. Blood *97*, 339-345.

Di Virgilio, F., Ferrari, D., Falzoni, S., Chiozzi, P., Munerati, M., Steinberg, T. H., and Baricordi, O. R. (1996). P2 purinoceptors in the immune system. Ciba Foundation symposium *198*, 290-302; discussion 302-295.

Diefenbach, A., Schindler, H., Donhauser, N., Lorenz, E., Laskay, T., MacMicking, J., Röllinghoff, M., Gresser, I., and Bogdan, C. (1998). Type 1 Interferon (IFNα/β) and Type 2 Nitric Oxide Synthase Regulate the Innate Immune Response to a Protozoan Parasite. Immunity *8*, 77-87.

Dirkx, A. E., Oude Egbrink, M. G., Kuijpers, M. J., van der Niet, S. T., Heijnen, V. V., Bouma-ter Steege, J. C., Wagstaff, J., and Griffioen, A. W. (2003). Tumor angiogenesis modulates leukocyte-vessel wall interactions in vivo by reducing endothelial adhesion molecule expression. Cancer research *63*, 2322-2329.

Draghiciu, O., Walczak, M., Hoogeboom, B. N., Franken, K. L. M. C., Melief, K. J. M., Nijman, H. W., and Daemen, T. (2014). Therapeutic immunization and local low-dose tumor irradiation, a reinforcing combination. International Journal of Cancer *134*, 859-872.

Drake, C. G. (2012). Combination immunotherapy approaches. Annals of Oncology *23*, viii41-viii46.

Dudley, M. E. (2011). Adoptive Cell Therapy for Patients with Melanoma. Journal of Cancer *2*, 360-362.

Ehlers, G., and Fridman, M. (1973). Abscopal effect of radiation in papillary adenocarcinoma. The British journal of radiology *46*, 220-222.

Elliott, M. R., Chekeni, F. B., Trampont, P. C., Lazarowski, E. R., Kadl, A., Walk, S. F., Park, D., Woodson, R. I., Ostankovich, M., Sharma, P.*, et al.* (2009). Nucleotides released by apoptotic cells act as a find-me signal to promote phagocytic clearance. Nature *461*, 282-286.

Engblom, C., Pfirschke, C., and Pittet, M. J. (2016). The role of myeloid cells in cancer therapies. Nat Rev Cancer *16*, 447-462.

Farlik, M., Reutterer, B., Schindler, C., Greten, F., Vogl, C., Müller, M., and Decker, T. (2010). Nonconventional Initiation Complex Assembly by STAT and NF-κB Transcription Factors Regulates Nitric Oxide Synthase Expression. Immunity *33*, 25-34.

Fensterl, V., and Sen, G. C. (2015). Interferon-Induced Ifit Proteins: Their Role in Viral Pathogenesis. Journal of Virology *89*, 2462-2468.

Flynn, J. L., Goldstein, M. M., Chan, J., Triebold, K. J., Pfeffer, K., Lowenstein, C. J., Schreiber, R., Mak, T. W., and Bloom, B. R. (1995). Tumor necrosis factor-alpha is required in the protective immune response against Mycobacterium tuberculosis in mice. Immunity *2*, 561-572.

Foley, E. J. (1953). Antigenic properties of methylcholanthrene-induced tumors in mice of the strain of origin. Cancer research *13*, 835-837.

Forssell, J., Öberg, Å., Henriksson, M. L., Stenling, R., Jung, A., and Palmqvist, R. (2007). High Macrophage Infiltration along the Tumor Front Correlates with Improved Survival in Colon Cancer. Clinical Cancer Research *13*, 1472-1479.

Förster, I., Hirose, R., Arbeit, J. M., Clausen, B. E., and Hanahan, D. (1995). Limited Capacity for Tolerization of CD4+ T Cells Specific for A Pancreatic ß cell Neo-Antigen. Immunity *2*, 573-585.

Fox, B. A., Schendel, D. J., Butterfield, L. H., Aamdal, S., Allison, J. P., Ascierto, P. A., Atkins, M. B., Bartunkova, J., Bergmann, L., Berinstein, N.*, et al.* (2011). Defining the critical hurdles in cancer immunotherapy. Journal of Translational Medicine *9*, 1-15.

Frey, B., Rubner, Y., Kulzer, L., Werthmöller, N., Weiss, E.-M., Fietkau, R., and Gaipl, U. S. (2014). Antitumor immune responses induced by ionizing irradiation and further immune stimulation. Cancer Immunology, Immunotherapy *63*, 29-36.

Gajewski, T. F., Schreiber, H., and Fu, Y.-X. (2013). Innate and adaptive immune cells in the tumor microenvironment. Nat Immunol *14*, 1014-1022.

Gallily, R., Warwick, A., and Bang, F. B. (1964). EFFECT OF CORTISONE ON GENETIC RESISTANCE TO MOUSE HEPATITIS VIRUS IN VIVO AND IN VITRO. Proceedings of the National Academy of Sciences *51*, 1158-1164.

Galon, J., Costes, A., Sanchez-Cabo, F., Kirilovsky, A., Mlecnik, B., Lagorce-Pages, C., Tosolini, M., Camus, M., Berger, A., Wind, P.*, et al.* (2006). Type, density, and location of immune cells within human colorectal tumors predict clinical outcome. Science *313*, 1960-1964.

Ganss, R., and Hanahan, D. (1998). Tumor microenvironment can restrict the effectiveness of activated antitumor lymphocytes. Cancer research *58*, 4673-4681.

Ganss, R., Ryschich, E., Klar, E., Arnold, B., and Hammerling, G. J. (2002). Combination of T-cell therapy and trigger of inflammation induces remodeling of the vasculature and tumor eradication. Cancer research *62*, 1462-1470.

Gao, Q., Qiu, S.-J., Fan, J., Zhou, J., Wang, X.-Y., Xiao, Y.-S., Xu, Y., Li, Y.-W., and Tang, Z.-Y. (2007). Intratumoral Balance of Regulatory and Cytotoxic T Cells Is Associated With Prognosis of Hepatocellular Carcinoma After Resection. Journal of Clinical Oncology *25*, 2586-2593.

Garbi, N., Arnold, B., Gordon, S., Hammerling, G. J., and Ganss, R. (2004). CpG Motifs as Proinflammatory Factors Render Autochthonous Tumors Permissive for Infiltration and Destruction. The Journal of Immunology *172*, 5861-5869.

Geissmann, F., Jung, S., and Littman, D. R. (2003). Blood Monocytes Consist of Two Principal Subsets with Distinct Migratory Properties. Immunity *19*, 71-82.

Ghosn, E. E., Cassado, A. A., Govoni, G. R., Fukuhara, T., Yang, Y., Monack, D. M., Bortoluci, K. R., Almeida, S. R., Herzenberg, L. A., and Herzenberg, L. A. (2010). Two physically, functionally, and developmentally distinct peritoneal macrophage subsets. Proc Natl Acad Sci U S A *107*, 2568-2573.

Giroux, M., Schmidt, M., and Descoteaux, A. (2003). IFN-gamma-induced MHC class II expression: transactivation of class II transactivator promoter IV by IFN regulatory factor-1 is regulated by protein kinase C-alpha. Journal of immunology *171*, 4187-4194.

Gordon, S. (2003). Alternative activation of macrophages. Nat Rev Immunol *3*, 23-35.

Grant, S. G., Jessee, J., Bloom, F. R., and Hanahan, D. (1990). Differential plasmid rescue from transgenic mouse DNAs into Escherichia coli methylation-restriction mutants. Proceedings of the National Academy of Sciences of the United States of America *87*, 4645-4649.

Griffioen, A. W. (2008). Anti-angiogenesis: making the tumor vulnerable to the immune system. Cancer Immunology, Immunotherapy *57*, 1553-1558.

Griffioen, A. W., Damen, C. A., Martinotti, S., Blijham, G. H., and Groenewegen, G. (1996). Endothelial Intercellular Adhesion Molecule-1 Expression Is Suppressed in Human Malignancies: The Role of Angiogenic Factors. Cancer research *56*, 1111-1117.

Hallahan, D., Kuchibhotla, J., and Wyble, C. (1996). Cell adhesion molecules mediate radiation-induced leukocyte adhesion to the vascular endothelium. Cancer research *56*, 5150-5155.

Hamzah, J., Jugold, M., Kiessling, F., Rigby, P., Manzur, M., Marti, H. H., Rabie, T., Kaden, S., Grone, H. J., Hammerling, G. J.*, et al.* (2008). Vascular normalization in Rgs5-deficient tumours promotes immune destruction. Nature *453*, 410-414.

Hanahan, D., and Coussens, Lisa M. (2012). Accessories to the Crime: Functions of Cells Recruited to the Tumor Microenvironment. Cancer cell *21*, 309-322.

Hanahan, D., and Weinberg, R. A. (2000). The hallmarks of cancer. Cell *100*, 57-70.

Hanahan, D., and Weinberg, R. A. (2011). Hallmarks of cancer: the next generation. Cell *144*, 646-674.

Handschel, J., Prott, F.-J., Sunderkötter, C., Metze, D., Meyer, U., and Joos, U. (1999). Irradiation induces increase of adhesion molecules and accumulation of β2-integrin-expressing cells in humans. International Journal of Radiation Oncology*Biology*Physics *45*, 475-481.

Heberle, H., Meirelles, G. V., da Silva, F. R., Telles, G. P., and Minghim, R. (2015). InteractiVenn: a web-based tool for the analysis of sets through Venn diagrams. BMC Bioinformatics *16*, 1-7.

Heise, M. T., Pollock, J. L., O'Guin, A., Barkon, M. L., Bormley, S., and Virgin, H. W. t. (1998). Murine cytomegalovirus infection inhibits IFN gamma-induced MHC class II expression on macrophages: the role of type I interferon. Virology *241*, 331-344.

Holzel, M., Bovier, A., and Tuting, T. (2013). Plasticity of tumour and immune cells: a source of heterogeneity and a cause for therapy resistance? Nat Rev Cancer *13*, 365-376.

Honda, K., and Taniguchi, T. (2006). IRFs: master regulators of signalling by Toll-like receptors and cytosolic pattern-recognition receptors. Nat Rev Immunol *6*, 644-658.

Houot, R., Schultz, L. M., Marabelle, A., and Kohrt, H. (2015). T-cell–based Immunotherapy: Adoptive Cell Transfer and Checkpoint Inhibition. Cancer Immunology Research *3*, 1115-1122.

Howlader, N., Noone, A.M., Krapcho, M., Miller, D., Bishop, K., Altekruse, S.F., Kosary, C.L., Yu, M., Ruhl, J., Tatalovich, Z., Mariotto, A., Lewis, D.R., Chen, H.S., Feuer, E.J., Cronin, K.A. (1975-2013). SEER Cancer Statistics Review. In, (Bethesda, MD: National Cancer Institute), p. based on November 2015 SEER data submission.

Huang, Y., Goel, S., Duda, D. G., Fukumura, D., and Jain, R. K. (2013). Vascular Normalization as an Emerging Strategy to Enhance Cancer Immunotherapy. Cancer research *73*, 2943-2948.

Iwamoto, K. S., and McBride, W. H. (1994). Production of 13-Hydroxyoctadecadienoic Acid and Tumor Necrosis Factor-α by Murine Peritoneal Macrophages in Response to Irradiation. Radiation Research *139*, 103-108.

Jablonski, K. A., Amici, S. A., Webb, L. M., Ruiz-Rosado, J. d. D., Popovich, P. G., Partida-Sanchez, S., and Guerau-de-Arellano, M. (2015). Novel Markers to Delineate Murine M1 and M2 Macrophages. PloS one *10*, e0145342.

Jain, R. K. (2013). Normalizing Tumor Microenvironment to Treat Cancer: Bench to Bedside to Biomarkers. Journal of Clinical Oncology *31*, 2205-2218.

James, R. F., Lake, S. P., Chamberlain, J., Thirdborough, S., Bassett, P. D., Mistry, N., and Bell, P. R. (1989). Gamma irradiation of isolated rat islets pretransplantation produces indefinite allograft survival in cyclosporine-treated recipients. Transplantation *47*, 929-933.

Johansson, A., Hamzah, J., Payne, C. J., and Ganss, R. (2012). Tumor-targeted TNFα stabilizes tumor vessels and enhances active immunotherapy. Proceedings of the National Academy of Sciences *109*, 7841-7846.

Jolliffe, I. (2014). Principal Component Analysis. In Wiley StatsRef: Statistics Reference Online, (John Wiley & Sons, Ltd).

Kalbasi, A., June, C. H., Haas, N., and Vapiwala, N. (2013). Radiation and immunotherapy: a synergistic combination. J Clin Invest *123*, 2756-2763.

Kamijo, R., Harada, H., Matsuyama, T., Bosland, M., Gerecitano, J., Shapiro, D., Le, J., Koh, S., Kimura, T., Green, S., and et, a. (1994). Requirement for transcription factor IRF-1 in NO synthase induction in macrophages. Science *263*, 1612-1615.

Kaplan, D. H., Shankaran, V., Dighe, A. S., Stockert, E., Aguet, M., Old, L. J., and Schreiber, R. D. (1998). Demonstration of an interferon γ-dependent tumor surveillance system in immunocompetent mice. Proceedings of the National Academy of Sciences *95*, 7556-7561.

Kawai, O., Ishii, G., Kubota, K., Murata, Y., Naito, Y., Mizuno, T., Aokage, K., Saijo, N., Nishiwaki, Y., Gemma, A.*, et al.* (2008). Predominant infiltration of macrophages and CD8(+) T Cells in cancer nests is a significant predictor of survival in stage IV nonsmall cell lung cancer. Cancer *113*, 1387-1395.

Kawai, T., and Akira, S. (2010). The role of pattern-recognition receptors in innate immunity: update on Toll-like receptors. Nat Immunol *11*, 373-384.

Kazemi, T., Younesi, V., Jadidi-Niaragh, F., and Yousefi, M. (2016). Immunotherapeutic approaches for cancer therapy: An updated review. Artificial Cells, Nanomedicine, and Biotechnology *44*, 769-779.

Kelly, P. M. A., Davison, R. S., Bliss, E., and McGee, J. D. (1988). Macrophages in human breast disease: a quantitative immunohistochemical study. Br J Cancer *57*, 174-177.

Kershaw, M. H., Devaud, C., John, L. B., Westwood, J. A., and Darcy, P. K. (2013). Enhancing immunotherapy using chemotherapy and radiation to modify the tumor microenvironment. OncoImmunology *2*, e25962.

Khan, B. V., Harrison, D. G., Olbrych, M. T., Alexander, R. W., and Medford, R. M. (1996). Nitric oxide regulates vascular cell adhesion molecule 1 gene expression and redox-sensitive transcriptional events in human vascular endothelial cells. Proceedings of the National Academy of Sciences of the United States of America *93*, 9114-9119.

Khong, H. T., and Restifo, N. P. (2002). Natural selection of tumor variants in the generation of “tumor escape” phenotypes. Nature immunology *3*, 999-1005.

Kim, D. W., Min, H. S., Lee, K. H., Kim, Y. J., Oh, D. Y., Jeon, Y. K., Lee, S. H., Im, S. A., Chung, D. H., Kim, Y. T.*, et al.* (2008). High tumour islet macrophage infiltration correlates with improved patient survival but not with EGFR mutations, gene copy number or protein expression in resected non-small cell lung cancer. British Journal of Cancer *98*, 1118-1124.

Klemm, F., and Joyce, J. A. (2015). Microenvironmental regulation of therapeutic response in cancer. Trends in Cell Biology *25*, 198-213.

Klug, F., Prakash, H., Huber, P. E., Seibel, T., Bender, N., Halama, N., Pfirschke, C., Voss, R. H., Timke, C., Umansky, L.*, et al.* (2013). Low-dose irradiation programs macrophage differentiation to an iNOS(+)/M1 phenotype that orchestrates effective T cell immunotherapy. Cancer cell *24*, 589-602.

Klune, J. R., Dhupar, R., Cardinal, J., Billiar, T. R., and Tsung, A. (2008). HMGB1: Endogenous Danger Signaling. Molecular Medicine *14*, 476-484.

Koebel, C. M., Vermi, W., Swann, J. B., Zerafa, N., Rodig, S. J., Old, L. J., Smyth, M. J., and Schreiber, R. D. (2007). Adaptive immunity maintains occult cancer in an equilibrium state. Nature *450*, 903-907.

Koh, T. J., and DiPietro, L. A. (2011). Inflammation and wound healing: the role of the macrophage. Expert Reviews in Molecular Medicine *13*.

Kratochvill, F., Neale, G., Haverkamp, J. M., Van de Velde, L. A., Smith, A. M., Kawauchi, D., McEvoy, J., Roussel, M. F., Dyer, M. A., Qualls, J. E., and Murray, P. J. (2015). TNF Counterbalances the Emergence of M2 Tumor Macrophages. Cell Rep *12*, 1902-1914.

Kreike, B., van Kouwenhove, M., Horlings, H., Weigelt, B., Peterse, H., Bartelink, H., and van de Vijver, M. J. (2007). Gene expression profiling and histopathological characterization of triple-negative/basal-like breast carcinomas. Breast Cancer Research *9*, 1-14.

Kwilas, A. R., Donahue, R. N., Bernstein, M. B., and Hodge, J. W. (2012). In the field: exploiting the untapped potential of immunogenic modulation by radiation in combination with immunotherapy for the treatment of cancer. Front Oncol *2*, 104.

Lamagna, C., Aurrand-Lions, M., and Imhof, B. A. (2006). Dual role of macrophages in tumor growth and angiogenesis. Journal of Leukocyte Biology *80*, 705-713.

Langley, R. E., Bump, E. A., Quartuccio, S. G., Medeiros, D., and Braunhut, S. J. (1997). Radiation-induced apoptosis in microvascular endothelial cells. British Journal of Cancer *75*, 666-672.

Lanitis, E., Irving, M., and Coukos, G. (2015). Targeting the tumor vasculature to enhance T cell activity. Current opinion in immunology *33*, 55-63.

Lauber, K., Ernst, A., Orth, M., Herrmann, M., and Belka, C. (2012). Dying cell clearance and its impact on the outcome of tumor radiotherapy. Frontiers in Oncology *2*.

Lawrence, T., and Natoli, G. (2011). Transcriptional regulation of macrophage polarization: enabling diversity with identity. Nat Rev Immunol *11*, 750-761.

Lee, H.-W., Choi, H.-J., Ha, S.-J., Lee, K.-T., and Kwon, Y.-G. (2013). Recruitment of monocytes/macrophages in different tumor microenvironments. Biochimica et Biophysica Acta (BBA) - Reviews on Cancer *1835*, 170-179.

Lee, M., Park, C.-S., Lee, Y.-R., Im, S.-A., Song, S., and Lee, C.-K. (2014). Resiquimod, a TLR7/8 agonist, promotes differentiation of myeloid-derived suppressor cells into macrophages and dendritic cells. Archives of Pharmacal Research *37*, 1234-1240.

Lee, Y., and Biswas, S. K. (2016). Rewiring macrophages for anti-tumour immunity. Nat Cell Biol *18*, 718-720.

Leroi, N., Lallemand, F., Coucke, P., Noel, A., and Martinive, P. (2016). Impacts of Ionizing Radiation on the Different Compartments of the Tumor Microenvironment. Frontiers in Pharmacology *7*.

Li, Y. M., Baviello, G., Vlassara, H., and Mitsuhashi, T. (1997). Glycation products in aged thioglycollate medium enhance the elicitation of peritoneal macrophages. Journal of immunological methods *201*, 183-188.

Lim, J. Y. H., Gerber, S. A., Murphy, S. P., and Lord, E. M. (2014). Type I interferons induced by radiation therapy mediate recruitment and effector function of CD8+ T cells. Cancer Immunology, Immunotherapy *63*, 259-271.

Loo, Y.-M., and Gale Jr, M. (2011). Immune Signaling by RIG-I-like Receptors. Immunity *34*, 680-692.

Lorimore, S. A., Coates, P. J., Scobie, G. E., Milne, G., and Wright, E. G. (2001). Inflammatory-type responses after exposure to ionizing radiation in vivo: a mechanism for radiation-induced bystander effects? Oncogene *20*, 7085-7095.

Luckheeram, R. V., Zhou, R., Verma, A. D., and Xia, B. (2012). CD4+T Cells: Differentiation and Functions. Clinical and Developmental Immunology *2012*, 12.

Lugade, A. A., Moran, J. P., Gerber, S. A., Rose, R. C., Frelinger, J. G., and Lord, E. M. (2005). Local Radiation Therapy of B16 Melanoma Tumors Increases the Generation of Tumor Antigen-Specific Effector Cells That Traffic to the Tumor. The Journal of Immunology *174*, 7516-7523.

Maeda, H., and Shiraishi, A. (1996). TGF-beta contributes to the shift toward Th2-type responses through direct and IL-10-mediated pathways in tumor-bearing mice. Journal of immunology *156*, 73-78.

Mahmoud, S. M. A., Paish, E. C., Powe, D. G., Macmillan, R. D., Grainge, M. J., Lee, A. H. S., Ellis, I. O., and Green, A. R. (2011). Tumor-Infiltrating CD8+ Lymphocytes Predict Clinical Outcome in Breast Cancer. Journal of Clinical Oncology *29*, 1949-1955.

Mako, V., Czucz, J., Weiszhar, Z., Herczenik, E., Matko, J., Prohaszka, Z., and Cervenak, L. (2010). Proinflammatory activation pattern of human umbilical vein endothelial cells induced by IL-1beta, TNF-alpha, and LPS. Cytometry A *77*, 962-970.

Mantovani, A., Biswas, S. K., Galdiero, M. R., Sica, A., and Locati, M. (2013). Macrophage plasticity and polarization in tissue repair and remodelling. The Journal of Pathology *229*, 176-185.

Mantovani, A., and Locati, M. (2013). Tumor-associated macrophages as a paradigm of macrophage plasticity, diversity, and polarization: lessons and open questions. Arteriosclerosis, thrombosis, and vascular biology *33*, 1478-1483.

Martinez, F. O., and Gordon, S. (2014). The M1 and M2 paradigm of macrophage activation: time for reassessment. F1000Prime Rep *6*, 13.

Martinez, F. O., Sica, A., Mantovani, A., and Locati, M. (2008). Macrophage activation and polarization. Frontiers in bioscience : a journal and virtual library *13*, 453-461.

Mattila, P., Majuri, M. L., Mattila, P. S., and Renkonen, R. (1992). TNF alpha-induced expression of endothelial adhesion molecules, ICAM-1 and VCAM-1, is linked to protein kinase C activation. Scand J Immunol *36*, 159-165.

Mattner, J., Schindler, H., Diefenbach, A., Rollinghoff, M., Gresser, I., and Bogdan, C. (2000). Regulation of type 2 nitric oxide synthase by type 1 interferons in macrophages infected with Leishmania major. Eur J Immunol *30*, 2257-2267.

McHale, J. F., Harari, O. A., Marshall, D., and Haskard, D. O. (1999). TNF-alpha and IL-1 sequentially induce endothelial ICAM-1 and VCAM-1 expression in MRL/lpr lupus-prone mice. Journal of immunology *163*, 3993-4000.

Melero, I., Rouzaut, A., Motz, G. T., and Coukos, G. (2014). T-Cell and NK-Cell Infiltration into Solid Tumors: A Key Limiting Factor for Efficacious Cancer Immunotherapy. Cancer Discovery *4*, 522-526.

Min, W., Pober, J. S., and Johnson, D. R. (1998). Interferon Induction of TAP1. The Phosphatase SHP-1 Regulates Crossover Between the IFN-α/β and the IFN-γ Signal-Transduction Pathways *83*, 815-823.

Misharin, A. V., Saber, R., and Perlman, H. (2012). Eosinophil contamination of thioglycollate-elicited peritoneal macrophage cultures skews the functional readouts of in vitro assays. J Leukoc Biol *92*, 325-331.

Mishra, K. P. (2004). Cell membrane oxidative damage induced by gamma-radiation and apoptotic sensitivity. Journal of environmental pathology, toxicology and oncology : official organ of the International Society for Environmental Toxicology and Cancer *23*, 61-66.

Monu, N. R., and Frey, A. B. (2012). Myeloid-Derived Suppressor Cells and anti-tumor T cells: a complex relationship. Immunological Investigations *41*, 595-613.

Mosser, D. M. (2003). The many faces of macrophage activation. Journal of Leukocyte Biology *73*, 209-212.

Mueller, M. M., and Fusenig, N. E. (2004). Friends or foes [mdash] bipolar effects of the tumour stroma in cancer. Nat Rev Cancer *4*, 839-849.

Munn, D. H., Shafizadeh, E., Attwood, J. T., Bondarev, I., Pashine, A., and Mellor, A. L. (1999). Inhibition of T Cell Proliferation by Macrophage Tryptophan Catabolism. The Journal of Experimental Medicine *189*, 1363-1372.

Murdoch, C., Muthana, M., Coffelt, S. B., and Lewis, C. E. (2008). The role of myeloid cells in the promotion of tumour angiogenesis. Nat Rev Cancer *8*, 618-631.

Murray, Peter J., Allen, Judith E., Biswas, Subhra K., Fisher, Edward A., Gilroy, Derek W., Goerdt, S., Gordon, S., Hamilton, John A., Ivashkiv, Lionel B., Lawrence, T., *et al.* (2014). Macrophage Activation and Polarization: Nomenclature and Experimental Guidelines. Immunity *41*, 14-20.

Murray, P. J., and Wynn, T. A. (2011). Protective and pathogenic functions of macrophage subsets. Nat Rev Immunol *11*, 723-737.

Nagorsen, D., Scheibenbogen, C., Marincola, F. M., Letsch, A., and Keilholz, U. (2003). Natural T cell immunity against cancer. Clinical cancer research : an official journal of the American Association for Cancer Research *9*, 4296-4303.

Nagy, J. A., Chang, S. H., Dvorak, A. M., and Dvorak, H. F. (2009). Why are tumour blood vessels abnormal and why is it important to know[quest]. Br J Cancer *100*, 865-869.

Nayar, S., Dasgupta, P., and Galustian, C. (2015). Extending the lifespan and efficacies of immune cells used in adoptive transfer for cancer immunotherapies–A review. Oncoimmunology *4*, e1002720.

Nemoto, K., Ishihara, H., Tanaka, I., Suzuki, G., Tsuneoka, K., Yoshida, K., and Ohtsu, H. (1995). Expression of IL-1β mRNA in Mice after Whole Body X-Irradiation. Journal of Radiation Research *36*, 125-133.

Noffz, G., Qin, Z., Kopf, M., and Blankenstein, T. (1998). Neutrophils but not eosinophils are involved in growth suppression of IL-4-secreting tumors. Journal of immunology *160*, 345-350.

Noy, R., and Pollard, J. W. (2014). Tumor-associated macrophages: from mechanisms to therapy. Immunity *41*.

O'Sullivan, T., Saddawi-Konefka, R., Vermi, W., Koebel, C. M., Arthur, C., White, J. M., Uppaluri, R., Andrews, D. M., Ngiow, S. F., Teng, M. W. L*., et al.* (2012). Cancer immunoediting by the innate immune system in the absence of adaptive immunity. The Journal of Experimental Medicine *209*, 1869-1882.

Ohba, K., Omagari, K., Nakamura, T., Ikuno, N., Saeki, S., Matsuo, I., Kinoshita, H., Masuda, J., Hazama, H., Sakamoto, I., and Kohno, S. (1998). Abscopal regression of hepatocellular carcinoma after radiotherapy for bone metastasis. Gut *43*, 575-577.

Ohno, S., Inagawa, H., Dhar, D. K., Fujii, T., Ueda, S., Tachibana, M., Suzuki, N., Inoue, M., Soma, G., and Nagasue, N. (2003). The degree of macrophage infiltration into the cancer cell nest is a significant predictor of survival in gastric cancer patients. Anticancer research *23*, 5015-5022.

Ohno, S., Ohno, Y., Suzuki, N., Kamei, T., Koike, K., Inagawa, H., Kohchi, C., Soma, G., and Inoue, M. (2004). Correlation of histological localization of tumor-associated macrophages with clinicopathological features in endometrial cancer. Anticancer research *24*, 3335-3342.

Oliveros, J. C. (2007-2015). Venny. An interactive tool for comparing lists with Venn's diagrams. In http://bioinfogp.cnb.csic.es/tools/venny/index.html.

Ortega-Gómez, A., Perretti, M., and Soehnlein, O. (2013). Resolution of inflammation: an integrated view. EMBO Molecular Medicine *5*, 661-674.

Ozdemir, B. C., Pentcheva-Hoang, T., Carstens, J. L., Zheng, X., Wu, C. C., and Simpson, T. R. (2014). Depletion of carcinoma-associated fibroblasts and fibrosis induces immunosuppression and accelerates pancreas cancer with reduced survival. Cancer cell *25*.

Pardoll, D. M. (2012). The blockade of immune checkpoints in cancer immunotherapy. Nat Rev Cancer *12*, 252-264.

Paris, F., Fuks, Z., Kang, A., Capodieci, P., Juan, G., Ehleiter, D., Haimovitz-Friedman, A., Cordon-Cardo, C., and Kolesnick, R. (2001). Endothelial apoptosis as the primary lesion initiating intestinal radiation damage in mice. Science *293*, 293-297.

Parish, C. R. (2003). Cancer immunotherapy: The past, the present and the future[ast]. Immunol Cell Biol *81*, 106-113.

Perrone, G., Ruffini, P. A., Catalano, V., Spino, C., Santini, D., Muretto, P., Spoto, C., Zingaretti, C., Sisti, V., Alessandroni, P*., et al.* (2008). Intratumoural FOXP3-positive regulatory T cells are associated with adverse prognosis in radically resected gastric cancer. European Journal of Cancer *44*, 1875-1882.

Petersen, R. P., Campa, M. J., Sperlazza, J., Conlon, D., Joshi, M.-B., Harpole, D. H., and Patz, E. F. (2006). Tumor infiltrating Foxp3+ regulatory T-cells are associated with recurrence in pathologic stage I NSCLC patients. Cancer *107*, 2866-2872.

Proia, D. A., and Kuperwasser, C. (2005). Stroma: tumor agonist or antagonist. Cell cycle (Georgetown, Tex) *4*, 1022-1025.

Pulit-Penaloza, J. A., Scherbik, S. V., and Brinton, M. A. (2012). Activation of Oas1a gene expression by type I IFN requires both STAT1 and STAT2 while only STAT2 is required for Oas1b activation. Virology *425*, 71-81.

Quail, D. F., and Joyce, J. A. (2013). Microenvironmental regulation of tumor progression and metastasis. Nat Med *19*.

Quezada, S. A., Peggs, K. S., Simpson, T. R., Shen, Y., Littman, D. R., and Allison, J. P. (2008). Limited tumor infiltration by activated T effector cells restricts the therapeutic activity of regulatory T cell depletion against established melanoma. The Journal of Experimental Medicine *205*, 2125-2138.

Ray, D., Shukla, S., Allam, U. S., Helman, A., Ramanand, S. G., Tran, L., Bassetti, M., Krishnamurthy, P. M., Rumschlag, M., Paulsen, M*., et al.* (2013). Tristetraprolin Mediates Radiation-Induced TNF-α Production in Lung Macrophages. PloS one *8*, e57290.

Reits, E. A., Hodge, J. W., Herberts, C. A., Groothuis, T. A., Chakraborty, M., K.Wansley, E., Camphausen, K., Luiten, R. M., de Ru, A. H., Neijssen, J*., et al.* (2006). Radiation modulates the peptide repertoire, enhances MHC class I expression, and induces successful antitumor immunotherapy. The Journal of Experimental Medicine *203*, 1259-1271.

Roche, P. A., and Furuta, K. (2015). The ins and outs of MHC class II-mediated antigen processing and presentation. Nat Rev Immunol *15*, 203-216.

Rodriguez, P. C., Quiceno, D. G., Zabaleta, J., Ortiz, B., Zea, A. H., Piazuelo, M. B., Delgado, A., Correa, P., Brayer, J., Sotomayor, E. M*., et al.* (2004). Arginase I Production in the Tumor Microenvironment by Mature Myeloid Cells Inhibits T-Cell Receptor Expression and Antigen-Specific T-Cell Responses. Cancer research *64*, 5839-5849.

Rosenberg , S. A., Packard , B. S., Aebersold , P. M., Solomon , D., Topalian , S. L., Toy , S. T., Simon , P., Lotze , M. T., Yang , J. C., Seipp , C. A*., et al.* (1988). Use of Tumor-Infiltrating Lymphocytes and Interleukin-2 in the Immunotherapy of Patients with Metastatic Melanoma. New England Journal of Medicine *319*, 1676-1680.

Rosenberg, S. A., and Restifo, N. P. (2015). Adoptive cell transfer as personalized immunotherapy for human cancer. Science *348*, 62-68.

Rosenberg, S. A., Restifo, N. P., Yang, J. C., Morgan, R. A., and Dudley, M. E. (2008). Adoptive cell transfer: a clinical path to effective cancer immunotherapy. Nature reviews Cancer *8*, 299-308.

Rosenberg, S. A., Yang, J. C., Sherry, R. M., Kammula, U. S., Hughes, M. S., Phan, G. Q., Citrin, D. E., Restifo, N. P., Robbins, P. F., Wunderlich, J. R.*, et al.* (2011). Durable Complete Responses in Heavily Pretreated Patients with Metastatic Melanoma Using T-Cell Transfer Immunotherapy. Clinical Cancer Research *17*, 4550-4557.

Rosenberg, S. A., Yannelli, J. R., Yang, J. C., Topalian, S. L., Schwartzentruber, D. J., Weber, J. S., Parkinson, D. R., Seipp, C. A., Einhorn, J. H., and White, D. E. (1994). Treatment of Patients With Metastatic Melanoma With Autologous Tumor-Infiltrating Lymphocytes and Interleukin 2. Journal of the National Cancer Institute *86*, 1159-1166.

Rusakiewicz, S., Semeraro, M., Sarabi, M., Desbois, M., Locher, C., Mendez, R., Vimond, N., Concha, A., Garrido, F., Isambert, N.*, et al.* (2013). Immune Infiltrates Are Prognostic Factors in Localized Gastrointestinal Stromal Tumors. Cancer research *73*, 3499-3510.

Rusinova, I., Forster, S., Yu, S., Kannan, A., Masse, M., Cumming, H., Chapman, R., and Hertzog, P. J. (2013). INTERFEROME v2.0: an updated database of annotated interferon-regulated genes. Nucleic acids research *41*, D1040-D1046.

Russell, J. S., and Brown, J. M. (2013). The irradiated tumor microenvironment: role of tumor-associated macrophages in vascular recovery. Frontiers in Physiology *4*, 157.

Ryschich, E., Schmidt, J., Hammerling, G. J., Klar, E., and Ganss, R. (2002). Transformation of the microvascular system during multistage tumorigenesis. International journal of cancer Journal international du cancer *97*, 719-725.

Sato, T., Terai, M., Tamura, Y., Alexeev, V., Mastrangelo, M. J., and Selvan, S. R. (2011). Interleukin 10 in the tumor microenvironment: a target for anticancer immunotherapy. Immunologic Research *51*, 170-182.

Schaue, D., Comin-Anduix, B., Ribas, A., Zhang, L., Goodglick, L., Sayre, J. W., Debucquoy, A., Haustermans, K., and McBride, W. H. (2008). T-cell responses to survivin in cancer patients undergoing radiation therapy. Clinical cancer research : an official journal of the American Association for Cancer Research *14*, 4883-4890.

Schaue, D., Micewicz, E. D., Ratikan, J. A., Xie, M. W., Cheng, G., and McBride, W. H. (2015). Radiation and Inflammation. Seminars in Radiation Oncology *25*, 4-10.

Schaue, D., Ratikan, J. A., Iwamoto, K. S., and McBride, W. H. (2012). Maximizing Tumor Immunity With Fractionated Radiation. International Journal of Radiation Oncology*Biology*Physics *83*, 1306-1310.

Schleicher, U., Hesse, A., and Bogdan, C. (2005). Minute numbers of contaminant CD8+ T cells or CD11b+CD11c+ NK cells are the source of IFN-gamma in IL-12/IL-18-stimulated mouse macrophage populations. Blood *105*, 1319-1328.

Schmidt, A., Oberle, N., and Krammer, P. (2012). Molecular Mechanisms of Treg-Mediated T Cell Suppression. Frontiers in immunology *3*.

Schmidt, J., Ryschich, E., Maksan, S. M., Werner, J., Gebhard, M. M., Herfarth, C., and Klar, E. (1999). Reduced basal and stimulated leukocyte adherence in tumor endothelium of experimental pancreatic cancer. International journal of pancreatology : official journal of the International Association of Pancreatology *26*, 173-179.

Schmitz-Winnenthal, F. H., Volk, C., Z'Graggen, K., Galindo, L., Nummer, D., Ziouta, Y., Bucur, M., Weitz, J., Schirrmacher, V., Buchler, M. W., and Beckhove, P. (2005). High frequencies of functional tumor-reactive T cells in bone marrow and blood of pancreatic cancer patients. Cancer research *65*, 10079-10087.

Schreiber, R. D., Old, L. J., and Smyth, M. J. (2011). Cancer Immunoediting: Integrating Immunity's Roles in Cancer Suppression and Promotion. Science *331*, 1565-1570.

Seibel, T. (2010) Local Low Dose Irradiation Triggers Tumor Infiltration by Adoptively Transferred and Host T Lymphocytes and Enhances Immunotherapy in Mice, Ruperto-Carola-University, Heidelberg, Germany.

Sektioglu, I. M., Carretero, R., Bender, N., Bogdan, C., Garbi, N., Umansky, V., Umansky, L., Urban, K., von Knebel-Döberitz, M., Somasundaram, V.*, et al.* (2016). Macrophage-derived nitric oxide initiates T-cell diapedesis and tumor rejection. OncoImmunology, e1204506.

Sgarbanti, M., Marsili, G., Remoli, A. L., Orsatti, R., and Battistini, A. (2007). IRF-7. Annals of the New York Academy of Sciences *1095*, 325-333.

Shah, W., Yan, X., Jing, L., Zhou, Y., Chen, H., and Wang, Y. (2011). A reversed CD4/CD8 ratio of tumor-infiltrating lymphocytes and a high percentage of CD4+FOXP3+ regulatory T cells are significantly associated with clinical outcome in squamous cell carcinoma of the cervix. Cell Mol Immunol *8*, 59-66.

Shan, Y.-X., Jin, S.-Z., Liu, X.-D., Liu, Y., and Liu, S.-Z. (2007). Ionizing radiation stimulates secretion of pro-inflammatory cytokines: dose–response relationship, mechanisms and implications. Radiation and Environmental Biophysics *46*, 21-29.

Shang, B., Liu, Y., Jiang, S.-j., and Liu, Y. (2015). Prognostic value of tumor-infiltrating FoxP3+ regulatory T cells in cancers: a systematic review and meta-analysis. Scientific Reports *5*, 15179.

Shankaran, V., Ikeda, H., Bruce, A. T., White, J. M., Swanson, P. E., Old, L. J., and Schreiber, R. D. (2001). IFN[gamma] and lymphocytes prevent primary tumour development and shape tumour immunogenicity. Nature *410*, 1107-1111.

Sharma, P., and Allison, J. P. (2015). The future of immune checkpoint therapy. Science *348*, 56-61.

Shimura, S., Yang, G., Ebara, S., Wheeler, T. M., Frolov, A., and Thompson, T. C. (2000). Reduced Infiltration of Tumor-associated Macrophages in Human Prostate Cancer: Association with Cancer Progression. Cancer research *60*, 5857-5861.

Sica, A., and Mantovani, A. (2012). Macrophage plasticity and polarization: in vivo veritas. J Clin Invest *122*, 787-795.

Sionov, R. V., Assi, S., Gershkovitz, M., Sagiv, J. Y., Polyansky, L., Mishalian, I., Fridlender, Z. G., and Granot, Z. (2015). Isolation and Characterization of Neutrophils with Anti-Tumor Properties. Journal of visualized experiments : JoVE, e52933.

Skowronski, J., Jolicoeur, C., Alpert, S., and Hanahan, D. (1990). Determinants of the B-cell response against a transgenic autoantigen. Proceedings of the National Academy of Sciences of the United States of America *87*, 7487-7491.

Soukup, K., and Wang, X. (2015). Radiation meets immunotherapy - a perfect match in the era of combination therapy? Int J Radiat Biol *91*, 299-305.

Stewart, T. J., and Abrams, S. I. (2008). How tumours escape mass destruction. Oncogene *27*, 5894-5903.

Sugihara, T., Murano, H., Nakamura, M., Ichinohe, K., and Tanaka, K. (2011). Activation of Interferon-Stimulated Genes by γ-Ray Irradiation Independently of the Ataxia Telangiectasia Mutated–p53 Pathway. Molecular Cancer Research *9*, 476-484.

Szklarczyk, D., Franceschini, A., Wyder, S., Forslund, K., Heller, D., Huerta-Cepas, J., Simonovic, M., Roth, A., Santos, A., Tsafou, K. P.*, et al.* (2015). STRING v10: protein-protein interaction networks, integrated over the tree of life. Nucleic acids research *43*, D447-452.

Takeshima, T., Pop, L. M., Laine, A., Iyengar, P., Vitetta, E. S., and Hannan, R. (2016). Key role for neutrophils in radiation-induced antitumor immune responses: Potentiation with G-CSF. Proceedings of the National Academy of Sciences.

Talmadge, J. E., Singh, R. K., Fidler, I. J., and Raz, A. (2007). Murine Models to Evaluate Novel and Conventional Therapeutic Strategies for Cancer. The American journal of pathology *170*, 793-804.

Tanigawa, N., Amaya, H., Matsumura, M., and Shimomatsuya, T. (1997). Association of tumour vasculature with tumour progression and overall survival of patients with non-early gastric carcinomas. British Journal of Cancer *75*, 566-571.

Teresa Pinto, A., Laranjeiro Pinto, M., Patrícia Cardoso, A., Monteiro, C., Teixeira Pinto, M., Filipe Maia, A., Castro, P., Figueira, R., Monteiro, A., Marques, M.*, et al.* (2016). Ionizing radiation modulates human macrophages towards a pro-inflammatory phenotype preserving their pro-invasive and pro-angiogenic capacities. Scientific Reports *6*, 18765.

Thomas, D. A., and Massagué, J. (2005). TGF-β directly targets cytotoxic T cell functions during tumor evasion of immune surveillance. Cancer cell *8*, 369-380.

Thomas, L. (1982). On immunosurveillance in human cancer. The Yale Journal of Biology and Medicine *55*, 329-333.

Tu, E., Chia, P. Z. C., and Chen, W. (2014). TGFβ in T cell biology and tumor immunity: Angel or devil? Cytokine & Growth Factor Reviews *25*, 423-435.

Tymoszuk, P., Evens, H., Marzola, V., Wachowicz, K., Wasmer, M.-H., Datta, S., Müller-Holzner, E., Fiegl, H., Böck, G., van Rooijen, N.*, et al.* (2014). In situ proliferation contributes to accumulation of tumor-associated macrophages in spontaneous mammary tumors. European Journal of Immunology *44*, 2247-2262.

Unterholzner, L. (2013). The interferon response to intracellular DNA: why so many receptors? Immunobiology *218*, 1312-1321.

Vacchelli, E., Semeraro, M., Enot, D. P., Chaba, K., Poirier Colame, V., Dartigues, P., Perier, A., Villa, I., Rusakiewicz, S., Gronnier, C.*, et al.* (2015). Negative prognostic impact of regulatory T cell infiltration in surgically resected esophageal cancer post-radiochemotherapy. Oncotarget *6*, 20840-20850.

Van Overmeire, E., Laoui, D., Keirsse, J., Van Ginderachter, J., and Sarukhan, A. (2014). Mechanisms Driving Macrophage Diversity and Specialization in Distinct Tumor Microenvironments and Parallelisms with Other Tissues. Frontiers in immunology *5*.

Vandenberk, L., Belmans, J., Van Woensel, M., Riva, M., and Van Gool, S. W. (2015). Exploiting the Immunogenic Potential of Cancer Cells for Improved Dendritic Cell Vaccines. Frontiers in immunology *6*, 663.

Vassalli, P. (1992). The pathophysiology of tumor necrosis factors. Annual review of immunology *10*, 411-452.

Vesely, M. D., Kershaw, M. H., Schreiber, R. D., and Smyth, M. J. (2011). Natural innate and adaptive immunity to cancer. Annual review of immunology *29*, 235-271.

Vinay, D. S., Ryan, E. P., Pawelec, G., Talib, W. H., Stagg, J., Elkord, E., Lichtor, T., Decker, W. K., Whelan, R. L., Kumara, H. M. C. S.*, et al.* (2015). Immune evasion in cancer: Mechanistic basis and therapeutic strategies. Seminars in Cancer Biology *35, Supplement*, S185-S198.

Viola, A., Sarukhan, A., Bronte, V., and Molon, B. (2012). The pros and cons of chemokines in tumor immunology. Trends Immunol *33*, 496-504.

Wang, J., Shirota, Y., Bayik, D., Shirota, H., Tross, D., Gulley, J. L., Wood, L., Berzofsky, J. A., and Klinman, D. M. (2015). Effect of TLR Agonists on the Differentiation and Function of Human Monocytic Myeloid Derived Suppressor Cells. Journal of immunology (Baltimore, Md : 1950) *194*, 4215-4221.

Wasserman, J., Blomgren, H., Rotstein, S., Petrini, B., and Hammarstrom, S. (1989). Immunosuppression in irradiated breast cancer patients: in vitro effect of cyclooxygenase inhibitors. Bulletin of the New York Academy of Medicine *65*, 36-44.

Watanabe, Y., and Jacob, C. O. (1991). Regulation of MHC class II antigen expression. Opposing effects of tumor necrosis factor-alpha on IFN-gamma-induced HLA-DR and Ia expression depends on the maturation and differentiation stage of the cell. Journal of immunology *146*, 899-905.

Weichselbaum, R., Fu, Y.-X., and Burnette, B. (2012). The confluence of radiotherapy and immunotherapy. Frontiers in Oncology *2*.

Weis, S. M., and Cheresh, D. A. (2011). Tumor angiogenesis: molecular pathways and therapeutic targets. Nat Med *17*, 1359-1370.

Weisman, G. A., Erb, L., Garrad, R. C., Theiss, P. M., Santiago-Pérez, L. I., Flores, R. V., Santos-Berríos, C., Méndez, Y., and González, F. A. (1998). P2Y nucleotide receptors in the immune system: Signaling by a P2Y2 receptor in U937 monocytes. Drug Development Research *45*, 222-228.

Welsh, T. J., Green, R. H., Richardson, D., Waller, D. A., O'Byrne, K. J., and Bradding, P. (2005). Macrophage and mast-cell invasion of tumor cell islets confers a marked survival advantage in non-small-cell lung cancer. Journal of clinical oncology : official journal of the American Society of Clinical Oncology *23*, 8959-8967.

Wersall, P. J., Blomgren, H., Pisa, P., Lax, I., Kalkner, K. M., and Svedman, C. (2006). Regression of non-irradiated metastases after extracranial stereotactic radiotherapy in metastatic renal cell carcinoma. Acta oncologica (Stockholm, Sweden) *45*, 493-497.

Willingham, S. B., Volkmer, J.-P., Gentles, A. J., Sahoo, D., Dalerba, P., Mitra, S. S., Wang, J., Contreras-Trujillo, H., Martin, R., Cohen, J. D.*, et al.* (2012). The CD47-signal regulatory protein alpha (SIRPa) interaction is a therapeutic target for human solid tumors. Proceedings of the National Academy of Sciences *109*, 6662-6667.

Wu, J., Su, W., Powner, M. B., Liu, J., Copland, D. A., Fruttiger, M., Madeddu, P., Dick, A. D., and Liu, L. (2016). Pleiotropic action of CpG-ODN on endothelium and macrophages attenuates angiogenesis through distinct pathways. Scientific Reports *6*, 31873.

Wu, N. Z., Klitzman, B., Dodge, R., and Dewhirst, M. W. (1992). Diminished leukocyte-endothelium interaction in tumor microvessels. Cancer research *52*, 4265-4268.

Wu, R., Forget, M.-A., Chacon, J., Bernatchez, C., Haymaker, C., Chen, J. Q., Hwu, P., and Radvanyi, L. (2012). Adoptive T-cell Therapy Using Autologous Tumor-infiltrating Lymphocytes for Metastatic Melanoma: Current Status and Future Outlook. Cancer Journal (Sudbury, Mass) *18*, 160-175.

Wu, Z. H., and Miyamoto, S. (2007). Many faces of NF-kappaB signaling induced by genotoxic stress. Journal of molecular medicine (Berlin, Germany) *85*, 1187-1202.

Xia, P., Gamble, J. R., Rye, K.-A., Wang, L., Hii, C. S. T., Cockerill, P., Khew-Goodall, Y., Bert, A. G., Barter, P. J., and Vadas, M. A. (1998). Tumor necrosis factor-α induces adhesion molecule expression through the sphingosine kinase pathway. Proceedings of the National Academy of Sciences *95*, 14196-14201.

Xiao, L., Liu, W., Li, J., Xie, Y., He, M., Fu, J., Jin, W., and Shao, C. (2014). Irradiated U937 Cells Trigger Inflammatory Bystander Responses in Human Umbilical Vein Endothelial Cells through the p38 Pathway. Radiation Research *182*, 111-121.

Xie, C., Liu, C., Wu, B., Lin, Y. A. N., Ma, T., Xiong, H., Wang, Q. I. N., Li, Z., Ma, C., and Tu, Z. (2016). Effects of IRF1 and IFN-β interaction on the M1 polarization of macrophages and its antitumor function. International Journal of Molecular Medicine *38*, 148-160.

Yannelli, J. R., Hyatt, C., McConnell, S., Hines, K., Jacknin, L., Parker, L., Sanders, M., and Rosenberg, S. A. (1996). Growth of tumor-infiltrating lymphocytes from human solid cancers: summary of a 5-year experience. International journal of cancer Journal international du cancer *65*, 413-421.

Youn, J.-I., and Gabrilovich, D. I. (2010). The biology of myeloid-derived suppressor cells: The blessing and the curse of morphological and functional heterogeneity. European Journal of Immunology *40*, 2969-2975.

Zhang, B., Bowerman, N. A., Salama, J. K., Schmidt, H., Spiotto, M. T., Schietinger, A., Yu, P., Fu, Y.-X., Weichselbaum, R. R., Rowley, D. A.*, et al.* (2007). Induced sensitization of tumor stroma leads to eradication of established cancer by T cells. The Journal of Experimental Medicine *204*, 49-55.

Zhang, D., and Zhang, D.-E. (2011). Interferon-Stimulated Gene 15 and the Protein ISGylation System. Journal of Interferon & Cytokine Research *31*, 119-130.

Zhang , L., Conejo-Garcia , J. R., Katsaros , D., Gimotty , P. A., Massobrio , M., Regnani , G., Makrigiannakis , A., Gray , H., Schlienger , K., Liebman , M. N.*, et al.* (2003). Intratumoral T Cells, Recurrence, and Survival in Epithelial Ovarian Cancer. New England Journal of Medicine *348*, 203-213.

Zhang, L., Khayat, A., Cheng, H., and Graves, D. T. (1997). The pattern of monocyte recruitment in tumors is modulated by MCP-1 expression and influences the rate of tumor growth. Laboratory investigation; a journal of technical methods and pathology *76*, 579-590.

Zhang, Q.-w., Liu, L., Gong, C.-y., Shi, H.-s., Zeng, Y.-h., Wang, X.-z., Zhao, Y.-w., and Wei, Y.-q. (2012). Prognostic Significance of Tumor-Associated Macrophages in Solid Tumor: A Meta-Analysis of the Literature. PloS one *7*, e50946.

Zhang, X., Goncalves, R., and Mosser, D. M. (2001). The Isolation and Characterization of Murine Macrophages. In Current Protocols in Immunology, (John Wiley & Sons, Inc.).

Zou, W. (2006). Regulatory T cells, tumour immunity and immunotherapy. Nat Rev Immunol *6*, 295-307.

6. SUPPLEMENTS

Table 28 Commonly upregulated genes

Gene	FC	FDR	FC	FDR	Description
	In vivo		*In vitro*		
Agrn	1.59	0.0346	2.77	0.0425	agrin
Arfgef3	2.72	0.0292	4.33	0.0150	ARFGEF family member 3
AW112010	2.78	0.0154	43.93	0.0008	expressed sequence AW112010
C3	1.61	0.0178	8.68	0.0014	complement component 3
Cd274	1.74	0.0003	10.64	0.0013	CD274 antigen
Cfb	4.89	0.0011	93.64	0.0010	complement factor B
Clec4n	1.94	0.0021	13.81	0.0021	C-type lectin domain family 4, member n
Cmpk2	2.40	0.0008	9.20	0.0015	cytidine monophosphate (UMP-CMP) kinase 2, mitochondrial
Col1a1	2.02	0.0302	4.45	0.0226	collagen, type I, alpha 1
Col1a2	2.01	0.0088	2.97	0.0429	collagen, type I, alpha 2
Col4a1	2.98	0.0280	8.16	0.0031	collagen, type IV, alpha 1
Col5a2	2.19	0.0199	6.10	0.0231	collagen, type V, alpha 2
Cxcl2	2.87	0.0119	4.05	0.0377	chemokine (C-X-C motif) ligand 2
Dcn	1.95	0.0035	4.34	0.0114	decorin
Ddx58	1.97	0.0000	4.26	0.0091	DEAD (Asp-Glu-Ala-Asp) box polypeptide 58
Dhx58	2.10	0.0000	2.86	0.0498	DEXH (Asp-Glu-X-His) box polypeptide 58
Ece1	1.52	0.0019	7.18	0.0042	endothelin converting enzyme 1
Egfr	2.71	0.0180	4.12	0.0498	epidermal growth factor receptor
Eif2ak2	1.68	0.0009	3.08	0.0192	eukaryotic translation initiation factor 2-alpha kinase 2
Fam46c	1.70	0.0037	4.20	0.0231	family with sequence similarity 46, member C
Fbln2	3.03	0.0000	5.24	0.0092	fibulin 2
Fcgr4	1.69	0.0000	4.15	0.0023	Fc receptor, IgG, low affinity IV
Gbp2	1.60	0.0231	10.61	0.0026	guanylate binding protein 2
Gbp4	3.40	0.0177	96.80	0.0008	guanylate binding protein 4
Gbp9	2.14	0.0226	16.40	0.0023	guanylate-binding protein 9
H2-T22	1.74	0.0065	2.90	0.0488	histocompatibility 2, T region locus 22
Havcr2	1.69	0.0039	3.89	0.0192	hepatitis A virus cellular receptor 2
Helz2	1.69	0.0001	4.67	0.0094	helicase with zinc finger 2, transcriptional coactivator
Ifi203	1.60	0.0001	3.28	0.0226	interferon activated gene 203
Ifi204	2.38	0.0000	3.79	0.0125	interferon activated gene 204
Ifi44	4.29	0.0000	10.42	0.0008	interferon-induced protein 44
Ifi44l	3.47	0.0000	8.94	0.0011	interferon-induced protein 44 like
Ifi47	2.70	0.0000	6.90	0.0044	interferon gamma inducible protein 47
Ifih1	2.08	0.0000	3.62	0.0125	interferon induced with helicase C domain 1
Ifit1	10.03	0.0000	14.47	0.0010	interferon-induced protein with tetratricopeptide repeats 1
Ifit1bl1	12.59	0.0020	10.02	0.0267	interferon induced protein with tetratricpeptide repeats 1B like 1
Ifit2	17.44	0.0000	22.53	0.0010	interferon-induced protein with tetratricopeptide repeats 2
Ifit3	27.57	0.0000	9.73	0.0014	interferon-induced protein with tetratricopeptide repeats 3
Iigp1	7.17	0.0356	448.20	0.0015	interferon inducible GTPase 1
Il2rb	2.64	0.0059	12.85	0.0342	interleukin 2 receptor, beta chain
Irf7	3.76	0.0000	14.14	0.0008	interferon regulatory factor 7
Irgm1	2.25	0.0000	8.92	0.0013	immunity-related GTPase family M member 1
Irgm2	1.96	0.0005	11.08	0.0018	immunity-related GTPase family M member 2
Isg15	5.07	0.0000	5.72	0.0092	ISG15 ubiquitin-like modifier
Kdr	1.64	0.0262	3.71	0.0308	kinase insert domain protein receptor

continued on the next page

Gene	FC	FDR	FC	FDR	Description
	In vivo		*In vitro*		
Lamc1	1.57	0.0001	2.45	0.0434	laminin, gamma 1
Lgals3bp	1.60	0.0000	4.93	0.0053	lectin, galactoside-binding, soluble, 3 binding protein
Ly6a	5.06	0.0057	121.26	0.0008	lymphocyte antigen 6 complex, locus A
Ly6c1	7.52	0.0000	87.12	0.0015	lymphocyte antigen 6 complex, locus C1
Ly6c2	8.06	0.0000	64.58	0.0023	lymphocyte antigen 6 complex, locus C2
Ly6e	1.94	0.0000	2.50	0.0259	lymphocyte antigen 6 complex, locus E
Met	2.06	0.0033	3.83	0.0071	met proto-oncogene
Ms4a4c	3.48	0.0001	13.61	0.0030	membrane-spanning 4-domains, subfamily A, member 4C
Ms4a6b	1.84	0.0039	13.04	0.0100	membrane-spanning 4-domains, subfamily A, member 6B
Mt2	2.28	0.0135	2.98	0.0366	metallothionein 2
Mx1	3.68	0.0000	6.85	0.0119	MX dynamin-like GTPase 1
Mxd1	1.93	0.0008	3.96	0.0179	MAX dimerization protein 1
Nlrc5	1.95	0.0008	6.99	0.0029	NLR family, CARD domain containing 5
Oas1g	3.13	0.0000	2.83	0.0431	2'-5' oligoadenylate synthetase 1G
Oas2	1.71	0.0018	7.38	0.0033	2'-5' oligoadenylate synthetase 2
Oas3	5.37	0.0000	8.78	0.0013	2'-5' oligoadenylate synthetase 3
Oasl2	3.38	0.0000	4.86	0.0057	2'-5' oligoadenylate synthetase-like 2
Parp12	1.69	0.0005	3.20	0.0275	poly (ADP-ribose) polymerase family, member 12
Parp14	1.79	0.0000	6.59	0.0018	poly (ADP-ribose) polymerase family, member 14
Parp9	1.71	0.0001	3.06	0.0424	poly (ADP-ribose) polymerase family, member 9
Pdgfra	2.27	0.0106	2.82	0.0480	platelet derived growth factor receptor, alpha polypeptide
Pf4	1.53	0.0178	6.56	0.0076	platelet factor 4
Plac8	2.04	0.0280	5.23	0.0425	placenta-specific 8
Rnf213	2.37	0.0000	8.16	0.0013	ring finger protein 213
Rsad2	5.97	0.0000	10.82	0.0022	radical S-adenosyl methionine domain containing 2
Rtp4	3.08	0.0000	8.19	0.0015	receptor transporter protein 4
Serpine1	3.06	0.0000	24.90	0.0010	serine (or cysteine) peptidase inhibitor, clade E, member 1
Siglec1	1.72	0.0000	4.22	0.0044	sialic acid binding Ig-like lectin 1, sialoadhesin
Slc39a2	4.25	0.0000	3.27	0.0171	solute carrier family 39 (zinc transporter), member 2
Slfn1	2.01	0.0002	22.60	0.0010	schlafen 1
Slfn4	2.40	0.0003	8.16	0.0029	schlafen 4
Slfn5	1.99	0.0000	3.31	0.0369	schlafen 5
Spon1	3.34	0.0014	80.62	0.0062	spondin 1, (f-spondin) extracellular matrix protein
Stat1	1.63	0.0430	4.07	0.0093	signal transducer and activator of transcription 1
Stat2	1.71	0.0000	4.99	0.0077	signal transducer and activator of transcription 2
Stfa3	2.32	0.0051	10.67	0.0377	stefin A3
Tgm2	2.15	0.0000	10.87	0.0010	transglutaminase 2, C polypeptide
Thbs1	1.78	0.0048	10.83	0.0144	thrombospondin 1
Tnc	25.58	0.0336	6.65	0.0091	tenascin C
Trim30a	1.59	0.0001	3.46	0.0109	tripartite motif-containing 30A
Trim30d	4.44	0.0000	27.13	0.0010	tripartite motif-containing 30D
Tulp4	1.51	0.0000	2.71	0.0184	tubby like protein 4
Usp18	5.33	0.0000	4.99	0.0086	ubiquitin specific peptidase 18
Vcan	2.67	0.0001	7.09	0.0084	versican
Xaf1	2.33	0.0000	5.01	0.0071	XIAP associated factor 1
Zbp1	4.57	0.0000	25.25	0.0010	Z-DNA binding protein 1
Znfx1	1.74	0.0000	3.39	0.0183	zinc finger, NFX1-type containing 1

92 genes commonly upregulated after *in vivo* and *in vitro* irradiation with the FC and FDR values from both datasets. With IRGs highlighted in bold.

Table 29 IPA Diseases and biological functions (listing the DEGs of the *in vivo* and *in vitro* dataset)

Diseases and Bio Functions	*in vivo*		*in vitro*	
	activation z-score	Genes in dataset	activation z-score	Genes in dataset
Innate immune response	**1.94**	*Mx1, Lgals9, Havcr2, Stat1, Zbp1, Isg15, Ifit2, Fn1, Clec4n, Eif2ak2, Ifih1, Ddx58, Bst2, Nlrc5, Igha*	**3.44**	*Havcr2, Mx2, Stat1, Zbp1, Tlr2, Mmp2, Isg15, Tlr8, Trem1, Ifit2, Nod2, Gbp5, Slpi, Clec4n, Eif2ak2, Lcn2, Ifih1, Clec4e, Ddx58, Fpr1, Fpr2, Nlrc5*
Activation of leukocytes	**2.76**	*Lck, Lgals9, Met, Gzmb, Vcan, Gzma, C3, Stat1, Fcgr2b, Il1rn, Itgav, Siglec1, Spp1, Npy, Mif, Ccl2, Card11, C1qa, Prf1, Bank1, Ddx58, Foxo1, Serpinb9, Cx3cr1, Timd4, Cxcl2, Fcgr4, Il2rb, Treml2, Cd274, Tnfaip3, Havcr2, Cd74, Csf1r, Fn1, Cfh, Cd19, Pou2af1, Thbs1, Cd300lf, Cxcr5, Retnla, Apoe, Cd79a, Hdac9, Blk, Fcgr1, Fos, Pf4, Nedd4, H2-Aa, H2-DMa, Tgm2, Cd79b, Nlrc3, Csf2rb2, C4b, H2-Ab1, H2-DMb1, Igha*	**4.42**	*Il12rb1, Trpm2, Met, Lyst, Nos2, Hif1a, Edn1, Vcan, Cd86, C3, Fas, Snca, Stat1, Lcn2, Notch1, Siglec1, Rasgrp1, Il1b, Il1a, Notch2, Tlr2, Cd1d1, Cd38, Clec4e, Cd69, Il4ra, Itgal, Ptgs2, Cish, Bmp2k, Ccl5, Ccl12, Nfkbiz, Icam1, Stx11, Saa3, Ddx58, Inhba, Cd1d2, Trem1, Itga1, Fpr1, Ptges, Cx3cr1, Cxcl2, Fcgr4, Il2rb, Hmox1, Mertk, Hsd11b1, Cd274, Slpi, Adora2b, Havcr2, Il15ra, Pag1, Cd2, Tgfbr2, Thbs1, Gja1, Tarm1, Slamf6, Nfkbia, Satb1, Pf4, Klrk1, Klrb1a, Il21r, Sbno2, H2-Q4, Tgm2, Socs1, Tlr8, Prkce, Cd24a, Kcna3, Spn, Fpr2*
Activation of myeloid cells	1.39	*Lgals9, Met, Gzma, C3, Stat1, Itgav, Spp1, Npy, Mif, Ccl2, Thbs1, Cx3cr1, Timd4, Cxcl2, Treml2, Apoe, Havcr2, Csf1r, Fn1, Cfh, Fcgr2b, Prf1, Cd300lf, Cxcr5, Retnla, Il1rn, Pf4, Tgm2, C4b*	**4.24**	*Il4ra, Icam1, Met, Cxcl2, Stat1, Cd86, Notch1, Cx3cr1, Itga1, Cd1d1, Ccl12, Trpm2, Trem1, C3, Thbs1, Tlr2, Clec4e, Ccl5, Edn1, Ptges, Snca, Il1b, Ptgs2, Saa3, Inhba, Nos2, Fpr1, Lcn2, Adora2b, Havcr2, Slpi, Gja1, Hmox1, Hsd11b1, Sbno2, Prkce, Tlr8, H2-Q4, Pf4, Tgm2, Socs1, Fpr2*
Activation of phagocytes	1.17	*Lgals9, Met, Gzma, C3, Stat1, Itgav, Spp1, Npy, Mif, Ccl2, Thbs1, Cx3cr1, Timd4, Cxcl2, Treml2, Apoe, Havcr2, Csf1r, Fn1, Cfh, Prf1, Cd300lf, Cxcr5, Retnla, Il1rn, Pf4, Tgm2, C4b*	**3.56**	*Trpm2, Met, Nos2, Edn1, Cd86, C3, Snca, Stat1, Lcn2, Notch1, Il1b, Tlr2, Cd1d1, Clec4e, Il4ra, Ptgs2, Ccl5, Ccl12, Icam1, Saa3, Thbs1, Inhba, Itga1, Fpr1, Ptges, Cx3cr1, Cxcl2, Hmox1, Mertk, Hsd11b1, Slpi, Adora2b, Havcr2, Cd24a, Gja1, Pf4, Sbno2, H2-Q4, Tgm2, Socs1, Tlr8, Trem1, Prkce, Fpr2*
Activation of macrophages	0.74	*Lgals9, Stat1, Il1rn, Itgav, Npy, Mif, Ccl2, Thbs1, Cx3cr1, Timd4, Apoe, Havcr2, Csf1r, Fn1, Prf1, Cxcr5, Retnla, C3, Tgm2*	**3.77**	*Trpm2, Nos2, Snca, Stat1, Lcn2, Notch1, Il1b, Tlr2, Cd1d1, Clec4e, Il4ra, Ptgs2, Ccl5, Ccl12, Icam1, Thbs1, Inhba, Ptges, Cx3cr1, Adora2b, Havcr2, Gja1, C3, Sbno2, H2-Q4, Tgm2, Socs1, Prkce*
Cell movement	**2.32**	*Lck, Apoe, Cdkn1b, Hdac9, Ccl24, Met, Hyal1, Sparc, Egfr, Sgpp1, Fos, Ctsl, Vcan, Plau, Ly6c2, Qpct, C3, Pdgfrb, Irf7, Stat1, Rgs18, Cfh, Fcgr2b, Itgav, Tnc, Spp1, Pf4, Flt1, Npy, Mgll, Mif, Ccl7, Ccl2, Tgm2, Rras, Thbs1, Ddx58, Fzd7, Irgm1, Mmp13, Cxcl2, Fcgr4, Sphk1, Kdr, Il2rb, Treml2, Csf2rb2, C4b, Cfb, Slfn4, Pdgfb, Trpv4, Cd274, Alox15, Tnfaip3, Dcn, Itgb3, Ciita, Cyp1b1, Cd74, Csf1r, Alox5, Fn1, Rgs1, Il1rn, Cd19, Cryab, Ccr3, Myrf, Prf1, Serpine1, Atp8a1, Stat2, Foxo1, Cd300lf, Cxcr5, Cx3cr1, Retnla, Hvcn1, Lyz1, Grk6, Col1a1, Cacna1e, Pltp, Net1, Podxl, Plxna2, Fbn1, Gba, Pdgfra, Dck, Cttn, Cd209a, Col4a1, Pou2af1, Selenbp1*	**6.25**	*Il12rb1, Mmp11, Mmp14, Ephb3, Trpm2, Met, Abca1, Kdm6b, Adora2b, Lsp1, Cxcl16, Ccl6, Esr1, Ctgf, Egfr, Rhbdf2, Nos2, Nfkbia, Hif1a, Lrrc16a, Edn1, Vcan, Ednrb, Osmr, Trio, Ly6i, Il15ra, C3, C2, Lox, Fosl1, Irf7, Nrp2, Stat1, Ralgds, Lcn2, Notch1, Rasgrp1, Il1b, Il1a, Tm4sf1, Tlr2, Cd1d1, Cyr61, Tnc, Pde4b, Lrp8, Cd38, Fosl2, Pf4, Cxcl1, Clec4e, Cd69, Furin, Ctsc, Il21r, Il4ra, Itgal, Hp, Mmp2, Adamts7, Ptgs2, Ccl5, Ccl12, Acta2, H2-Q4, Lrrk2, Icam1, Tgm2, Rara, F13a1, Itga9, Prex1, Fgl2, Thbs1, Ddx58, Pvr, Inhba, Cmklr1, Trem1, Itga1, S1pr1, Fpr1, Irgm1, Kcna3, Ptges, Gja1, Fpr2, Nod2, Cxcl2, Fcgr4, Serpinb2, Kdr, Il2rb, Cfb, Slfn4, Hmox1, Mmp8, Sod2, Cav1, Cd274, Slpi, Abr, Dcn, Cdk1, Timp3, Pttg1, Cd86, Lmnb1, Jag1, Cd2, Olr1, Siglece, Nt5e, Lif, Apln, Serpine1, Socs1, Stat2, Mmp10, Gpr183, Spn, Cx3cr1, Socs3, Wfdc17, Sod3, Col1a1, Epha2, Chdh, Cd34, Lyst, Fas, Vldlr, Epha4, Serpine2, Marco, Pdgfra, Cxcl3, Tjp1, Col4a1, Dusp4, Tgfbr2, Nfkbiz, Tgfbi, Saa3, Prkce, Cd24a, Rapgef2*
Cell movement of myeloid cells	**2.26**	*Apoe, Ccl24, Hyal1, Ctsl, Vcan, Plau, Qpct, C3, Spp1, Pf4, Ccl2, Tgm2, Thbs1, Irgm1, Cxcl2, Sphk1, Kdr, Il2rb, Treml2, C4b, Cfb, Trpv4, Tnfaip3, Cd74, Csf1r, Alox5, Il1rn, Flt1, Cttn, Ccr3, Myrf, Cxcr5, Col1a1, Itgb3, Gba, Col4a1, Mif, Serpine1, Cx3cr1, Grk6*	**3.92**	*Il12rb1, Trpm2, Abca1, Lsp1, Ctgf, Nos2, Hif1a, Edn1, Vcan, Il15ra, C3, C2, Fas, Lcn2, Il1b, Il1a, Tlr2, Cyr61, Pde4b, Pf4, Cxcl1, Cd69, Il4ra, Itgal, Hp, Ptgs2, Ccl5, Ccl12, Nfkbiz, Icam1, Tgm2, Prex1, Thbs1, Inhba, Trem1, S1pr1, Fpr1, Irgm1, Ptges, Fpr2, Cxcl2, Kdr, Il2rb, Cfb, Hmox1, Mmp8, Cav1, Timp3, Lmnb1, Cd2, Nt5e, Tgfbr2, Socs1, Cmklr1, Itga1, Mmp10, Spn, Socs3, Sod3, Col1a1, Slpi, Nfkbia, Cxcl3, Col4a1, Serpine1, Itga9, Cx3cr1, Nod2*

Cell movement of phagocytes	1.97	*Col1a1, Apoe, Ccl24, Hyal1, Trpv4, Tnfaip3, Itgb3, Ctsl, Vcan, Plau, Qpct, C3, Cd74, Csf1r, Alox5, Il1rn, Itgav, Gba, Spp1, Pf4, Flt1, Cttn, Cd209a, Col4a1, Mif, Ccl2, Myrf, Serpine1, Thbs1, Irgm1, Cx3cr1, Cxcl2, Sphk1, Kdr, Treml2, C4b, Grk6, Cfb*	**4.01**	*Il12rb1, Trpm2, Abca1, Lsp1, Ctgf, Nos2, Hif1a, Edn1, Vcan, Il15ra, C3, C2, Fas, Nrp2, Lcn2, Il1b, Il1a, Tlr2, Cyr61, Pde4b, Cd38, Pf4, Cxcl1, Cd69, Itgal, Hp, Ptgs2, Ccl5, Ccl12, Nfkbiz, Icam1, Prex1, Thbs1, Inhba, Cmklr1, Trem1, S1pr1, Fpr1, Irgm1, Ptges, Fpr2, Cxcl2, Kdr, Cfb, Hmox1, Mmp8, Cav1, Timp3, Cd86, Lmnb1, Nt5e, Tgfbr2, Socs1, Itga1, Mmp10, Spn, Socs3, Sod3, Col1a1, Slpi, Nfkbia, Marco, Cxcl3, Il4ra, Col4a1, Serpine1, Itga9, Cx3cr1, Nod2*
Cell movement of macrophag-es	1.09	*Apoe, Vcan, Plau, Spp1, Pf4, Ccl2, Thbs1, Irgm1, Cx3cr1, Kdr, Trpv4, Tnfaip3, Csf1r, Il1rn, Mif, Myrf, Itgb3, Cd74, Gba, Flt1, Serpine1*	**2.90**	*Il12rb1, Hmox1, Nos2, Hif1a, Edn1, Vcan, Il15ra, Il1b, Il1a, Tlr2, Cyr61, Pf4, Itgal, Ptgs2, Ccl5, Ccl12, Icam1, Thbs1, S1pr1, Irgm1, Ptges, Fpr2, Cx3cr1, Kdr, Cav1, Timp3, Lmnb1, Tgfbr2, Socs1, Itga1, Mmp10, Sod3, Ctgf, Il4ra, Serpine1*
Viral Infection	**-2.39**	*Lck, Lgals9, Cd274, Ctsl, Cd74, Itgav, Spp1, Oasl1, Hmga1, Cxcl2, Sphk1, H2-Ab1, Pou3f1, Igha, Mx1, Apoe, Gzmb, Dhx58, Rsad2, Itgb3, Gzma, Eif2ak2, C3, Irf7, Stat1, Fn1, Fcgr2b, Ifih1, Il1rn, Zbp1, Oasl2, Cd19, Cd209a, Ccl2, Isg15, Prf1, Stat2, Ddx58, Serpinb9, Ifit2, Bst2, Ifit1bl1, Pf4*	**-2.50**	*Mertk, Cd274, Nos2, Il1b, Tlr2, Klrk1, Itgal, Tgfbr2, Socs1, Fpr1, St3gal5, Cxcl2, Hmox1, Cav1, Slpi, Dhx58, Lsp1, Irf1, Rsad2, Mx2, Eif2ak2, C3, Irf7, Cflar, Stat1, Ifih1, Zbp1, Oasl2, Ccl5, Nfkbiz, Isg15, Stx11, Stat2, Ddx58, Tlr8, Abcb1a, Ifit2, Ch25h, Socs3, Ifit1bl1, Nfkbia, Fas, Pf4, Ccl12, H2-Q4, Apln, Icam1*

Diseases and biological functions predicted by IPA to be increased (red) or decreased (blue) in PECs after *in vivo* or *in vitro* irradiation. The DEGs of the two datasets for each Disease and biological function are listed under 'Genes in dataset'. Activation z-score ≥ |2|; p-value <0.0001 considered significant. Insignificant values shown in black.

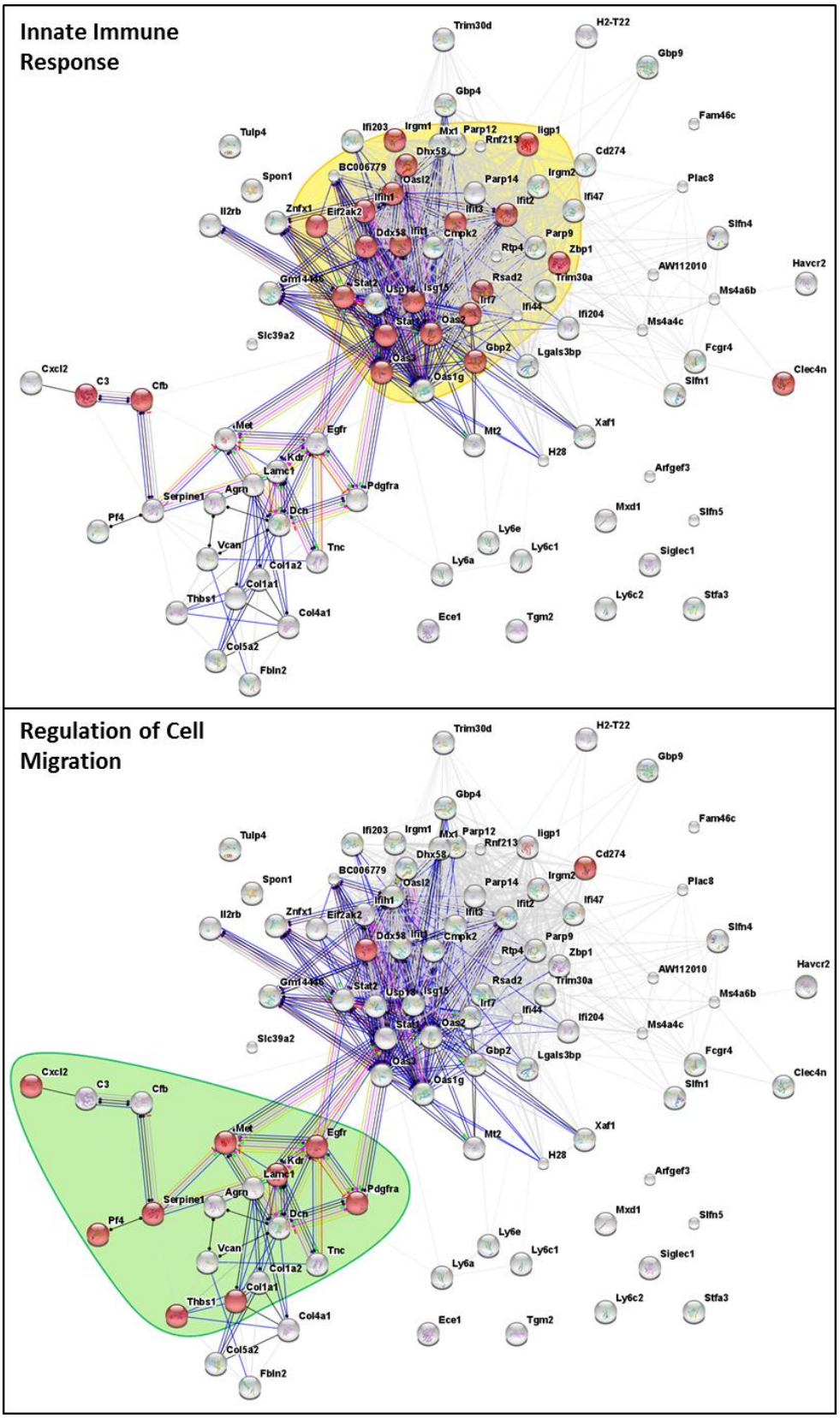

Figure S33 Protein network of genes upregulated in PECs in response to LDI

Protein-protein interactions of the proteins encoded by the 92 genes upregulated after both *in vivo* and *in vitro* irradiation, visualized by STRING. The nodes represent proteins. Highlighted in red are the proteins associated with the respective GO term indicated in the upper left corner of the subfigure. The coloured areas highlight the protein clusters which predominantly comprise proteins involved in an innate immune response (yellow) or cell migration (green).The edges represent physical and functional connections between the proteins.

Table 30 IPA Upstream regulators (IFN signalling) (listing the DEGs of the *in vivo* and *in vitro* dataset)

Upstream regulator	*in vivo*		*in vitro*	
	activation z-score	Genes in dataset	activation z-score	Genes in dataset
IRF3	5.63	*Stat1, Parp12, Helz2, Oas2, Stat2, Ube2l6, Nt5c3, Parp14, Irgm2, Ddx58, Slfn1, Plac8, Phf11b, Ifih1, Dhx58, Irgm1, Ifi204, Cmpk2, Oasl1, Ifi47, Fcgr1, Oas1g, Oasl2, Mx1, Irf7, Trim30d, Isg15, Usp18, Rsad2, Ifit1, Ifit1bl1, Ifit2, Ifit3*	6.01	*Oas1g, Dhx58, Samd9l, Parp12, Phf11d, Ifih1, Stat1, Cd86, Ddx58, Helz2, Oasl2, Usp18, Stat2, Tap1, Plac8, Isg15, Cd69, Parp14, Ifi47, Igtp, Oas2, Fam26f, Mx2, Irgm1, Cmpk2, Ifit1bl1, Rsad2, Irgm2, Ifi205, Ifit3b, Irf7, Ccl5, Ifit1, Ifit2, Slfn1, Trim30d, Gbp5, Nos2*
IRF7	5.47	*Stat1, Parp12, Helz2, Oas2, Stat2, Ube2l6, Nt5c3, Parp14, Irgm2, Ddx58, Slfn1, Plac8, Phf11b, Ifih1, Dhx58, Irgm1, Ifi204, Cmpk2, Oasl1, Ifi47, Fcgr1, Oas1g, Oasl2, Mx1, Irf7, Trim30d, Isg15, Usp18, Rsad2, Ifit2, Ifit3, Ifit1bl1*	5.73	*Oas1g, Dhx58, Samd9l, Parp12, Phf11d, Ifih1, Stat1, Ddx58, Helz2, Oasl2, Usp18, Stat2, Tap1, Plac8, Isg15, Cd69, Parp14, Ifi47, Igtp, Oas2, Fam26f, Mx2, Irgm1, Cmpk2, Rsad2, Irgm2, Ifi205, Ifit3b, Irf7, Ccl5, Ifit2, Slfn1, Trim30d, Gbp5, Ifit1bl1*
IRF5	4.17	*Stat1, Parp12, Oas2, Stat2, Ube2l6, Nt5c3, Ddx58, Ifih1, Dhx58, Cmpk2, Oasl1, Oas1g, Oasl2, Irf7, Isg15, Rsad2, Ifit2, Ifit3*	3.93	*Oas1g, Dhx58, Parp12, Ifih1, Stat1, Ddx58, Oasl2, Stat2, Isg15, Cxcl1, Oas2, Cmpk2, Rsad2, Ifit3b, Irf7, Ifit2, Dapk2*
IFN-γ	4.09	*Fcgr2b, Ece1, Pf4, Csf1r, Hmga1, Gbp2, C3, Stat1, Eif2ak2, Fcgr4, Stat2, Cd274, Thbs1, Rab20, Ly6e, Nlrc5, Irgm2, Ddx58, Slfn1, Il1rn, Ifih1, Plau, Col5a2, Bst2, Irgm1, Ifi204, Slfn4, Spp1, Chst3, Ifi47, Fcgr1, Angptl4, Serpine1, Oas1g, Gbp4, Mx1, Irf7, Retnla, Cd163, Cfb, Isg15, Flt1, Rsad2, Iigp1, Ly6c2, Ccl7, Ccl2, Ifit2, Fos, Mgl2, Il7r, Kdr, Ciita, Col1a2, H2-DMa, Col1a1, Fn1, H2-Ab1, H2-Eb1, Cd74, H2-Aa, Cxcl2, H2-Ob, Ms4a4c*	7.67	*Cflar, Ly6e, Sbno2, Hif1a, Oas1g, Ctsh, Nfkbia, Ifi202b, Eif2ak2, Adora2b, Fas, Itgal, Ifih1, Icam1, Nfkbiz, Serpina3f, Stat1, Cd86, Fcgr4, Ddx58, Bst1, Stat2, Tap1, Wfdc17, Sod2, Ndrg4, Nod2, C2, Isg15, Col5a2, Irf1, Cxcl1, Il12rb1, Pf4, Ifi47, Igtp, Nlrc5, Ece1, Il1a, C1rb, Ccl12, Slfn4, C3, Mx2, Irgm1, Mefv, Ass1, Gbp2, Cd274, Rsad2, Thbs1, Tlr2, Irgm2, Il15ra, Socs1, Clec4e, Gm4070, Ifi205, Cp, Cish, Gbp2b, Irf7, Ccl5, Edn1, Ch25h, Tjp1, Ptges, Flt4, Mmp2, Ifit2, Slfn1, Crlf1, Serpine1, Gbp7, Gbp3, Il1b, Ptgs2, Socs3, Tgtp2, Timp3, Il18bp, Inhba, Gbp5, Nos2, Acod1, Cfb, Gbp4, Gbp8, Ly6i, Iigp1, Lcn2, Ubd, Trem1, Il23r, Col1a2, Acta2, Kdr, Cxcl2, Col1a1, Ccnd2, Ctsc, Abcb1a, Abca1, Vldlr, Hmox1, Ms4a4c, Arg2, Saa3, Ctgf*
IFN-α	4.95	*Fcgr2b, C3, Stat1, Eif2ak2, Oas2, Stat2, Siglec1, Ddx58, Slfn5, Slfn1, Il1rn, Phf11b, Ifih1, Dhx58, Bst2, Ifi204, Slfn4, Egfr, Fcgr1, Oas1g, Mx1, Irf7, Prf1, Zbp1, Isg15, Usp18, Ifit1bl1, Ifit2, Gzmb, Ifit3, Ifitm2, Fos*	5.88	*Oas1g, Dhx58, Eif2ak2, Slfn5, Fas, Phf11d, Ifih1, Icam1, Stat1, Prkce, Egfr, Cd86, Siglec1, Ddx58, Ccnd2, Usp18, Stat2, Isg15, Cd69, Irf1, Oas2, Ccl12, Slfn4, C3, Mx2, Mefv, Ifit1bl1, Il15ra, Socs1, Ifi205, Gbp2b, Ifit3b, Irf7, Ch25h, Ifit2, Slfn1, Zbp1, Socs3, Tgtp2, Cd38, Nos2, Il21r, Il12rb1*
IFN-β1	3.76	*Gbp2, Stat1, Eif2ak2, Parp12, Stat2, Itgb3, Ddx58, Ifih1, Dhx58, Bst2, Oas1g, Gbp4, Mx1, Irf7, Zbp1, Isg15, Ifit1, Ccl2, Ifit2, Cd274, Thbs1, Nt5c3, Nfix, Irgm2, Irgm1, Ifi27l2a, Ifi204, Cmpk2, Fbn1, Ifi47, Cryab, Fbln2, Trim30d, Usp18, Rsad2, Ifit3, Itgav, Fos*	5.16	*Oas1g, Dhx58, Eif2ak2, Parp12, Ifih1, Stat1, Cd86, Ddx58, Stat2, Nod2, Isg15, Irf1, Ccl12, Mx2, Gbp2, Socs1, Gm4070, Irf7, Ccl5, Ifit1, Ch25h, Ifit2, Gbp7, Zbp1, Gbp3, Tgtp2, Gbp5, Nos2, Gbp4, Gbp8, Nfkbie, Cd24a, Lamb1, Ctla2b, Usp18, Fbln2, Cxcl1, Ifi47, Igtp, Irgm1, Cmpk2, Serpinb2, Cd274, Rsad2, Thbs1, Irgm2, Clec4e, Ifi205, Ifit3b, Trim30d, Acod1, Notch1*
STAT1	3.50	*Fcgr2b, Pf4, C3, Stat1, Eif2ak2, Irgm1, Fos, Rnf213, H2-Eb1, Oasl1, Fcgr1, Mx1, Irf7, Prf1, Retnla, Isg15, Ifit1, Gzmb, Gbp2, Ciita, Ly6e, Apoe, Cfb, Ifitm2, Cxcl2*	4.47	*Eif2ak2, Fas, Icam1, Stat1, Cd86, Ccnd2, Tap1, Abca1, Isg15, Irf1, Pf4, Igtp, Klrk1, Rnf213, C3, Mx2, Irgm1, Il15ra, Socs1, Gbp2b, Irf7, Ccl5, Ifit1, Ch25h, Socs3, Nos2, Acod1, Lcn2, Ly6e, Gbp2, Ptgs2, Cfb, Hif1a, Cxcl2, Tgtp2*

Upstream regulators, associated with IFN signalling, predicted by IPA to be activated in PECs after *in vivo* or *in vitro* LDI. The DEGs of the two datasets for each Upstream regulator are listed under 'Genes in dataset'. Activation z-score ≥ |2|; p-value <0.0001 considered significant.

Table 31 Upstream regulators (TLR agonists) (listing the DEGs of the *in vivo* and *in vitro* dataset)

Upstream regulator	*in vivo*		*in vitro*	
	activation z-score	Genes in dataset	activation z-score	Genes in dataset
LPS	6.31	Slc15a3, Pf4, Csf1r, Plin2, Ctsl, Hmga1, Gbp2, C3, Stat1, Cd300lf, Irak2, Eif2ak2, Stat2, Cd274, Thbs1, Nt5c3, Tnfaip3, Mif, Rgs1, Dcn, Nlrc5, Irgm2, Slfn1, Il1rn, Odc1, Met, Tgm2, Alox5, Alox15, Irgm1, Fos, Ifi204, Cmpk2, Sphk1, Spp1, Apoe, Chst3, Fbn1, Treml2, Ifi47, H2-Aa, Cxcl2, Cryab, Angptl4, Fbln2, Serpine1, Serpinb9, Oas1g, Gbp4, Mmp13, Ifi44l, Mx1, Irf7, Serpina3n, Cd163, Trim30d, Cfb, Isg15, Ccl24, Usp18, Flt1, Rsad2, Ly6c2, Ccl7, Ifit1, Ccl2, Ifit2, Tnc, Ifit3, Itgav, Kdr, Rab20, Herpud1, Ifrd1, Col1a2, Plau, Col5a2, Col3a1, Col6a1, Oasl1, Il2rb, Vcan, Col4a1, Iigp1, Fcgr2b, Birc3, Pdgfb, Foxo1, Ptgs1, Nfix, Tgfb2, Col1a1, Sparc, Fn1, H2-Ab1, Cd74, Cxcr5, Ccr3	9.65	Cflar, Dusp4, Hif1a, Oas1g, Notch2, Nfkbia, Ifi202b, Eif2ak2, Birc3, Adora2b, Il4ra, Fas, Itgal, Cd24a, Icam1, Osmr, Met, Nfkbiz, Cxcl2, Stat1, Cd86, Lamb1, Il1f9, Dcn, Ccnd2, H2-Q4, Usp18, Stat2, Tap1, Wfdc17, Sod2, Fbln2, Notch1, Satb1, Il21r, Isg15, Cd69, Zc3h12c, Irf1, Slc7a11, Cxcl1, Pde4b, Pf4, Tnc, Cxcl16, Jag1, Ifi47, Cd1d1, Igtp, Nlrc5, Il1a, Gja1, Ccl12, Trem1, C3, Mx2, Irgm1, Ifi44l, Cmpk2, Lif, Ass1, Hp, Mmp14, Serpinb2, Gbp2, Cd274, Rsad2, Thbs1, Tgm2, Hmox1, Tlr2, Irgm2, Il15ra, Socs1, Clec4e, Ifi205, Cish, Gbp2b, Ifit3b, Irf7, Ccl5, Ifit1, Cyr61, Edn1, Ptges, Flt4, Mmp2, Ifit2, Slfn1, Arg2, Serpine1, Gbp3, Il1b, Trim30d, Ptgs2, Socs3, Tarm1, Tgtp2, Cd38, Saa3, Inhba, Ctgf, Fpr2, Nos2, Acod1, Fpr1, Marco, Cfb, Gbp4, Ly6i, Lcn2, Tsc22d1, Col1a2, Stx11, S1pr1, Cdc42ep2, Slc31a2, Kdr, Ctsc, Abcb1a, Ralgds, Serpine2, Col5a2, Col5a1, Vcan, Col4a1, Mefv, Col5a3, Olr1, Gpr84, Il2rb, Ch25h, Timp3, H2-M2, Iigp1, Lmnb1, Rara, Nfkbie, Col1a1, Abca1, Slc40a1
poly I:C	5.65	Gbp2, C3, Stat1, Eif2ak2, Oas2, Stat2, Sp100, Cd274, Thbs1, Tnfaip3, Rgs1, Ly6e, Nlrc5, Ddx58, Ifih1, Dhx58, Bst2, Fos, Slfn4, Oasl1, Fcgr1, Cxcl2, Oas1g, Oasl2, Mx1, Irf7, Trim30d, Zbp1, Isg15, Oas3, Rsad2, Iigp1, Ifit1, Ccl2, Ifit2, Gzmb, Ifit3, Fcgr2b, Birc3	7.02	Ly6e, Oas1g, Dhx58, Eif2ak2, Etnk1, Birc3, Il4ra, Fas, Ifih1, Icam1, Cxcl2, Stat1, Cd86, Ddx58, Oasl2, Stat2, Abca1, C2, Isg15, Cd69, Irf1, Cxcl1, Nlrc5, Oas2, Il1a, Klrk1, Slfn4, C3, Mx2, Oas3, Olr1, Gbp2, Cd274, Rsad2, Thbs1, Tlr2, Il15ra, Socs1, Ifit3b, Irf7, Ccl5, Ifit1, Ifit2, Zbp1, Il1b, Trim30d, Ptgs2, Tarm1, Nos2, Fpr1, Marco, Iigp1
CpG oligonucleotide	1.24	Thbs1, Serpine1, Gbp4, Mmp13, Trim30d, Ccl7, Rassf4, Fcgr2b	4.45	Notch2, Fas, Icam1, Nfkbiz, Cd86, Sod2, Notch1, Abca1, C2, Cxcl1, Olr1, Gpr84, Thbs1, Tlr2, Clec4e, Gbp2b, Serpine1, Il1b, Trim30d, Ptgs2, Nos2, Marco, Gbp4, Ptges
Resiquimod	1.83	Irak2, Cxcl2, Irf7, Ccl7, Ccl2, Plau, Spp1, Ccl24, Herpud1	3.39	Nfkbiz, Cxcl2, Sod2, Cxcl1, Gpr84, Tlr2, Clec4e, Irf7, Ccl5, Il1b, Ptgs2, Nos2, Fas, Il1a, Ccl12, Inhba

TLR agonist upstream regulators predicted by IPA to be activated in PECs after *in vivo* or *in vitro* LDI. The DEGs of the two datasets for each Upstream regulator are listed under 'Genes in dataset'. Activation z-score ≥ |2|; p-value <0.0001 considered significant. Grey shaded values are below the threshold.

Table 32 Upstream regulators (PRR signalling) (listing the DEGs of the *in vivo* and *in vitro* dataset)

Upstream regulator	*in vivo*		*in vitro*	
	activation z-score	Genes in dataset	activation z-score	Genes in dataset
DDX58	3,05	Stat1, Eif2ak2, Stat2, Ifih1, Mx1, Irf7, Ifi44, Isg15, Rsad2, Ifit1, Ifit2, Ifit3, Ddx58	4,02	Tor1aip2, Eif2ak2, Ifih1, Stat1, Gem, Stat2, Isg15, Irf1, Mx2, Ifi44, Rsad2, Socs1, Gbp2b, Ifit3b, Irf7, Ccl5, Ifit1, Ifit2, Socs3, Ddx58
MAVS	4,23	Stat1, Parp12, Oas2, Stat2, Ube2l6, Nt5c3, Ddx58, Dhx58, Cmpk2, Oasl1, Oas1g, Oasl2, Irf7, Isg15, Rsad2, Ifit1, Ifit2, Ifit3	4,07	Oas1g, Dhx58, Parp12, Stat1, Ddx58, Oasl2, Stat2, Isg15, Oas2, Cmpk2, Rsad2, Ifit3b, Irf7, Ccl5, Ifit1, Ifit2, Il1b
TBK1	2,81	Mx1, Cmpk2, Rsad2, Irf7, Ifit1, Ifit2, Iigp1, Cxcl2	4,08	Sh3bp5, Icam1, Nfkbiz, Cxcl2, Cxcl1, Il1a, Fgl2, Mx2, Cmpk2, Rsad2, Tlr2, Il15ra, Irf7, Ccl5, Ifit1, Edn1, Ifit2, Ptgs2, Inhba, U90926, Marco, Iigp1, Tsc22d1, Il1b
IFIH1	2,75	Oas2, Bst2, Oas1g, Mx1, Irf7, Lck, Isg15, Ly6c2	2,76	Oas1g, Fas, Isg15, Oas2, Mx2, Cish, Irf7, Ly6i
TLR3	4,94	Mx1, Gzmb, Cd274, Cmpk2, Rsad2, Rgs1, Ifih1, Gbp2, Tnc, Oasl2, Npy, Usp18, Ccl7, Ccl2, Serpine1, Oasl1, Serpinb9, Ifit2, Iigp1, Stfa3, Cxcl2, Stfa2l1, Treml2, Ifi204, Ifit3, Irf7, Stat1, Il1rn, Isg15, Ddx58, Oas1g, Ifi47	6,16	Ifi202b, Fas, Ifih1, Nfkbiz, Cxcl2, Cd86, Furin, Oasl2, Usp18, Abca1, Cd69, Irf1, Cxcl1, Tnc, Il1a, Klrk1, Ccl12, Mx2, Cmpk2, Ier3, Gbp2, Cd274, Stfa3, Rsad2, Hmox1, Ifi205, Gbp2b, Ifit3b, Ccl5, Edn1, Ifit2, Arg2, Serpine1, Gbp3, Il1b, Ptgs2, Socs3, Saa3, Nos2, Acod1, Iigp1, Lcn2, Oas1g, Stat1, Ddx58, Isg15, Ifi47, Irf7, Ptges
TLR7	2,22	Stat2, Tnfaip3, Cxcl2, Mx1, Irf7, Isg15, Rsad2, Cdkn1b	3,13	Nfkbia, Cxcl2, Cd86, Stat2, Sod2, Isg15, Cxcl1, Mx2, Gpr84, Rsad2, Socs1, Irf7, Ccl5, Il1b, Irf1, Ccl12
TLR9	4,53	Stat2, Cd274, Npy, Stfa3, Ifi204, Sphk1, Cxcl2, Serpine1, Oasl2, Mx1, Irf7, Isg15, Usp18, Rsad2, Ccl7, Ifit1, Ccl2, Ifit2, Tnc, Ifit3, Stfa2l1	6,01	Ugcg, Ifi202b, Fas, Sgms2, Nfkbiz, Cxcl2, Cd86, Furin, Oasl2, Usp18, Stat2, Wfdc17, Abca1, Isg15, Smpdl3b, Cd69, Tnc, Il1a, Mx2, Ier3, Cd274, Stfa3, Rsad2, Hmox1, Socs1, Ifi205, Cish, Ifit3b, Irf7, Ccl5, Ifit1, Edn1, Ifit2, Arg2, Serpine1, Il1b, Ptgs2, Socs3, Saa3, Nos2, Acod1, Lcn2, St3gal5, Lyst
MYD88	4.16	C3, Tnfaip3, Il1rn, Met, Cmpk2, Spp1, Oasl1, Cxcl2, Serpine1, Ms4a4c, Mgl2, Irf7, Isg15, Rsad2, Ifit1, Ccl2, Ifit2, Gzmb	6.80	Cflar, Hif1a, Nfkbia, Sh3bp5, Icam1, Met, Nfkbiz, Cxcl2, Cd86, Pstpip2, Ednrb, Isg15, Zc3h12c, Cxcl1, Pde4b, Jag1, Acsl1, Il1a, Gdap10, C3, Mefv, Cmpk2, Hp, Acpp, Mmp14, Olr1, Rsad2, Tlr2, Cish, Ms4a4c, Irf7, Ccl5, Ifit1, Ch25h, Ptges, Mmp2, Ifit2, Serpine1, Il1b, Ptgs2, Socs3, Mmp8, Cd38, Saa3, Inhba, Fpr2, Nos2, Acod1, Fpr1, U90926, Marco, Irf1, Tsc22d1
TICAM1	4.41	Tnfaip3, Irgm2, Met, Irgm1, Ifi204, Cmpk2, Oasl1, Ifi47, Cxcl2, Serpine1, Ms4a4c, Mx1, Irf7, Cfb, Isg15, Rsad2, Ifit1, Ccl2, Ifit2, Ifit3	6.48	Tor1aip2, Cflar, Nfkbia, Icam1, Met, Nfkbiz, Cxcl2, Cd86, Pstpip2, Ednrb, Isg15, Irf1, Cxcl1, Pde4b, Jag1, Ifi47, Igtp, Acsl1, Il1a, Gdap10, Ccl12, Mx2, Irgm1, Mefv, Cmpk2, Rsad2, Tlr2, Irgm2, Il15ra, Socs1, Ifi205, Ifit3b, Ms4a4c, Irf7, Ccl5, Ifit1, Ch25h, Ifit2, Serpine1, Ptgs2, Socs3, Cd38, Il18bp, Fpr2, Acod1, Fpr1, Cfb, Tsc22d1, Il1b

Upstream regulators, associated with PRR signalling, predicted by IPA to be activated in PECs after *in vivo* or *in vitro* LDI. The DEGs of the two datasets for each Upstream regulator are listed under 'Genes in dataset'. Activation z-score ≥ |2|; p-value <0.0001 considered significant.

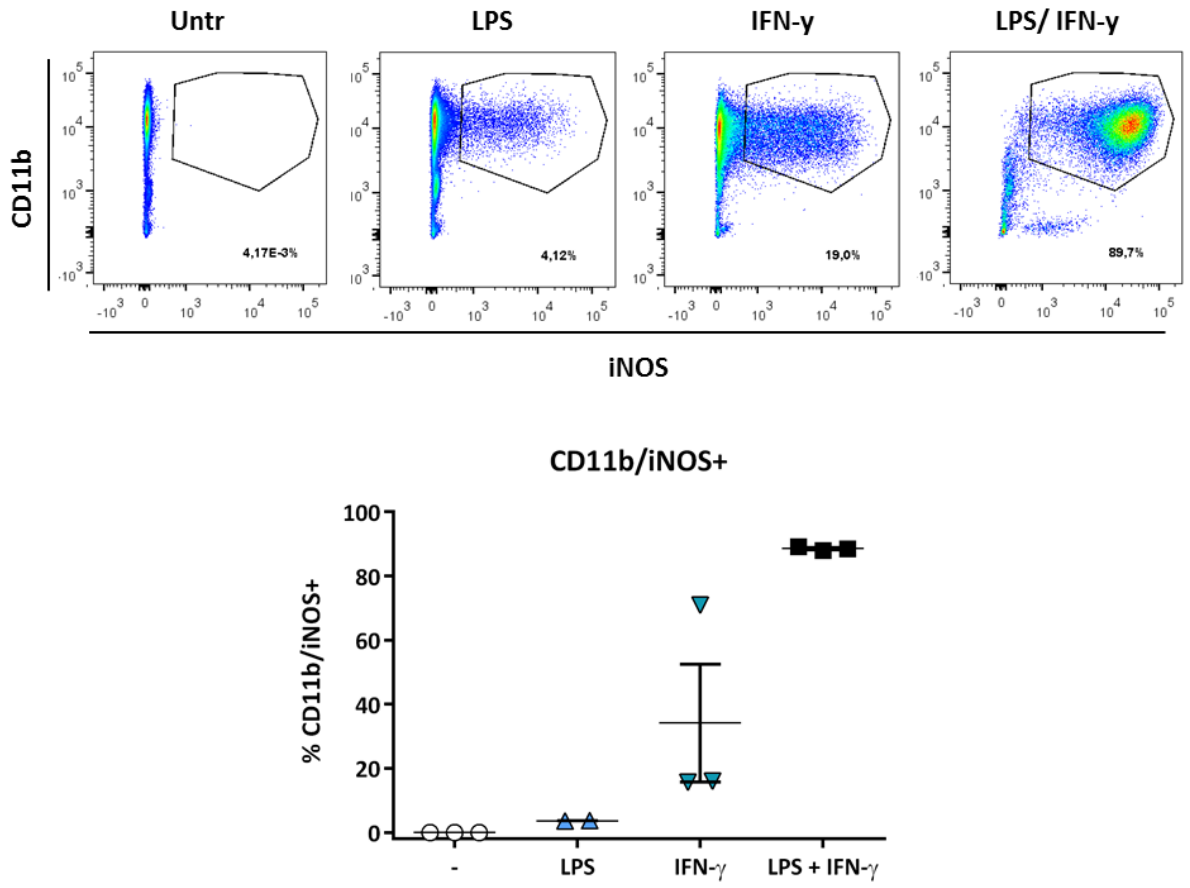

Figure S34 Effects of proinflammatory stimuli on iNOS levels of peritoneal macrophages
iNOS expression in peritoneal macrophages following *in vitro* stimulation with LPS and or IFN-γ. Flow cytometric analysis of thioglycolate-elicited PECs from C3H wt mice after stimulation with 20 ng/ml LPS and/or 20 ng/ml IFN- γ for 24 hrs. Control cells were cultured in medium only. Representative dot plots and quantitative analysis of CD11b/iNOS^{+} PECs. Only single, viable cells were included in the analysis. Data shown as mean ± SEM (n=2-3 mice per group).

7. DANKSAGUNG

Hiermit möchte ich mich bei den vielen Menschen bedanken, die mich bei der Entstehung dieser Arbeit unterstützt haben.

Mein großer Dank gilt Prof. Dr. **Philipp Beckhove** für die Möglichkeit meine Doktorarbeit in seinem Labor anfertigen zu können, sowie für sein Vertrauen und die wissenschaftlichen Freiräume in denen ich lernen und wachsen konnte. Besonders möchte ich mich für die Bereitstellung des interessanten und spannenden Themas bedanken, an dem ich arbeiten durfte.

Bei Prof. Dr. **Knut Schäkel** und Prof. Dr. **Viktor Umansky**, den Mitgliedern meines ‚thesis advisory committees', möchte ich mich für die wertvollen Anregungen zu meinem Projekt und für das Interesse an dessen Fortschritt bedanken. Danke auch an Prof. Dr. **Michael Lanzer** für die Bereitschaft den Prüfungsvorsitz meiner Disputation zu übernehmen, Prof. Dr. **Stefan Eichmüller** für die Erstellung des Zweitgutachten und Prof. Dr. **Rainer Zawatzky** für die Teilnahme an meinem Prüfungskomitee.

Prof. Dr. **Günter Hämmerling** und Dr. **Ibrahim Sektioglu** danke ich für die gute Zusammenarbeit im Rahmen unserer Kooperation, die mein Projekt vorangebracht hat. Gleicher Dank gilt Dr. **Kay Klapproth** für die Methoden, die ich von ihm lernen durfte und die hilfreichen wie auch interessanten wissenschaftlichen Diskussionen und nicht zuletzt für die vielen Nächte am Sorter.

Danke auch an **Andreas Griesbach**, **Jens Lang** und **Barbara Kahn-Schapowal** für die Unterstützung bei der Bestrahlung meiner Mäuse; an Dr. **Damir Krunic** und Dr. **Manuela Brom** der Einheit 'Lichtmikroskopie' für ihre Hilfe mit den IF-Aufnahmen; an Dr. **Kerstin Dell**, Dr. **Michaela Socher** und die Tierpfleger der ZTL für die tolle Zusammenarbeit; sowie and die Mitarbeiter der ‚High Throughput Sequencing' Einheit der ‚GPCF' für das RNA Sequencing.

Auch danke ich den Mäusen, die für die Anfertigung dieser Arbeit ihr Leben lassen mussten.

Mein besonderer Dank gilt den aktuellen und ehemaligen Mitarbeitern der AG Beckhove (& Bayer Joint Lab) für die großartige Arbeitsatmosphäre und all die gemeinsamen wissenschaftsfernen Aktivitäten:

Dr. **Felix Klug** für die ausgezeichnete Einarbeitung und die gemeinsame Arbeit an den Cancer Cell Revisions. **Lukas Nögel**, meinem fleißigen Masteranden, für den Perspektivwechsel und die Denkanstöße. Dr. **Jasmin Quandt**, für ihre Hilfe mit den Mäuschen, dem CANTO und der DIVA, aber vor allem für ihr offenes Ohr. Dr. **Maria Xydia**, einer exzellenten Wissenschaftle-

rin, für ihre professionellen und auch persönlichen Ratschläge. Dr. **Hans-Henning Böhm** für seine Weisheit und seinen Humor. Dr. **Anna-Lena Krause**, für ihre Kreativität, für die alternative Karriereplanung und das Niveau. **Tillmann Michels** für die Unterstützung bei der RNA-Sequencing Analyse und Dr. **Maria Pritsch** für ihre Unterstützung bei den statistischen Analysen. Dr. **Diane Egger-Adam**, Dr. **Lilli Podola** und Dr. **Mudita Pincha** für die wissenschaftlichen, wie auch nicht-wissenschaftlichen Gespräche und fürs Zuhören. Dr. **Slava Stamova**, Dr. **Anchana Rathinasamy**, Dr. **Nisit Khandelwal**, **Antonio Sorrentino**, **Valentina Volpin** and **Chih-Yeh Chen** for a great time – not only in the cell culture. **Melanie Neubauer** für ihre Assistenz bei größeren Mausexperimenten und nicht zuletzt **Simone Jünger**, **Mariana Bucur** und **Ludmila Umansky**, für die hervorragende Organisation des Labors und ihre uneingeschränkte Hilfsbereitschaft, sowie **Miriam Schimmelmann** und **Irmtraud Williams** für die administrative Unterstützung.

Bei den Mitarbeitern der AG Sültmann, möchte ich mich für die herzliche Aufnahme (wenn auch inoffiziell) in den letzten Monaten bedanken. Bei **Sabrina Gerhardt** und **Simon Ogrodnik** für die Unterstützung bei meinen Bioanalyzerversuchen, aber vor allem bei **Leonie Ratz.** Danke für unsere Unterhaltungen, für deine Korrekturen und besonders für die lustigen und schönen (Sushi-) Abende.

Von ganzem Herzen danke ich meinen Freunden. Insbesondere **Katha** für ihre aufbauenden Worte und moralische Unterstützung während meines Studiums und meiner Promotion und **Jan** und **Rebecca** für die Spieleabende, die tiefsinnigen Gespräche und die Erweiterung meines Horizonts.

Mein größter Dank gilt meiner Familie und Patrick. Meiner **Mutter**, dafür, dass sie immer an mich glaubt, immer für mich da ist und mich in all meinen Entscheidungen bedingungslos unterstützt. Meiner Schwester **Adina** und meinem Bruder **Severin** für die Unbeschwertheit und das Chaos, wenn wir zusammen sind.

Patrick, ohne deinen Rückhalt, deine Unterstützung und dein Verständnis wäre ich nicht so weit gekommen. Auch wenn ich es nicht immer zum Ausdruck bringen konnte habe ich das nie als selbstverständlich angesehen.
Ich bin dir unendlich dankbar für alles.